Targeted approaches to C5 high-grade serous ovarian cancer through novel patient derived xenografts

Valerie Yue Ming Heong

A dissertation submitted in total fulfillment of the requirements of the degree of

Doctor of Philosophy

August 2017

The Walter and Eliza Hall Institute of Medical Research

Department of Medical Biology

The University of Melbourne

PhD thesis

Dr Valerie Heong

Walter and Eliza Hall Institute of Medical Research

Supervisors:

Associate Professor Clare Scott

Professor Geoff Lindeman

Seconded to the laboratory of Dr. Ruby Huang, Cancer Science Institute, National University Singapore

Abstract:

Epithelial ovarian carcinoma (EOC) is the fifth most common cause of cancer death in western women. It can be classified into five main histological subtypes – endometrioid, clear cell, mucinous and high grade serous ovarian carcinoma (HGSOC), as well as low grade serous ovarian carcinoma. HGSOC can be further subclassified into four sub-groups based on molecular characteristics - C1, C2, C4 and C5. The C5 subtype, which is also known as the proliferative or Stem-A subtype, is associated with stem cell-like behavior and confers a poor prognosis. Little is known about this poor prognostic subtype of HGSOC. In addition, limited pre-clinical models are available to date for therapeutic exploration. This thesis has therefore focused on establishing a clinically relevant cohort of C5/proliferative/ Stem-A HGSOC patient-derived xenografts (PDX), and subsequently undertaking detailed molecular characterization to further understand the biology of this molecular subtype as well as performing drug response analyses.

Here we showed that the C5/proliferative/ Stem-A HGSOC molecular subtype is heterogenous. We also showed through a cohort of clinically relevant PDX that the MYCN expression was not a good predictor of response to the MYCN inhibitor, M606 despite promising *in vitro* data from neuroblastoma cell lines and transgenic mouse models. Furthermore, we showed that *MYCN* expression was not a faithful predictor of response to BET bromodomain inhibitor, I-BET-762. In addition, we demonstrated that resistance to BET bromodomain inhibitor, I-BET-762 in C5/proliferative/ Stem-A HGSOC, was regulated by the *FZD7-TWIST1* axis. Lastly, we identified the vinca alkaloid, vinorelbine as an effective therapeutic agent in C5/proliferative/ Stem-A HGSOC, relevant for further exploration in the clinical setting.

Taken together, research completed in this thesis has greatly enhanced our understanding of C5/proliferative/ Stem-A HGSOC biology. The established cohort of clinically relevant C5/proliferative/ Stem-A HGSOC PDXs are an invaluable laboratory resource to enable accurate *in vivo* testing of novel therapies in the future. Furthermore, we identified a suitable effective therapeutic strategy to inform a C5/proliferative/ Stem-A -specific clinical trial.

Declaration

This is to certify that:

1. This thesis comprises only my original work towards the PhD, except where indicated in the Preface.

2. Due acknowledgement has been made in text to all other material presented.

3. This thesis is less than 100,000 words in length, exclusive of figures, tables and bibliographies.

Valerie Heong Yue Ming

The Walter and Eliza Hall Institute of Medical Research

Department of Medical Biology

The University of Melbourne

Parkville, Victoria 3052

Australia

Preface

Pursuant to the regulations of The University of Melbourne, the author's contribution to each Chapter was as follows:

Chapter 3 90%

Dr. Jan Pyman performed immunostaining on sections collected from PDX and primary patient tumours. Thuan Phoung performed one set of immunoblotting for BCL2 protein to complete three biological replicates for each PDX characterized during my secondment to Singapore.

Chapter 4 80%

Dr Tan Ming performed the *TWIST1* ChIP-qPCR. Dr Tony Tan Tuan Zea performed bioinformatics analyses for the *FZD7-TWIST1* signature for the patient tumours as well as the PDX data presented.

Chapter 5 95%

Mohammad Asad performed the anoikis assay and FACS experiment. Dr Tony Tan Tuan Zea performed bioinformatics analyses for the MASH analysis on the PDX.

Thus, the author's overall contribution to work in this thesis was > 88%.

Acknowledgements

I would like to thank my supervisors, Dr. Clare Scott and Dr. Geoff Lindemann (WEHI, Australia) and Dr. Ruby Huang (CSI, Singapore) for giving me the opportunity to study in their lab. Thank you for mentoring me and teaching me about science and life. I will never be able to put it into words how much you both inspired me with your tenacity, integrity and relentless perseverance. You have both given me a glimpse of what good leaders should be and I will always be grateful.

I would also like to acknowledge my PhD committee, Dr. Kate Sutherland, Dr. Ian Street, Dr. Sumitra Ananda and Dr. Matt Wakefield for all the support, advice and encouragement throughout the years.

This thesis would not be possible without Dr. Monique Topp, who taught me all I know about PDX and *in vivo* experiments, Dr. Tony Tan Tuan Zea, for all the bioinformatics and general IT support, Dr. Chung Vin Yee, for teaching me everything I know about epigenetics and Ye Jieru, thank you for your patience and for being a sounding board for literally everything.

I would also like to thank all my past and current lab members from both WEHI, Australia and CSI, Singapore for their friendship and guidance. From WEHI, Elizabeth Lieshke – thank you for your patience and for helping me out with last minute house-keeping issues, Monique Topp, Thuan Phuong, Gwo Ho, Liz Kyran, Emma Boehm, Venetia Kumbatta, Robert Holian, Alison Hadley, Holy Barker, Olga Kondroshova, Ksenija (Kas) Nesic and Michelle Cook. From CSI, Vin Yee Chung, Jieru Ye, Tan Ming, Tony Tan Tuan Zea, Mohammad Asad, Angele Koh, Theng Kuay Kuee, Eddy Pang and Tang Hei Mui.

I would also like to thank our collaborators from the Royal Womens Hospital (RWH), Melbourne and the Australian Ovarian Cancer Study (AOCS). In particular, Dr.

Jan Pyman for immunohistochemistry staining of the PDX, Dr. Orla McNally, Dr. Michael Quinn, Dr. Sumitra Ananda, Dr. Anne Hamilton, Prof David Bowtell, Julene Harrow and Pauline Thomas for their collaboration in the generation of the PDX. I would also like to acknowledge our collaborators at the Mayo clinic, Rochester, USA, Dr. Paul Haluska and Dr. John Weroha for contributing to the C5/Stem-A PDX, and Children's Cancer Institute Australia (CCIA), Australia, Dr. Michelle Henderson for collaboration on the MYCN project. I would also like to take this opportunity to thank all the women with ovarian cancer who donated their samples and participated in the AOCS.

I would like to acknowledge both WEHI and CSI services that played a crucial role in my research. The media kitchen, bioservices, histology and the animal facility. In particular, the animal techs Silvia Stoev and Kim Birchall.

Most importantly, I want to thank God for not only providing the opportunity but for giving me the strength, perseverance and favor for this journey. My parents for their unwavering support, encouragement and words of wisdom, my brothers and sisters- in- law for their endless support, my friends both in Australia – Hari, Yao, Su Chin, Mahen, Sarah, Ben, Lip Jin and Von – thanks for your friendship and my new and old friends in Singapore/ Malaysia – Hazel, Wong TF, Chi yen, Janice, Li- Ann, Jean, Jin Yu, BQ, Madam SS, Mark, Jason, Aunty Angie and Uncle Robert – thank you for the laughs, for feeding me and for keeping me sane. This journey wouldn't have been the same without all of you.

List of publications

Tan TZ*, **HEONG V***, Ye J, Lim D, Low J, Choolani M, Scott C, Tan DSP and Huang RYJ. Deciphering intra tumoral heterogeneity using Molecular Assessment of Subtype Heterogeneity to guide personalized medicine in ovarian cancer. *Equal contributing authors. *Under review*. ***EMBO Mol Med*** 2017. *Part of this manuscript arises from work presented in Chapter 5 of this thesis. Data from this manuscript was also alluded to in the discussion (Chapter 6) of this thesis.*

Tan M*, Asad M*, **HEONG V***, Wong MK, Tan TZ, Thiery JP, Scott C, Huang RYJ. The *FZD7-TWIST1* axis driven anoikis resistance and tumorigenesis is a therapeutic target for Wnt pathway in ovarian cancer. *Equal contributing authors. *Under review*. ***Cell Death and Differentiation*** 2017. *Part of this manuscript arises from work performed in chapter 4 of this thesis.*

Bowtell D, Bohm S, Ahmed A, Aspuria PJ, Bast R, Beral V, Birrer M, Blagden S, Bookman M, Brenton J, Chippinelli K, Martins F, Coukos G, Drapkin R, Edmondson R, Fotopoulou C, Gabra H, Galon J, Gourley C, **HEONG V**, Huntsman D, Iwanicki M, Karlan B, Kaye A, Lengyel E, Levine D, Lu K, McNeish I, Menon U, Narod S, Nelson B, Nephew K, Pharoah P, Powell D, Ramos P, Romero I, Scott C, Sood A, Stonach E and Balkwill F. Rethinking ovarian cancer II: reducing moretality from high-grade serous ovarian cancer. ***Nature Reviews Cancer***. 2015. 15(11):668-79. *This manuscript is a consensus statement from the Helene Harris Memorial Trust Meeting in Spain. It is addressed in the introduction and some of chapter 3. It arises from work conducted by me that contributed to Chapter 3 of my thesis which led me to be selected for the travel fellowship award and attendance to the meeting that resulted in this manuscript.*

Topp M, Hartley L, Cook M, **HEONG V**, Boehm E, McShane L, Pyman J, McNally O, Ananda S, Harrell M, Etemadmoghadam D, Galletta L, Alsop K, Mitchell G, Fox SB, Kerr JB, Hutt KJ, Kaufmann SH, Australian Ovarian Cancer Study, Swisher EM, Bowtell DD, Wakefield M and Scott CL. Molecular correlates of platinum response in human high-grade serous ovarian cancer patient-derived xenografts. ***Molecular Oncology***. 2014. 8(3):656-68. *This manuscript was not included in my PhD. However, it arises from work performed during my PhD.*

Table of Contents

Index of figures

Index of Tables

Non – standard abbreviations

ACTB	Actin, beta
BCA	Bicinchoninic acid
bHLH	basic helix–loop–helix
BRCA1/2	Breast cancer susceptibility gene 1/2
B2M	Beta-2-microglobulin
CA125	Cancer antigen 125
ChIP-qPCR	Chromatin immunoprecipitation-quantitative polymerase chain reaction
ChIP-seq	Chromatin immunoprecipitation-sequencing
CSC	Cancer stem cell
CTC	Circulating tumour cell
CSI	Cancer Science Institute
DMEM	Dulbecco's modified eagle medium
DMSO	dimethyl sulfoxide
EOC	Epithelial ovarian carcinoma
EpiA/B	Epithelial A/B
FACS	fluorescence-activated cell sorting
FCS	fetal calf serum
FFPE	formalin fixed paraffin embedded
FIGO	International Federation of Gynecology and Obstetrics
GEMM	genetically engineered mouse model
G150	half growth inhibitory concentration
H + E	hematoxylin and eosin
HGSOC	High-grade serous carcinoma

HPRT1	Hypoxanthine phosphoribosyltransferase 1
IC50	half maximal inhibitory concentration
IGF	Insulin-like growth factor
IL-6	Interleukin 6
LGSC	Low-grade serous carcinoma
Mes	Mesenchymal
MET	Mesenchymal-epithelial transition
MTS	(3-(4,5-dimethylthiazol-2-yl)-5-(3-carboxymethoxyphenyl)-2-(4- sulfophenyl)-2H-tetrazolium)
NSG	non-obese severe combined immune deficient IL2r$\gamma^{J/J}$
OCCC	Ovarian Clear Cell cancer
OS	Overall survival
OSE	Ovarian surface epithelium
PFS	Progression-free survival
PARP	Poly ADP-ribose polymerase
PDX	patient – derived xenograft
RPL13A	Ribosomal protein L13a
RPMI	Roswell Park Memorial Institute
RTK	Receptor tyrosine kinase
SEM	Standard error of mean
siRNA	Small interfering RNA
shRNA	Short hairpin RNA
T1	first passage of patient – derived xenograft transplanted from patient tumour
TCGA	The Cancer Genome Atlas Research Network
TSS	Transcription start site

TGF-α	Transforming growth factor-α
TSS	Transcription start site
TWIST1	Twist family bHLH transcription factor 1
VEGF	Vascular endothelial growth factor
WEHI	The Walter and Eliza Hall Institute of MedicalResearch
Wnt	Wingless-type MMTV integration site family

The abbreviations of gene and protein names have been expanded in the text upon their first use in the thesis

Chapter I:

Introduction

1. Introduction

Ovarian cancer is the seventh most common cancer and eighth most common cause of cancer-related death in women worldwide (Ferlay et al., 2014). With no validated screening schedule, and paucity of symptoms at disease onset, more than 50% of ovarian cancers are diagnosed at an advanced stage (Vaughan et al., 2011). In the year 2012, global statistics listed 238,719 new diagnoses of ovarian cancer and 151,905 cases of ovarian cancer death were reported (Ferlay et al., 2014). In Australia there are an estimated 1500 new cases annually and almost 1000 deaths from OC reported in 2010 (AIHW, 2012) while in Singapore, from 2009 – 2013, 1646 new cases of ovarian cancer were diagnosed over five years and 583 deaths were attributed to ovarian cancer (Singapore Cancer Registry, 2015). Ovarian cancers can arise from three main types of ovarian tissues: surface epithelial cells, sex cord-stromal tissues and germ cells (V. W. Chen et al., 2003; Scully, 1987). Of all malignant ovarian tumours, epithelial ovarian carcinoma (EOC) is the most common type, accounting for about 90% of cases (Chuaqui et al., 1998). Cytoreductive surgery integrated with platinum based chemotherapy has become the initial standard treatment (Cadron et al., 2007; McGuire et al., 1996). However, approximately 70% of patients' experience disease relapse after a varying disease-free interval

1.1. Epithelial ovarian cancer (EOC)

1.1.1 Histological and molecular classification of EOC

EOC consist of a series of molecularly and aetiologically distinct diseases (Vaughan et al., 2011). Conventionally, EOC were divided into five main histological subtypes based on their histopathological features, namely serous, mucinous, endometrioid, clear cell and transitional/Brenner type (Scully et al., 1987). Within each histological subset, the tumours were further classified into benign, if they lack profuse proliferative and cytological atypia; borderline (low malignant potential), if they show exuberant growth but limited invasiveness; or as malignant if there was invasive behavior (Chen et al., 2003). Furthermore, endometriod and mucinous carcinomas are graded using a three point scale, usually referred to as grade1, grade 2 or grade 3 (Chen et al., 2003).

When describing EOC, conventionally they were divided into two broad categories, type 1 and type II tumours, based on two molecular pathways of tumourigenesis (Shih and Kurman, 2004) (Table 1). Type I tumours comprise mainly low-grade tumours which include low-grade serous carcinoma (LGSC), mucinous ovarian tumours, endometrioid ovarian cancer, clear cell ovarian cancer (OCCC) and malignant Brenner tumours; while type II tumours tend to consist of high-grade tumours such as the most common high-grade serous carcinomas (HGSOC), carcinosarcomas and undifferentiated carcinomas (Shih and Kurman, 2004). Most type I tumours develop in a stepwise fashion from recognizable precursors, such as cystadenomas, adenofibromas or borderline tumors; while type II tumours tend to develop *de novo* from epithelial inclusion cysts of the ovary or from tubal intraepithelial carcinoma.

Despite the histological similarities, LGSC and HGSOC differ clinically and molecularly, with *BRAF* or *KRAS* mutations (65%) prominent in LGSC while *TP53* mutations are ubiquitous in HGSOC (Ahmed et al., 2010). Clinically, these tumours

vary in their responses to standard therapy, with LGSCs (generally not highly proliferative) responding poorly to chemotherapy whereas HGSOC (highly proliferative) generally experience high response rates to initial standard chemotherapy with varying disease free intervals, however, the majority will invariably experience disease recurrence (Bowtell et al., 2015; Shih and Kurman, 2004).

Table 1.1: Type I and Type II EOC

Classes	Histotype (Percentage)	Precursors	Genetic abnormalities
Type I	Low-grade serous carcinomas (<5%)	Serous cystadenoma/adenofibroma Borderline serous tumour Noninvasive serous carcinoma	BRAF, KRAS, NRAS, ERBB2 mutations
	Mucinous carcinomas (3%)	Mucinous cystadenoma Borderline mucinous tumour Intraepithelial carcinoma	KRAS mutations ERBB2 amplification
	Endometrioid carcinomas (10%)	Atypical endometriosis Endometrioid adenofibroma Borderline endometrioid tumour Intraepithelial carcinoma	PTEN mutations/LOH CTNNB1, KRAS, PIK3CA, PPP2R1A, ARID1A mutations Microsatellite instability MMR deficiency
	Clear cell carcinomas (10%)	Atypical endometriosis Clear cell adenofibroma Borderline clear cell tumour Intraepithelial carcinoma	KRAS, HNF1, ARID1A, CTNNB1, TGF-b RII, PIK3CA, PPP2R1A mutations PTEN mutations/LOH Microsatellite instability
	Malignant Brenner tumours	Brenner tumour Borderline Brenner tumour	Not yet identified
Type II	High-grade serous carcinomas (70%)	De novo in epithelial inclusion cysts Tubal intraepithelial carcinoma	TP53, BRCA1/2 mutations ERBB2 amplification AKT2 amplification CDKN2A inactivation NF1, CDK12 mutations Homologous recombinant repair genes mutations PI3/Ras/Notch/FoxM1 signaling alterations
	Malignant mixed mesodermal tumours (carcinosarcomas)	Not yet identified	TP53 mutations
	Undifferentiated carcinoma	Not yet identified	Not yet identified

Adapted from Chung VY *et al*, 2015; Hennessy *et al*, 2009; Jayson *et al*, 2014; Prat, 2012; Shih and Kurman, 2004**)**

1.1.2 Cell of origin of histological subtypes of EOC

Recent pathological and genomic findings indicate that the majority of the histological subtypes are likely derived from non-ovarian tissues and share few

molecular similarities (Kurman and Shih, 2010) (Figure 1.1). The distal fallopian tube has been identified as a source of HGSOC (Lee et al., 2007; Levanon et al., 2010; Piek et al., 2001). The fallopian tube compared with the ovarian surface epithelium in the genesis of HGSOC is still being hotly debated, however, published mouse models now support the fallopian tube secretory cells as the cell of origin of most human HGSOC (Perets et al., 2013)

OCCC and endometrioid cancers have a strong epidemiological link with endometriosis with high-frequency of somatic mutations of the PI3K catalytic subunit *PIK3CA* and AT-rich interactive domain-containing protein 1A (*ARID1A*) (Jones et al., 2010; Kuo et al., 2009). Finally, the majority of invasive mucinous ovarian tumours are thought to have metastasized to the ovary from other solid cancer types, including gastrointestinal tumours (Kelemen and Köbel, 2011; Zaino et al., 2011) (figure 1.1). It is becoming increasingly clear that some EOC have more in common with certain types of renal cancer or breast cancer than they do with other histological subsets of ovarian cancer. In essence, HGSOC share transcriptional and genomic features with basal like breast cancers (Bowtell et al., 2015; Tothill et al., 2008) while OCCC have very similar phenotypes to renal clear cell cancers (Zorn et al., 2005). Indeed, more robust classification using immunological markers and genomic studies have resulted in previously designated tumours being reclassified (Köbel et al., 2009). Therefore, the different ovarian histological subsets should not be regarded as a single entity, as their cell of origin, driver mutations and epidemiology are indeed very different.

With regards to low-grade invasive tumours, these tumours are still regarded as ovarian-derived but the initiating cells are still unclear. It is possible that their site of origin will be re-evaluated in the future. However, it is clear that LGSC are not precursor lesions to HGSOC as they have a very distinct range of mutational events.

1.1.3 High- grade serous ovarian cancer (HGSOC)

As previously mentioned, HGSOC shares substantial molecular similarities with basal-like breast cancer and accounts for the most death from ovarian cancer (Bowtell et al., 2015). Hitherto, there has been minimal improvement in overall survival rates from this disease for decades (Bowtell et al., 2015) (figure 1.2).

1.1.3.1 Cell of origin of HGSOC

Despite the term ovarian cancer, several pathological, epidemiological, molecular and mouse model studies suggests the likely progenitor cell of HGSOC is the secretory epithelial cell of the distal fallopian tube (FTSEC) (Kindelberger et al., 2007; Kuhn et al., 2012; Perets et al., 2013) (figure 1.2). Nevertheless, despite the improved methods of pathological assessment of fallopian tubes, there appears to be some HGSOC lesions that seem to arise without fallopian tube involvement. This is consistent with experimental mouse model studies of HGSOC where some models show a direct evolution from precursor cells in the fallopian tube (Perets et al., 2013) while others appear to primarily involve precursor cells in the ovary (Kim et al., 2015). It is still unclear whether tumours that appear to arise without fallopian tube involvement are associated with earlier seeding of the ovaries with fallopian tube secretory epithelial cells through a process known as endosalpingosis or whether they are truly ovary-derived diseases (Bowtell et al., 2015; Kim et al., 2015; Perets et al., 2013). Currently, the earliest known molecular event in HGSOC is the acquisition of mutations in the tumour suppressor gene, *TP53*. It is the pathognomonic feature of serous tubal intraepithelial carcinoma (STIC) and invariably present in HGSOC (Ahmed et al., 2010; TCGA., 2011)

1.1.3.2. Markers of drug response and resistance in HGSOC

Generally, point mutations in oncogenes or tumour suppressor genes are relatively uncommon in HGSOC (TCGA., 2011). Instead, they are characterized by significant genomic and structural variation, with frequent copy number changes, making this cancer an example of a chromosomally unstable (C-class) malignancy (Ciriello et al., 2013). Approximately 50% of HGSOC have been shown to be defective in the homologous recombination (HR) DNA repair pathway (TCGA., 2011). The majority of HR defects arise mainly from germline, somatic and/or epigenetic mutations in *BRCA1* or *BRCA2* (~33% of HGSOC) (Alsop et al., 2012; TCGA., 2011) and, to a lesser extent, from mutations in other components of the HR pathway (Walsh et al., 2011) (figure 1.3). Indeed, HR deficiency is an important determinant of platinum sensitivity and provides a rational basis for the use of poly(ADP- ribose) polymerase (PARP) inhibitors, which further inactivate DNA repair in already compromised HR-defective tumours (Fong et al., 2009; Ledermann et al., 2012; Scott et al., 2015). Somatic and germline mutations in components of HR are generally mutually exclusive (Bowtell et al., 2015; George et al., 2013)

Cyclin E1 (*CCNE1*) amplification represents an important subset of mostly HR-intact tumours. Approximately 30% of HR-intact tumours have amplification of *CCNE1* (which encodes the G1/S-specific cyclin E1) (TCGA., 2011), and this is likely an early event in the development of HGSOC (Karst et al., 2011). The loss of *BRCA1* and *CCNE1* amplification were observed to be mutually exclusive as the acquisition of both these events were shown to result in synthetic lethality (Etemadmoghadam and Weir, 2013). Moreover, HGSOC cell lines in which *CCNE1* is amplified undergo cell cycle arrest or apoptosis following the loss of cyclin E1 or its protein partner, cyclin-dependent kinase 2 (CDK2) (Etemadmoghadam et al., 2010). The proportion of HGSOC with *NF1* (neurofibromin 1) and *RB1* loss has recently been

shown to be more prevalent than previously thought increasing to 17% and 15% respectively (Bowtell et al., 2015) (figure 1.3) although the exact clinicopathologic outcomes of these molecular events are still unclear.

1.1.3.3 Prevention and screening of HGSOC

HGSOC is usually diagnosed at an advanced stage in about 70% of patients and these women have a substantially worse outcome compared to women diagnosed with early stage disease. As such, it is important to identify patients who are at increased risk and to implement effective preventative strategies for this disease. Notable preventive strategies include the oral contraceptive pill (OCP) that provides lasting risk reduction in all women (Kotsopoulos et al., 2015) and the duration of OCP used correlating with the reduction in risk (Bowtell et al., 2015). The exact mechanism of the ovarian protection with OCP is still unclear and further research is needed. Chronic use of asprin for non-malignant conditions has also been shown to be associated with the reduction in the incidence of EOC (Trabert et al., 2014).

In contrast, the use of hormonal therapy in menopausal women was found to increase the risk of ovarian cancer, in particular HGSOC, in a meta-analysis of more than 50 epidemiological studies (Collaborative Group on Epidemiological Studies of Ovarian Cancer., 2015, 2015). Obesity has also been shown to be a risk factor for HGSOC, more significantly in women who have never used hormonal therapy (Collaborative Group on Epidemiological Studies of Ovarian Cancer., 2012). Accounting for increase in BMI alone, if all other relevant remains constant, for every 5mg/m2 increase in BMI is associated with a 3% increase in ovarian cancer incidence per decade (Collaborative Group on Epidemiological Studies of Ovarian Cancer., 2012). Lastly, and certainly the most studied risk factor, is the presence of a germline mutation in *BRCA1* or *BRCA2* which are present in approximately 15%-17% of HGSOC patients (Alsop et al., 2012).

As such, germline testing should be offered to all women irrespective of age or family history at diagnosis as it not only provides prognostic information (Alsop et al., 2012; Pennington et al., 2014) as previously outlined, but also enables population testing for founder mutations in family members and high risk population groups.

Early detection methods are paramount for this disease as the disease is often asymptomatic before peritoneal spread. The Prostate, Lung, Colorectal and Ovarian (PLCO) Cancer Screening Trial using blood based tumour marker CA125 accompanied with Trans-vaginal ultrasound showed no reduction in mortality (Buys et al., 2011). While the more recent United Kingdom Collaborative Trial of Ovarian Cancer Screening (UKCTOCS) performed incidence screening based on a multimodal strategy in which annual serum CA125 was interpreted together with the risk of ovarian cancer algorithm (ROCA) (Menon et al., 2015). Women were subsequently triaged into normal risk, intermediate risk and elevated risk depending on the ROCA and either returned to annual screening, repeat CA125 or transvaginal ultrasound and repeat CA125 respectively depending on their individual risk (Menon et al., 2015). Using the algorithm and multimodality screening tools doubled the screen detected invasive EOC ($p = 0.0027$) compared with a fixed single-threshold biomarker (Menon et al., 2015). Evidence of a mortality impact is still awaited. Future screening strategies could focus on detection of specific DNA aberrations in the plasma (Forshew et al., 2012) or cervical secretions (Kinde et al., 2013) such as *TP53* mutations for screening of high risk HGSOC.

1.1.3.4 Current treatment paradigm in HGSOC

Cytoreductive surgery integrated with platinum based chemotherapy has become the initial standard treatment (Cadron et al., 2007; McGuire et al., 1996). HGSOC tend to be sensitive to first line platinum-based chemotherapy and other DNA-damaging

agents, and are frequently amenable to retreatment, even with the same or similar cytotoxic therapy to those that were used during the initial treatment period (platinum – sensitive disease). Pre-operative tumour load and post-operative residual disease are some of the most important prognostic factors for survival in advanced stage disease (Bois et al., 2009; Horowitz et al., 2015). Nonetheless, several key questions still remain unclear. This includes patient selection of those most likely to benefit from primary cytoreductive surgery (debulking surgery), timing and extent of surgery and the value of neoadjuvant chemotherapy and interval debulking particularly in specialized centres with experienced gynecological surgeons (Vergote et al., 2010). Hence, it seems pertinent to carefully select patients who would derive the greatest benefit from these surgical options. The development of biomarkers that reliably predict surgical resectability, or rapid relapse despite optimal surgical effort, is important for patient stratification (van Meurs et al., 2013) and thus, integration of molecular markers with clinical and histological factors should be included in the assessment of every newly diagnosed HGSOC patient.

Nevertheless, despite maximal efforts, treatment resistance eventually develops in 80% -90% of patients with relapsed disease (Bowtell et al., 2015). Recurrent EOC is incurable and it remains unclear why patients develop recurrent disease despite the high response rates (~70%) observed during initial chemotherapy. Besides retreatment with a platinum agent, chemotherapy agents such as pegylated liposomal doxorubicin (Gordon et al., 2000), topotecan (Sehouli et al., 2011) and gemcitabine (Mutch et al., 2007) are among the cytotoxic agents used in the relapsed setting, with generally low response rates (Gordon et al., 2004; Mutch et al., 2007; Sehouli et al., 2011). In contrast, targeted therapeutic approaches with the anti-vascular endothelial growth factor (VEGF) antibody, bevacizumab in high risk patients (Perren et al., 2011) or platinum-resistant disease (Pujade-Lauraine et al., 2014), and olaparib, an inhibitor of the enzyme poly-

(ADP ribose) polymerase inhibitor (PARPi) (Ledermann et al., 2012; Ledermann et al., 2014; Pennington et al., 2014) in patients who harbor a *BRCA1/2* mutation, have demonstrated significant improvement in outcomes for a subgroup of patients with advanced ovarian cancer.

In the relapsed setting, several retrospective studies have associated total macroscopic tumour clearance with secondary cytoreductive surgery with significant prolonged progression free survival and overall survival (Fotopoulou et al., 2013; Harter et al., 2006). However, there is currently no prospective evidence of survival benefit for secondary cytoreduction post completion of first-line treatment in platinum-sensitive tumours (Bowtell et al., 2015) and thus, we await with interest several large multicentre, prospective, randomized surgical trials (AGO-OVAR OP.4/AGO DESKTOP OVAR III and GOG0213 studies) that are expected to define the value of secondary debulking surgery in the relapsed setting.

1.2 Ovarian cancer intertumoural heterogeneity - Molecular subtyping of ovarian cancer (mesenchymal, immune reactive, differentiated, proliferative)

The major stumbling block for the application of personalised medicine approaches is the significant inter-tumoural heterogeneity that exist in ovarian cancer. For personalised strategies to be successful, clinically relevant validated biomarkers along with the development of companion diagnostic test to evaluate responses are required. Hitherto, robust platforms such as these are lacking in ovarian cancer. Furthermore, identifying the underlying biology and molecular pathogenesis of ovarian cancer is crucial to enhance our understanding and improve treatment of this devastating disease.

Co-ordinated molecular analyses identified four independent molecular subtypes of HGSOC with associated prognostic significance based on gene expression profiling in several independent studies (Tan, Miow et al., 2013; TCGA., 2011; Tothill et al., 2008). The subsets have each been termed differently by the authors of the individual analyses but have been found to show clear correlation with distinct clinical outcomes (figure 1.4). An enrichment of genes, ontology terms, and signaling pathways associated with immune cells was found to be associated with the immunoreactive subtype (C2/Epi B) with genes related to the adaptive immune response found to be significantly overexpressed, including markers of T-cell activation (CD8A) and T-cell trafficking (CXCL9) (TCGA., 2011; Tothill et al., 2008). The immunoreactive/C2 subtype is not only immunogenic but is also associated with *BRCA1* mutations (George et al., 2013) which leads to defects in the homologous recombination DNA repair (HR) pathway (Patch et al., 2015). Tumours with DNA repair deficiencies are thought to stimulate the immune system through their high mutational load and expression of neoantigens resulting in higher levels of tumour infiltrating lymphocytes in these tumours (Le et al., 2015; Schwarz et al., 2015). Notably, the C2/immunoreactive molecular subtype has been associated with a better clinical outcome compared to other subtypes (C1, C4, C5) (Tan, Miow et al., 2013a; TCGA.,

2011). The differentiated (C4) subtype was associated with a more mature stage of development due to high expression of *MUC16* and *MUC1* as well as expression of the secretory fallopian tube marker *SLP1*. Markers suggestive of increased stromal components such as markers of activated myofibroblasts (*FAP*), vascular endothelial cells and pericytes (*PDGFRB*) (TCGA., 2011; Tothill et al., 2008) as well as enrichment pathways defining extracellular matrix production and remodelling, cell adhesion, cell signalling and angiogenesis (Tothill et al., 2008) were characteristic for the mesenchymal (C1/Mes) subtype. This subtype also correlated with enrichment of the TGF-beta pathway, which is consistent with enrichment of the epithelial-mesenchymal transition (EMT) signatures in this subtype (Miow et al., 2014; Tan, Miow et al., 2013) partly accounting for the poor outcomes of this molecular subtype.

1.2.1 Characteristics and classification of the proliferative (C5/Stem-A) subtype

The proliferative C5/Stem-A subtype comprises 20% of HGSOC (Tothill et al., 2008) is associated with maintenance of an undifferentiated state in cancer cells (Helland et al., 2011) leading to poorer outcomes (Tothill et al., 2008). The proliferative subtype of HGSOC (TCGA., 2011), also known as the C5 subtype by Tothill et al (Tothill et al., 2008) and the Stem-A subtype by Tan et al (Tan, Miow et al., 2013), is characterized by high expression of developmental transcription factors such as *HMGA2*, *TCF7L1* and *SOX11*, low expression of ovarian tumour markers (*MUC1* and *MUC16*) and high expression of proliferation markers such as *MCM2* and *PCNA* (TCGA., 2011). Notably, Wnt and cadherin signalling pathway members were highly enriched in tumours from this molecular subtype (Tan, Miow et al., 2013a; Tothill et al., 2008). They are further defined by very low expression of immune cell markers (Tothill et al., 2008) (*CD45, CD2, CD3D, CD8A*).

1.2.2 Relevance of molecular subtyping in HGSOC and potential targets of therapy

The high-grade molecular subtypes were correlated with various clinicopathological parameters and showed significant differences in both progression free survival (PFS) and overall survival (OS) in a univariate analysis (Tothill et al., 2008) as well as in a multivariate cox regression analysis when taking into account other clinically relevant parameters (Tan, Miow et al., 2013) (Figure 1.4). Importantly, the Mesenchymal/C1 subtype and the C5/Stem-A subtype were linked to poorer outcomes compared to the other subtypes (Tan, Miow et al., 2013; Tothill et al., 2008) (Figure 1.4). When individual subtypes were interrogated, the Mes subtype had more advanced stage disease and higher incidence of metastasis whereas the Stem-A subtypes were more prominent in the older patients (Tan, Miow et al., 2013)

Although there is limited clinical evidence currently to suggest these transcriptomic subtypes can robustly predict therapeutic outcomes in patients with ovarian cancer, recent retrospective analysis suggests that bevacizumab had greater benefit in the poor prognosis molecular subtypes (Mesenchymal/C1 and proliferative/C5/Stem-A), compared to the other subtypes (Gourley et al., 2014; Kommoss et al., 2017). There have also been reports to suggest molecular subtypes with enrichment of certain genomic and transcriptomic pathways exhibit preferential responses to certain cytotoxic agents, such as platinum, paclitaxel, vincristine and vinorelbine (George et al., 2013; Miow et al., 2014; Tan et al., 2008; Tan, Miow et al., 2013). With novel therapeutic options for ovarian cancer in the horizon, the need to explore the clinical relevance of these transcriptomic subtypes and how it may inform personalized therapeutic strategies is of paramount importance.

1.2.3 Role of MYCN in proliferative/C5/ Stem-A subtype

This subtype of HGSOC was observed to activate a highly specific pathway involving *MYCN* amplification and over-expression associated with over-expression of MYCN targets including *Let-7* repressor *LIN28B,* and *HMGA2* amplification and over-expression (Helland et al., 2011) (figure 1.5). The deregulation of the MYCN pathway and downstream targets, involving multiple genes that contribute to stem cell renewal, was found to be altered in this particular molecular subtype of HGSOC (Helland et al., 2011).

Hitherto, the role of *MYCN* in HGSOC is still unclear. However, in neuroblastoma (NB), the most common extracranial solid tumor in infants and children, and accounts for 15% of cancer-related mortalities, largely due to metastatic disease progression, *MYCN* amplification is considered the most important oncogenic marker (Brodeur et al., 1984; Maris and Matthay, 1999). *MYCN* amplification occurs in up to 25% of primary neuroblastoma tumors and strongly correlates with advanced-stage disease and treatment failure (Brodeur et al., 1984; Seeger et al., 1985). Targeted inhibition of *MYCN* was observed to induce growth arrest and apoptosis in neuroblastoma cells (Kang et al., 2006; Nara et al., 2007) and may also be relevant for the proliferative/C5/Stem-A HGSOC subtype that is characterized by over-expression of the MYCN pathway. Therefore, therapeutic strategies that include inhibition of the transcription factor, MYCN, may prove efficacious for this molecular subtype.

1.2.4 Enrichment of Wnt pathway and chromatin modification in proliferative/C5/ Stem-A subtype

The proliferative/C5/Stem-A subtype has been demonstrated to characteristically display enrichment of the chromatin modification gene sets (Tan, Miow et al., 2013) (figure 1.5). In addition to deregulation of the MYCN pathway, the

proliferative/C5/Stem-A subtype were also found to upregulate Wnt/PCP pathway genes and cadherin signaling pathway members, including N-cadherin and P-cadherin (Asad et al., 2014; Tothill et al., 2008), all of which could be relevant for biomarker selection and therapeutic targeting.

Through interrogation of the Wnt pathway, Frizzled 7(FZD7), a receptor for Wnt signalling, was observed to be responsible for driving the aggressiveness in C5/Stem-A ovarian cancer by regulating cell proliferation, cell cycle progression, maintenance of the aggressive phenotype, and cell migration via CK1e-mediated non-canonical Wnt/PCP pathway (Asad et al., 2014). FZD7, is one of the FZD receptors that mediates both canonical and non-canonical Wnt signals (Zhang et al., 2013) (figure 1.5) and has been found to be an important regulator of pluripotency and the undifferentiated phenotype (Zhang et al., 2013) in embryonic stem (ES) cells. *FZD7* contributes to cell stemness in several types of normal cells and cancer cells (Mei et al., 2014; Song et al., 2006).

TWIST1, a transcription factor with a basic helix loop helix (bHLH) domain (Thisse et al., 1988), plays an important role in epithelial to mesenchymal transition (EMT) and cancer metastasis. It causes resistance to apoptosis (Ansieau et al., 2008; Maestro et al., 1999), chemoresistance (Cheng et al., 2007; Li et al., 2009), enrichment of cancer stem cell (CSC) populations (Mani et al., 2008; Vesuna et al., 2009), and cell invasiveness (Yang et al., 2004). Several groups have reported the association of *TWIST1* with many types of aggressive tumors, including breast, prostate (Yuen et al., 2007), and gastric cancers (Feng et al., 2009; Luo et al., 2008). In ovarian cancer, *TWIST1* over-expression has been reported to predict for poorer clinical outcomes (Hosono et al., 2007) and is associated with both the canonical and non-canonical Wnt pathways. In the canonical pathway, *TWIST1* acts as a downstream effector of *WNT3A* (Reinhold et al., 2006), *WNT1* (Howe et al., 2003) and β-catenin (Goodnough et al.,

2016) while in the non-canonical pathway, high expression of *TWIST1* correlates with the expression of FZD receptor 6 (FZD6), which is associated with poor survival in neuroblastoma (Cantilena et al., 2011).

The blocking of the FZD7/PCP pathway has been suggested through small molecule inhibitors of FZD7 (Fujii et al., 2007) or inhibition of porcupine, an enzyme that is essential for palmitoylation of wnt for secretion and subsequent binding of wnt to its receptors (Madan and Virshup, 2015), to demonstrate reduction of tumour-initiating cell populations in a range of tumour types (Gurney et al., 2012) and could potentially be exploited to improve outcomes of patients from this poor prognostic subtype.

1.2.5. Microtubules as a potential target in proliferative/C5/ Stem-A subtype

The proliferative/C5/Stem-A molecular subtype will be referred to as the C5/Stem-A subtype from here onwards. Gene expression analysis of the proliferative/C5/Stem-A subtype revealed enrichment of the microtubule/tubulin - related pathway compared to the non-C5/Stem-A subtype (Tan, Miow et al., 2013) suggesting targeting microtubule targeting agents (MTA) like vinca alkaloids and taxol may be efficacious in this subtype. Hence, not surprisingly, *in vitro* analysis using C5/Stem-A cell lines, revealed increased sensitivity of this subtype to inhibitors of microtubule polymerizing agents like vinorelbine and vincristine compared to non-C5/Stem-A cell lines (Tan, Miow et al., 2013). Strikingly, when cells were treated with vincristine, apoptotic activity was detected only in the C5/Stem-A cells with no apoptotic activity detected in non-C5/Stem-A cells (Tan, Miow et al., 2013). Although the underlying molecular mechanisms are still unclear and in vivo validation will need to be performed, this suggests that inhibition of tubulin polymerization could potentially be an effective avenue to target this poor prognostic subtype.

1.3 Preclinical models to evaluate novel cancer therapeutics

The utility of preclinical models to test hypotheses is central to cancer research. Increased understanding of the genomic landscape through massively parallel sequencing has revealed somatic mutations and molecular aberrations common to specific subsets of ovarian cancer, provided new prognostic and predictive markers and highlighted the potential therapeutic targets relevant for personalized medicine approaches. A frequently cited reason for failure of targeted therapies in clinical practice is the lack of adequate preclinical models that recapitulate the diversity and intra - tumoural heterogeneity often seen in patients (Whittle et al., 2015) and evaluating these new targets using established cell lines is limited by the poor correlation between responsiveness observed in cell lines versus that elicited in the patient (Johnson et al., 2001; Scott et al., 2013). Long-established human cell lines, and to a certain extent transgenic mouse models, often fail to reflect the key features of human malignancies and tend to not adequately predict therapeutic response in clinical settings.

1.3.1 Ovarian cancer cell lines as preclinical models

Whilst cancer cell lines serve as useful tools for understanding mechanistic drug interactions, there are significant limitations, because continual passage of these cell lines inherently leads to clonal selection and consequent loss of heterogeneity (Ellis and Fidler, 2010; Gillet et al., 2011). Furthermore, many of these cell lines have been cultured *in vitro* for decades and are more closely aligned to each other, regardless of tissue of origin, than the clinical samples to which they were intended to model (Domcke et al., 2013; Gillet et al., 2011). Indeed, their lack of predictive value is highlighted by the limited translational correlation between clinical results and *in vitro* and *in vivo* data obtained with cell lines (Johnson et al., 2001) making them poor surrogates of the source patients

and in part, contributing to the high failure rate of new oncology drugs (Bowtell et al., 2015; Whittle et al., 2015)

Despite multiple recent studies highlighting the inadequacies of the commonly used ovarian cancer cell lines as models of HGSOC (Beaufort et al., 2014; Domcke et al., 2013) much of the published literature in HGSOC still focuses heavily on these cell lines. As such, after the recent HHMT Ovarian Cancer Action 13th International Research Meeting which has been fostering communication between international ovarian cancer experts for more than 25 years, a consensus article was published outlining research priorities, strategies and recommendations for improving outcomes for women with HGSOC (Bowtell et al., 2015). Amongst them, it was strongly recommended that HGSOC research should be performed on extensively characterized cell lines that adequately reflect the disease and that detailed characteristics should be provided in all manuscripts (Bowtell et al., 2015). Furthermore, much emphasis was placed on improved approaches to generate primary cell cultures from patients (Ince et al., 2015; O Donnell et al., 2014) as more effective preclinical models as well as encouraging a concerted effort at creating large sets of genomically and functionally characterized HGSOC cell lines which are representative of key clinical mutational drivers (Bowtell et al., 2015). In addition, culture conditions such as three dimensional (3D) matrices and co-cultures of fibroblasts and mesothelial cells with malignant cells that more closely resemble the tumour microenvironment (Kenny et al., 2014; 2015) may enhance success in obtaining continuous, biologically relevant cell lines with stable biologic features. The use of *in vivo* models reflecting characteristics of human disease were also recommended.

1.3.2. Genetically engineered mouse models (GEMM)

GEMM provides a model in which to study the early pathogenesis of ovarian cancer. Considerable progress has been made in recent years in the development of mouse models of ovarian cancer. Currently, several GEMM that specifically direct transformation to the distal fallopian tube secretory epithelial cell (FTSECs) and histologically and molecularly reflect human HGSOC, including models with *Tp53* mutations and conditional inactivation of *Pten* and *Brca1* and *Brca2* (Kindelberger et al., 2007; Perets et al., 2013). The benefit of GEMMs is that the oncogenic mutation/s is often a mimic of those found in human tumours, and so can generate a phenotypically similar tumour (Baust et al., 2014; Perets et al., 2013). Importantly, these models recapitulate the development of the STIC lesions - ovarian cancer precursor lesions (Baust et al., 2014).

Disadvantages of GEMMs include the inability to recapitulate the heterogeneity of human tumours and the long latency for tumour development. Furthermore, GEMMs are expensive, require breeding strategies that are time consuming and have thus far not reported to have better predictive power for testing new therapies than cheaper models (Peterson and Houghton, 2004; Sausville and A. M. Burger, 2006). However, they are good models to study single oncogenic driver pathways such as *CCNE1* or *MYCN* amplification, which are relevant for certain subsets of HGSOC. Moreover, novel genome editing technologies, such as CRISPR-Cas9 techniques may simplify and improve the generation and utility of these models (Platt et al., 2014). The utility of these models will be further enhanced by derivation of resultant transplantable tumour cell lines in an immunocompetent, fully syngeneic environment that allows for well-controlled *in vitro* and *in vivo* experiments.

1.3.3. Patient derived organoids

Organotypic cultures derived from patient tumour tissues involves surgically resected or biopsy samples being established in 3D organoid *in vitro* cultures, which can then be passaged, preserved and used in *in vitro* and *in vivo* drug studies and have been shown to be useful pre-clinical models studies (Sachs and Clevers, 2014). Organoid cultures have been developed for cancers like pancreatic cancer, where mutations in *Kras* present in the patient tumour were continuously maintained in the resulting organoid (Boj et al., 2015) and also for colorectal tumours, which have been observed to maintain their expression profile in culture and is reflective of the original human tumour (Sato et al., 2011). Furthermore, therapeutic studies have been performed in cystic fibrosis and gastric cancer which have been encouraging (Dekkers et al., 2013). The model has also been used in ovarian cancer to support the association between chronic inflammation and ovarian cancer formation as well as established a novel *in vitro* model for studying of early events of ovarian cancer (Kwong et al., 2009). Therefore, organoids have thus been found to provide a useful and renewable resource for pre-clinical studies that are flexible and adaptable to high throughput screening for identification of novel therapeutic strategies (van de Wetering et al., 2015). In addition, the organoid cultures' relatively time efficient establishment allows data from *in vitro* culture studies to potentially be used in parallel with the patient from whom the organoids were derived to inform and guide personalised treatment strategies (Dekkers et al., 2013). Furthermore, the ability of organoids to enable establishment of early tumour stages at a higher success rate than cancer cell lines or patient derived xenograft (PDX) allows for a more comprehensive representation of the respective tumour spectrum. Nevertheless, there have not been any studies to date that have successfully demonstrated the ability of organoid cultures to predict a patient's response to therapy and certainly none in an ovarian cancer model.

Similarly to many other pre-clinical models, organoids as pure epithelial structures lack tumour stroma and vasculature and do not allow therapeutic interrogation that target

the host-tumour interactions (Sachs and Clevers, 2014). Tumour heterogeneity is also limited in organoids due to culture stress, and clonal selection (Sachs and Clevers, 2014). Collectively, organoid cultures are useful however, vigorous validation studies are required before organoid cultures can be utilized widely. Given time, a collection of validated human organoid lines that is representative of the respective cancer group could be used as preclinical models of cancer for therapeutic studies.

1.3.4. Patient derived xenografts

Patient derived xenografts (PDX) are renewable tumour resources generated from fresh human tumors engrafted into mice or cell suspensions derived from pleural or peritoneal fluid for injection into mice without prior *in vitro* exposure (Scott et al., 2013; Topp et al., 2014; Whittle et al., 2015) Considerable efforts have been employed to enhance the take rates of PDX and include implantation into the orthotopic site of the tumour, estrogen supplementation, utility of highly immunosuppressed mice (Quintana et al., 2008) as well as altering the microenvironment (Fleming et al., 2010). Early passage PDX tumours are often cryopreserved as viable samples to create a live biobank of early passage PDX tumour cells for further experimental studies (Figure 1.7(A). HGSOC PDX models have been shown to accurately reflect the histopathlogy, gene expression, molecular profiles and therapeutic response of the patient's tumor and are biologically stable (Scott et al., 2014; Topp et al., 2014; Weroha et al., 2014). In contrast, xenografts derived from cell lines reflect the *in vitro* culture system and do not recapitulate the heterogeneity and complexity of what is seen in clinical practice (Scott et al., 2013; Topp et al., 2014). Hence, the most clinically relevant utility of the PDX will stem from direct comparison of a patient's clinical response with that of the corresponding PDX to the same therapy (figure 1.7(B)

PDX have successfully been used to examine drug response and effects of targeted treatment (Scott et al., 2014). Although limited in number, PDX have also been shown to be useful for screening drug sensitivity that may be used to inform personalized strategies of patients, particularly in the relapsed setting (Scott et al., 2013). Several studies have indeed demonstrated high concordance between the clinical response with that of the corresponding xenograft model (Kolfschoten et al., 2000; Topp et al., 2014; Weroha et al., 2014). Moreover, Kolfschoten *et al* further expanded *in vitro* findings of drug response in the PDX model by identifying a correlation between glutathione reductase activity and efficacy of cytotoxic agents cisplatin and cyclophosphamide suggesting that glutathione-related enzymes could be useful as a predictor of drug sensitivity (Kolfschoten et al., 2000).

PDX models show increasing utility for identification of resistance mechanisms and for providing further insight into the mechanism of action of certain therapies (Kortmann et al., 2011; Press et al., 2008) (Figure 1.7(B). In HGSOC, prolonged exposure to a particular treatment, like cisplatin, is used to create drug – resistant models (Vidal et al., 2012). The utility of drug-resistant PDX models lie in its ability to identify therapies that may be effective in patients who harbor non-responsive tumours and to demonstrate mechanism of action of potential efficacious combination treatments (Vidal et al., 2012).

As previously mentioned, most OC patients present late in the course of the disease, following intra-peritoneal dissemination. OC PDX models generated intra-peritoneally have been used to investigate tumor progression and examine metastasis of human ovarian tumors (Vidal et al., 2012). Using this model, it was found that tumor spread in the mice reflected clinical patterns of metastasis with ascites formation and elevated CA-125 (Vidal et al., 2012). Each tumor's molecular phenotype has an impact on response to therapy. Hence, a detailed molecular annotation of each PDX is necessary for the evaluation of novel targeted therapies (Figure 1.7(B). However, numerous

published reports still lack detail regarding histologic subtype, molecular annotation and description of methods used to generate and maintain the PDX cohort (Scott et al., 2013)

Despite the usefulness of the PDX model, there are several limitations. The most notable is the use of immunocompromised mice which lack natural killer cells and both B and T lymphoid cells, precluding the use of these models for preclinical testing of immunotherapies. The loss of human stroma gradually post engraftment, replaced by murine stroma may be problematic, although the architecture of the donor derived stroma is often observed through repeated passaging if tumours are passaged as fragments. Humanized mouse models enabling co-engraftment of human bone marrow cells may circumvent some these issues but inherently introduces another layer of complexity (Garcia and Freitas, 2012). Furthermore, researchers need to be cognizant that the majority of PDX cohorts generated are biased towards more aggressive tumours. Indeed, the rate of engraftment by a PDX serves as a poor prognostic indicator (DeRose et al., 2013). Another consideration is the high likelihood for viral contamination in PDX cohorts and has been proven to be difficult to eradicate (Liu et al., 2010).

In summary, these studies prove that PDX models provide an avenue of renewable resource that recapitulates the diversity of HGSOC, maintains biological fidelity relative to the tumour of origin, is useful to optimize novel therapies and to evaluate mechanisms of drug resistance. Furthermore, the ability of PDXs to recapitulate treatment responses of parental tumours and its potential to be used as models to predict metastatic behavior makes them a valuable and important preclinical research tool.

1.4 Project Aims

1. **To determine the complexity of C5/Stem-A HGSOC biology through characterization of a clinically relevant cohort of C5/ Stem-A PDX**

Little is known about the biology of the C5/Stem-A/proliferative subtype of HGSOC other than the associated poor prognosis. Pre-clinical models currently available for exploration of HGSOC are suboptimal. The first aim of the project was to develop clinically relevant C5/Stem-A PDX and to undertake in-depth molecular characterization as a tool to interrogate and enhance our understanding of this subtype. By generating a cohort of C5/Stem-A HGSOC PDX we were not only able to generate a renewable resource to enable future exploration but the PDX could also serve as discovery tools for novel compounds and biomarkers of therapeutic response.

2. **To test efficacy of novel candidate inhibitors of C5/Stem-A HGSOC in the established PDX**

   The second aim of this project was to identify candidate inhibitors for this specific subtype due to the absence of therapeutic strategies available for this poor prognostic subtype. Common *in vivo* models used to test novel compounds employ cell line xenografts that often do not correlate with clinical trial results in patients. We aimed to use the molecularly characterized PDX generated in aim one to test novel therapies. With the use of PDX, tissue can be obtained easily during the course of treatment. This would enable biomarker exploration through pharmacodynamic analysis and interrogation for markers of response or resistance to the novel agent in light of their individual molecular aberrations.

3. **To understand biology relevant for response or resistance of C5/Stem-A HGSOC to specific therapy**

   The third aim of the project was to understand the underlying mechanisms of response and resistance to the novel therapeutic inhibitors used in this subtype.

Through exploration of these underlying mechanisms, we could attempt to identify vulnerabilities in this molecular subtype for targeting through novel combination strategies. By drawing on expertise from Singapore, where I spent two years of my PhD at the Cancer Science Institute, Singapore under the supervision of Dr. Ruby Huang on secondment from my parent institution, relevant therapeutic combinations were further explored.

4. **To identify the most promising compound for C5/Stem-A HGSOC to inform a clinical trial**

   Except for *BRCA1/2* mutations, there are currently no approved biomarkers of interest for which to target therapy in ovarian cancer. However, recent retrospective translational studies have suggested that the molecular subtypes may be clinically relevant. As a proof-of-concept, by using the C5/Stem-A subtype as a biomarker, we aim to provide sufficient preclinical data to inform a prospectively selected clinical trial. This bench-to-bedside trial will spawn a pipeline of other similar trials for the other molecular subtypes.

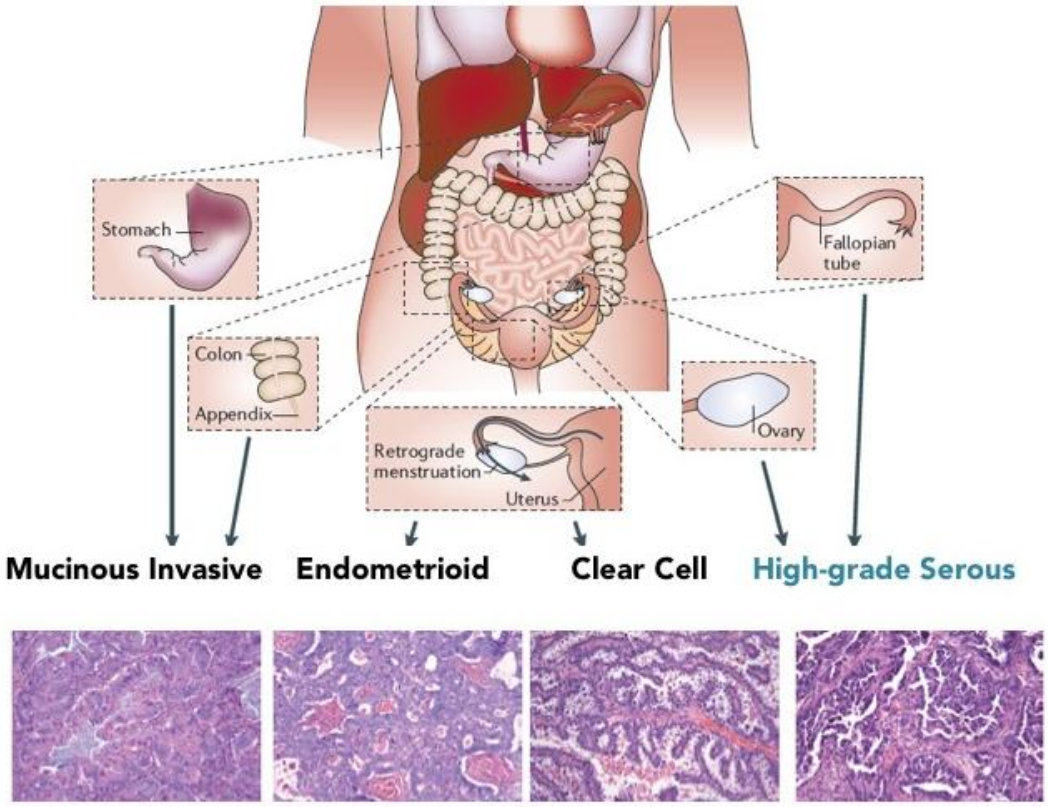

Figure 1.1: Diverse origins of ovarian cancer. Ovarian cancers, despite collectively referred to as a single entity, do not have the same cell of origin. The majority of mucinous ovarian cancers are metastases to the ovary, often from the gastrointestinal tract. Endometrioid and clear cell ovarian cancers are largely derived from endometriosis which in turn is associated with retrograde menstruation. High grade serous ovarian cancers have been shown to originate from the surface of the ovary and/or fallopian tube. Figure adapted from Vaughan et al Nature Reviews Cancer 2011

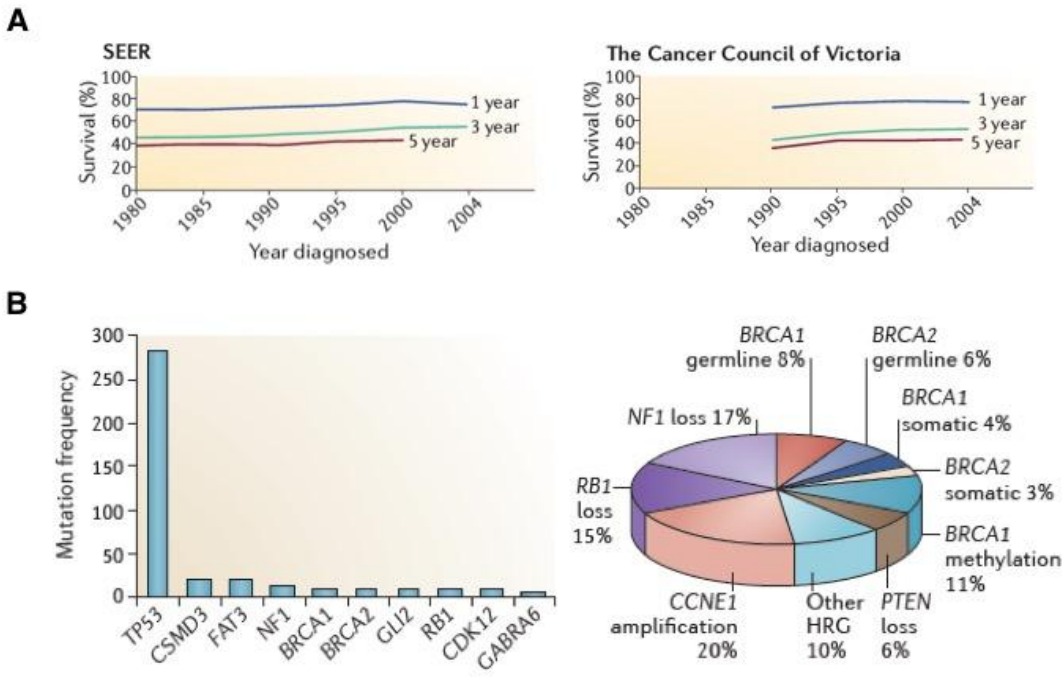

Figure 1.2: Clinical outcomes and molecular features of high grade ovarian cancer. **(A)** One-, three- and five-year survival post-diagnosis of ovarian cancer patients over the past 20 years. Data from (Left panel: Surveillance, Epidemiology and End Results (SEER, 1980–2004); (Right panel: The Cancer Council of Victoria, Victoria, Australia (1990–2004). **(B) (Left panel):** *TP53* mutations are ubiquitous in HGSOC (Ahmed et al., 2010) but somatic point mutations in other driver genes occur at a low frequency. The data shown here were taken from 300 HGSOC tumours in The Cancer Genome Atlas database (TCGA., 2011). **(Right panel):** The frequency of key driver mutations in HGSOC (TCGA., 2011). Approximately half of all HGSOCs show mutational and functional evidence of putative homologous recombination (HR) deficiency, Cyclin E1 (*CCNE1*) amplification represents an important subset of HR-intact tumours, and recent data have increased the proportion of tumours with *NF1* (neurofibromin 1) and *RB1* loss. Figure adapted from Bowtell et al Nature Reviews Cancer 2015 and Vaughan et al Nature Reviews Cancer 2011

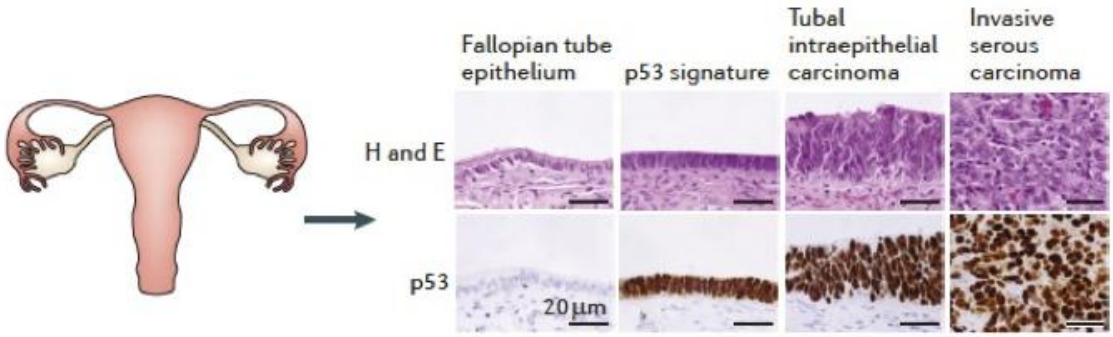

Figure 1.3: Origins of HGSOC. Evolution of the different stages of development of HGSOC in the human fallopian tube marked by p53 staining and cellular morphology. A large proportion of HGSOC is thought to arise from secretory epithelial cells of the fallopian tube, which express the marker, PAX8. p53 staining marks clonal expansion of cells (p53 signatures) in the absence of morphological transformation of the fallopian tube epithelium. Piling up of cells and loss of epithelial architecture occurs in early lesions (tubal intraepithelial carcinoma (TIC)), finally leading to invasive cancer. Figure adapted from Bowtell et al Nature Reviews Cancer 2015

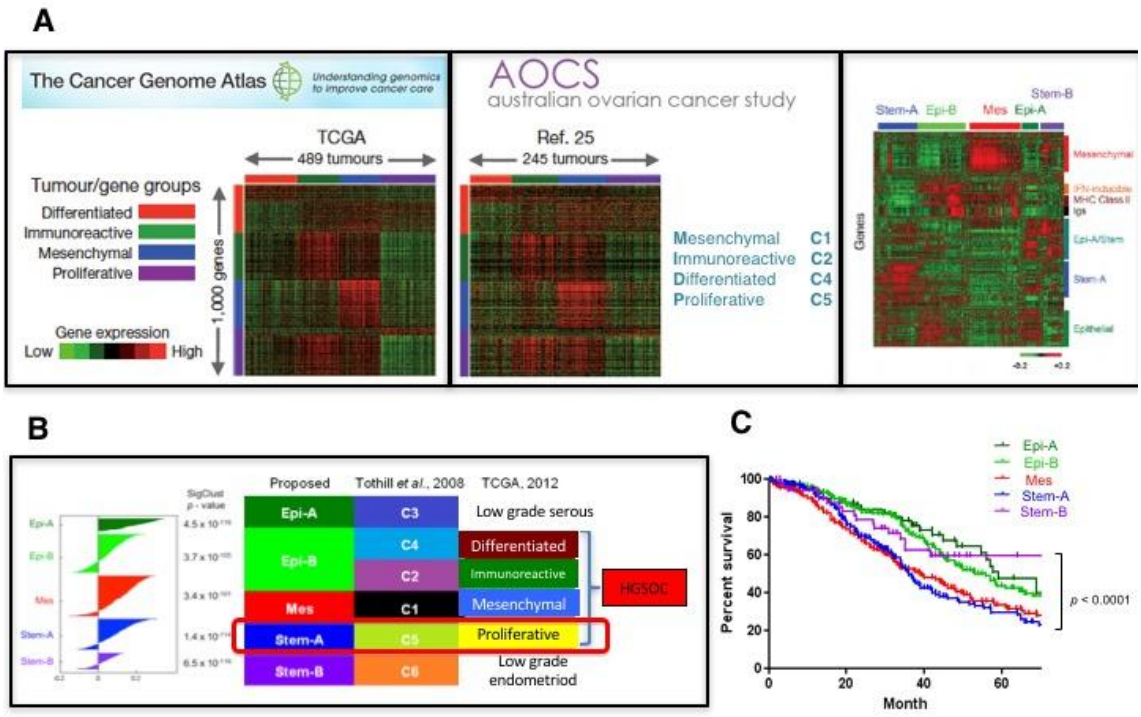

Figure 1.4: Molecular subtypes in HGSOC. (A) HGSOC can be divided into four molecular subtypes based on gene expression and are reproducible and validated independently. Data shown are from (Left panel): Cancer Genome Atlas Reseach Network (n=489 HGSOC samples) (TCGA., 2011); (Middle panel): Australian Ovarian Cancer Study (n=245 HGSOC and high grade endometriod samples); (Right panel): Cancer Science Institute, Singapore (n=1429 HGSOC and high grade endometriod samples). **(B)** Schematic diagram shows concordant results when all three independent datasets were compared. (C) Survival outcomes of the independent molecular subtypes shows Stem-A and Mes subtypes have the poorest prognosis. Figure adapted from Cancer Genome Atlas Reseach Network Nature 2011, Tothill et al, Clin Canc Res 2008, Tan et al, EMBO Mol Med 2013

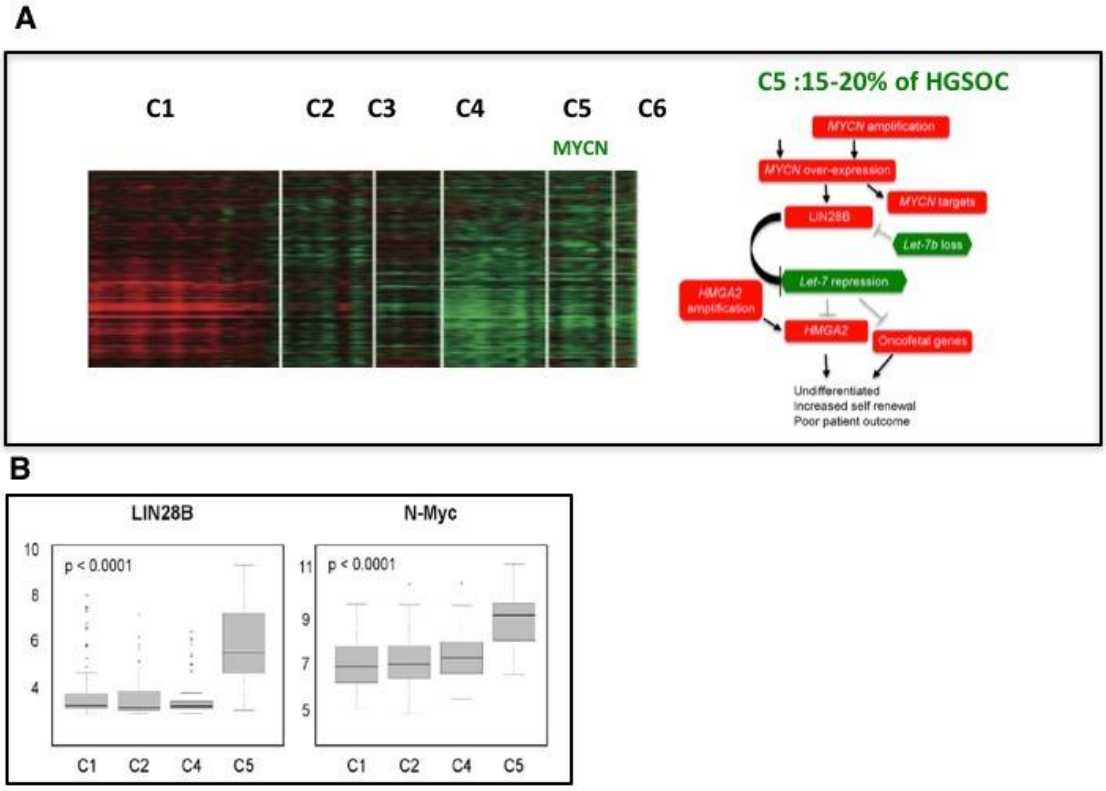

Figure 1.5: MYCN pathway deregulation in C5/Stem-A HGSOC. The C5/Stem-A tumours consist of 15-20% HGSOC and are characterized by highly specific signaling events involving amplification and overexpression of *MYCN* which influences a regulatory loop involving *LIN28B*, *Let-7* and *HMGA2* in C5 high-grade serous tumours. (B) Boxplots depict differential expression of *LIN28B* and *MYCN* in different molecular subtypes of serous ovarian cancers from the Australian Ovarian Cancer Study dataset demonstrating significant upregulation of *MYCN* and *LIN28B* in C5 HGSOC. Figure adapted from Tothill et al Clinc Canc Res 2008 and Helland et al, PLoS One 2011

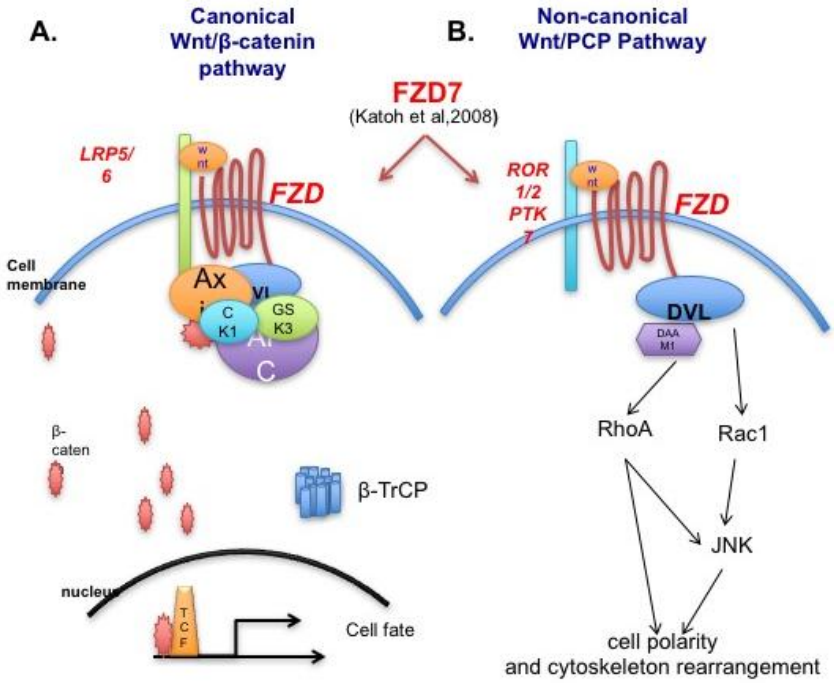

Figure 1.6: FZD7 regulates both canonical wnt and non-canonical wnt pathway.

FZD7 can transduce both **(A)** canonical and **(B)** non-canonical WNT signaling pathway and orchestrates cellular proliferation, epithelialization, migration and tissue movement in a context-dependent manner during embryogenesis, adult-tissue homeostasis and carcinogenesis. Figure adapted from Clevers et al, Cell 2011 and Raymond et al 2005

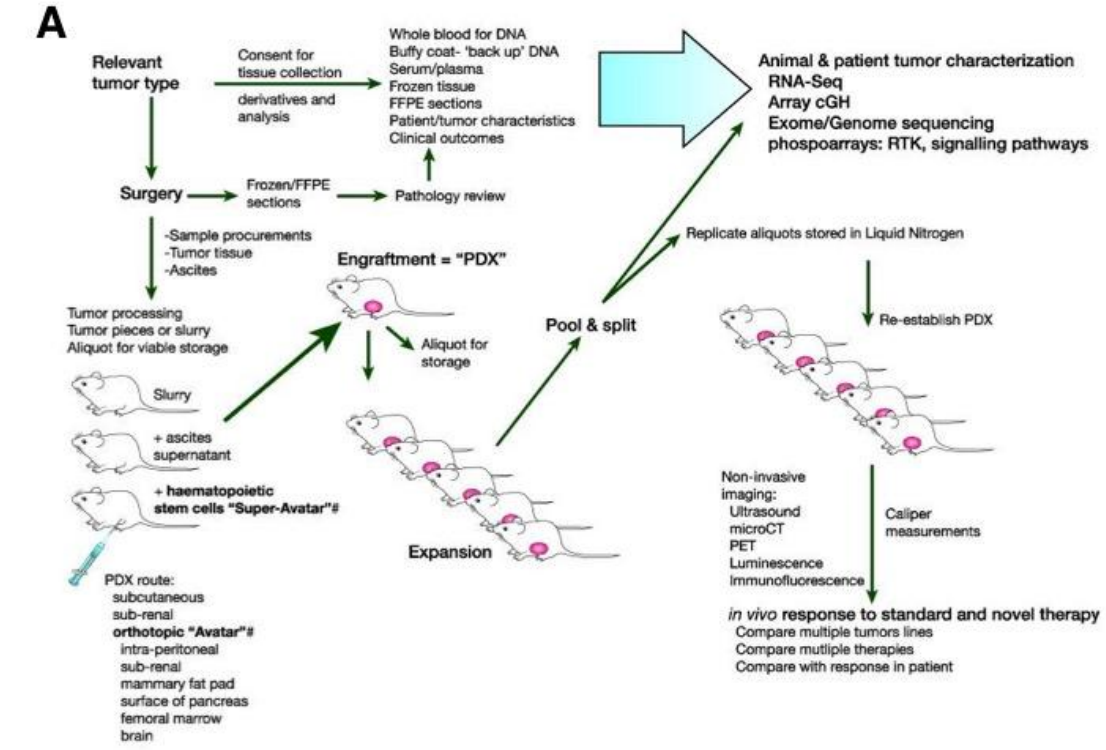
A
Relevant tumor type
Consent for tissue collection
derivatives and analysis
Whole blood for DNA
Buffy coat- 'back up' DNA
Serum/plasma
Frozen tissue
FFPE sections
Patient/tumor characteristics
Clinical outcomes
Animal & patient tumor characterization
RNA-Seq
Array cGH
Exome/Genome sequencing
phospoarrays: RTK, signalling pathways
Surgery
Frozen/FFPE sections
Pathology review
-Sample procurements
-Tumor tissue
-Ascites
Engraftment = "PDX"
Replicate aliquots stored in Liquid Nitrogen
Tumor processing
Tumor pieces or slurry
Aliquot for viable storage
Aliquot for storage
Pool & split
Re-establish PDX
Slurry
+ ascites supernatant
+ haematopoietic stem cells "Super-Avatar"#
Expansion
Non-invasive imaging:
Ultrasound
microCT
PET
Luminescence
Immunofluorescence
Caliper measurements
PDX route:
subcutaneous
sub-renal
orthotopic "Avatar"#
intra-peritoneal
sub-renal
mammary fat pad
surface of pancreas
femoral marrow
brain
in vivo response to standard and novel therapy
Compare multiple tumors lines
Compare mutliple therapies
Compare with response in patient

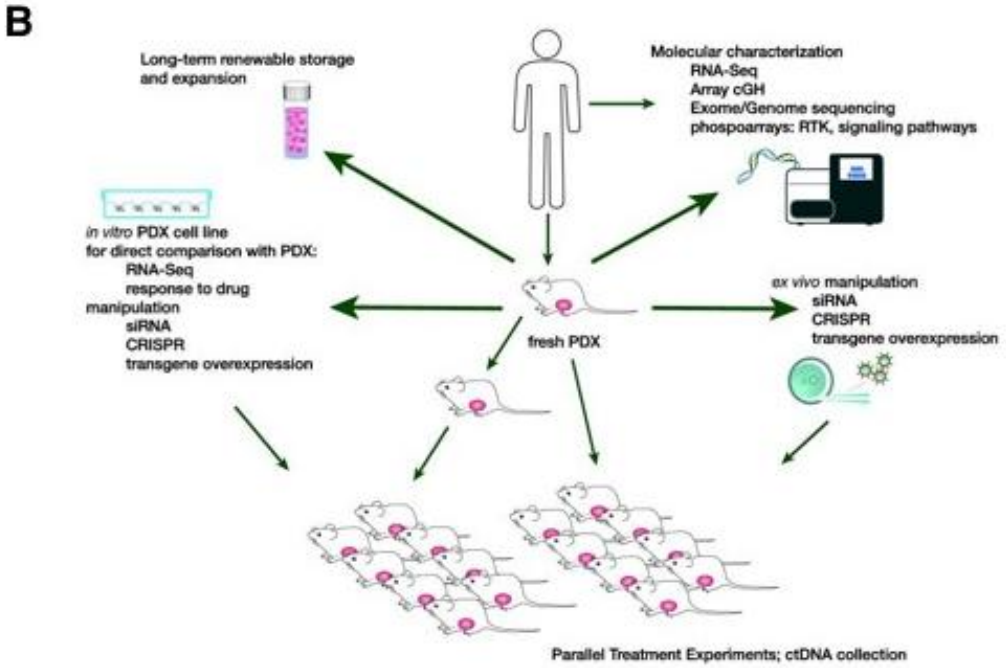
B
Long-term renewable storage and expansion
Molecular characterization
RNA-Seq
Array cGH
Exome/Genome sequencing
phospoarrays: RTK, signaling pathways
in vitro PDX cell line
for direct comparison with PDX:
RNA-Seq
response to drug
manipulation
siRNA
CRISPR
transgene overexpression
fresh PDX
ex vivo manipulation
siRNA
CRISPR
transgene overexpression
Parallel Treatment Experiments; ctDNA collection

Figure 1.7: Generation and utility of the PDX model. (A) The transplanting of fresh, unmanipulated patient tumor at the time of biopsy or surgery into mice allows the generation of stable patient-derived xenografts (PDX) with considerable biological fidelity to the primary human cancer. Detailed functional and molecular analysis can be performed and compared with the primary human sample and with patient outcome. A renewable resource can be generated by freezing viable tumour material of minced tissue slurry. Once PDX have been generated and annotated, additional derivatives can be generated, which further increase the utility of the original model, adding to its functionality. **(B)** *In vivo* response to conventional and novel therapy can be performed in parallel for multiple drugs or sequentially, in order to drive drug resistance, as occurs in the clinic. Generation of a cell line, which once validated to be molecularly and biological similar to the baseline tumor and PDX, can be manipulated using techniques such as siRNA, CRISPR or transgene over-expression. Similar techniques may be applied directly to fresh PDX material using a short *ex vivo* process (24–48 hours *in vitro* culture) while parallel treatment experiments can incorporate surveillance for markers of drug resistance using ctDNA analysis. Figure adapted from Lodhia et al Bichim Biophys Acta 2015

Chapter II:

Materials and Methods

Materials and Methods

Materials and methods for work performed at Walter and Eliza Hall Institute, Victoria, Australia

2.1 Human tissue

2.1.1 Clinical sample collection and processing

Samples were collected fresh in RPMI media from chemotherapy naïve patients with suspected high grade EOC on frozen section during primary debulking surgery at the Royal Women's Hospital. All patients were enrolled in the Australian Ovarian Cancer Study. Written informed consent was obtained from all patients prior to inclusion in the study. The Australian Ovarian Cancer Study was approved by the Human Research Ethics Committees at the Peter MacCallum Cancer Centre, Queensland Institute of Medical Research, University of Melbourne and all participating hospitals. Additional approval was obtained from the Human Research Ethics Committees at the Royal Women's Hospital and the Walter and Eliza Hall Institute. The histologic diagnoses of all patients from whom samples were collected, were subsequently verified by an expert panel of gynaecological histopathologists (Royal Women's Hospital or MAYO Clinic). Clinical follow-up of patient outcome was obtained via the CONTRO-engined gemma database, Royal Women's Hospital or by the MAYO Clinic. Only samples verified as HGSOC were expanded as PDX and analysed. Samples obtained were divided into several parts and processed immediately. A portion of tumour material was transplanted into at least four mice while remaining tissue were further divided into three portions and subsequently 1) fixed in 10% formalin at room temperature for 24 – 72 h depending on tissue size before paraffin embedding by standard histology procedures, 2) minced and viably frozen in 10% DMSO in liquid nitrogen ensuring continuation of the resource and 3) frozen for use at a later time.

2.1.2 Immunohistochemistry

Automated staining was performed with a Ventana BenchMark Ultra (Roche Diagnostics, USA). The following clones from Ventana were used: for WT1 (6F-H2); PAX8 (MRQ-50), ER (SP1); PR (1E2); Ki67 (30-9); p53 (DO-7) and Anti-Pan Keratin (AE1/AE3/PCK26). All first generation (T1) xenografts (human tumour tissue transplanted into a mouse, arising as a xenograft), were screened with IHC for human CD45 (RP2.18, Ventana), in order to exclude occasional donor-derived hematologic malignancy (transplantable). Sections stained for Bcl-2 were scored by two investigators blinded as to HG-SOC/PDX number. Consecutive high-powered fields and 200 consecutive tumor cells were assessed for staining. Percent of strong (+++), moderate (++), low (+) and absent staining was documented ((+++% x 3) + (++% x 2) + (+% x 1) + (0% x 0), out of a possible total score of 300).

2.2 *in vivo* mouse studies

2.2.1 Generation of patient-derived xenografts (PDX).

Immuno-compromised nonobese diabetic–severe combined immunodeficient, interleukin -2 receptor-γ-null (NOD-SCID-IL-2rγ) mice (4-8 wk old; WEHI animal breeding facility) were used for animal studies with approval from the Melbourne Health Animal Ethics Committee and the WEHI Animal Ethics Committee. Under anaesthesia, a fragment of fresh tumor was placed subcutaneously (1 - 3 mm^3) or via the intra-ovarian bursal (< 1 mm^3) approach. Tumor growth was monitored by measuring 2 perpendicular axes using calipers once weekly and tumor volume calculated as $\pi/6$ x [larger diameter x smaller $diameter^2$]). The mouse was sacrificed once the tumor volume reached 0.7 cm^3. The tumor was harvested and prepared as above for analysis as well as being transplanted into new recipient mice to generate serial propagation. Tumor material was minced and viably frozen in 10% DMSO in liquid nitrogen ensuring

continuation of the resource.

2.2.2 *in vivo* drug studies

Recipient mice bearing tumors ~0.2 cm^3 in size (0.18-0.3 cm^3) were randomly assigned to weekly treatment with vehicle or study drug using individual dose/titration and timing studies in NOD-SCID-IL-2rγ mice based on toxicity of the study drug. For all in vivo drug studies, tumor growth was monitored as above 2-3 x weekly and tumor volume calculated. The mouse was sacrificed once the tumor volume reached 0.7 cm^3. Mice were bled at cull for hematologic analysis if unwell or for storage of plasma at -80°C.

In all *in vivo* drug studies, time to Progressive disease (PD) was defined as the time (in days) from beginning of treatment to an increase in average tumor volume (for that treatment group) of >20% from the nadir (taken as the smallest average tumor volume recorded since treatment started or 0.2 cm^3 if nadir was < 0.2 cm^3 as lesions smaller than this are difficult to measure with accuracy). Time to Harvest (TTH) was defined as the time (in days) from the beginning of treatment to day of harvest at 0.7 cm^3 and the median TTH was calculated and plotted using Kaplan-Meier curves (Prism version 7)

2.2.2.1 *in vivo* cisplatin drug studies

Recipient mice bearing tumors ~0.2 cm^3 in size (0.18-0.3 cm^3) were randomly assigned to weekly treatment with vehicle or cisplatin (4 mg/kg) on days 1, 8 and 18. This regimen was chosen based on dose titration/timing studies in tumor-bearing NOD-SCID-IL-2rγ mice. One hundred days was chosen as a conservative measure to differentiate between cisplatin sensitivity versus resistance for PDX, as PD usually occurred around 50 d or earlier, or in contrast, sustained remission was also observed (>200 d). The six-month timeline used to determine platinum sensitivity in the clinic was not reasonable, as that represents one quarter of a mouse's lifetime, and around one

third of the life-time of an immuno-compromised mouse.

2.2.2.2 *in vivo* M606 drug studies

Recipient mice bearing tumors ~0.2 cm^3 in size (0.18-0.3 cm^3) from relevant PDX were randomly assigned to treatment with vehicle (DMSO) or M606 diluted in DMSO (40mg/kg) via the peritoneum daily (Monday- Friday). This regimen was chosen based on efficacy data from our collaborators as well as dose titration/timing studies in tumor-bearing NOD-SCID-IL-2rγ mice.

2.2.2.3 *in vivo* JQ1 drug studies

Recipient mice bearing tumors ~0.2 cm^3 in size (0.18-0.3 cm^3) from relevant PDX were randomly assigned to treatment with vehicle (DMSO) or JQ1 diluted in DMSO (50mg/kg) via oral gavage daily. This regimen was chosen based on efficacy data as well as dose titration/timing studies in tumor-bearing NOD-SCID-IL-2rγ mice from our collaborators.

2.2.2.4 *in vivo* I-BET-762 drug studies

Recipient mice bearing tumors ~0.2 cm^3 in size (0.18-0.3 cm^3) from relevant PDX were randomly assigned to treatment with vehicle (DMSO + cyclodextrin) or I-BET-762 (25mg/kg) via oral gavage every alternate day. This regimen was chosen based on dose titration/timing studies in non-tumour bearing and tumor-bearing NOD-SCID-IL-2rγ mice.

2.2.2.5 *in vivo* vinorelbine drug studies

Recipient mice bearing tumors ~0.2 cm^3 in size (0.18-0.3 cm^3) from relevant PDX were randomly assigned to treatment with vehicle or vinorelbine (15mg/kg) on days 1, 8 and 18 intravenously via the tail vein. This regimen was chosen based on dose titration/timing studies in tumor-bearing NOD-SCID-IL-2rγ mice.

2.2.2.6 *in vivo* paclitaxel drug studies

Recipient mice bearing tumors ~0.2 cm^3 in size (0.18-0.3 cm^3) from relevant PDX were randomly assigned to treatment with vehicle or paclitaxel (25mg/kg) twice a week for 3 weeks intraperitoneally. This regimen was chosen based on dose titration/timing studies in tumor-bearing NOD-SCID-IL-2rγ mice

2.2.3 Mutational analysis

The BROCA panel identifies all classes of mutations, including single-base substitutions, small insertions and deletions, and large gene rearrangements (Walsh et al., 2011). Sequence alignment and variant calling were performed against the reference human genome (UCSC hg19) as previously described (Walsh et al., 2011). Each variant was annotated with respect to gene location and predicted function in HGVS nomenclature. Deletions and duplications of exons were detected by a combination of depth of coverage and split read analysis. Missense variants without clear deleterious impact were not routinely included. For somatic large gene rearrangements or copy number variations (CNVs), any intragenic deletion or duplication was considered deleterious. Homozygous whole gene deletions were considered deleterious; hemizygous whole gene deletions (i.e., loss of heterozygosity (LOH)) were excluded. All sequence variants were confirmed with Sanger sequencing. Germline analysis of *BRCA1/2* mutations identified in baseline HGSOC (WEHI#91, WEHI#95) was performed in germline DNA with confirmatory Sanger Sequencing yielding concordant results.

2.3 General molecular biology

2.3.1 Isolation, quantitation and analysis of RNA

RNA was extracted from fresh frozen tumour material using the Qiagen AllPrep DNA/RNA/protein mini kit (Qiagen, Hilden, Germany). Total RNA was precipitated in RNA free water as per manifacturer' s guidelines.

2.3.2 Complementary DNA (cDNA) synthesis and RT-PCR

Total RNA was extracted from snap frozen tumor material and converted to cDNA and analysed in qPCR 15 uL reaction volume using primers for *MYCN, LIN28B, LIN28A, HMGA2, CCNE1, HPRT* and, as an endogenous normalization control, *ACTB (β-actin)* with SYBR-green reagent (Qiagen) and assessed on an ABI-PRISM 7900 thermal cycler (both from Applied Biosystems). Data analyses were performed by the comparative threshold cycle method (Narita et al., 2003). For each baseline HGSOC, one aliquot of RNA was generated and used in 3-7 independent experiments. The positive control for the MYCN pathway was the CH1 cell line, which has increased expression of MYCN, although not copy number gain (Helland et al., 2011). The positive control for *CCNE1* overexpression was the OVCAR3 cell line, which has high-level amplification of *CCNE1* (log2 CN ratio >2 by qRT-PCR and SNP microarray) (Etemadmoghadam et al., 2010). Primers were purchased from SAbiosciences (Qiagen), including five housekeeping genes *B2M, HPRT1, RPL13A, GAPDH* and *ACTB* that were used for normalization. For all RT-qPCR data, the mRNA expression level of each gene of interest was normalized to the expression of housekeeping genes and presented either as average $2^{-\Delta Ct}$, or as average fold change ($2^{-\Delta\Delta Ct}$) with respect to control, from at least two biological replicates of the sample. Primers used are detailed below

List of primers used for experiments at Walter and Eliza Hall Institute, Australia

qRT-PCR was performed using the following forward and reverse primers:

Gene	sense (5' – 3')	antisense (5' – 3')
MYCN	CACAAGGCCCTCAGTACCTC	ACCACGTCGATTTCTTCCTC
LIN28B	TCTTCCAAAGGCCTTGAGTC	ATGATGATCAAGGCCACCAC
LIN28	AGGAAAGAGCATGCAGAAGC	GCTACCATATGGCTGATGCTC
HMGA2	ACTTCAGCCCAGGGACAAC	CTTGTTTTTGCTGCCTTTGG
CCNE1	GAAATGGCCAAAATCGACAG	TCTTTGTCAGGTGTGGGGA
HPRT1	GTTATGGCGACCCGCAG	ACCCTTTCCAAATCCTCAGC
ACTB	GCACAGAGCCTCGCCTT	GTTGTCGACGACGAGCG

2.3.3 Protein isolation and western blot

Whole-cell lysates were prepared using 2D lysis buffer containing protease inhibitor PMSF, and protein concentrations were assessed by Pierce Coomassie (Bradford) Protein Assay (Thermo Fisher Scientific). Equal protein loads of 8ug were resolved on precast 8% to 16% Bis-Tris gels (Bio-Rad) under reducing conditions. Protein was transferred to PVDF membranes using Bio-Rad criterion wet transfer method (Bio-Rad), then probed with antibodies against Cyclin E (Clone HE12; Santa Cruz), MYCN (B8.4.B; Santa Cruz), LIN28B (#4196; cell signaling), BCL2 (clone: 100; WEHI) and β-actin (clone AC-74, Sigma; also used as a loading control). Blots were visualized by enhanced chemi-luminescence (Amersham ECL Prime, GE Healthcare Life Sciences) according to the manufacturer's instructions.

Materials and Methods for work performed at Cancer Science Institute, Singapore

2.4 Human cell lines

2.4.1 Cell culture and tissue culture maintenance

21 EOC cell lines from the SGOCL library (Huang et al., 2013) were used in this study. The cell lines were previously characterized into five molecular phenotypes (Huang et al., 2013) and were maintained in their respective culture media.

EOC cell lines used with their respective molecular subtypes and culture media

Cell lines	Molecular subtypes	Media
A1847	Mesenchymal	RPMI 1640, 10% FBS, 10 µg/ml insulin
A2780	C5/Stem-A	RPMI 1640, 10% FBS
Caov3	Epi- B	DMEM, 10% FBS
CH1	C5/Stem-A	DMEM, 10% FBS
FUOV1	C5/Stem-A	DMEM/F12 (1:1), 10% FBS
Hey	Mesenchymal	RPMI 1640, 10% FBS
JHOS2	Epi- A	DMEM/F12 (1:1), 10% FBS, 0.1 mM NEAA
JHOS3	Epi- B	DMEM/F12 (1:1), 10% FBS, 0.1 mM NEAA
JHOS4	C5/Stem-A	DMEM/F12 (1:1), 10% FBS, 0.1 mM NEAA
OAW42	C5/Stem-A	DMEM, 10% FBS, 0.7 µg/ml insulin
OV17R	C5/Stem-A	DMEM/F12 (1:1), 5% FBS, 0.4 µg/ml hyrocortisone, 10 µg/ml insulin
OVCA432	Epi- B	DMEM, 10% FBS
OVCA433	Epi- A	DMEM, 10% FBS
OVCAR3	C5/Stem-A	RPMI 1640, 20% FBS, 10 µg/ml insulin
OVCAR5	Stem-B	RPMI 1640, 10% FBS, 10 µg/ml insulin
OVK18	C5/Stem-A	DMEM, 10% FBS
PEO1	Epi- A	RPMI 1640, 10% FBS
SKOV3	Mesenchymal	DMEM, 10% FBS
TOV112D	C5/Stem-A	MCDB105/M199 (1:1), 10% FBS
PA1	C5/Stem-A	DMEM, 10% FBS
COV318	C5/Stem-A	DMEM, 10% FBS

2.4.2 Complementary DNA (cDNA) synthesis and RT-PCR

Total RNA of EOC cell lines and EOC tumour samples was extracted with RNeasy mini kit or miRNeasy mini kit (Qiagen) according to manufacturer's protocol. For gene expression qPCR, 500ng mRNA was reverse-transcribed to cDNA using RT^2 first strand kit (SAbiosciences, Qiagen) and subsequently mixed with SYBR green master mix (SAbiosciences, Qiagen) for qPCR analysis by ABI 7900HT (Life Technologies). Thermal cycling conditions were set as: 1 cycle of 95ºC incubation for 10 minutes for initial DNA denaturation and the activation of HotStart

DNA Taq Polymerase, followed by 40 cycles of 95ºC for 15 seconds (denaturation) and 60ºC for 1 minute (primer annealing and extension). Primers were purchased from SAbiosciences (Qiagen), including five housekeeping genes *B2M, HPRT1, RPL13A, GAPDH* and *ACTB* that were used for normalization. Details of the primers are listed in below. For all RT-qPCR data, the mRNA expression level of each gene of interest was normalized to the expression of housekeeping genes and presented either as average $2^{-\Delta Ct}$, or as average fold change ($2^{-\Delta\Delta Ct}$) with respect to control, from at least two biological replicates of the sample. Primers used are detailed below:

Commercially available primers (SAbiosciences, Qiagen)

Target	**Cat. No.**	**Target**	**Cat. No.**
ACTB	PPH00073E	FZD7	PPH02420A
B2M	PPH01094E	TWIST1	PPH02132A
GAPDH	PPH00150E	RPL13A	PPH01020B
HPRT1	PPH01018C		

Other primers:

BCL2	CTGCACCTGACGCCCTTCACC	CACATGACCCCACCGAACTCAAAGA

2.4.3 Protein isolation and western blot analysis

Cell lysates were harvested by RIPA buffer (#R0278, Sigma-Aldrich) added with protease inhibitor (#539134) and phosphatase (#524625) inhibitor cocktails from Calbiochem, Millipore. BCA assay (#23225, Thermo Scientific) was performed for protein quantification. Lysates were resolved by standard reducing SDS-PAGE, transferred on PVDF membranes, blocked with 5% skim milk (Nacalai Tesque) and immunoblotted with specific antibodies: anti-BRD4 (Clone:#13440; cell signaling), anti-NAT10 (Clone:133651-AP; proteintech), anti-alpha tubulin (clone: DM1A; sigma Aldrich), anti-acetylated tubulin (Clone:611B1; Sigma Aldrich) and anti-TWIST1 (clone:#sc-81417; Santa Cruz). Infrared dye-conjugated secondary antibodies from Li-COR Biosciences were used at 1:10000 dilution: IRDye 800CW goat anti-mouse or anti-rabbit (#926-32210, #926-32211), IRDye 680LT goat anti-mouse or anti-rabbit (#926-

68020, #926-68021) and IRDye 800CW donkey anti-goat (#926-32214). Blots were scanned using the Odyssey Infrared Imaging System (Li-COR). Images were converted to gray scale.

2.4.4 Knockdown of *NAT10* by siRNA for cell proliferation assay

Dharmacon SMART pool siGENOME siRNA (sequences not available) and Dharmacon SMART pool ON-TARGETplus siRNA (OTP) formats (Thermo Fisher Scientific, Lafayette, CO) were used to knockdown *NAT10* in ovarian cell lines. PA-1, COV318, CH1 cells were used as representative cell lines for the C5/Stem-A subtype. SKOV3 and HEY cells were used as representative non-C5/Stem-A cell lines. Optimization experiments for each cell line was performed using four different transfection reagents (DF1, DF2, DF3, DF4). Cells were reverse-transfected with each individual siRNA per well in a 96-well format in the following conditions: PA-1, 1200 cells with 0.22 ml of DF2 (T-2002); COV318, 4000 cells with 0.15ml of DF4; SKOV-3, 2500 cells with 0.12 ml of DF2 (T-2002); HEY, 1000 cells with 0.08 ml of DF4 (T-2004); CH1, 1800 cells with 0.17 ml of DF4 (T-2004). We used two negative controls for Dharmacon SMART pool siGENOME siRNA transfection (#D-001206-13-20 and #D-001206-14-20), and one negative control for Dharmacon SMART pool ON-TARGETplus siRNA transfection (#D-001810-10-20). Assays were performed in quadruplicate. After 72-h incubation, an MTS assay was used to measure cell growth using a CellTiter 96 AQueous Non-Radioactive Cell Proliferation Assay following the manufacturer's recommendations (#G5430, Promega, Madison, WI).

2.4.5 Generation of stable *TWIST1* overexpression and *FZD7* knockdown cell lines

For generation of stable *TWIST1* overexpressed and *FZD7* knockdown clones, *TWIST1* lentiviral plasmids encoding full-length wild type *TWIST1* with a pLenti-GIII-CMV-GFP-2A-Puro backbone (ABM) and shRNA clones (#TRCN0000020541 and #TRCN0000020542, Sigma-Aldrich) were selected with pLKO.1-puro Luciferase shRNA plasmid (#SHC007, Sigma-Aldrich) as a control while shRNA plasmids (pLKO.1) for *FZD7* from Sigma Aldrich (shFZD7-1 #**Clone ID:** NM_003507.1-2030s21c1 & shFZD7-2 # **Clone ID:** NM_003507.1-778s21c1) and shRNA luciferase control (MISSION pLKO.1-puro Luciferase shRNA Control) were used for *FZD7* knockdown stable clones. Plasmids were mixed with MISSION® Lentiviral Packaging Mix (#SHP001, Sigma-Aldrich) before addition to a mixture of transfection reagent Fugene 6 (#11814443001, Roche) and OptiMEM. After 10-15 minutes of incubation at room temperature, they were added to 293T cells seeded in the 6cm dishes. For infection, virus-containing supernatants were harvested 48 and 72 hours after transfection, filtered and added to selected cells, together with polybrene (Sigma-Aldrich). 24 hours after infection, cells were treated with puromycin at appropriate concentrations decided by their respective puromycin kill curve.

2.4.6 *in vitro* growth assay

Cells were seeded in 96 well plates (# 167008, Nunclon, Thermo) at 1000 per well at day 0. From day1 to day7, MTS assays (#G5430, Promega) were performed everyday according to standard protocol. The cells were incubated with MTS reagent mix for 2 hours and 490nm absorbance was read using a plate reader (Tecan infinite 200).

2.4.7 *in vitro* apoptotic assay

For the caspase 3/7 activity assay, cells were seeded in ultra-low attachment 96-well plates (#7007, Corning) at a density of 5,000 (OV17R clones) or 3,000 (CH1 clones) cells per well. After 72h or 96h incubation, 20μL of CellTiter-Fluor reagent (for cell viability, #TB371, Promega) was added to all the wells and the fluorescence was measured using a Tecan plate reader (Tecan infinite 200) after 1h incubation at 37°C. 100μL of Caspase-Glo 3/7 reagent (#TB323, Promega) was then added to all the wells and the luminescence was measured after 1~2h incubation at room temperature. The caspase 3/7 activities were divided by the cell viabilities and then normalized to their respective controls.

2.4.8 cell line *in vitro* drug study

C59 and I-BET-762

Stable FZD7 knockdown clones of CH1 and OV17R cell lines were tested for their sensitivity to I-BET-762 and C59 (obtained from our collaborator, Dr. David Virshup, DUKE-NUS, Singapore). Cells were seeded in 96-well plates at an optimal density, which was determined for each cell line to ensure that it reached 80% confluency by the end of the assay. Following an overnight incubation, cells were treated with nine concentrations of each drug (twofold dilution series over a 128-fold concentration range) for 48 h. The percentage of the cell population responding to the drug relative to the negative controls was measured using a CellTiter 96 AQueous Non-Radioactive Cell Proliferation Assay, following the manufacturer's recommendations (#G5430, Promega). Dose-response curves were plotted using GraphPad Prism, to derive a growth inhibitory concentration of 50% (GI50; drug concentration for 50% growth inhibitory effects on cells) for each cell line in at least three independent experiments

Vinorelbine and paclitaxel

Dharmacon SMART pool siGENOME siRNA and Dharmacon SMART pool ON-TARGETplus siRNA (OTP) formats (Thermo Fisher Scientific, Lafayette, CO) were used to knockdown *NAT10* in PA-1, COV318, CH1, SKOV3 and HEY cells as detailed above. Assays were performed in quadruplicate. After 48 - 72hr incubation, cells were treated with nine concentrations of either vinorelbine or paclitaxel (twofold dilution series over a 128-fold concentration range) for 48 h and an MTS assay was used to measure cell growth using a CellTiter 96 AQueous Non-Radioactive Cell Proliferation Assay following the manufacturer's recommendations (#G5430, Promega, Madison, WI). Dose-response curves were plotted using GraphPad Prism (version 7), to derive a growth inhibitory concentration of 50% (GI50; drug concentration for 50% growth inhibitory effects on cells) for each cell line in at least three independent experiments.

2.4.9 Suspension culture and FACS

For FACS, cells were seeded in ultra-low attachment 10cm dish (#3263, Corning) at a density of 500,000 cells per dish. After incubated at 37°C, 5% CO2 for 48-72h, cells were collected, trypsinized to get single cell suspension, and stained with PI and Annexin V (#V13242, Sigma) for 15min at room temperature in dark. LSRII FACS analyzer was used to do the FACS with proper gating.

2.4.10 Chromatin immunoprecipitation assays (ChIP-qPCR)

Cells grown in 100 mm or 150 mm dishes were cross-linked by adding formaldehyde to a final concentration of 1% and incubated at room temperature for 10 minutes. To quench the formaldehyde, glycine was added to a final concentration of 0.125 M and incubated for 5 minutes. The fixed cells were rinsed twice with 1x TBS and harvested by scraping in SDS buffer (100 mM NaCl, 50 mM Tris-Cl at pH 8.1, 5 mM EDTA, 0.5% SDS, 0.02% NaN_3 and protease inhibitors). For lysis and shearing of DNA, the cells were sonicated by either Bioruptor® or Branson digital sonifier for

7 to 10 pulses (20” on 20” off intervals). The size of chromatin fragments (200 bp to 500 bp) was checked by agarose gel electrophoresis. Prior to immunoprecipitation, the chromatin samples were pre-cleared with blocked Protein G sepharose beads for one hour at 4°C. Inputs (2.5%) were collected and the rest of the pre-cleared samples were incubated with IgG control antibodies or anti-BRD4 antibodies (clone: #13440, cell signaling), 3 µg each, overnight at 4°C. The samples were then incubated with blocked Protein G sepharose beads for two hours at 4°C followed by a number of high stringency washes. The bound DNA was eluted, reverse cross-linked at 65°C overnight in 1% SDS, 0.1 M $NaHCO_3$ and subsequently purified using QIAquick PCR purification kit from Qiagen. The purified samples and input controls were subjected to either qPCR analysis. For ChIP-qPCR, the primer pairs used include:

BCL2 promoter	(forward) 5' TTAGGACGGTGGGCCTGAAAG 3'
	(reverse) 5' CCCGAGCGTGGTGTTTACTTT 3'
C-MYC promoter	(forward) 5' GAGCAGCAGAGAAAGGGAGA 3'
	(reverse) 5' CAGCCGAGCACTCTAGCTCT 3'
MYCN1 promoter	(forward) 5'TTTGCACCTTCGGACTACCC 3’
	(reverse) 5' TTTGACTGCGTGTTGTGCAG 3’
MYCN2 promoter	(forward) 5' TCCTGGGAACTGTGTTGGAG 3’
	(reverse) 5' TCCTCGGATGGCTACAGTCT 3'
MYCN neg promoter	(forward) 5' GTATCACCGTCCATTCCCCG 3'
	(reverse) 5' TTGGAGGCAGCTCAAAGACC 3'
WNT5A promoter	(forward) 5' CAAATAGGCAGCCGAGAGAC 3'
	(reverse) 5' CTCTAGCGTCCACGAACTCC 3'

2.5 *FZD7-TWIST1* signature

To derive *FZD7-TWIST1* signature, we extracted pre-processed gene expression data from CSIOVDB (Tan et al., 2015). The 77 genes (Appendix 1) whose expression most positively correlate to the average expression of *FZD7* and *TWIST1* (Spearman Correlation Coefficient *Rho*>0.3) were selected as an *FZD7-TWIST1* signature. To compute the enrichment score of the signature, a two-sample Kolmogorov–Smirnov-based test was used. Kaplan-Meier analyses were performed using GraphPad Prism ® version 7 (GraphPad Software; La Jolla, CA). Patients were categorized into low and high groups corresponding to the first (lowest 25%) and last quartiles (highest 25%) of signature enrichment score, respectively. P-values of survival analyses were computed using log-rank test.

To assess the enrichment of FZD7--TWIST1 signature for the PDX, microarray data (Weroha et al., 2014) previously generated by our collaborator from the Mayo clinic, Dr. Paul Haluska, single-sample GSEA version 4 was applied. A numerical score was given to each PDX based on the resemblance of their gene expression profile to the 77-gene signature. Spearman correlation coefficient test was performed using GraphPad Prism ® version 7 (GraphPad Software; La Jolla, CA). P-values of Kaplan-Meier survival analyses were computed using log-rank test.

2.6 Molecular assessment of subtype heterogeneity (MASH) analysis

To estimate intra-tumoral heterogeneity, a quantitative measurement scheme was derived based on the scores computed by the five subtype predictors. This score is based on the assumption that a tumor must show at least one primary molecular subtype, and that the secondary subtypes constitute the intra-tumor molecular subtype heterogeneity. Given the molecular subtype scores, $Score_s$, where $s \in$ **SUBTYPE**, and **SUBTYPE** =

{Epi-A, Epi-B, Mes, Stem-A, Stem-B}, the intra-tumoral heterogeneity, denoted as $Tumor_{Heterogeneity}$, is estimated as

$$Tumor_{Heterogeneity} = \sum_{s\in \mathrm{SUBTYPE}}^{5} Score_s - \max_{s\in \mathrm{SUBTYPE}} (Score_s),$$

$$Tumor_{Heterogeneity} \in [-1.0, 4.0]$$

The intra-tumoral heterogeneity score was applied to the clinical samples. Tumors with more than one subtype annotation expectantly showed a higher heterogeneity score, indicating the validity of the scoring system (Fig. EV3A).

MASH assay

In order to have a reduced set of genes for MASH assessment, the subtype signature identified by Lasso regression in this study was limited to genes overlap in subtype signature identified previously in a cohort of 1,538 samples that formed subset of CSIOVDB (Tan et al., 2013a). Only 56 genes out of the 1971 were retained and used for MASH assay on NanoString platform. The regression coefficients were re-trained using Lasso regression and CSIOVDB leaving NUH cohort (n = 3,331) out as the corresponding FFPE samples form NUH cohort will be used as validation set. Youden's index was adopted to select threshold for subtype classification.

To derive the MASH analysis for the PDX, microarray data (Weroha et al., 2014) previously generated by our collaborator from the Mayo clinic, Dr. Paul Haluska, was used to select the relevant genes of interest and computed. Test of correlation was performed using GraphPad Prism ® version 7 (GraphPad Software; La Jolla, CA). P-values of survival analyses were computed using log-rank test.

2.7 Statistical Analysis

Prism (Version 7; GraphPad) and Excel (Version 12.2.8) software were used for statistical analysis. Mean and standard deviations were calculated using Excel. Two group comparisons were made using 2-tailed *t* tests assuming equal variances. The time taken for a PDX to develop to the pre-defined tumor volume at which euthanasia of the animal was required, was calculated and plotted using Kaplan-Meier curves (Prism version 7). Differences in time taken to volume required for cull post treatment, between cohorts of treatment mice were tested using log-rank tests. *P* values less than 0.05 were considered to indicate statistical significance

Chapter III:

Generation and characterization of C5/Stem-A HGSOC PDX

3.1 Introduction

Epithelial Ovarian Carcinoma (EOC) is one of the most challenging cancers to treat partly due to the advanced stage of disease (FIGO Stage III or IV) at diagnosis and lack of effective screening (Vaughan et al., 2011). Since 1996, platinum/taxane based combination therapy has become the standard-of-care first line chemotherapy with response rates of around 80% (Bois, 2003; Cadron et al., 2007; McGuire et al., 1996; Ozols, 2003). However, the success of this approach is limited and approximately 70% of patients fail to achieve complete responses, or experience disease relapse after a varying disease-free interval and this is often accompanied by eventual acquired resistance to further chemotherapy. High grade serous ovarian carcinoma (HGSOC), the most common form of EOC, accounts for 70% of patient mortality. This disease is one of the most chromosomally variant malignancies and is characterized by genomic instability with relatively few validated oncogenic drivers (Bowtell et al., 2015; Patel et al., 2011; TCGA., 2011).

Four independent molecular subtypes of HGSOC with associated prognostic significance have been identified based on gene expression profiling in several independent studies (Helland et al., 2011; S. Tan et al., 2015; TCGA., 2011; Tothill et al., 2008). The C5/Stem-A subtype comprises 20% of HGSOC, is associated with maintenance of an undifferentiated state in cancer cells (Helland et al., 2011) leading to poorer outcomes (Tothill et al., 2008). The C5 subtype of HGSOC, also known as the proliferative subtype (TCGA., 2011) and the Stem-A subtype by Tan et al, is characterized by high expression of transcription factors such as HMGA2 and SOX11, low expression of ovarian tumour markers (MUC1 and MUC16) and high expression of proliferation markers such as MCM2 and PCNA (TCGA., 2011). This subtype of HGSOC was observed to activate a highly specific pathway involving *MYCN*

amplification and over-expression associated with over-expression of MYCN targets including *Let-7* repressor *LIN28B,* and *HMGA2* amplification and over-expression (Helland et al., 2011). The deregulation of the MYCN pathway and downstream targets, involving multiple genes that contribute to stem cell renewal, was found to be altered in this particular molecular subtype of HGSOC (Helland et al., 2011).

Currently, the role of *MYCN* in HGSOC is still unclear. However, in neuroblastoma (NB), the most common extracranial solid tumor in infants and children, and accounts for 15% of cancer-related mortalities, largely due to metastatic disease progression, *MYCN* amplification is considered the most important oncogenic marker (Brodeur, 2003; Maris and Matthay, 1999). The role of *MYCN* amplification in neuroblastoma has been outlined in the introduction section of this thesis (section "Role of MYCN in proliferative/C5/ Stem-A subtype"). Given the significant role of *MYCN* amplification in neuroblastoma, the targeting of *MYCN* may also be relevant for the C5/Stem-A HGSOC subtype that is characterized by over-expression of the MYCN pathway.

Another independent study has linked this subtype to the regulation of microtubule dynamics and observed an increased sensitivity to microtubule polymerizing agents (Tan, Miow et al., 2013). This will be further discussed in-depth in Chapter V of this thesis. Recently, studies have observed clinically relevant implications for the robust molecular subtypes of HGSOC, implying potential for relevant therapeutic targeting based on molecular signatures (Gourley et al., 2014; Konecny et al., 2014)

As the molecular subtypes become more clinically relevant, it will be prudent to determine other factors within each subtype that will impact on therapeutic response and resistance. Certain molecular aberrations with the potential to affect standard cytotoxic

and/or targeted therapeutics have been observed in HGSOC. Patients whose HGSOC harbors a HR DNA repair pathway defect in either of the breast or ovarian cancer predisposition gene, *BRCA1* or *BRCA2*, have been observed to have higher response rates to platinum based chemotherapy(Alsop et al., 2012; Bolton et al., 2012; Pennington et al., 2014; Tan et al., 2008) and to targeted inhibitor, Poly(ADP-ribose) polymerase (PARP) inhibitor, (Ledermann et al., 2014; Swisher et al., 2017) leading to improved prognosis and better overall survival (Alsop et al., 2012; Pennington et al., 2014; Tan, Yap et al., 2013). Indeed, recent reports now show that even without germline or somatic mutations in *BRCA1/2*, mutations in other homologous recombination-related genes, such as *RAD51C* or a high percentage of genome-wide loss of heterozygosity (LOH) in the tumour is associated with similar phenotypic outcomes and PARP inhibitor response (Swisher et al., 2017). Hence, to understand the biology of C5/Stem-A HGSOC, it would be crucial to factor in aberrations in genes related to HR DNA repair pathway.

CCNE1 amplification or gain is a key driver mutation in about 20% HGSOC (Bowtell et al., 2015). It represents an important subset of HR-intact tumours, generally occurs mutually exclusive from *BRCA1* and *BRCA2* mutations and have been shown to confer relative resistance to conventional chemotherapy and a reduced overall survival (Etemadmoghadam et al., 2010). Overexpression of pro-survival oncogenic members of the *BCL2* family has also been observed and their role in resistance to targeted therapeutics as well as standard cytotoxics is becoming apparent (Cragg et al., 2009; Deng et al., 2007; Kuroda et al., 2006). Genomic studies have shown substantial clonal diversity exist in chemo-naïve HGSOC patients. As such, a better understanding of the factors that impact on response to treatment is central to improving outcomes.

To further understand the biology and detect oncogenic drivers or vulnerabilities relevant for the C5/Stem-A HGSOC, we established a cohort of 12 independent chemo-

naïve PDX with in-depth molecular and functional annotation to increase the therapeutic utility of the PDX cohort. We subsequently utilised this unique resource to explore the therapeutic relevance of candidate inhibitors based on their druggable molecular characteristics.

3.2 Results

Generation of molecularly annotated C5/Stem-A HGSOC PDX

Tumour samples were collected from chemo-naïve patients at time of diagnosis during primary cytoreductive surgery for high-grade serous ovarian cancer (HGSOC). Unmanipulated tumour fragments were transplanted into immunocompromised NOD-SCID-IL-2rγ recipient mice subcutaneously to generate patient-derived xenografts (PDX). As both the orthotopic intra-bursal and subcutaneous routes were observed to result in reliable transplantation with preservation of serous papillary structures and similar histologic appearance of H+E stained sections (Topp et al., 2014), the subcutaneous route was chosen as it is less invasive and allows for a more accurate measurement of tumour volume. Molecular, functional and clinical outcome features of the first twelve consecutive cases have been described (Topp et al., 2014). Three of the twelve cases (25%) were consistent with a C5/Stem-A molecular subtype of HGSOC, as evidenced by over-expression of either *MYCN* and/or *LIN28B* mRNA via RT-qPCR(Topp et al., 2014) which resulted in two engrafted PDX (figure 3.1).

To expand our cohort of C5/Stem-A PDX, a second cohort of 10 additional post-surgical HGSOC samples were obtained from the same centre and screened for MYCN pathway over-expression (*MYCN* and *LIN28B*) by RT-qPCR. Four out of ten (40.0%) from the partially selected second cohort over-expressed *MYCN* and/or *LIN28B* mRNA (figure 3.1), which gave rise to two C5/Stem-A PDX from this second HGSOC cohort (Figure 3.1). mRNA expression of *MYCN* and *LIN28B* was determined relative to the cohort and control cell lines.

To further enrich for C5/Stem-A tumours, a third cohort, consisting of eight C5/Stem-A HGSOC PDX samples were obtained from our collaborator at another institution, derived from a consecutive cohort of EOC PDX deemed to be C5/Stem-A-

like based on microarray gene expression analysis (Weroha et al., 2014). Collectively, this resulted in a cohort of 12 C5/Stem-A HGSOC PDX (figure 3.1).

Sequencing of DNA extracted from tumour tissue confirmed the presence of pathogenic mutations in the tumour suppressor gene, *TP53*, known to be ubiquitously involved in HGSOC(Ahmed et al., 2010), in all samples(Topp et al., 2014)(table 3.1: TP53 mutation for cohort1; cohort2 and cohort3). Immunohistochemical (IHC) staining of tumour tissue for p53 protein was consistent with a mutation in all cases (either absent or strongly positive). IHC analysis of baseline human tumour tissue from the WEHI cohort confirmed positive expression of WT1 and PAX8, consistent with the diagnosis of HGSOC and variable expression of the proliferative marker, Ki67. Consistent with this, all PDX were proved to be of epithelial origin, with positive staining by IHC for pan-CK and negative staining for CD45 (excluding the possibility of a host-derived lymphoma) (figure 3.2). Similar analysis were performed by our collaborator for cohort 3 (Weroha et al., 2014) prior to shipping minced PDX tissue and stored in DMSO to us for enrichment of our C5/Stem-A HGSOC cohort and thus baseline human tissue were not available to us for comparisons.

C5/Stem-A PDX selection based on MYCN pathway over-expression

The C5/Stem-A subtype of HGSOC includes MYCN pathway deregulation which contributes to altered stem cell renewal and differentiation associated with poor outcomes (Helland et al., 2011). As such, we screened for members of the MYCN pathway (*MYCN, LIN28B* and *HMGA2*) via RT-qPCR on baseline chemo-naïve HGSOC tumour samples for the first and second cohort while early passage PDX tumours were used to determine MYCN pathway members for the third cohort. MYCN and LIN28B protein expression were subsequently determined for all the C5/Stem-A PDX from all three cohorts.

For the two successfully engrafted C5/Stem-A PDX from the initial first cohort (Topp et al., 2014), we observed one PDX overexpressed MYCN and LIN28B protein (WEHI#29) (figure 3.3(B). For the second cohort of 10 HGSOC chemo-naïve cases, three overexpressed *MYCN* mRNA and 2 overexpressed *LIN28B* mRNA while five overexpressed mRNA for the oncofetal protein *HMGA2* that regulates differentiation and stem cell renewal (figure 3.3(C). Only two out of the three C5/Stem-A tumours successfully engrafted (WEHI#91 WEHI#95) with one PDX (WEHI#95) observed to overexpress MYCN and LIN28B protein (figure 3.3(C) (table 3.2). In the C5/Stem-A-enriched cohort of HGSOC based on microarray gene expression analysis (Weroha et al., 2014)(third cohort), we observed that seven out of eight putative C5/Stem-A PDX overexpressed either *MYCN* or *LIN28B* mRNA (except for #PH034) (figure 3.3(A) while five out of eight showed appreciable protein overexpression in either MYCN or LIN28B protein levels (figure 3.4(B). All eight PDX overexpressed mRNA for *HMGA2* (figure 3.3(C).

Protein expression was found to be concordant with the mRNA expression for *MYCN* and *LIN28B* across all three cohorts (figure 3.4(A). MYCN and/or LIN28B protein was overexpressed in seven of 12 C5/Stem-A PDX (figure 3.4(B). Seven out of 12 overexpressed MYCN protein; three out of 12 overexpressed LIN28B protein) (figure 3.4(B) (table 3.2).

Determining relevant prognostic markers in the C5/Stem-A HGSOC PDX

Currently, one of the main prognostic indicators of clinical outcomes besides stage of disease and surgical debulking status, is the response of the HGSOC to platinum-based therapy (Vaughan et al., 2011), in which the status of DNA repair pathway in the tumour has significant relevance (Alsop et al., 2012; Bowtell et al., 2015; Pennington et al., 2014; Swisher et al., 2017; Vaughan et al., 2011). To determine characteristics

relevant for prognosis of the C5/Stem-A subtype of HGSOC PDX, we explored DNA repair gene status including *BRCA1/2* and other genes in the FA-BRCA-HR pathway (Table 3.3) (Walsh et al., 2011) in this cohort of 12 C5/Stem-A PDX. Three PDX were found to harbor a mutation in *BRCA2* (PDX WEHI#91, WEHI#95, #PH077) (table 3.3). Mutations in other potentially relevant genes were observed in *FANCM* (PDX #PH039) and *CHEK1* (PDX#PH041). One PDX (#PH048) harbored a mutation in the *SMARCA4* gene, an inactivating mutation in the SWI/SNF chromatin remodelling gene (Table 3.2).

Functional platinum response of C5/Stem-A HGSOC PDX

In order to further understand the disease biology of the individual C5/Stem-A HGSOC PDX within the cohort, we determined *in vivo* responses to platinum based chemotherapy using cisplatin monotherapy, for each of the 12 PDX. Similar to Topp *et al*, we defined response as being "cisplatin sensitive" if the average PDX tumor volume of the recipient mice underwent initial tumor regression with complete remission (CR, defined as tumor volume < 0.2 cm^3) or partial remission (PR, defined as reduction in tumor volume of > 30% from baseline) followed by progressive disease (PD, an increase in tumor volume of >20% from 0.2 cm^3 or nadir post-treatment, if nadir ≥ 0.2 cm^3) occurring ≥ 100 days from start of treatment; "cisplatin resistant" if initial tumor regression (CR or PR) or stable disease (SD) was followed by PD within 100 days; or "cisplatin refractory" if three or more mice bearing that PDX had tumors which failed to respond (no CR, PR or SD) during cisplatin treatment (day 1 - 18) (Topp et al., 2014).

Of the 12 C5/Stem-A HGSOC PDX analysed, four PDX were sensitive to cisplatin with PD observed ≥ 100 days following treatment (#PH038, #PH054, #PH077 and #PH039) (figure 3.4; table 3.4); two of five cisplatin-sensitive PDX harbored mutations in DNA repair genes, with one carrying a mutation in *BRCA2* (#PH077) and the other in the putative HRD gene, *FANCM* (#PH039). One PDX was resistant to

cisplatin (#PH034) with initial tumour regression followed by PD at 45 days and 55 days respectively (figure 3.5) (Table 3.4). Five of the 12 PDX were refractory to cisplatin (#PH036, #PH041, #PH048, WEHI#29 and WEHI#36) with PD observed at 3 - 22 days following commencement of treatment concordant with the previously reported poor prognosis in this subtype (Tan et al., 2015; Tothill et al., 2008) (figure 3.5)(Table 3.4). Mature cisplatin treatment data for two PDX (WEHI#91 and WEHI#95) are still pending with preliminary data suggesting platinum sensitivity in PDX WEHI#91 (data not shown) which also harbors a *BRCA2* mutation.

We subsequently compared platinum response of patients with the PDX from which they were derived. Treatment response data were available from five patients and was observed to be concordant with the platinum response of the corresponding PDX. Patients from which PDX #PH039 and #PH077 were derived were observed to be sensitive to platinum- based treatment, defined as time from last dose of platinum to disease recurrence of 6 months or more, with platinum free interval (PFI) of 11 months and 9 months, respectively while patient from which PDX #PH041 was derived was resistant to platinum – based treatment, defined as time from last dose of platinum to disease recurrence of less than 6 months. PFI for patient which PDX #PH041 was derived was 5 months. As previously published, patients from which PDX WEHI#29 and WEHI#36 were derived was observed to be refractory to platinum- based treatment corresponding to the platinum response of the PDX (Topp et al., 2014).

Determining relevant markers for drug resistance in the C5/Stem-A HGSOC PDX

Next, to determine the impact of relevant oncogenes on response to therapy, we interrogated the C5/Stem-A HGSOC PDX for several oncogenes, *CCNE1* and *BCL2*, with the potential to affect response to primary treatment. Two of the 12 (15%) C5/Stem-A PDX overexpressed mRNA and protein levels of CCNE1 (PDX #PH041 and

WEHI#29) (figure 3.6(A,B). Of note, baseline tumour WEHI#36 had high expression of CCNE1, however the resultant PDX WEHI#36 did not. Not surprisingly, both PDX were refractory to primary platinum therapy (Table 3.4). *CCNE1* mRNA demonstrated concordance to protein expression in the 12 HGSOC C5/Stem-A PDX analysed (Table 3.5).

We subsequently interrogated individual PDX for *BCL2* expression. The intrinsic apoptotic pathway in mammals is regulated by the balance between pro-survival members, BCL2 or MCL-1, and pro-apoptotic members of the BCL2 family(Cragg et al., 2009). We identified overexpression of *BCL2* mRNA levels in 8 of 12 C5/Stem-A HGSOC PDX (figure 3.7(A). As overexpression of *BCL2* mRNA may not always translate to increase in protein levels (Liu et al., 2016), BCL2 protein levels were subsequently evaluated in each of the individual PDX by western blotting or immunohistochecmistry (figure 3.7(B). We observed four PDX overexpressed BCL2 protein (PDX #PH048, WEHI#29, WEHI#91, WEHI#95) (figure 3.7(B). Two of the four PDX were refractory to platinum (#PH048 and WEHI#29) (Table 3.4) (Table 3.5). This observation was consistent with observations made from other solid malignancies demonstrating primary resistance to standard therapy (Vaillant et al., 2013). BCL2 protein overexpression was also identified in PDX WEHI#91 and WEHI#95. Mature cisplatin treatment data for these PDXs are still pending.

Targeting *MYCN* using a novel MYCN inhibitor (M606) in C5/Stem-A HGSOC PDX

Having established the relative platinum sensitivity of each of the C5/Stem-A PDX, we subsequently ventured to examine the response of these PDXs to novel therapeutics predicted to target this molecular subset. The novel MYCN inhibitor, M606, was derived from a drug library screen by our collaborator at the Children's Cancer

Institute, Australia, with selective cytotoxicity only for *MYCN*-amplified neuroblastoma cells (Cheung, 2012). This novel compound appeared to demonstrate anti-tumour activity in neuroblastoma cell lines (figure 3.8(A) and transgenic *MYCN*-amplified neuroblastoma mice models (figure 3.8(B) as monotherapy. When used in combination, anti-tumour activity was observed in combination with cisplatin compared to either vehicle or M606 alone in transgenic *MYCN*-amplified neuroblastoma models (figure 3.7(B). Using the MYCN status previously assessed, we evaluated three MYCN over-expressing PDXs *in vivo* initially using 25mg/kg of M606 daily (Monday to Friday) I/P for 3 weeks (data not shown) and subsequently switched to 40mg/kg of M606 daily (Monday to Friday) I/P for 3 weeks as dosing schedules were performed by our collaborator showing that this dose was efficacious and tolerable in neuroblastoma mouse models.

Of the three C5/Stem-A HGSOC PDX tested, #PH038, #PH077 and #PH048, none demonstrated an anti-tumour response to single agent M606 with median TTH with M606 of 27.5d, 22d and 17d respectively compared to vehicle treated controls 24d, 23.5d and 31d respectively (Table 3.6) (figure 3.9(A-C). To assess the utility of this novel inhibitor in combination, M606 (40mg/kg) was administered in combination with low-dose cisplatin (2mg/kg) in PDX #PH038 and #PH077. Significant toxicity was observed in the form of weight loss limiting the ability to expand the treatment to more mice. Of the two PDX treated, #PH038 and #PH077, when compared with cisplatin monotherapy (4mg/kg), combination therapy of M606 with cisplatin (2 mg/kg) was no better as evidenced by the K-M curves (HR: none; p value: 0.045 and HR:2.01; p value: 0.56, respectively) (figure 3.9 (D,F). Of note, efficacy for cisplatin (2mg/kg) as a single agent was tested in n=2 mice with similar (> 90days) sensitivity to that seen for 4 mg/kg (data not shown). Therefore, the combination efficacy observed in these two cisplatin-sensitive PDX was likely the result of the cytotoxic agent. Cisplatin-resistant C5/Stem-A PDX

models were not assessed as the toxicity/benefit ratio did not support ongoing investigation.

Next, we assessed MYCN protein expression pre- and post- treatment with M606 for PDX #PH077 and for the transgenic *MYCN*-amplified neuroblastoma mice to ascertain on-target activity of the drug. We observed no appreciable reduction in MYCN protein levels pre and post M606 in both models, perhaps explaining the lack of efficacy of the drug (figure 3.10) and further emphasizing the need for therapeutic testing of new compounds in PDX models as part of the validation process in drug development.

3.3 Discussion:

Here, we have successfully established a cohort of C5/ Stem-A HGSOC PDXs from predominantly surgical specimens. In accordance with our previous work and other published literature, we found that the subcutaneous route of transplant to be tolerable, feasible and maintained the relevant features of the primary tumour when analysed by IHC (Topp et al., 2014; Weroha et al., 2014; Whittle et al., 2015)(Figure 2). As the cohort of 12 C5/Stem-A HGSOC PDX was derived from two separate sources with differing workflows and processes, it will be difficult to comment on the transplantation success rate of this cohort with the methods used. Nonetheless, we demonstrated, that the PDXs were amenable to expansion in mice, freeze/thaw cycles and reseeding in mice to provide a valuable, renewable source of material that is reflective of patient tumours.

Helland and colleagues reported that *MYCN* over-expression was highly C5-specific and mechanisms in addition to gene amplification are likely to contribute to the C5 phenotype (Helland et al., 2011). Furthermore, significant over-expression of *MYCN* target genes, including *LIN28B* and *HMGA2* were highly enriched in the C5/Proliferative, supporting the view that *MYCN* is functionally active in this C5/Stem-A subtype (Helland et al., 2011; TCGA., 2011; Tothill et al., 2008). As such, *MYCN* and/or *LIN28B* mRNA expression levels were used to stratify primary tumours into two nominal groups of C5/Stem-A versus non-C5/Stem-A subtypes. Although established datasets have used several different platforms such as nanostring (Tothill et al., 2008) and microarray (Tan, Miow et al., 2013; TCGA., 2011) to classify HGSOC into individual subtypes, there is a lack of general consensus as to the most appropriate method for subset analysis. Furthermore, the emphasis on degree of stroma architecture within a tumour sample analysed using one of these platforms made tumours derived

from PDX, which generally lack human stroma due to replacement by mouse stroma, difficult to ascertain. Hence, a RT-qPCR technique which is cost effective, feasible to perform in a laboratory setting and accurate was employed when stratifying the tumour samples.

Based on cohort one and two, 7/22 (31.8%) tumours were identified as C5/Stem-A HGSOC which is higher than expected in a general population(Tan et al., 2013a; TCGA., 2011; Tothill et al., 2008). While cohort one was derived from consecutive HGSOC tumours, cohort two, which consisted of 4/10 (40%) C5/Stem-A HGSOC, was not. This and the small sample size may have confounded the analysis. Interestingly, none of the PDX harbored a *BRCA1* mutation while three PDX harbored a *BRCA2* mutation (Table 3.3). While it is generally more common to harbor a *BRCA1* mutation compared to a *BRCA2* mutation, the increased representation of *BRCA2* mutations in our cohort likely due to the fact that this PDX cohort is made up of a highly selective group of tumours, makes drawing any meaningful conclusions from this observation challenging. Nonetheless, it is encouraging to observe that the PDX (#PH077) harboring a *BRCA2* mutation with corresponding mature platinum response data showed sensitivity to platinum therapy consistent with the patient from which it was derived from as well as observations made in large patient cohorts (Alsop et al., 2012; D. S. P. Tan et al., 2008).

Several reports have demonstrated that PDX tumour response to therapy was reflective of patient responses (Topp et al., 2014; Weroha et al., 2014; Whittle et al., 2015). Hitherto, we only have five patients with clinically available data on patterns of platinum-response. The clinical patient data was observed to correlate with cisplatin treatment responses in the PDX from which they were derived. From our cohort, 63.6% of C5/Stem-A HGSOC PDX was refractory or resistant to platinum response. This appears to be relatively high even accounting for the poorer prognostic and more

aggressive biology of this subtype. As corroborative clinical patient treatment response data was not available for most of the PDX treated and is beyond the scope of this project, only general conclusions can be drawn from this small sample size. The data however, does allude to the more aggressive nature of this subtype and warrants further investigation (TCGA., 2011).

When focusing on oncogenic drivers, particularly in *CCNE1* and *BCL2*, in the C5/Stem-A HGSOC PDX, we observed that *CCNE1* mRNA expression was concordant with protein expression and 25% (3/12) overexpressed both *CCNE1* mRNA and protein. Interestingly, this correlated with resistance/refractory response to primary platinum therapy in the corresponding PDX as predicted in the literature(Etemadmoghadam et al., 2010). Similarly, BCL2 protein expression was observed to be overexpressed in the 40% (4/10) PDX and two of the PDX with corresponding platinum response data appeared to be refractory to platinum therapy. This is first time BCL2 and CCNE1 expression patterns are described in C5/Stem-A HGSOC, albeit in the PDX model. It is tempting to speculate this may be reflective in the clinical setting however, subsequent passaging of tumours with each transplantation tend to result in clonal selection pressure which may potentially result in overexpression of oncogenic drivers. Future work could focus on understanding the interplay and tumorigenic/apoptotic relevance between members of the BCL2-family in HGSOC and assess the role of BH3-mimetic combinatorial treatments in light of the recently approved BH3-mimetic, venetoclax (ABT-199) (Roberts et al., 2016).

One of the major issues in drug development is the limited translational correlation between clinical results and *in vitro* as well as *in vivo* cell line data (Johnson et al., 2001) making them poor surrogates of the source patients, and in part contributing to the high failure rate of new oncology drugs (Bowtell et al., 2015; Whittle et al., 2015). The novel MYCN inhibitor, M606, was a compound derived from a drug library

screen using *MYCN* amplified neuroblastoma cell lines, *MYCN* single copy neuroblastoma cell lines and non-malignant human cell lines. M606 was designed to inhibit MYCN with on-target activity evident in cell lines and some anti-tumour activity in the transgenic mice model but none demonstrated in the MYCN over-expressed C5/Stem-A HGSOC PDX model. The activity observed in both the cell lines and the transgenic mice model may result from off-target activity and is unlikely to be recapitulated in the clinical setting. This highlights the importance of testing novel compounds during drug discovery in preclinical models that reflects the heterogeneity observed in the clinic.

In conclusion, we have established a cohort of C5/Stem-A HGSOC PDXs that recapitulate their parental/primary tumours at the phenotypic level. We have used these PDXs to identify prognostic markers and oncogenic drivers of relevance to enhance our insights into the biology of this subtype. Despite their similar gene expression profiles, being C5/Stem-A, they appear highly heterogeneous both molecularly and in their patterns of response to standard platinum therapy. This will be a useful resource to test novel compounds as it recapitulates the heterogeneity of HGSOC and reflect histopathologic properties of the original tumour. Hence, future work could leverage on this resource by focusing on enhancing the molecular characterization of this cohort in light of new druggable targets and testing of suitable combinatorial approaches to inform a clinical trial.

Table 3.1. *TP53* mutations identified by BROCA analysis.

C5/Stem-A HGSOC	**Gene**	Consequence	Mutation – GRCh37	c.DNA	Protein
#PH038	*TP53*	missense	chr17:7578403C>T	c.527G>A	p.C176Y
#PH039	*TP53*	missense	chr17:7577565T>G	c.4609G>T	p.E1537X
#PH077	*TP53*	splice|SPL	chr17:7578176C>T	c.276+1G>A	**-**
#PH054	*TP53*	missense	chr17:7578259A>C	c.590T>G	**p.**V197G
#PH034	*TP53*	missense	chr17:7577539G>A	c.742C>T	**p.**R248W
#PH036	*TP53*	missense	chr17:7577547C>T	c.734G>A	**p.**G245D
#PH041	*TP53*	missense	chr17:7577538C>A	c.743G>T	**p.**R248L
#PH048	*TP53*	missense	chr17:7578550G>T	c.380C>A	**p.**S127Y
WEHI#29	*TP53*	missense	Chr17:7577098T>G	c.804A>C	p.R280S
WEHI#36	*TP53*	missense	Chr17:7578190T>C	c.659A>G	p.Y220C
WEHI#91	*TP53*	missense	chr17:7577129A>C	c.809T>G	p.F270C
WEHI#95	*TP53*	missense	chr17:7578394T>C	c.536A>G	p.H179R

Table 3.1. *TP53* mutations identified by BROCA analysis. DNA was prepared from C5/Stem-A HGSOC PDX for all PH annotated samples while baseline DNA was used for WEHI annotated samples. DNA were analysed by massively parallel sequencing for mutations in DNA repair genes, including *TP53* (BROCA sequencing (Walsh et al., 2011)). A *TP53* mutation was found in each of the 12 HG-SOC. Presence of mutated p53 protein by IHC is shown.

Table 3.2. Molecular Characteristics of C5/Stem-A HGSOC cohort.

HG-SOC	Platinum response	Mutation [a]	*MYCN* [c]	MYCN [d]	*LIN28B* [c]	LIN28B [c]
#PH038	**Sensitive**	nmf [b]	++	-/+	++	++
#PH039	**Sensitive**	*FANCM*	++	+	-/+	-/+
#PH077	**Sensitive**	*BRCA2*	+++	++	-/+	+
#PH054	**Sensitive**	nmf [b]	++	-/+	-	+
#PH034	**Resistant**	nmf [b]	+	-/+	+	-/+
#PH036	**Refractory**	nmf [b]	+++	++	+	-/+
#PH041	**Refractory**	*CHEK2*	++	++	+++	+
#PH048	**Refractory**	*SMARCA4*	+++	++	+++	+++
WEHI#29	**Refractory**	nmf [b]	+	-	+++	++
WEHI#36	**Refractory**	nmf [b]	+	-	++	-
WEHI#91	**Sensitive[e]**	*BRCA2*	+++	++	-	-
WEHI#95	**Pending**	*BRCA2*	+++	+++	++	+

Molecular Characteristics of HG-SOC transplanted. Analysis of baseline HG-SOC: DNA repair genes by BROCA sequencing (by Walsh et al (Walsh et al., 2011)); qRT-PCR. Five HGSOC were found to harbor a mutation in a DNA repair gene, other than *TP53*. [a]BROCA sequencing(Walsh et al., 2011); [b] nmf – no mutation found in DNA repair genes (apart from in *TP53*); [c] RT-qPCR; [d]western blot; -/+ negligible expression, + low expression, ++ intermediate expression, +++ high expression relative to this cohort and control cell lines. [e]Preliminary data shows PDX WEHI#91 is sensitive to cisplatin therapy. CH1, known to have over-expression of *MYCN, LIN28B and HMGA2*(Helland et al., 2011). RT-qPCR data represents mean expression patterns +/- SEM of at least 3 experiments. Where reported, error bars represent SEM.

Table 3.3. DNA repair gene mutations identified by BROCA analysis

C5/Stem-A HGSOC	Gene	Consequence	Mutation - GRCh37	Location [a]	Protein
PH#077	*BRCA2*	frameshift	chr13:32913532_32913534delTG	c.5040_5041delTG	p.S1680fs*11
PH#041	*CHEK2*	frameshift	chr22:29091857_29091858delC	c.1229_1230delC	p.T410fs*12
WEHI#91	*BRCA2*	frameshift	chr13:32911652_32911655delGATA	c.3160_3163delGATA	p.D1054fs*5
WEHI#95	*BRCA2*	frameshift	chr13:32912897_32912901delGACAT	c.4405_4409delGACAT	p.D1469fs*11

Table 3.3. DNA repair gene mutations identified by BROCA analysis of C5/Stem-A HGSOC. DNA was prepared from C5/Stem-A HGSOC PDX for all PH annotated samples while baseline DNA was used for WEHI annotated samples. DNA were analysed by massively parallel sequencing for mutations in DNA repair genes other than *TP53* (reported in Supplementary Table 2). (BROCA (Walsh et al., 2011)). [a] Locations in reference sequences (Start codon = 1) BRCA2: NM_000059, NP_000050.

Table 3.4. Relative growth rates of independent C5/Stem-A HGSOC PDX and median survival following platinum therapy

HG-SOC PDX	Time to PD (d) cisplatin	Median TTH (d) vehicle	Median TTH (d) cisplatin	n (recipient mice)	Hazard ratio (95% CI)
Sensitive					
#PH038	>120d	18.5	>120d	10, 6	0.07*** (0.02 – 0.22)
#PH039	>100d	11	>100d	11, 5	0.09** (0.02 – 0.36)
#PH077	>120d	19	>120d	13, 13	0.08*** (0.02 – 0.26)
#PH054	>120d	31	>120d	8, 8	0.12*** (0.03 – 0.45)
Resistant					
#PH034	55	36	94	8, 9	0.22*** (0.07 – 0.69)
Refractory					
#PH036	3	68.5	88.5	6, 8	0.5^{ns} (0.15 – 1.7)
#PH041	8	57	89	8, 9	0.48^{ns} (0.16 – 1.4)
#PH048	3	19	39	6, 8	0.56^{ns} (0.23 – 1.4)
WEHI#29	3	19	29	4, 6	<0.3704
WEHI#36	22	22	48	11, 9	<0.0001

Table 3.4. Relative growth rates of independent PDX and median survival following cisplatin therapy. Recipient mice PDX were randomized to treatment with vehicle or cisplatin 4mg/kg, D1, 8, 18 when tumour volume reached 0.18-0.3 cm^3. Time to Progressive disease (PD) was defined as the time (in days) from beginning of cisplatin treatment to an increase in average tumor volume (for that treatment group) of >20% from the nadir (used to categorise PDX as sensitive (PD≥100 days), resistant (PD <100 days) or refractory to cisplatin). Time to Harvest (TTH) was defined as the time (in days) from the beginning of treatment to day of harvest at 0.7 cm^3 and the median TTH was calculated and plotted using Kaplan-Meier curves (Prism version 7). Control growth rates (treatment with vehicle) for independent PDX reveal that the slowest growth rates were observed for the most sensitive PDX, PH#038 and PH#039. As seen with the relatively early measure of time to PD, response to cisplatin was most durable for cisplatin-sensitive PDX, PH#038, PH#039, PH#077 and PH#054 (TTH > 120 d); intermediate for PH#034 (cisplatin-resistant PDX; median TTH 86-94d) and PH#036, PH#041, PH#048, WEHI#29 and WEHI#36 with median TTH of only 29-92d (p value for difference between cisplatin and vehicle significant for all except PH#036, PH#048 and WEHI#29 indicating that two of five "refractory" PDX derived some short-term benefit from treatment). For the Kaplan Meier analysis of median TTH, all data were censored at 120 days except for PH#039 which was censored at 100 days. Cisplatin data for mice WEHI#29 and WEHI#36 were previously reported in(Topp et al., 2014) and only p values are reported here. Significance determined by Mantel-Cox test. ^{ns} p value not significant; *p value <0.05; **p value <0.01; *** p value <0.005. Hazard Ratio and 95% CI determined by Log Rank analysis

Table 3.5 Analysis of putative oncogenic drivers of C5/Stem-A HGSOC PDX.

HG-SOC	Platinum response	*CCNE1* [c]	CCNE1 [d]	*BCL2* [c]	BCL2 [d]
#PH038	**Sensitive**	+	-	++	-
#PH039	**Sensitive**	-	-	++	-
#PH077	**Sensitive**	+	-	+++	-
#PH054	**Sensitive**	+	-	+	-
#PH034	**Resistant**	-	-	+++	+
#PH036	**Refractory**	++	+	+++	+
#PH041	**Refractory**	+++	+++	+++	+
#PH048	**Refractory**	-	-	+++	+++
WEHI#29	**Refractory**	+++	+++	+++	+++
WEHI#36	**Refractory**	+++	++	ND	+
WEHI#91	**Sensitive[f]**	-	-	+++	++
WEHI#95	**Pending**	-	-	+++	++

Analysis of relevant oncogenic drivers of C5/Stem-A HGSOC PDX cohort: Where mature platinum response was available, CCNE1 and BCL2 protein expression correlated with resistant/refractory response to primary platinum therapy. *CCNE1* mRNA expression was concordant with protein expression. Three HGSOC PDX were found to overexpress *CCNE1* mRNA. Majority overexpress *BCL2* mRNA, only four PDX overexpress BCL2 protein. [c]qRT-PCR; [d]western blot -/+ negligible expression, + low expression, ++ intermediate expression, +++ high expression relative to this cohort and control cell lines. [f] Preliminary data shows PDX WEHI#91 is sensitive to cisplatin therapy. OVCAR3, known to have over-expression of *CCNE1*(Etemadmoghadam et al., 2010) and WEHI#29 known to overexpress BCL2 protein(Topp et al., 2014). qRT-PCR data represents mean expression patterns +/- SEM of at least 3 experiments. Where reported, error bars represent SEM

Table 3.6. Relative growth rates of independent C5/Stem-A HGSOC PDX and median survival following M606 therapy

HG-SOC PDX	Time to PD (d) M606	Median TTH (d) vehicle	Median TTH (d) M606	n (recipient mice)	Hazard ratio (95% CI)
#PH038	3d	24d	27.5d	7, 4	HR: 0.88^{ns} (0.2 – 2.97)
#PH048	3d	23.5d	22d	7, 4	HR: 1.6^{ns} (0.35 – 7.9)
#PH077	3d	17d	31d	6, 3	HR: 2.1^{ns} (0.59 – 13)

Table 3.6. Relative growth rates of independent PDX and median survival following M606 therapy. Recipient mice PDX were randomized to treatment with vehicle or M606 40mg/kg daily (Monday – Friday) for 3 weeks, when tumour volume reached 0.18-0.3 cm^3. Time to Progressive disease (PD) was defined as the time (in days) from beginning of cisplatin treatment to an increase in average tumor volume (for that treatment group) of >20% from the nadir. Time to Harvest (TTH) was defined as the time (in days) from the beginning of treatment to day of harvest at 0.7 cm^3 and the median TTH and Hazard Ratio was calculated and plotted using Kaplan-Meier curves (Prism version 7). As seen with the relatively early measure of time to PD, there was no response to M606 in PDX, PH#038, PH#048 and PH#077 with TTH similar for M606 and vehicle treated mice. (p value for difference between M606 and vehicle was not significant for all PDX treated indicating that none of the PDX derived benefit from treatment). Significance determined by Mantel-Cox test. ^{ns} p value not significant; *p value <0.05; **p value <0.01; *** p value <0.005. Hazard Ratio and 95% CI determined by Log Rank analysis

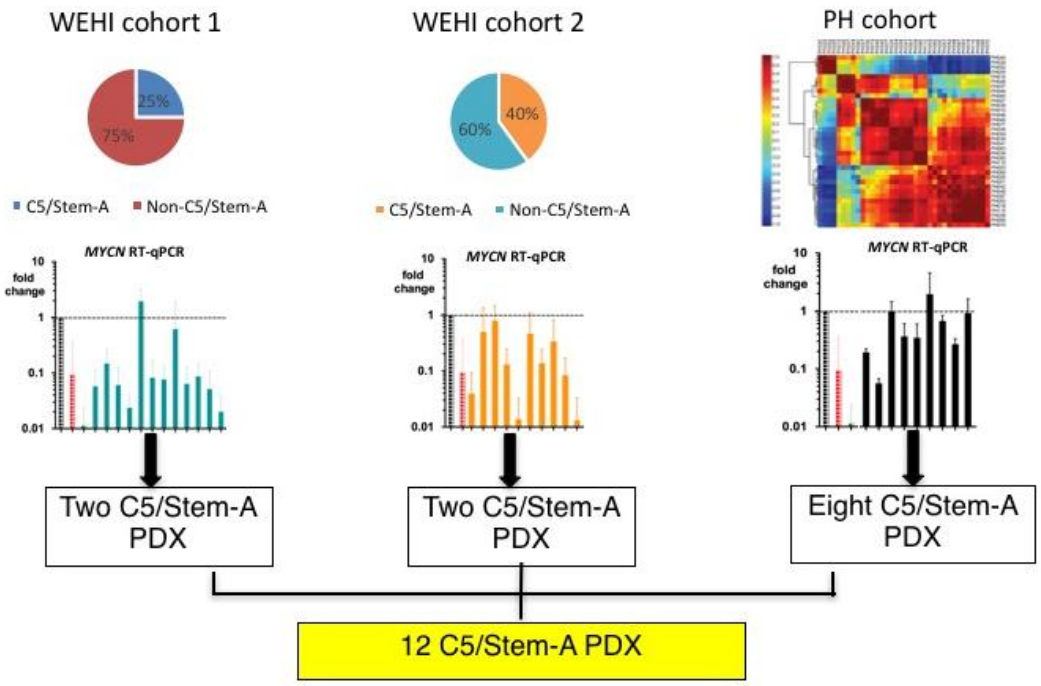

Figure 3.1: Schematic representation of the generation of the C5/Stem-A HGSOC PDX cohort. Tumour material were obtained from three separate cohorts. The first cohort (WEHI cohort 1) was derived from consecutive patient samples of HGSOC from the Royal Women's Hospital, Victoria, Australia while the second cohort (WEHI cohort 2) was derived from a partially selected group of women with HGSOC from the same hospital. Both these cohorts were screened for *MYCN* and *LIN28B* expression via RT-qPCR and deemed to be C5 based on high expression of either of these genes relative to control. CH1 cell line was used as control (Helland et al., 2011). The third cohort (PH cohort) was a C5 enriched cohort based on affy array analysis and PDX tumour samples were given to us by our collaborator from the Mayo clinic, Rochester, USA. All samples deemed to be C5 were transplanted into reservoir mice and 12 successfully gave rise to C5 PDXs.

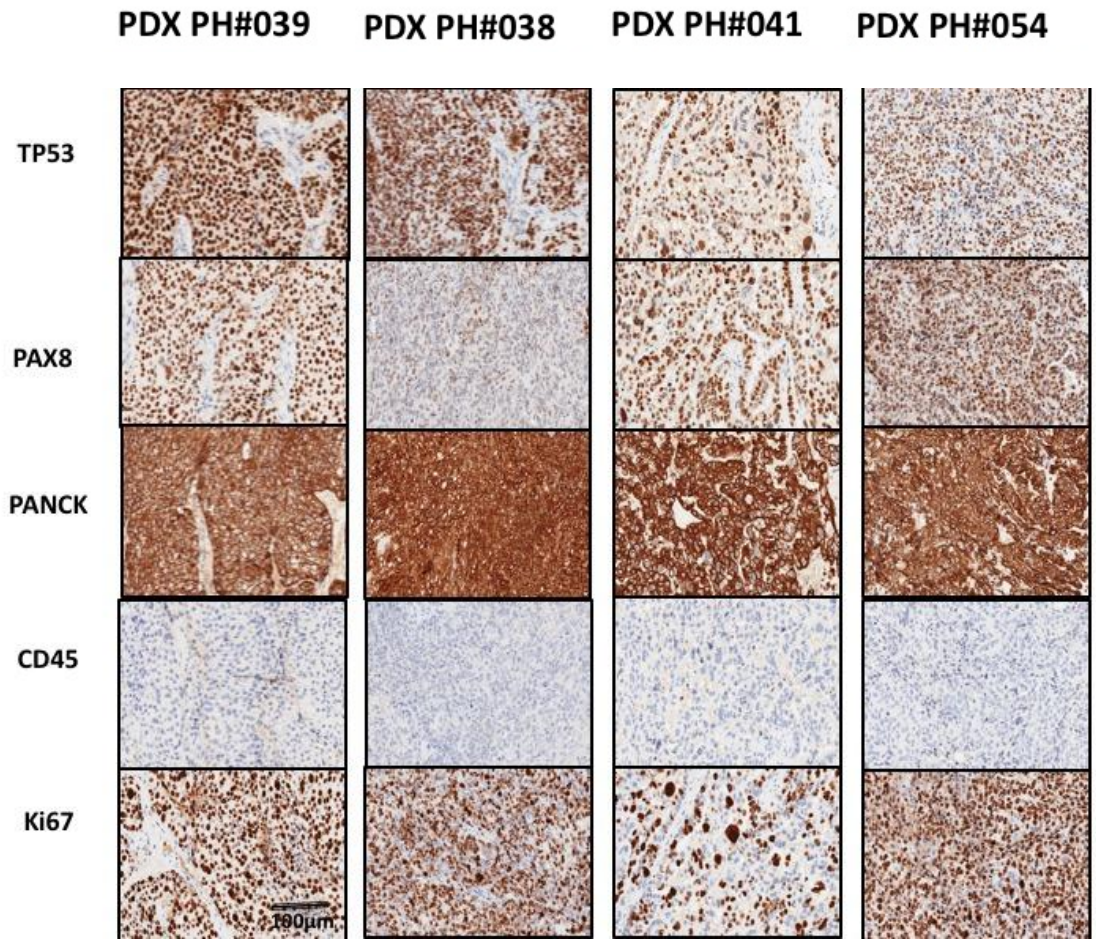

Figure 3.2: C5/Stem-A PDX resembles HGSOC. T1 C5/Stem-A PDX derived tumours were stained by immunohistochemistry for TP53, PAX8, panCK, CD45 and Ki67. Four representative T1 PDX IHC stains are shown. All PDX demonstrated positive staining for the epithelial marker, pan-CK, TP53 and PAX8 and negative for the hemopoietic marker, CD45, indicative that the tumours are indeed of human epithelial origin consistent with HGSOC and not murine based.

T1 = first passage of patient – derived xenograft transplanted from human tumour

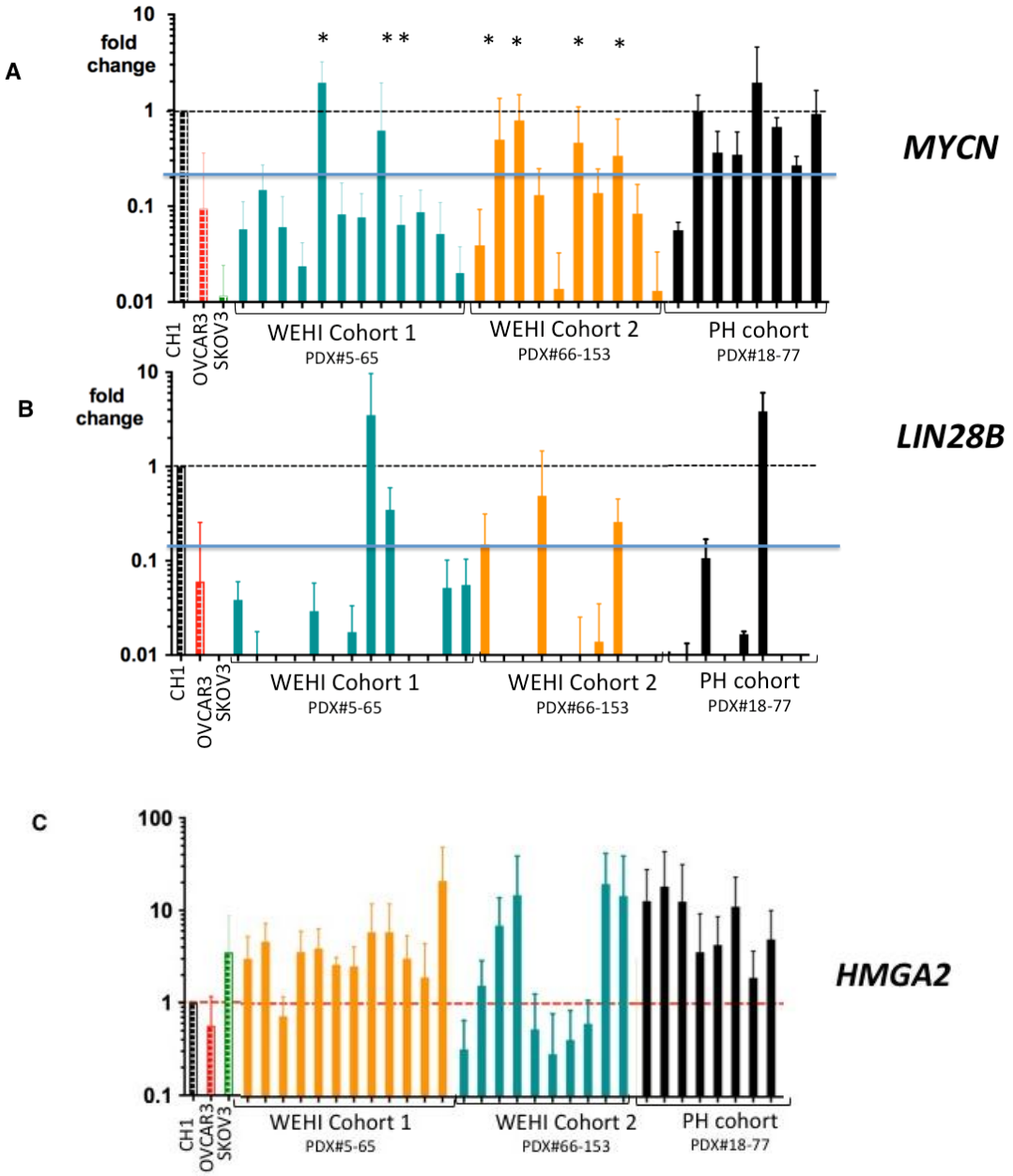

Figure 3.3: Expression patterns of MYCN pathway members in the baseline (WEHI cohort) and PDX (PH cohort) tumours screened. mRNA expression of MYCN pathway members demonstrates (A) *MYCN* expression in the tumours screened shows increased expression in the C5/Stem-A enriched PH cohort compared to the unselected/partially selected WEHI cohort (B) No obvious pattern of expression seen in *LIN28B* expression in tumours screened and (C) heterogeneous *HMGA2* expression among the tumours screened. * denotes C5/Stem-A tumours. Tumours with MYCN and LIN28B mRNA expression > black dotted line = high expression (+++); between black and blue lines were regarded as having intermediate expression (++). Data represents mean ± SEM of at least 3 independent experiments. Where reported, error bars represent SEM

A

PDX #ID	C5 PDX	MYCN mRNA	MYCN protein	LIN28B mRNA	LIN28B protein
Mayo 4	#PH038	++	+	+	-
Mayo 5	#PH039	++	++	-	-
Mayo 11	#PH077	+++	+++	-	-
Mayo 9	#PH054	++	+	-	-
Mayo 1	#PH018	++	-	++	+++
Mayo 2	#PH034	+	-	-	-
Mayo 3	#PH036	+++	++	-	-
Mayo 6	#PH041	+++	++	+	-
Mayo 7	#PH048	++	++	+++	+++
WEHI #29	WEHI #29	++	++	+++	++
WEHI #36	WEHI #36	++	-	++	-
WEHI #91	WEHI #91	+++	+	-	-
WEHI #95	WEHI #95	+++	+++	++	+

MYCN ab: clone number B8.4.B (monoclonal)
LIN28B Ab: Cat#4196 (polyclonal)

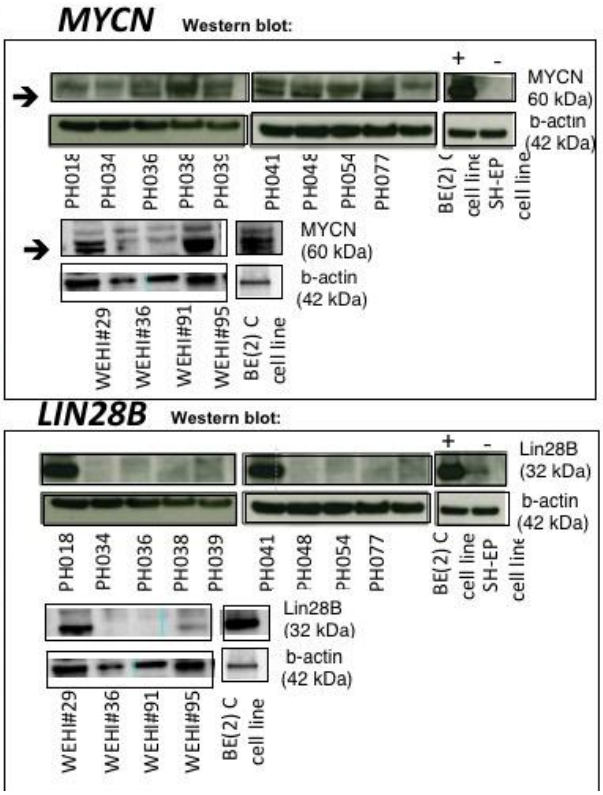

Figure 3.4: MYCN and LIN28B protein and mRNA expression of 12 C5/Stem-A PDX. (A) Table shows average expression levels of RT-qPCR and western blot analysis of MYCN and LIN28B expressions; MYCN protein band as indicated by the black arrow (the lower of the two bands at 60kDa); -/+ negligible expression, + low expression, ++ intermediate expression, +++ high expression relative to this cohort and control cell lines. CH1, known to have over-expression of *MYCN, LIN28B and HMGA2* (Helland et al., 2011). RT-qPCR and western blot data represents mean expression patterns of at least 3 experiments. Where reported, error bars represent SEM (B) Representative western blot analysis of MYCN and LIN28B protein from one blot. Westen blot analysis using biological replicates in 3 independent mice were performed for each PDX and average expression was documented in the table. BE(2)C neuroblastoma cell line known to over-express MYCN and LIN28B protein was used as control. B-actin was used as loading control.

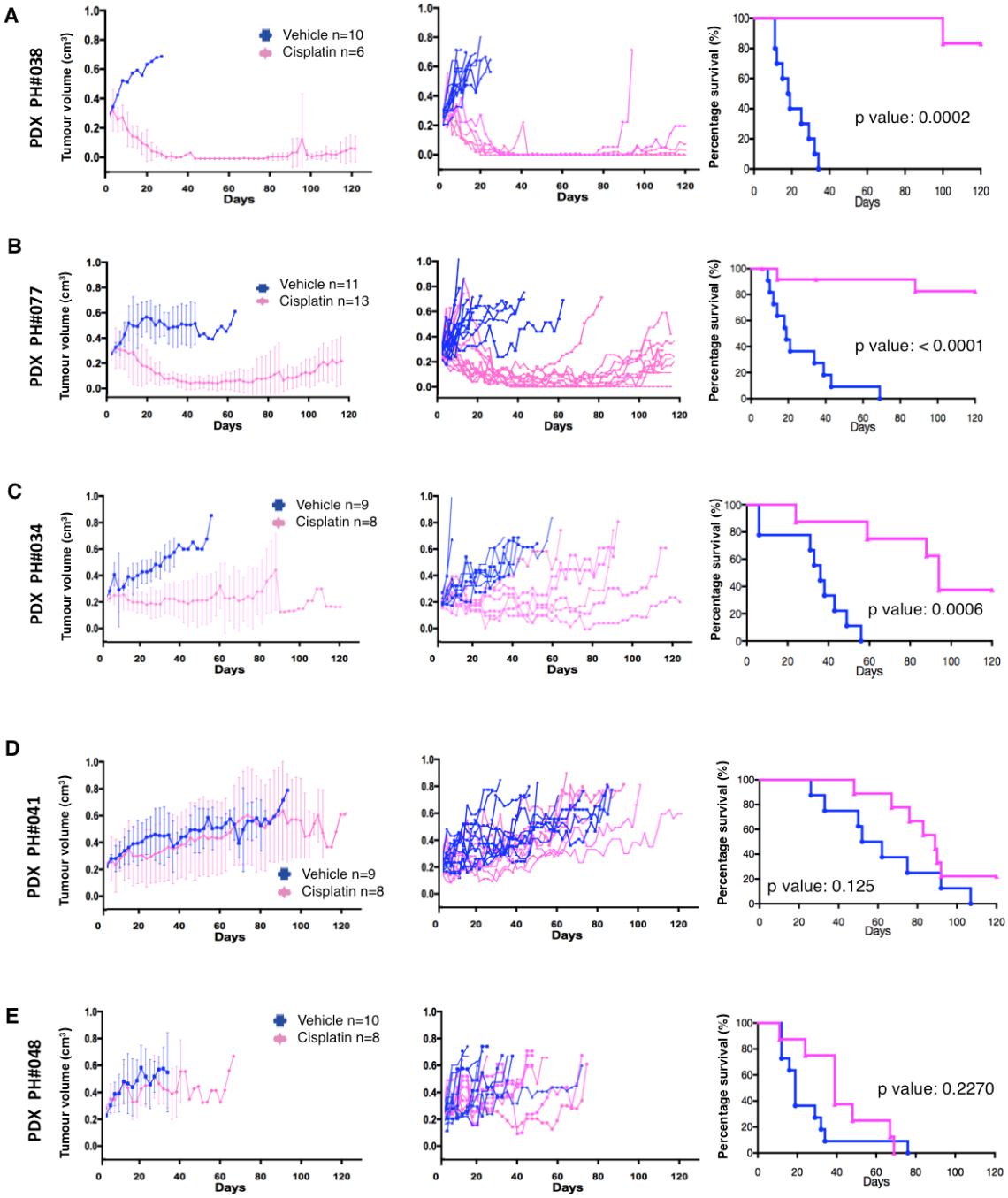
A
PDX PH#038
Tumour volume (cm³)
Vehicle n=10
Cisplatin n=6
Days
Percentage survival (%)
p value: 0.0002
B
PDX PH#077
Vehicle n=11
Cisplatin n=13
p value: < 0.0001
C
PDX PH#034
Vehicle n=9
Cisplatin n=8
p value: 0.0006
D
PDX PH#041
Vehicle n=9
Cisplatin n=8
p value: 0.125
E
PDX PH#048
Vehicle n=10
Cisplatin n=8
p value: 0.2270

Figure 3.5: Heterogeneous response to platinum therapy in C5/Stem-A PDX cohort. Representative patterns of cisplatin response in five C5/Stem-A PDX ranging from (A,B) cisplatin sensitive, (C) cisplatin resistant and (D,E) cisplatin refractory. Left panel: shows average tumour volume for each PDX treated with cisplatin (pink) and vehicle (blue); Middle panel: Individual spaghetti plots of each mouse treated with cisplatin (pink) and vehicle (blue) and Right panel: Kaplan-Meier survival analysis demonstrating TTH of cisplatin treated mice compared to vehicle treatment. Cisplatin was administered at 4mg/kg on D1, D8 and D18 via the peritoneum. PDX were deemed "cisplatin sensitive" if the average PDX tumor volume of the recipient mice underwent initial tumor regression with complete remission (CR, defined as tumor volume < 0.2 cm^3) or partial remission (PR, defined as reduction in tumor volume of > 30% from baseline) followed by progressive disease (PD, an increase in tumor volume of >20% from 0.2 cm^3 or nadir post-treatment, if nadir ≥ 0.2 cm^3) occurring ≥ 100 days from start of treatment; "cisplatin resistant" if initial tumor regression (CR or PR) or stable disease (SD) was followed by PD within 100 days; or "cisplatin refractory" if three or more mice bearing that PDX had tumors which failed to respond (no CR, PR or SD) during cisplatin treatment (day 1 - 18)(Topp et al., 2014). Data represents mean ± SEM. Where reported, error bars represent SEM

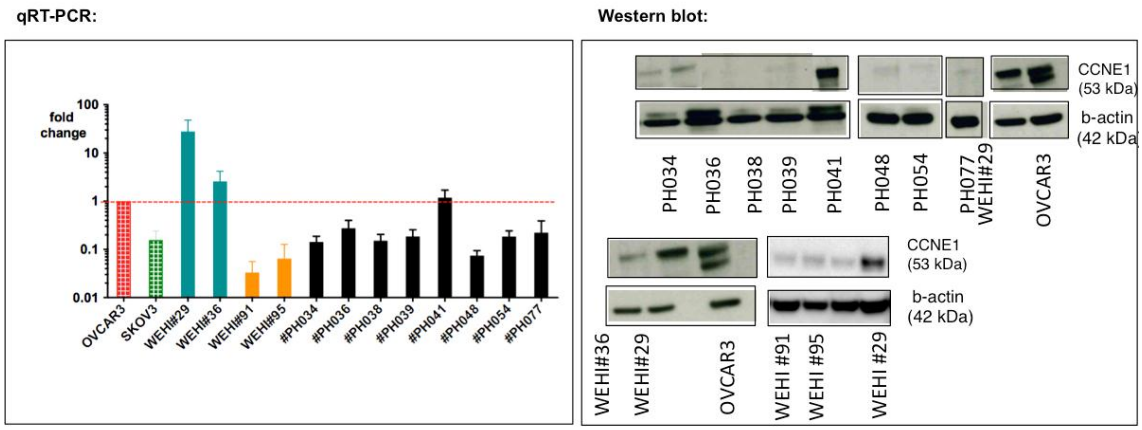

Figure 3.6: CCNE1 mRNA and protein expression of 12 C5/Stem-A PDX. (A) Table shows average mRNA expression levels from RT-qPCR analysis of *CCNE1* mRNA expressions relative to OVCAR3 control. OVCAR3 (Etemadmoghadam et al., 2010) , previously shown to have over-expression of *CCNE1*. Data represents mean ± SEM of at least 3 experiments. Where reported, error bars represent SEM. (B) Representative western blot analysis of CCNE1 protein from one blot. Westen blot analysis using biological replicates in 3 independent mice were performed for each PDX and average expression was documented in table 3.5. OVCAR3 (Etemadmoghadam et al., 2010) cell line and WEHI #29 (Topp et al., 2014), known to over-express CCNE1 protein was used as control. B-actin was used as loading control.

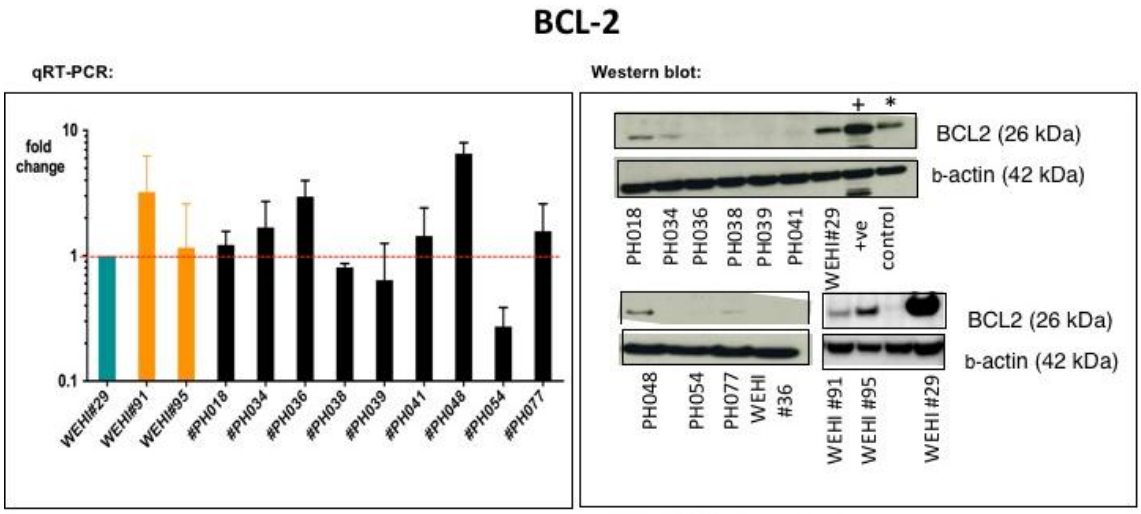

Figure 3.7: BCL2 mRNA and protein expression of 12 C5/Stem-A PDX. (A) Table shows average mRNA expression levels from RT-qPCR analysis of *BCL2* mRNA expressions relative to WEHI#29 control. WEHI#29 (Topp et al., 2014), known to have over-expression of *BCL2.* Data represents mean ± SEM of at least 3 experiments. Where reported, error bars represent SEM. (B) Representative western blot analysis of BCL2 protein from one blot. Westen blot analysis using biological replicates in 3 independent mice were performed for each PDX and average expression was documented in (table 3.5). WEHI#29 (Topp et al., 2014) and HL60 (Benito et al., 1997) known to over-express BCL2 protein was used as positive control. B-actin was used as loading control.

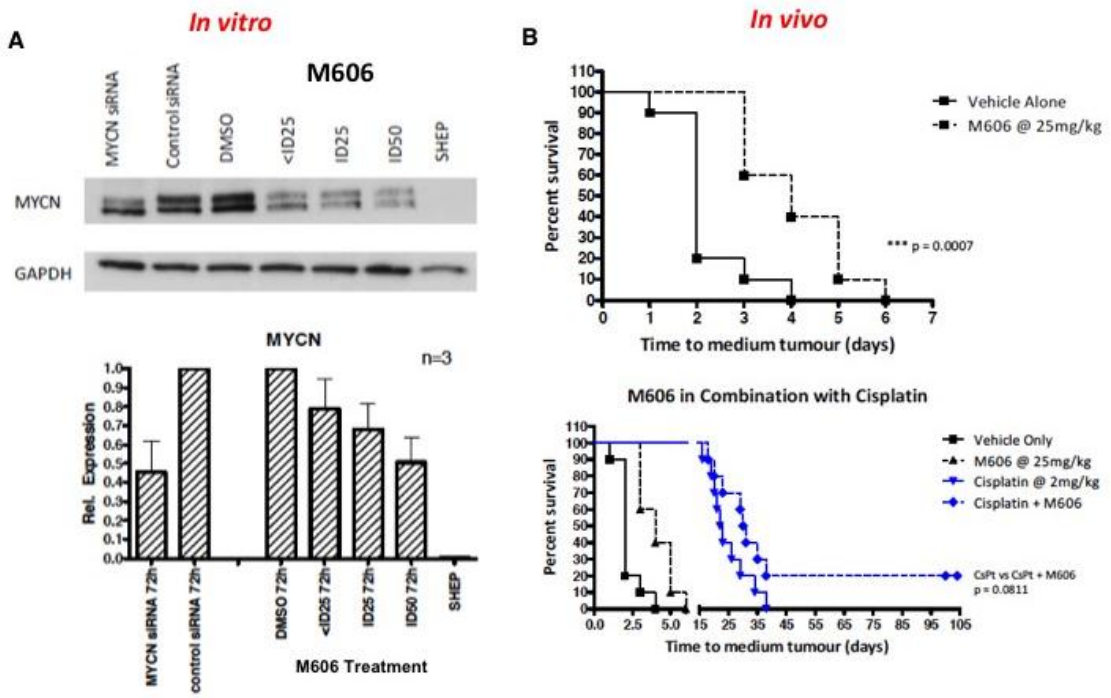

Figure 3.8: M606 inhibits MYCN and shows activity *in vitro* and *in vivo*. (A) *in vitro* analysis shows M606 inhibits MYCN protein. (B) *in vivo* activity of M606 in transgenic MYCN amplified neuroblatoma mice models. Figure adapted from collaborator at Children's Cancer Institute Australia, Sydney (Cheung, 2012). ID25 = growth inhibitory concentration at 25%; ID50 = growth inhibitory concentration at 50%

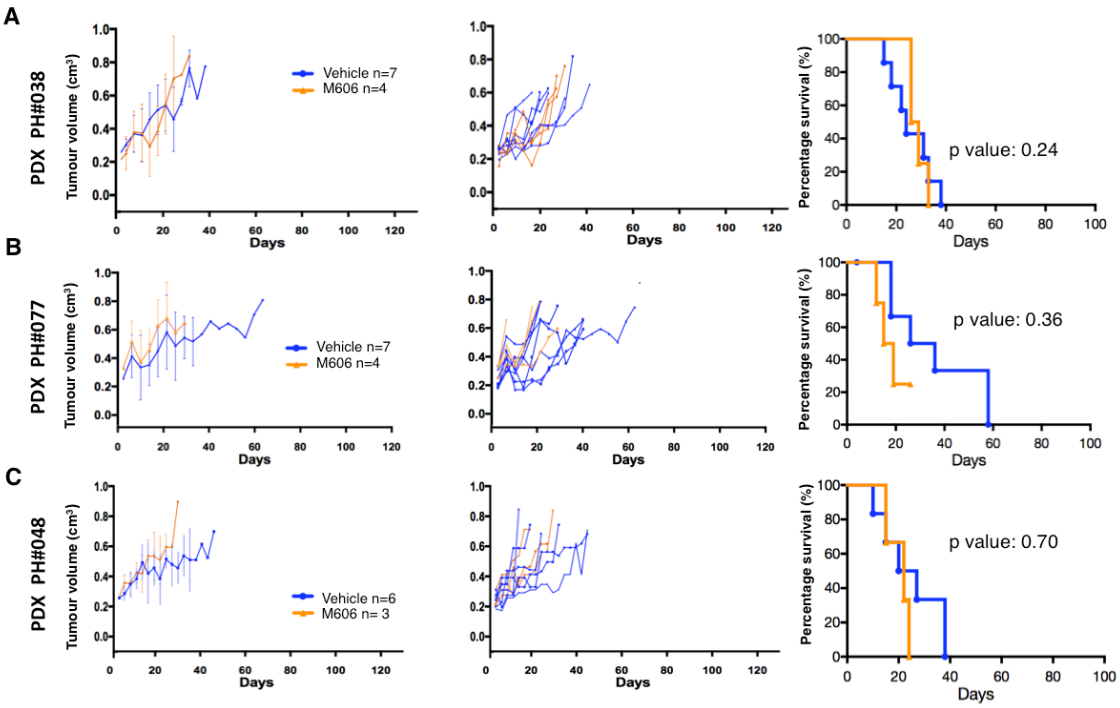
A
PDX PH#038
Tumour volume (cm³)
Vehicle n=7
M606 n=4
Days
Percentage survival (%)
p value: 0.24
B
PDX PH#077
Vehicle n=7
M606 n=4
p value: 0.36
C
PDX PH#048
Vehicle n=6
M606 n= 3
p value: 0.70

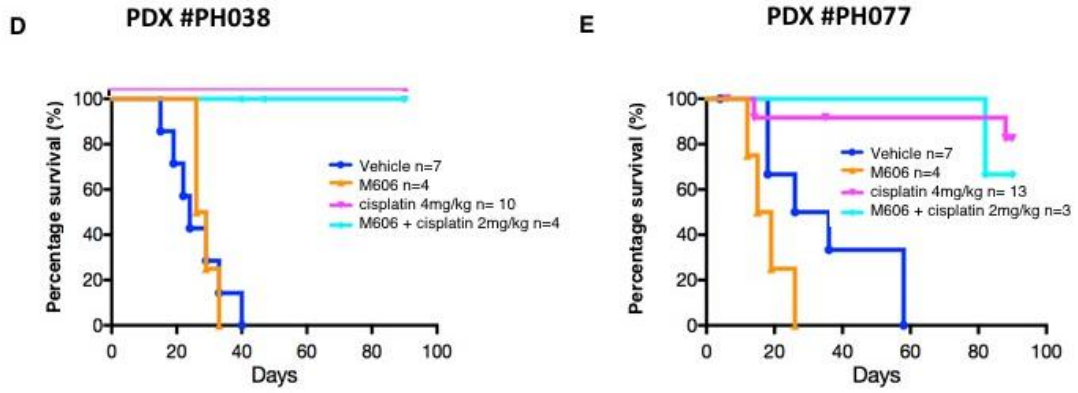
D
PDX #PH038
Percentage survival (%)
Vehicle n=7
M606 n=4
cisplatin 4mg/kg n= 10
M606 + cisplatin 2mg/kg n=4
Days
E
PDX #PH077
Vehicle n=7
M606 n=4
cisplatin 4mg/kg n= 13
M606 + cisplatin 2mg/kg n=3

Figure 3.9: No response to M606 in *MYCN* over-expressed C5/Stem-A PDX. M606 response in three C5/Stem-A PDX (A, B, C) shows no response to M606 monotherapy. Left panel: shows average tumour volume for each PDX treated with M606 (yellow) and vehicle (blue); Middle panel: Individual spaghetti plots of each mouse treated with M606 (yellow) and vehicle (blue) and Right panel: Kaplan - Meier survival analysis demonstrating TTH of M606 (yellow) treated mice compared to vehicle (blue) treatment. M606 was administered at 40mg/kg on daily Monday to Friday for 3 weeks via the peritoneum. Combination treatment with M606 and cisplatin was used in two PDX (D,E) shows no increase in TTH between combination of M606 and cisplatin (light blue) compared to cisplatin alone (pink). Combination regimen: M606 was administered at 40mg/kg on daily Monday to Friday for 3 weeks via the peritoneum while cisplatin was administered at 2mg/kg on D1, D8 and D18 via the peritoneum (light blue) and cisplatin monotherapy was administered at 2mg/kg on D1, D8 and D18 via the peritoneum with vehicle DMSO daily Monday to Friday for 3 weeks via the peritoneum (pink). Number of mice used as depicted in the figure. Data represents mean ± SEM. Where reported, error bars represent SEM.

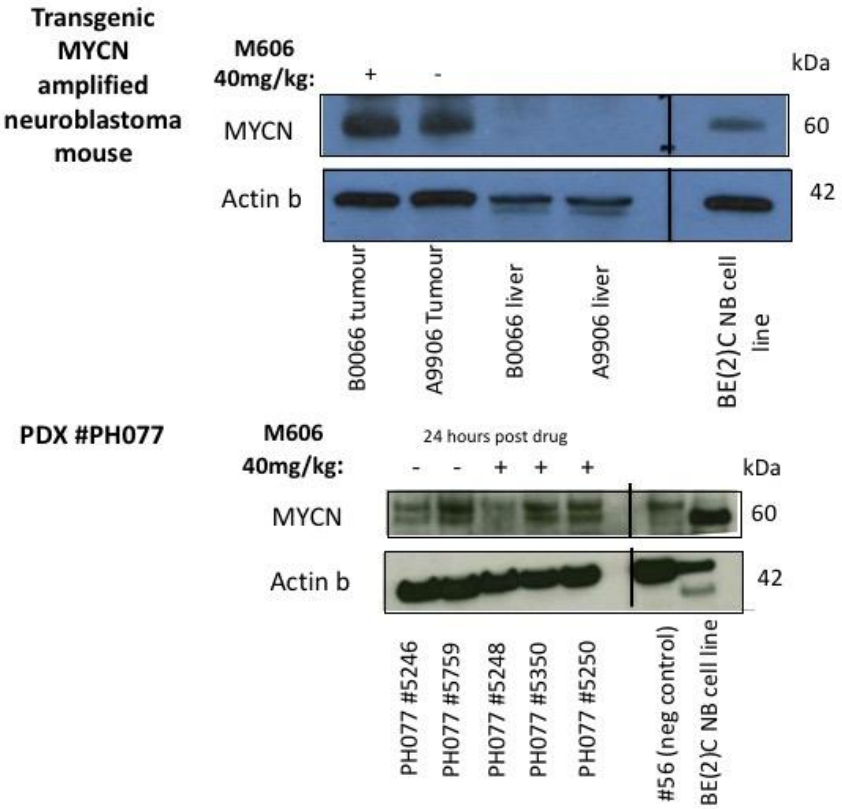

Figure 3.10: No appreciable inhibition of MYCN in PDX and transgenic MYCN amplified neuroblastoma mouse model. Western blot analysis performed on M606 treated transgenic MYCN amplified neuroblastoma mouse (upper panel) and PDX #PH077 (lower panel) shows no appreciable inhibition of MYCN protein. Mice were treated with 40mg/kg M606 or vehicle (DMSO) and harvested 12 hours post treatment for western blot analysis. Three separate mice from PDX #PH077 were treated with M606 with the above mentioned doses and tumours were analysed using western blot analysis. BE(2)C neuroblastoma cell line known to over-express MYCN protein was used as control. B-actin was used as loading control.

Chapter IV:

Utility of BET Bromodomain inhibitors in C5/ Stem-A HGSOC

4.1 Introduction

As the novel inhibitor identified by a generic screen (M606) did not induce durable tumour regression in the C5/Stem-A HGSOC PDX tested, we considered alternative targeting strategies. As previously described, the C5/Stem-A subtype of HGSOC is characterized by high expression of transcription factors such as *SOX11*, *HOXA7*, *HOXA9*, *HMGA2*, and *TCF7L1* and low expression of ovarian tumour markers (MUC1 and MUC16) (Tothill et al., 2008). This subtype also characteristically displays enrichment of the chromatin modification gene sets (Tan et al., 2013a) (figure 4.1). In addition to deregulation of the MYCN pathway, the Stem-A/C5 subtype has also been shown to upregulate WNT/PCP pathway genes and cadherin signaling pathway members, including N-cadherin and P-cadherin (Asad et al., 2014; Tothill et al., 2008), all of which could be relevant for biomarker selection and therapeutic targeting.

Our increasing understanding of cancer genetics and epigenetics not only implicates epigenetic regulators in the initiation and maintenance of cancer but also highlights an opportunity for therapeutic intervention (Fong et al., 2015). One of the most promising class of epigenetic modulating compounds to emerge, is that of small molecule inhibitors targeting the bromodomains of BET family proteins (BRD2, BRD3, BRD4 and BRDT). Recent research has established a compelling rationale for targeting BRD4 in cancer. BRD4 influences mitotic progression (Dey et al., 2009) and is a critical regulator of transcriptional elongation, by mediating the interaction with the positive transcription elongation factor B (pTEFb) (Yang et al., 2005). BRD4 is a chromatin reader that regulates transcription through linking histone acetylation and core components of the translational apparatus (Rathert et al., 2015). Additionally, BRD4 has also been detected in oncogenic rearrangements that lead to highly tumorigenic fusion proteins, as in the case of the BRD4-NUT fusion gene, which product is driven by the BRD4 promoter (Filippakopoulos et al., 2010). Small molecule BET inhibitors prevent binding of BET

proteins (ie: BRD4) to acetylated histones (Nicodeme et al., 2011) and inhibit transcriptional activation of BET target genes attenuating cell growth and survival through several mechanisms including down-regulation of critical oncogenes like *MYC/MYCN/BCL-2* (Delmore et al., 2011; Puissant et al., 2013; Wyce et al., 2013).

Recently, reports have emerged to suggest BRD4 inhibitor sensitivity is associated with *c-MYC* expression in AML (Zuber, 2011) and multiple myeloma (Delmore et al., 2011) or with MYCN expression in neuroblastoma (Puissant et al., 2013) and HGSOC (Baratta et al., 2015). Specifically in HGSOC, JQ1 sensitivity correlated with *c-MYC/MYCN* mRNA levels *in vitro* (Baratta et al., 2015). JQ1 is a potent, selective small-molecule inhibitor of BET bromodomains (Filippakopoulos et al., 2010). It is a thieno-triazolo-1,4-diazepine that displaces BET bromodomains from chromatin by competitively binding to the acetyl-lysine recognition pocket. Baratta et al subsequently performed *in vivo* studies, using one *MYCN* overexpressing HGSOC PDX and one PDX with high *c-MYC* expression, which resulted in abrogation of tumour growth when treated with JQ1 compared to vehicle controls over 30-50 days. No effect was observed in the HGSOC PDX that did not overexpress either *MYCN* or *c-MYC* (Baratta et al., 2015). In addition, exposure to BET inhibitors lead to rapid transcriptional suppression of key proto-oncogenes, such as *c-MYC, MYCN* and *BCL2* (Dawson et al., 2011; Delmore et al., 2011; Wyce et al., 2013). Importantly, overexpression of these proto-oncogenes from a heterologous promoter have been reported to partially alleviate the anticancer effects of the BET bromodomain inhibitor (JQ1/ I-BET) (Dawson et al., 2011; Delmore et al., 2011) suggesting the downstream effects on the proto – oncogenes are mediated by BRD4 inhibition.

Most data suggesting correlation between *MYCN/c-MYC* and BRD4 inhibition were obtained from drug screen analysis using relatively few representative cell lines from any single cancer histiotype (Marcotte et al., 2016). When an shRNA screen and

integrated molecular analyses was performed on a large panel of breast cancer cell lines (77 cell lines), contrary to previous published reports, JQ1 sensitivity did not reflect impaired *MYC* expression with both sensitive and resistant cell lines displaying similar *MYC* mRNA levels and the addition of exogenous *MYC* did not convert JQ1 sensitive lines to resistant cell lines (Marcotte et al., 2016). Instead, the use of comprehensive integrative analysis revealed an alternative explanation that correlated JQ1 resistance with PIK3CA mutation in breast cancer cell lines (Marcotte et al., 2016; Shu and Polyak, 2017). Similarly, in acute myeloid leukemia, the Wnt/ b-catenin pathway was implicated in resistance to BET bromodomain inhibitor therapy as chromatin-bound BRD4 was globally reduced in resistant cells, replaced by b-catenin, but the expression of key target genes, such as *MYC,* remained unaltered (Fong et al., 2015) (figure 4.2(A). In addition, inhibition of the Wnt/b-catenin signalling restored BET bromodomain inhibitor sensitivity *in vitro* and *in vivo* (Fong et al., 2015). Of potential relevance, enrichment of the Wnt/PCP pathway in the C5/ Stem-A subtype of HGSOC has been previously described (Asad et al., 2014). There is now convincing evidence demonstrating phenotypic outcomes may depend on the level at which the Wnt pathway is activated, and that the strength of the signal is regulated at multiple points in the signalling cascade including the Wnt/Fzd receptor complex (Phesse et al., 2016). FZD7 is of particular interest, as it is the Wnt receptor most commonly up-regulated in several different cancers and can also transmit signals through the different arms of the Wnt pathway referred to broadly as canonical (Wnt/β-catenin dependent) and non-canonical (Wnt/β-catenin independent) (figure 1.6). The Wnt - FZD interaction is promiscuous with a single Wnt ligand able to bind multiple FZD protein receptors and vice versa. FZD7 is able to form a complex with R-Spo3 to bind WNT5A and activate the Wnt/PCP signalling by inducing Sdc4-dependent, clathrin-mediated endocytosis

(Ohkawara et al., 2011), relevant for the C5/ Stem-A subtype of HGSOC (Asad et al., 2014)

Furthermore, in basal-like breast cancer cells the recruitment of BRD4 at the *WNT5A* super-enhancer was shown to be dependent on the interaction between TWIST, a key transcription activator of epithelial- mesenchymal transition (EMT), and BRD4 (Shi et al., 2014) (figure 4.2(B). Indeed, supporting the hypothesis that Wnt-FZD7-BRD4 is relevant for C5/ Stem-A HGSOC, *FZD7* and *MYCN* gene expression were compared across a cohort of ovarian cancer patient samples and a direct correlation between these two genes were observed (figure 4.3(A). Also of note was the high levels of *FZD7* expression in tumour samples within the C5/Stem-A molecular subtype observed in 2 separate sets of ovarian tumour samples analysed (figure (4.3 (B).

Much emphasis has focused on transcriptional effects of BET inhibitors being highly specific to the cell type being examined. Therefore, in this chapter the utility of BRD4 inhibitor therapy *in vitro* and *in vivo* in C5/Stem-A HGSOC PDX will be described. Using a larger number of C5/Stem-A HGSOC PDX, the efficacy of BRD4 inhibitor therapy was explored and ChIP-qPCR analysis employed to validate some known BRD4 target genes in order to enhance our understanding of the mechanisms underlying its anti-tumour activity.

4.2 Results

In vivo BRD4 inhibition in C5/ Stem-A PDX

The suggested hypothesis that *MYCN* expression levels might predict for sensitivity to BET bromodomain inhibitor therapy in HGSOC (Baratta et al., 2015) was evaluated using a larger number of C5/ Stem-A HGSOC PDX than had been previously characterised by Baratta *et al*. To identify whether BET bromodomain inhibition impacted on tumour regression, JQ1 and I-BET-762 (previously shown to have BRD4 anti-tumour activity (Baratta et al., 2015)) were used to determine treatment response in a range of MYCN pathway over-expressing C5/Stem-A HGSOC PDX.

One PDX (#PH077) was initially treated intra-peritoneally (i/p) with 50mg/kg daily of JQ1 or vehicle for 21 days. However, due to treatment toxicity (weight loss) observed in this PDX (figure 4.4), JQ1 treatment was subsequently ceased.

Alternatively, a second BET bromodomain inhibitor, I-BET762, was evaluated, as prior studies observed BRD4 anti-tumour activity in several solid malignancies including HGSOC and multiple myeloma (Baratta et al., 2015; Chaidos et al., 2014; Wyce et al., 2013), importantly, with an improved tolerability profile. In light of our previous experience with the BET bromodomain inhibitor, JQ1, non-tumour bearing mice were initially tested using escalating doses of I-BET762 up to 30 mg/kg alternate days. When no toxicities were observed, two tumour bearing *MYCN* high C5/Stem-A HGSOC PDX (#PH038, #PH041) were subsequently treated by oral gavage with I-BET-762 or vehicle at a low dose of 15 mg/kg on alternate days. Stabilisation of disease was observed in one PDX (PH#041), compared with increased tumour growth in vehicle-treated mice (figure (4.5 (A). No tumour regression or stabilisation of disease was observed in the other PDX tested (PH#038) (figure 4.5 (B). Median TTH for PDX with stabilisation of disease on I-BET-762, PH#041, was 51.5 days compared to 33 days (p value <0.0896) for vehicle treated mice (Table 4.1). Although there was no obvious tumour regression with PDX

PH#038, median TTH for I-BET-762 treated PDX was 28 days compared to 16 days for vehicle treated controls (Table 4.1) suggesting potential drug activity at higher doses. Importantly, no significant toxicity was observed and treatment was well tolerated.

This encouraging preliminary data led to parallel *in vivo* studies in the Scott laboratory using an increased dose of I-BET-762, 25mg/kg alternate days via oral gavage and the cohort was expanded to include a total of five C5/Stem-A HGSOC PDX (four *MYCN* overexpressing PDX and one with normal *MYCN* expression: #PH038, #PH077, #PH041, #PH048 and #PH034, respectively). Intriguingly, only one of the five C5/Stem-A HGSOC PDX treated resulted in tumour regression (#PH041, median time to tumour harvest (TTH) of > 120 days compared to 68 days in vehicle treated mice) while the four other PDXs did not (three *MYCN* high PDX and one *MYCN* low PDX) (data not shown). Collectively, the data suggest that BRD4 inhibitor therapy appeared to have anti-tumour activity, however, *MYCN* expression alone may not be a faithful predictive marker for BET bromodomain inhibitor therapy in the C5/Stem-A HGSOC and its effect is likely to be restricted to a subset of HGSOC. Understanding this restriction may allow more successful targeting of this intriguing therapeutic approach. Subsequently, I moved to explore the mechanistic basis for response to BET bromodomain inhibitors in C5/Stem-A HGSOC using *in vitro* models.

Depletion of *FZD7* increases sensitivity to BET bromodomain inhibitor, I-BET-762.

To study the function of *FZD7* in C5/Stem-A HGSOC, stable knockdown of *FZD7* was performed using two different FZD7-targeting shRNA hairpins (referred to as shFZD7.1 and shFZD7.2) (Asad et al., 2014) on two C5/Stem-A HGSOC human cell lines with high endogenous expression of *FZD7* and *TP53* mutation, CH1 and OV17R (figure 4.6(A). shRNA sequences targeting luciferase (shLuci) were used as controls.

Cells were subsequently selected for 48hours with puromycin and plated for further experiments. The PA1 cell line which is a terato-carinoma cell line, which although was molecularly subtyped as Stem-A by Tan *et al* (Tan, Miow et al., 2013) was not used in these experiments as it did not harbor a *TP53* mutation. Unfortunately, the OV17R knockdown shFZD7.2 cells did not survive after subsequent passaging, thus experiments performed exploring the effects of *FZD7* on BET bromodomain inhibitors for OV17R involved only one stable knockdown line, shFZD7.1 (figure 4.6(B).

When cellular proliferation was assessed, the knockdown of *FZD7* alone did not appear to impair cell viability over the 6-day timeframe compared to luciferase controls of both the C5/Stem-A HGSOC representative cell lines (Figure 4.7 – left panel). However, when cells were treated with 1um BET bromodomain inhibitor, I-BET-762 (~IC30 for both cell lines), a non-significant reduction in cellular proliferation in the luciferase control cells were observed in both CH1 and OV17R cells (Figure 4.7 – middle panel). The suppression of cellular proliferation with I-BET-762 was further enhanced by the depletion of *FZD7* (figure 4.7 – right panel).

To determine whether the I-BET-762 effect was influenced by *FZD7*, I-BET-762 dose-response curves were performed on the same *FZD7* knockdown cell lines and their luciferase controls. Cells lacking *FZD7* were more sensitive to BET bromodomain inhibition in both cell lines as evident by a lower IC50 (Figure 4.7(C). Upon *FZD7* depletion, there was a consistent and significant > 9 fold average reduction of the half maximal effective concentration (IC50) of I-BET-762 in CH1 (figure 5.7 (D – left panel) and ~2 fold reduction in OV17R (figure 5.7 (D – right panel).

Depletion of *FZD7* makes C5/Stem-A cells more vulnerable to I-BET-762 mediated cell death.

Next, to determine the mechanism behind the increased sensitivity to BET bromodomain inhibitor therapy with depletion of *FZD7*, an apoptosis assay was used to detect caspase 3 and 7 activity in the *FZD7* knockdown and luciferase control cells following treatment with DMSO, 1um, 2.5um and 5um I-BET-762 respectively. Cells were initially treated with DMSO (control) or I-BET-762 at concentrations shown in Figure 4.8 for five days prior to analysis of cell viability via luminescence and apoptotic activity via fluorescence. As shown in figure 4.8, there was no significant difference in caspase 3/7 activity when *FZD7* depleted cells were treated with DMSO control compared to luciferase control. However, when 1um, 2.5um and 5um I-BET-762 was added to OV17R cell lines, an increase in caspase 3/7 activity of >2 fold was observed in *FZD7* depleted cell lines compared to their luciferase controls (Figure 4.8(B). A similar significant trend was observed in the shFZD7.2 stable clone of CH1 with an increase in caspase 3/7 activity of >1.6 fold following treatment with 1um, 2.5um and 5um I-BET-762 respectively (figure 4.8(A).

TWIST1 is regulated by *FZD7* and *FZD7-TWIST1* axis

Through parallel work performed in the Huang lab at Cancer Science Institute, Singapore, we found that *FZD7* regulated the transcription factor, TWIST1 via epigenetic modulation (Tan, Asad, Heong et al; manuscript submitted). The relationship between *FZD7* and *TWIST1* was subsequently explored in greater detail using ovarian patient tumour samples (figure 4.9(A-C). The mRNA expression of *TWIST1* and *FZD7* were observed to correlate with one another (R^2=0.48) (figure 4.9(A). In addition, using genes that were highly correlated with both *FZD7* and *TWIST1* genes, a signature was devised, *FZD7-TWIST1* signature, consisting of 77 genes that have a positive Spearman correlation (Rho > +0.3)(Appendix 1). This signature was subsequently tested on ovarian tumour samples according to their known individual molecular subtypes and

observed that the two subtypes with the worst prognosis, Stem-A and Mes subtype, had the highest *FZD7-TWIST1* signature score (figure 4.9 (B). The *FZD7-TWIST1* signature was also tested on ovarian tumours with correlated clinical outcomes of overall survival and disease free survival (Tan, T.Z., Yang, H., 2015) and showed that tumours with high *FZD7-TWIST1* signatures were associated with a poorer outcome (figure 4.9(C).

We then employed the *FZD7-TWIST1* signature on the C5/Stem-A HGSOC PDXs previously treated with I-BET-762 as a proof-of-principle exercise. Based on the small numbers, we observed that the *FZD7-TWIST1* signature score inversely correlated with duration of response (Rho=-0.445; p 0.45). The PDX with the highest *FZD7-TWIST1* signature score, PH#048, was observed to have the shortest response to bromodomain inhibitor therapy while lower scores (<1.0) had a longer TTH (figure 4.9(D). This signature will need to be further validated in other datasets of bromodomain inhibitor treated PDX/ patient population in the future.

Reduced BRD4 recruitment to *MYCN, WNT5A* and *BCL2* promoter region with depletion of *FZD7*

BRD4 has been previously shown in both haematological and solid tumour malignancies to regulate transcription of several key genes including *WNT5A* in breast cancer (Shi et al., 2014), *MYCN* in neuroblastoma (Henssen et al., 2016; Puissant et al., 2013), *c-MYC* in leukemia (Dawson et al., 2011), and *BCL2* in neuroblastoma (Wyce et al., 2013). Hitherto, BRD4 has not been shown to directly regulate these genes in EOC. To explore the role of *FZD7* and its influence on BRD4 on the direct regulation of these genes (ie: *MYCN, c-MYC, BCL2* and *WNT5A*) in C5/Stem-A HGSOC, BRD4 ChIP-qPCR was performed using specific primers (figure 4.10). Primers for *MYCN, c-MYC* and *WNT5A* were validated from the literature albeit in other tumour types while primers used for *BCL2* were specifically designed (figure 4.10(E).

From the BRD4 ChIP-qPCR results (figure 4.10), significant reduction in BRD4 enrichment was detected at the promoter regions of *MYCN* (MYCN1)(figure 5.10(A) and *WNT5A* (figure 5.10(B) at 543bp to 523bp and at 129bp to 109 bp downstream of TSS respectively in *FZD7* depleted CH1 cells compared to their luciferase controls. A similar trend was observed in OV17R cells with depleted *FZD7* at these regions when compared to their luciferase control counterparts, but did not reach statistical significance (figure 4.10 (A,B). BRD4 enrichment at exon1 region of *MYCN* 36bp to 56bp upstream of TSS (*MYCN2*) showed reduction in BRD4 enrichment in *FZD7* depleted OV17R cells and in one knockdown clone in CH1 cells (shFZD7.1), but did not reach significance likely due to low efficiency of the primer pair (figure 4.10(A). A similar trend of reduced BRD4 enrichment in depleted *FZD7* cells of both cell lines was also observed at the *BCL2* promoter region -4207bp to -3825bp downstream from the TSS (Figure 4.10(C), albeit not statistical significant. Intriguingly, contrary to the trend observed in other genes, BRD4 enrichment was detected at the exon 1 region of c-myc (figure 4.10(D) 14bp to 34 bp upstream of TSS in *FZD7* depleted CH1 and OV17R cell lines.

TWIST1 recruits BRD4 to *MYCN, WNT5A* and *BCL2* promoter

Shi *et al* previously reported that the BRD4 – TWIST interaction is mediated by binding of BD2 of BRD4 to lysine-acetylated TWIST and this interaction is required for the recruitment of BRD4 to the *WNT5A* superenhancer in basal like breast cancer cells (Shi et al., 2014). To evaluate whether this interaction occurs in the C5/Stem-A HGSOC model, a BRD4 IP (figure 4.11(A) was initially performed to establish that the monoclonal BRD4 antibody (clone number: #13440) used can indeed successfully pull down BRD4 proteins and would be suitable as a positive control. To test if *TWIST1* recruited BRD4 via a similar mechanism as observed by Shi *et al*, TWIST1 antibody

(clone number: #2F8E7) was used in the Co-IP. However, when we attempted to probe for the TWIST1 protein on the blot containing proteins from the BRD4 pulldown, the concentration of protein loaded was insufficient to detect a TWIST1 band. Instead, we used the TWIST1 antibody for immunoprecipitation and BRD4 antibody for immunoblotting in a Co-IP performed on CH1 and OV17R cells which proved TWIST1 - BRD4 interaction (figure 4.11(B). Due to certain difficulties with the TWIST1 antibody, this will need to be further validated using mass spectrometry analysis to prove whether BRD4 was indeed present in the TWIST1 pulldown.

A *TWIST1* ChIP-qPCR was subsequently performed in parallel on parental CH1 cell lines using primer pairs shown in figure 4.11(C) (Tan, Asad, Heong et al; manuscript submitted). *TWIST1* enrichment was observed on the *MYCN1, WNT5A* and *BCL2* regions previously shown to also bind BRD4 (figure 4.10).

Collectively, the BRD4 and *TWIST1* ChIP-qPCR data confirms the findings that *MYCN, BCL2* and *WNT5A* are *TWIST1* target genes. The depletion of *FZD7*, which results in reduction of *TWIST1* (figure 4.9(A), leads to decreased BRD4 binding to promoters of *TWIST1* target genes (*MYCN, BCL2* and *WNT5A*) but not to *c-MYC* which does not appear to be a *TWIST1* target gene (figure 4.11(C).

TWIST1 mediates response to the bromodomain inhibitor, I-BET-762

When *TWIST1* levels were interrogated in C5/Stem-A HGSOC *FZD7* depleted model, *TWIST1* mRNA expression was found to significantly correlate with the mRNA levels of *FZD7* (figure 4.12 (A). Therefore, to further explore the role of *TWIST1*, *FZD7* knockdown stable clones in CH1 and OV17R cells, which have consequently low levels of *TWIST1* were manipulated to induce an increase in *TWIST1* expression which we coined *TWIST1* rescue (shFZD7.1^{twist1}). Using these cells, I-BET-762 dose response curves were performed which showed that the increased sensitivity of sh*FZD7* to BET

bromodomain inhibitor could be reversed by inducing the expression of the *TWIST1* gene (figure 4.12 (B).

The *TWIST1* rescue cells were shown to significantly overexpress *BCL2*, a pro-survival gene, in both the cell lines and *WNT5A* in the CH1 cell line compared to their sh*FZD7* counterpart (figure5.12(C). Collectively, the data would suggest that BET bromodomain inhibitor sensitivity in C5/Stem-A HGSOC is heavily influenced by *TWIST1* expression and that the FZD7-TWIST1 axis may be relevant to predict sensitivity to bromodomain inhibitor therapy in these cell lines.

Synergism between sh*FZD7* and bromodomain inhibitor in the suppression of TWIST1 target genes

To evaluate whether depletion of *FZD7,* with consequent TWIST1 depletion, in combination with BET bromodomain inhibition lead to further downregulation of the TWIST1 target genes in the C5/Stem-A HGSOC. From the RT-qPCR results of CH1 and OV17R cell lines used (figure 4.13), depletion of *FZD7* consistently downregulated *WNT5A, MYCN and BCL2* expression in both CH1 and OV17R cell lines (figure 4.13(A,B). *c-MYC* was downregulated only in the CH1 cell lines (figure 4.13(C) while *LIN28B* mRNA was observed to be overexpressed with knockdown of *FZD7* in both the cell lines (figure 4.13 (C, D). With the addition of 1um I-BET-762 therapy, a reduction in *WNT5A*, *MYCN* and *BCL2* levels were observed compared to luciferase control DMSO treated cells, of which, the *BCL2* down-regulation was significant in the CH1 cell line (figure 4.13 (A,B). There were no obvious changes to the *c-MYC and LIN28B* expression levels in both these cell lines with I-BET-762 treatment (figure 4.13 (C,D). However, when cells were both *FZD7* depleted and treated with 1um of a BRD4 inhibitor, synergistic down-regulation of expression was observed in *WNT5A, MYCN* and *BCL2* in both CH1 and OV17R cells, of which the down-regulation of *MYCN* and

BCL2 expression was significant. Intriguingly, *c-MYC* expression remained unchanged with the addition of 1um I-BET-762 in CH1 cell lines (figure 4.13 (C) but was significantly down-regulated only in the *FZD7* depleted OV17R cell line (figure 4.13 (D). A similar observation was observed with the expression of *LIN28B* mRNA. In *FZD7* replete cells, BET bromodomain inhibitor therapy had no effect on *LIN28B* levels however, in the *FZD7* depleted state, the addition of 1um I-BET-762 did not result in significant down-regulation of *LIN28B* expression in both CH1 and OV17R cell lines compared to luciferase control cells (figure 4.13 (C,D).

Collectively, these data would suggest synergy between the BET bromodomain inhibitor therapy and depletion of the FZD7-TWIST1 axis. The inhibition of *FZD7* results in reduced proliferation (figure 4.6) and increase in apoptosis (figure 4.8) through reduction of *TWIST1* mediated direct regulation of *WNT5A*, *MYCN* and *BCL2*. When coupled with a BET bromodomain inhibitor, this results in further reduction of these genes.

Inhibition of *FZD7-TWIST1* axis by porcupine inhibitor, compound 59 (C59), mimics inhibition of *FZD7*

The data thus far would suggest that the Wnt pathway plays a role in modulating I-BET-762 activity. Inhibition of PORCN blocks the secretion of wnt by inhibiting their interaction with Wntless (WLS) that transports them to the plasma membrane (figure 4.14(A) (Madan and Virshup, 2015). In data obtained in parallel performed in the Huang Lab, Cancer Science Institute, Singapore, we observed that C59, a porcupine inhibitor, inhibited the *FZD7-TWIST1* axis (Appendix 2) (Tan, Asad, Heong et al; manuscript submitted). Hence, C59 (red box) was used in subsequent experiments (figure 4.14(B). Using a growth assay, cells were treated at varying drug concentrations of I-BET-762 with the addition of 10 nm porcupine inhibitor, C59, and cell viability

was subsequently assessed after 5 days. In the luciferase control cells C59, significantly enhanced I-BET-762 sensitivity, more significantly in the CH1 cells, as evident by a lower IC50 (figure 4.14(B). Conversely, C59 did not further enhance sensitivity to I-BET-762 in *FZD7* depleted CH1 and OV17R cells (figure 5.13(B).

4.3 Discussion

In this chapter, including additional experiments performed in parallel in the lab, we established that *MYCN* overexpression was not a faithful predictor of BET bromodomain inhibitior sensitivity in C5/Stem-A HGSOC. This was highlighted in several other studies demonstrating that although BET inhibitors appear to show great potential, the anti-proliferative and anti-tumour effects were quite variable (Kurimchak et al., 2016; Lockwood et al., 2012; Mertz et al., 2011). In addition, cancer cells were observed to not only acquire resistance to BET bromodomain inhibitors (Fong et al., 2015) but reports have also emerged specifically in ovarian cancer demonstrating acquired resistance through adaptive kinome reprogramming, suggesting single agent BET inhibitor treatment may not provide durable responses (Kurimchak et al., 2016)

Recent studies investigating resistance mechanisms of BET bromodomain inhibitors demonstrated the relevance of the Wnt/b-catenin pathway in promoting downstream signalling of BRD4 and that blockade of the b-catenin pathway restored sensitivity to BET inhibition (Fong et al., 2015; Rathert et al., 2015). Indeed, using C5/Stem-A HGSOC representative cell lines, *FZD7-TWIST1* axis was shown to play an essential role in the regulation of BET bromodomain inhibitor sensitivity. Depletion of *FZD7*, which consequently lead to the inhibition of *TWIST1* (figure 4.12(A), resulted in increased sensitivity to I-BET-762 with consequent attenuation of cell proliferation (figure 4.7) and increased apoptosis (figure 4.8). Alternatively, rescuing the *TWIST1*expression in sh*FZD7* clones nullified the effect of sh*FZD7* to BET bromodomain inhibitors (figure 4.12(B) demonstrating that *TWIST1* mediated the increased in sensitivity to BET bromodomain inhibitor, I-BET-762, in the sh*FZD7* clones.

TWIST1 has been associated with many types of aggressive solid tumor malignancies and is implicated in cancer initiation, progression and metastasis (Qin et

al., 2011). Importantly, *TWIST1* has been reported to override oncogene-induced cell senescence and apoptosis (Ansieau et al., 2008; Valsesia-Wittmann et al., 2004), has been shown to be implicated in chemotherapy resistance (Cheng et al., 2007), enhances cancer stem cell properties through EMT (Mani et al., 2008), and facilitate metastasis (Qin et al., 2009; Qin et al., 2011). In our model, *FZD7* and *TWIST1* expression appeared to correlate as depletion of *FZD7* resulted in reduction in *TWIST1* expression and interestingly, the exogenous overexpression of *TWIST1* lead to increased resistance to BET bromodomain inhibitor therapy.

The depletion of *FZD7* reduced BRD4 recruitment to the promoter region of *MYCN*, *WNT5A* and *BCL2* (figure 4.10) with consequent reduction in the mRNA expression of these genes (figure 4.13). Conversely, at the *c-MYC* promoter, BRD4 recruitment was increased in *FZD7* depleted cell lines. Intriguingly, the synergistic effects previously observed in the other genes with the combination of *FZD7* and BET inhibition was not demonstrated in this gene. We hypothesize that TWIST1, as a transcription factor, recruits BRD4 to its target genes and stabilizes BRD4 to the promoter regions of TWIST1 target genes, which includes *MYCN, WNT5A* and *BCL2,* to exert its effect as an epigenetic reader. *C-MYC* has been shown to be down-regulated in the C5/Stem-A HGSOC subtype (TCGA., 2011) and does not appear to be a *TWIST1* target gene (Figure 4.11(C). Hence, its regulation is independent of the *FZD7-TWIST1* axis. In addition, suppression of *TWIST1* results in an increase in global histone acetylation (Appendix 3) (Tan, Asad, Heong et al; manuscript submitted) through modulation of the p300/PCAF histone acetyltransferase further explaining the increase in BRD4 enrichment at the c-*MYC* promoter region.

Emerging studies have suggested that intrinsic resistance mechanisms observed following BET inhibitor therapy may be tumour-type specific (Kurimchak et al., 2016; Shi et al., 2014) and the data thus far would suggest that the Wnt pathway plays a role in

modulating I-BET-762 activity in C5/Stem-A HGSOC. Indeed, when a porcupine inhibitor, C59, was combined with the BET bromodomain inhibitor, I-BET-762, treated luciferase control cells of CH1 and OV17R demonstrated sensitivity to BET bromodomain inhibitor therapy similar to *FZD7* depleted cells further suggesting that the Wnt pathway via *FZD7-TWIST1* axis influenced BET bromodomain inhibitor sensitivity in C5/Stem-A HGSOC cells. Therefore, this further strengthens the hypothesis that in order to improve BRD4 sensitivity in C5/Stem-A HGSOC, modulating the *FZD7-TWIST1* axis may yield greater success. Future works should focus on validating this data in the PDX model in an effort to inform a clinical trial and improve our understanding of resistance mechanisms to BET bromodomain inhibitors in C5/Stem-A HGSOC

Strikingly, *BCL2* mRNA was observed to be consistently elevated in both the shFZD7.1^{twist1} rescue cell lines (figure 4.12 (C). *BCL2* is an oncogene that prevented cell death and promotes tumorigenesis by enabling cells that would normally undergo apoptosis to survive thereby facilitating acquisition of additional oncogenic lesions to drive neoplastic transformation (Delbridge et al., 2016). Based on this data, it would appear at least theoretically, that combining a BH3-mimetic with BET bromodomain inhibitor therapy could provide more durable responses in C5/Stem-A HGSOC. In light of the recently approved BH3-mimetic, venetoclax, future works could focus on understanding the role of *BCL2*, if any, in the resistance of C5/Stem-A HGSOC to BET bromodomain inhibitors and utility of BH3-mimetic in combination with BET bromodomain inhibitors

Furthermore, Kurimchak *et al* further demonstrated that ovarian cancer cells rewire their receptor tyrosine kinase (RTK) networks uniquely to BET protein inhibition. In ovarian cancer cells sensitive to BET inhibition, RTK and downstream AKT/ PI3K signalling activity was reduced, whereas in a subset of ovarian cancer cells

inherently resistant to BRD4 inhibitors, BET inhibition activated RTKs (fibroblast growth factor receptor 1-3, EGFR and IGR1R) and their downstream signalling pathways, which included AKT and RAF-MEK-ERK activity (Kurimchak et al., 2016). Importantly, combination treatment of BET inhibitor concurrently with a PI3K/mTOR inhibitor or MEK inhibitor in JQ1 resistant cell lines, blocks cell growth, RNA polymerase II phosphorylation and MYC protein levels to a greater extent than single agent therapy in a selected subset of ovarian cancer cell lines (Kurimchak et al., 2016). Collectively, these findings would suggest that single agent BET bromodomain therapy may not provide durable therapeutic responses in ovarian cancer and will likely require combination therapies. The ability to accurately select the right combination strategies based on a biomarker would be crucial as the effects of BET bromodomain inhibitor therapy appear to be cell-type specific.

Despite their molecular similarity, it is clear that the C5/Stem-A HGSOC subtype is heterogenous and a single underlying common genetic aberration is unlikely to be the only driver of tumorigenesis in this subtype. Hence, using a signature, like the *FZD7-TWIST1* signature, which includes a constellation of genes relevant for this subtype may be more useful to predict the sensitivity of tumours to BET bromodomain inhibitors. Future work could focus on refining and validating the FZD7-TWIST1 signature score on both PDX models and patient tumours.

In conclusion, we have established that *MYCN* is not a faithful predictor of BET bromodomain inhibitor sensitivity in C5/Stem-A HGSOC. We have also demonstrated that the wnt pathway via *FZD7-TWIST1* axis influences sensitivity to BET bromodomain inhibition. Through the overexpression of *TWIST1*, (TWIST1 rescue) overexpression of *BCL2* was strikingly observed in *FZD7* depleted cell lines and this was associated with increased resistance to BET bromodomain inhibition. Future work could focus on the role of *TWIST1* and *BCL2* in the regulation of histone acetylation to

enhance our understanding of the relevant epigenetic regulators responsible for BET bromodomain inhibition sensitivity and thus allow for better prediction of their activity in C5/Stem-A HGSOC.

Table 4.1

HGSOC PDX	Time to PD (d) I-BET762	Median TTH (d) vehicle	Median TTH (d) I-BET762	n (recipient mice)	Hazard ratio (HR) 95% CI
#PH038	12	16	28	4, 3	HR 0.52^{ns} (0.10-2.57)
#PH041	29	33	51.5	2, 2	HR 0.19^{ns} (0.01 – 2.4)

Table 4.1: Relative growth rates of independent PDX and median survival following I-BET762 therapy. Recipient mice PDX were randomized to treatment with vehicle or I-BET762 monotherapy 15mg/kg, alternate days when tumour volume reached 0.18-0.3 cm^3. Time to Progressive disease (PD) was defined as the time (in days) from beginning of I-BET762 treatment to an increase in average tumor volume (for that treatment group) of >20% from the nadir. Time to Harvest (TTH) was defined as the time (in days) from the beginning of treatment to day of harvest at 0.7 cm^3 and the median TTH was calculated and plotted using Kaplan-Meier curves (Prism version 7). Preliminary data showed PDX #PH038 did not have an appreciable response to I-BET762 when treated at a dose 15mg/kg alternate days. However, PDX #PH041 appeared to have initial regression however this was not durable lasting 29 days (time to PD). (p value for difference between 15mg/kg I-BET-762 and vehicle was not significant for all PDX treated however, PDX PH#041 had a trend towards significance with a p value < 0.08). Significance determined by Mantel-Cox test. ^{ns} p value not significant; *p value <0.05; **p value <0.01; *** p value <0.005. Hazard Ratio and 95% CI determined by Log Rank analysis.

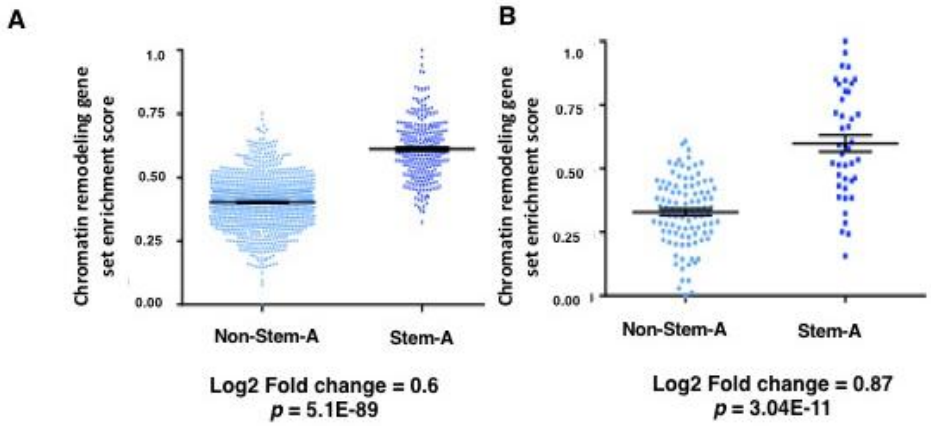

Figure 4.1: Stem-A/C5 ovarian cancer tumours upregulate chromatin remodeling genes. Enrichment of chromatin remodeling gene set (http://software.broadinstitute.org/gsea/msigdb/cards/CHROMATIN_REMODELING.html) consisting of 25 genes in ovarian cancer. Increased chromatin remodelling enrichment score (mean ± SEM) in Stem-A subtype compared to non- Stem-A subtype of A) ovarian cancer tumors (n = 1142; (Tan, Miow et al., 2013)), and similarly, B) ovarian cancer cell lines (n=142; (Tan, Miow et al., 2013)). The enrichment score is computed by single sample GSEA [(Verhaak et al., 2013); Pubmed ID: 23257362]. (Huang Lab, unpublished)

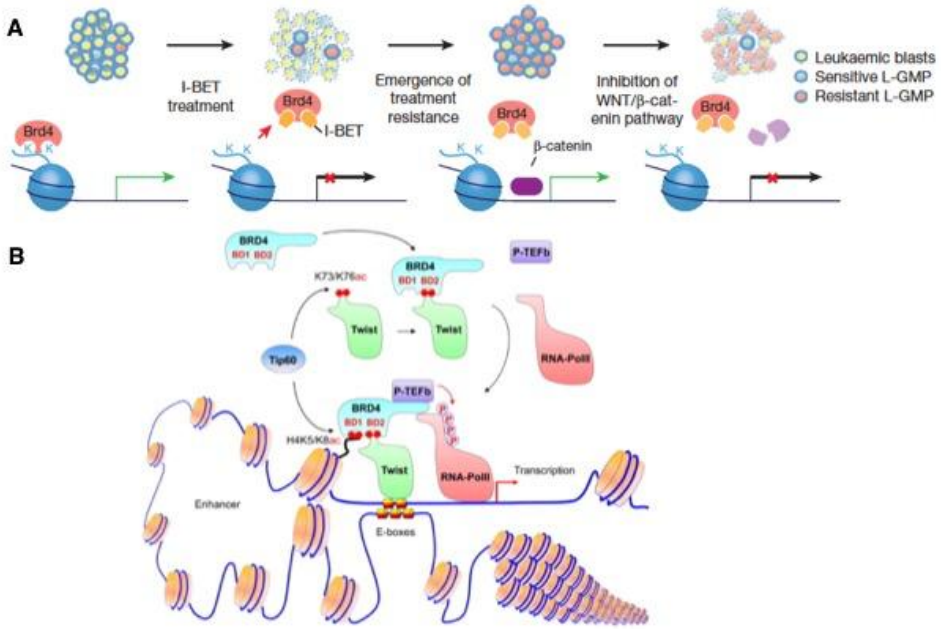

Figure 4.2: Wnt pathway responsible for BET bromodomain inhibitor resistance in leukemia models and regulates tumorigenesis via BRD4 in breast cancer. (A) Proposed model illustrating the role WNT/b-catenin pathway in BET bromodomain resistance in leukemic cells. Image adapted from Fong et al Nature 2015. (B) Proposed model illustrating the interaction of TWIST and BRD4 at the enhancer/ promoter of *WNT5A* reduced WNT5A expression and suppressed invasion, cancer stem cell (CSC)-like properties, and tumorigenicity of basal like breast cancer cells. Image adapted from Jian Shi et al Cancer Cell 2014

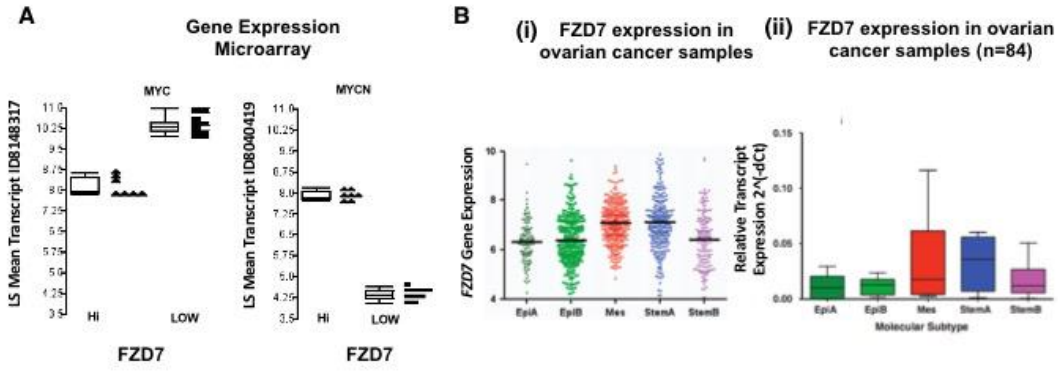

Figure 4.3: **FZD7 expression levels in ovarian cancer tumour samples and its relationship to *c-MYC* and *MYCN*** (A) Boxplot of *MYCN* (red box) and *c-MYC* expression stratified by *FZD7* expression level. The box indicates 1st quantile , median and 3rd quantile while the whiskers indicate the min and max expression level (Huang Lab; unpublished). (B) *FZD7* expression levels stratified by molecular subtypes on two independent ovarian tumour cohorts (i) data obtained from CSIOVDB database (n=3431) (Tan et al., 2015) and (ii) Ovarian tumour samples from our collaborators in japan (n=84). Adapted from M Asad et al; Cell Death and Disease 2015

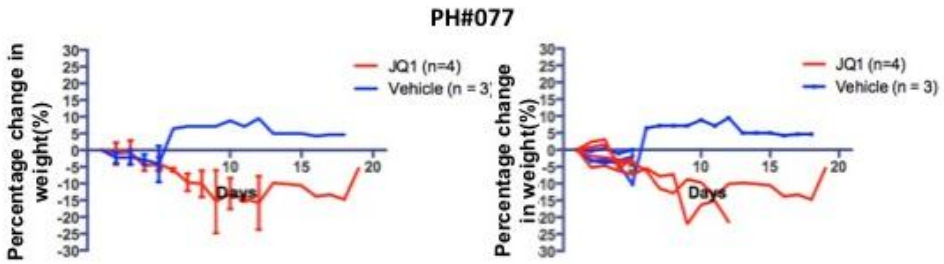

Figure 4.4: JQ1 *in vivo* toxicity. Percentage weight loss from baseline of PDX#077 treated with JQ1 monotherapy 50mg/kg or vehicle (DMSO) intraperitoneally. Left panel: mean percentage change ± SEM; right panel: percentage change in weight for each individual mice treated with JQ1 or vehicle. Where reported, error bars represent SEM.

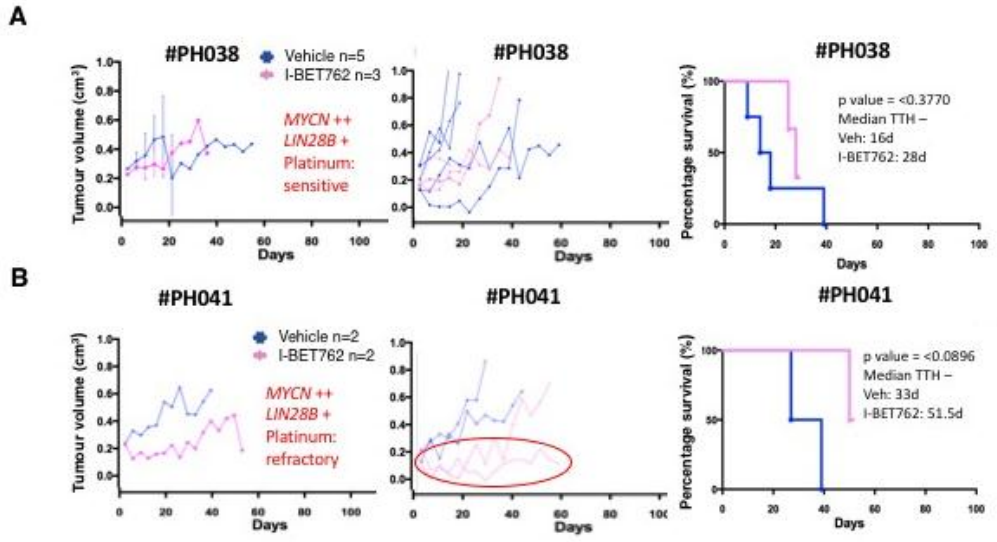

Figure 4.5: Low dose I-BET-762 demonstrates tumour stabilisation in one out of two PDX in vivo. I-BET-762 anti-tumour activity was evaluated in two PDX. Mice bearing PDX #PH038 and #PH041 were treated with vehicle (DMSO) or I-BET-762 15mg/kg alternate days intraperitoneally for maximum of 3 weeks starting on day 1. (A) #PH039 shows no appreciable anti-tumour activity and (B) #PH041 shows initial tumour stabilisation. Left panel: Graphs showing mean tumour volume ± SEM; Middle panel: individual spaghetti graphs; and right panel: KM curves shows tumour response to I-BET762 on two different PDX. P-value determined using log-rank tests with p value < 0.05 were considered to indicate statistical significance. Where reported, error bars represent SEM.

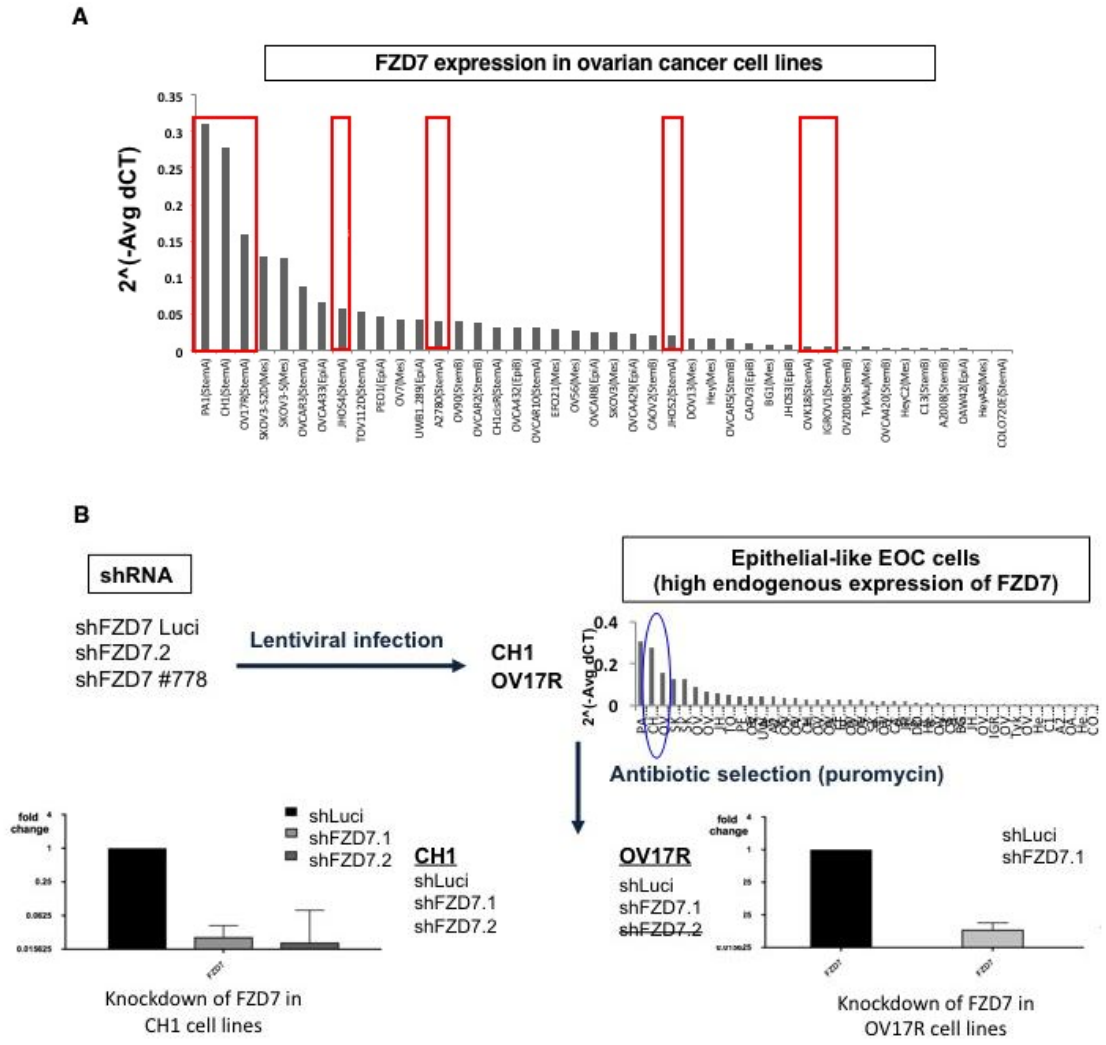

Figure 4.6: *FZD7* expression in ovarian cancer cell lines and experimental scheme of the in vitro shRNA knockdown using two C5/Stem-A HGSOC cell lines. (A) RT-qPCR showing variable endogenous *FZD7* expression observed in ovarian cancer cell lines. Red boxes indicate Stem-A cell lines with CH1 and OV17R displaying the highest endogenous FZD7 expression in Stem-A ovarian cancer cell lines. (PA1 was not used as it was not a HGSOC cell lines). (B) Diagram illustrating the workflow of CH1 and OV17R cells that were infected with each of the indicated shRNA, selected for 48hours with puromycin and plated for further experiments. shLuci is a control lentivirus.

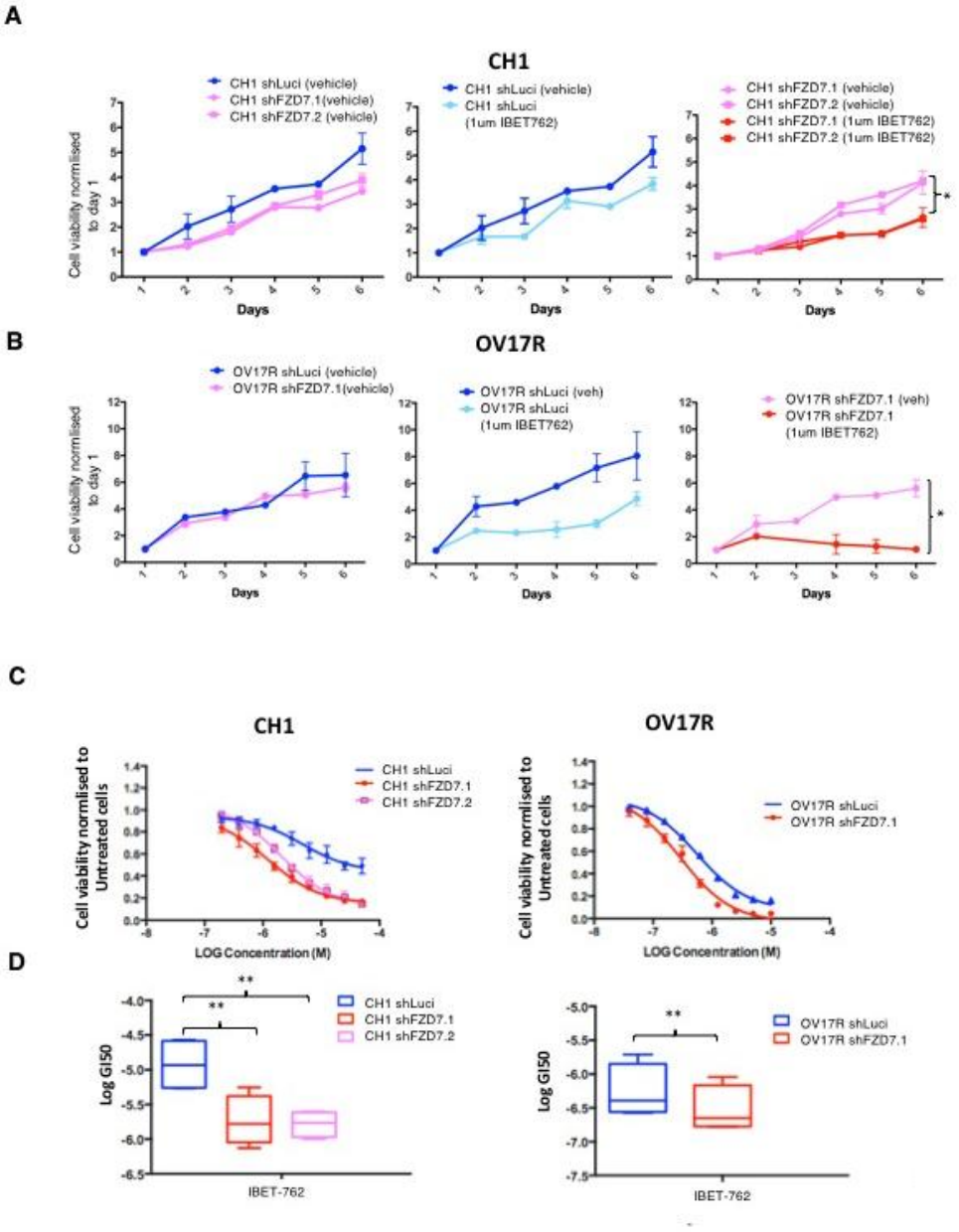
A
CH1
CH1 shLuci (vehicle)
CH1 shFZD7.1(vehicle)
CH1 shFZD7.2 (vehicle)
CH1 shLuci (vehicle)
CH1 shLuci
(1um IBET762)
CH1 shFZD7.1 (vehicle)
CH1 shFZD7.2 (vehicle)
CH1 shFZD7.1 (1um IBET762)
CH1 shFZD7.2 (1um IBET762)
Cell viability normlised to day 1
Days
B
OV17R
OV17R shLuci (vehicle)
OV17R shFZD7.1(vehicle)
OV17R shLuci (veh)
OV17R shLuci
(1um IBET762)
OV17R shFZD7.1 (veh)
OV17R shFZD7.1
(1um IBET762)
C
CH1
OV17R
Cell viability normlised to Untreated cells
LOG Concentration (M)
CH1 shLuci
CH1 shFZD7.1
CH1 shFZD7.2
OV17R shLuci
OV17R shFZD7.1
D
Log GI50
IBET-762

Figure 4.7: *FZD7* depletion impairs CH1 and OV17R proliferation and sensitizes cells to BRD4 inhibition. Line graphs shows mean proliferation curves ± SEM of at least 3 independent experiments, for days 1-6, with and without 1um of the active BRD4 inhibitor I-BET-762 for (A) CH1 cell lines and (B) OV17R cell lines. Left plane: vehicle treated shFZD7 and luciferase control cells; middle plane: vehicle and 1um I-BET-762 treated luciferase control cells, and right plane: vehicle and 1um I-BET-762 treated FZD7 depleted cells. Cell viability was measured using MTS assay and for each time point, was reported after normalization to the value obtained on day1. (C) I-BET-762 dose response curves in CH1 and OV17R cells infected with each of the indicated shRNA. Cell viability was measured using MTS assay and for each value was reported as a percentage of the effect obtained by employing the vehicle alone. Cells were treated for 5 days at varying concentrations of I-BET-762. (D) Comparison of the IC50 values obtained from the I-BET-762 dose response curves performed in the various conditions. Where reported, error bars represent SEM. Statistical significance was determined by student's t test * $p < 0.05$; ** $p < 0.01$.

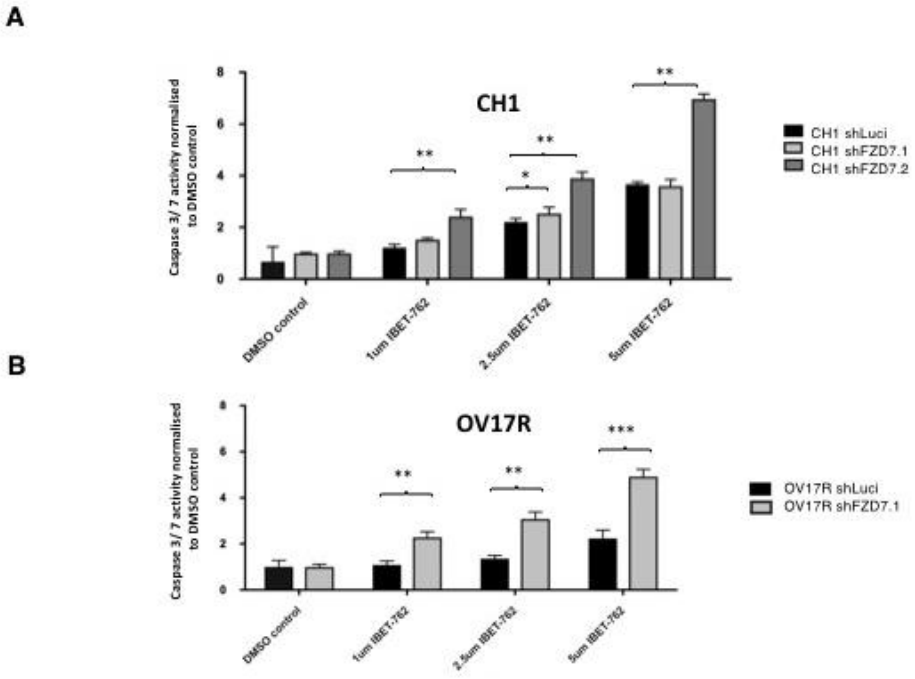

Figure 4.8: Depletion of *FZD7* makes C5/Stem-A cells more vulnerable to I-BET-762 mediated cell death. Apoptosis assay was used to detect caspase 3 and 7 activity in CH1 and OV17R cells infected with each of the indicated shRNA and subsequently treated with either vehicle (DMSO), 1um, 2.5um or 5um IBET762, respectively. Data represents mean ± SEM of at least 3 independent experiments. Statistical significance was determined by unpaired t test * $p < 0.05$; ** $p < 0.01$

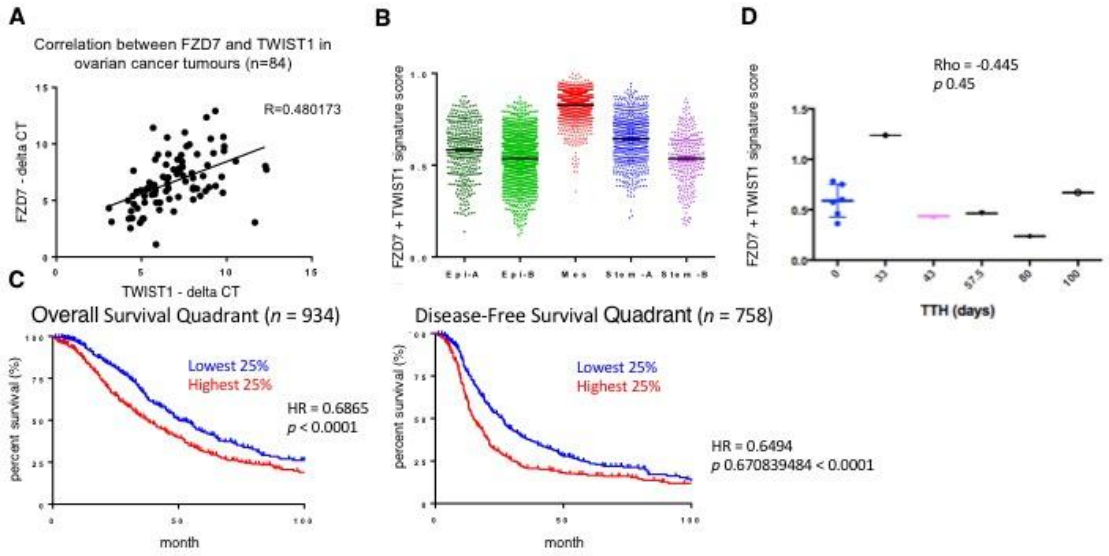

Figure 4.9: *FZD7-TWIST1* signature score in ovarian cancer patient tumours and PDX correlated with outcomes. (A) Correlation between mRNA expression of *FZD7* and *TWIST1* in ovarian cancer patient samples (n=84). (B) *FZD7-TWIST1* signature score stratified according to molecular subtypes in ovarian cancer patient samples from publicly available database, CSIOVDB (n=3431). Stem-A and Mes subtype has the highest *FZD7-TWIST1* signature score. Data represents mean ± SEM. (C) High *FZD7-TWIST1* signature score correlated with poorer overall and disease – free survival. Data from CSIOVDB (Tan et al., 2015). Disease – Free Survival is defined as time from date of diagnosis to date of first local or distant recurrence or disease progression whichever occurs first. Statistical significance was determined by log rank analysis. (D) FZD7-TWIST1 signature scores of all eleven C5/Stem-A HGSOC PDX from the Mayo cohort. Correlation of FZD7-TWIST1 signature scores with I-BET-762 treatment response was performed on five PDX that received drug (PH#048, PH#034, PH#038, PH#077, PH#041). (Blue dots) Six PDX that did not receive I-BET-762. TTH is the median time to tumour harvest in days.

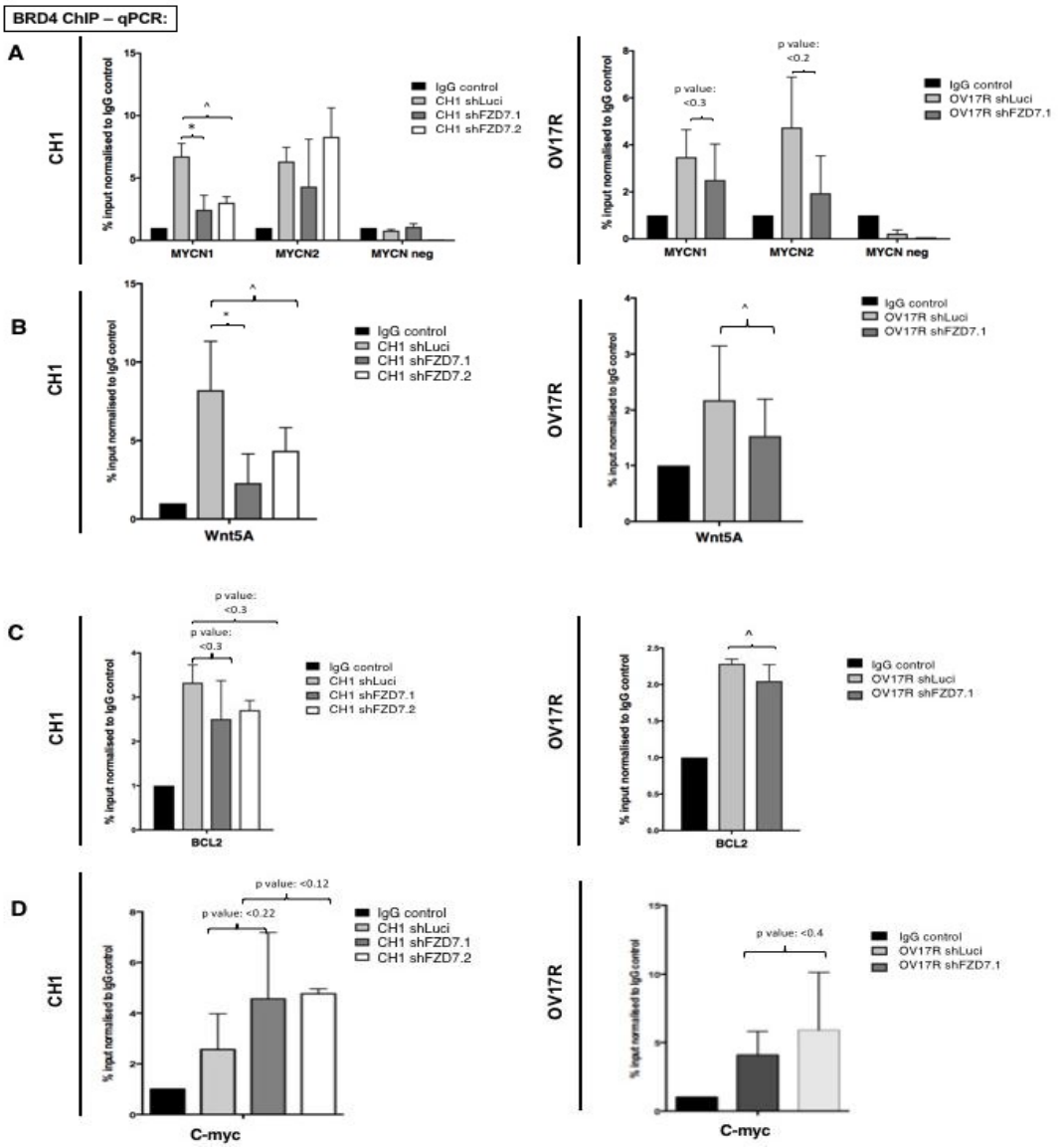

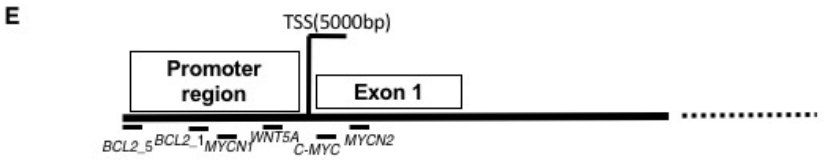

Flanking primers

	Distance relative to TSS			Reference
***MYCN* 1 promoter**	-543bp	to	-523bp	Puissant et al, Cancer Discovery 2013
***MYCN* 2 promoter**	+36bp	to	+56bp	Puissant et al, Cancer Discovery 2013
***Wnt5A* promoter**	-129bp	to	-109bp	Shi et al, Cancer Cell 2014
***C-MYC* promoter**	+14bp	to	+34bp	Dawson et al,
***BCL2_1* promoter**	-1859bp	to	-1547bp	Self – designed (sequence in methods)
***BCL2_5* promoter**	-4207bp	to	-3825bp	Self – designed (sequence in methods)

Figure 4.10: BRD4 recruitment at the promoter regions of *MYCN, WNT5A, BCL2* and *c-MYC* genes detected by ChIP-qPCR. Bar charts shows BRD4 ChIP-qPCR in FZD7 depleted CH1 and OV17R cell lines. Signals of IgG control and ChIP samples were normalised to input DNA and subsequently, results from ChIP samples were normalised again to IgG control. Reduced BRD4 enrichment at (A) *MYCN, (B)WNT5A* and (C)*BCL2* genes in *FZD7* depleted cells compared to luciferase controls and (D) increase in BRD4 enrichment at the *c-MYC* promoter region in both cell lines. (E) Promoter primers used in the ChIP-qPCR experiment arranged in order of their relative positions in relation to the TSS of the individual gene. Data represents mean ± SEM of at least 3 independent experiments. Statistical significance was determined by unpaired t test. ^$p<0.1$, * $p<0.05$; **$p<0.01$

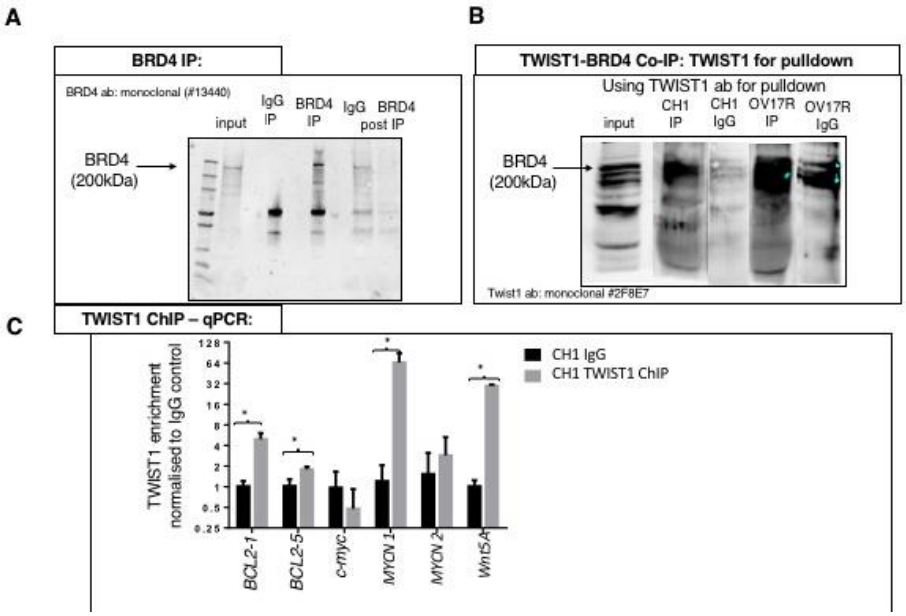

Figure 4.11: TWIST1 recruits BRD4 to *MYCN, WNT5A* and *BCL2* promoter.

(A) Endogenous BRD4 was immunoprecipitated using antibody (#13440) and examined by western blotting. (B) TWIST1-BRD4 Co-IP. TWIST1 was immunoprecipitated using #2F8E7 and analysed using BRD4 antibody #13440 by immunoblotting (Tan Ming; Huang Lab, Tan M, Asad M, Heong et al, manuscript submitted). (C) Bar charts shows TWIST1 ChIP-qPCR CH1 cell line. Signals of IgG control and ChIP samples were normalised to input DNA and subsequently, results from ChIP samples were normalised again to IgG control (Tan Ming; Huang Lab. Tan M, Asad M, Heong et al, manuscript submitted). Primer pairs used depicted previously in figure 5.10(E). Significant TWIST1 enrichment at *MYCN1* region, two regions of *BCL2* (BCL2-1 and BCL2-5) and *WNT5A* genes. Data represents mean ± SEM of at least 3 independent experiments. Statistical significance was determined by unpaired t test. ^$p<0.1$, * $p<0.05$; **$p<0.01$

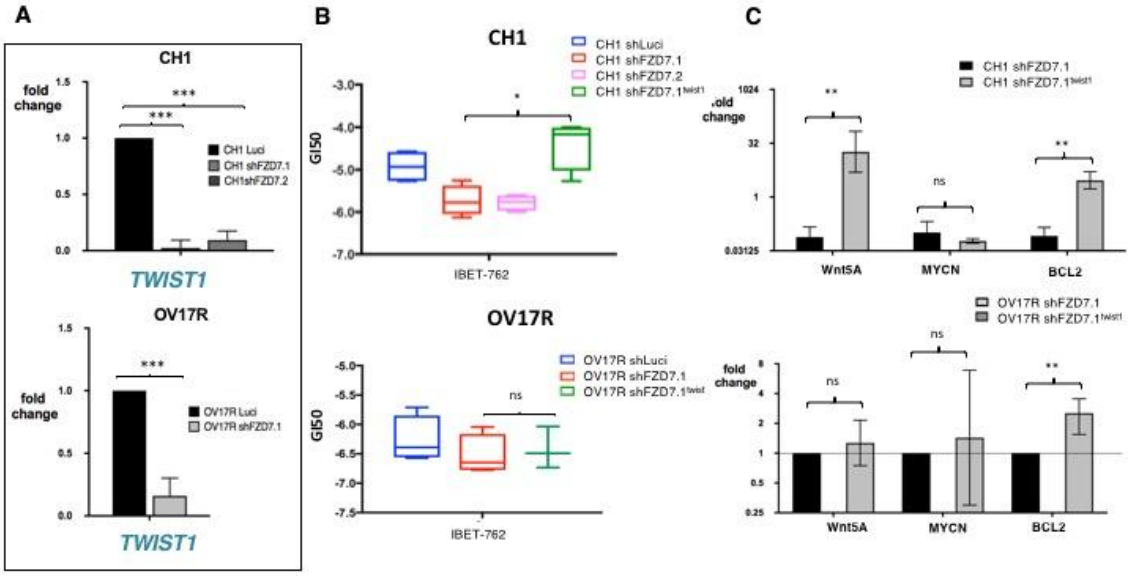

Figure 4.12: Depletion of *FZD7* results in down-regulation of *TWIST1* and rescue of *TWIST1* in *FZD7* knockdown leads to bromodomain inhibitor resistance. (A) RT-qPCR results show reduction of mRNA expression of *TWIST1* with inhibition of *FZD7*. Data represents mean ± SEM of at least 3 independent experiments. (B) Comparison of IC50 values obtained from I-BET-762 dose response curves performed in cells infected with each of the indicated shRNAs shows resistance to I-BET-762 in *TWIST1* rescue cells compared to their *FZD7* depleted controls. (C) RT-qPCR of *TWIST1* rescue CH1 and OV17R cells consistently overexpressed *BCL2* mRNA. Data represents mean ± SEM of at least 3 independent experiments. Where reported, error bars represent SEM. Statistical significance was determined by student's t test * p <0.05; **p<0.01

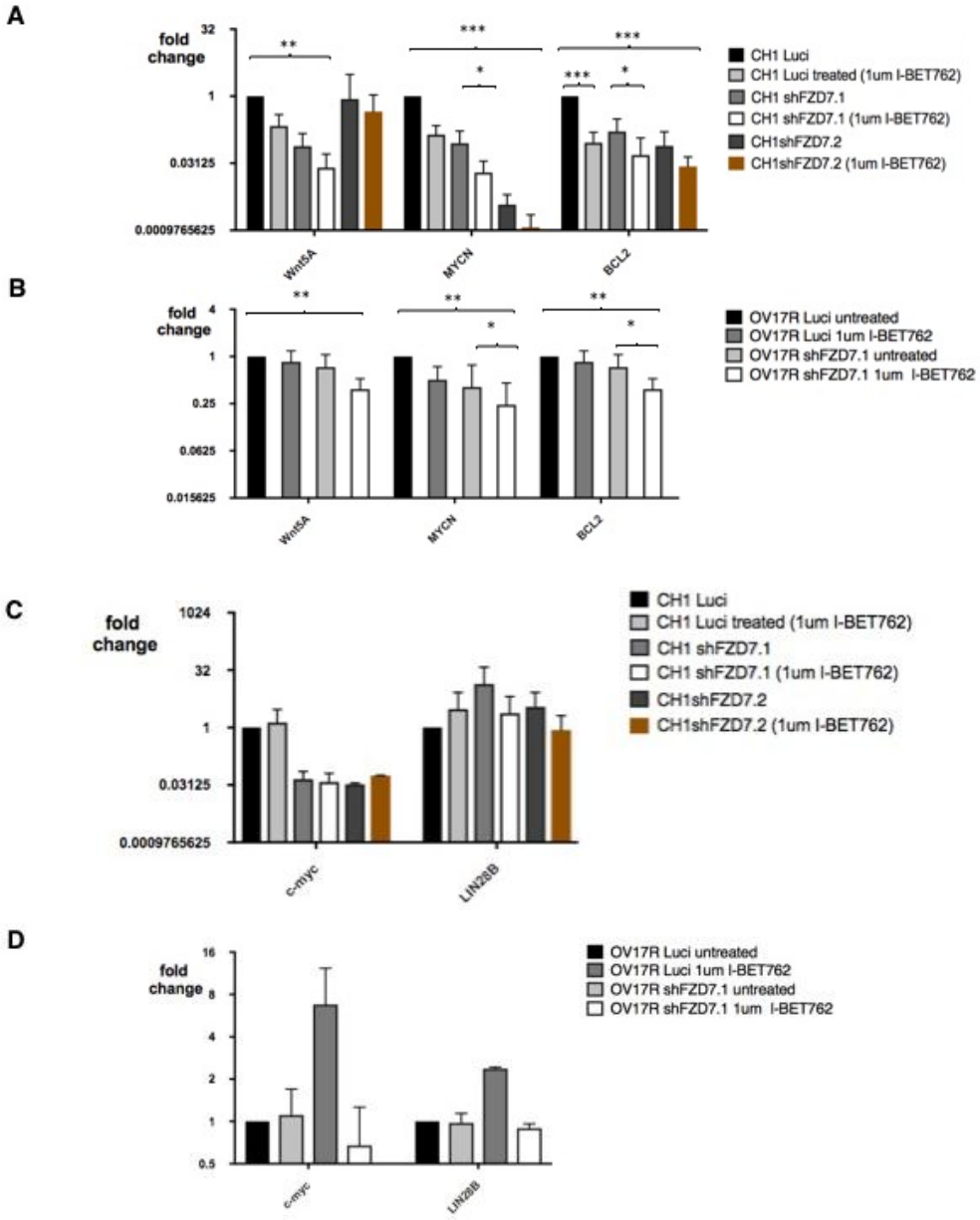

Figure 4.13: Synergistic effect between BET bromodomain inhibition with I-BET-762 and *FZD7* depletion in downregulation of TWIST1 target genes. Synergism between BRD4 inhibition and *FZD7* depletion was consistently observed in both (A) CH1 and (B) OV17R cell lines in the downregulation of *MYCN, WNT5A* and *BCL2* genes. (C,D) Synergism was not observed in *c-MYC* and *LIN28B* genes in both the cell lines. Data represents mean ± SEM of at least 3 independent experiments. Where reported, error bars represent SEM. Statistical significance was determined by unpaired t test * p <0.05; **p<0.01

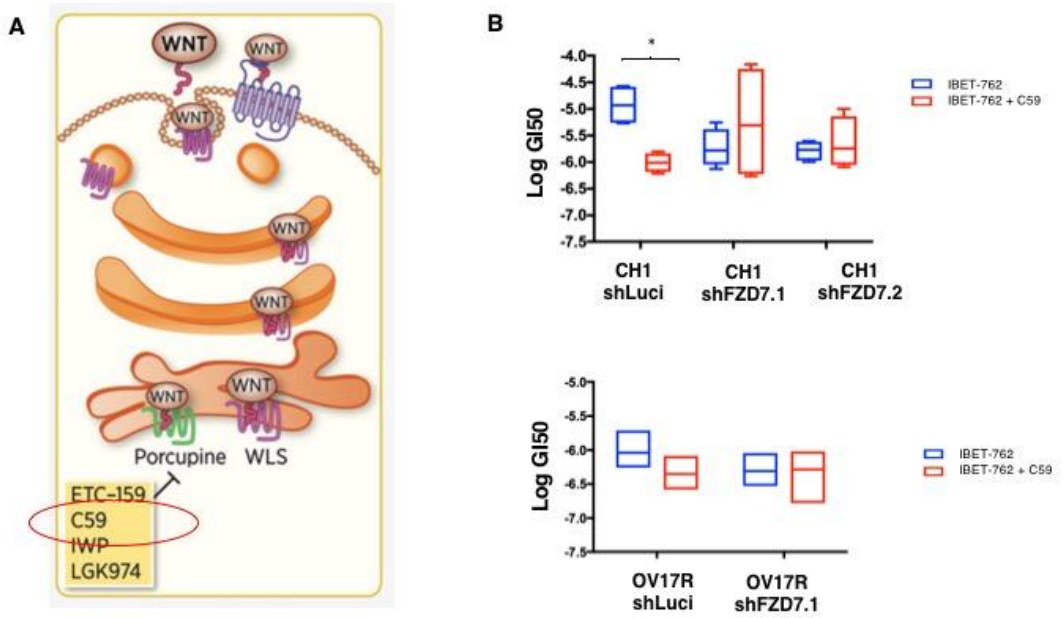

Figure 4.14: No synergism observed with combination of porcupine inhibitor and BET bromodomain inhibitor, I-BET-762, in *FZD7* depleted cells. (A) Mechanism of action of PORCN inhibitor. Compound C59 (red box) was used in subsequent experiments. Image adapted from Madan et al. Mol Cancer Ther 2015. (B) Addition of C59 to I-BET-762 treated CH1 and OV17R cells only increased sensitivity to I-BET-762 in *FZD7* replete cells. Comparison of the IC50 values obtained from monotherapy I-BET-762 (blue) and combination of I-BET-762 and 10nm C59 (red) dose response curves. Cell viability was measured using MTS assay and for each value was reported as a percentage of the effect obtained by employing the vehicle alone. Data represents mean ± SEM of at least 3 independent experiments Where reported, error bars represent SEM. Statistical significance was determined by student's t test * p <0.05; **p<0.01.

Chapter V:

Microtubule dynamics and association with C5/Stem-A HGSOC

5.1 Introduction

Approximately 70% of EOC patients' experience disease relapse post adjuvant chemotherapy, albeit after a varying disease-free interval. Recurrent EOC is incurable and it remains unclear why patients develop recurrent disease despite the high response rates (~70%) observed during initital chemotherapy. At disease recurrence, tumours may be platinum sensitive or resistant. Besides retreatment with a platinum agent, chemotherapy agents such as pegylated liposomal doxorubicin (Gordon et al., 2000), topotecan (Sehouli et al., 2011) and gemcitabine (Mutch et al., 2007) are among the cytotoxic agents used in the relapsed setting, with low response rates (Gordon et al., 2004; Mutch et al., 2007; Sehouli et al., 2011). The paucity of responses is due to ovarian cancer being treated as a single entity with lack of stratification of the diverse histological and molecular subtypes. In contrast, targeted approaches with anti-vascular endothelial growth factor (VEGF) antibody, bevacizumab (Perren et al., 2011), and olaparib, an inhibitor of the enzyme poly-(ADP ribose) polymerase inhibitor (PARPi) (Ledermann et al., 2012), have demonstrated significant improvement in outcomes for a subgroup of patients with advanced ovarian cancer.

Hitherto, much of the underlying mechanisms that underpin drug sensitivity and efficacy in EOC remains largely elusive. Several studies have emerged demonstrating that analysis of transcriptomic and genomic EOC tumour profiles may identify certain EOC subgroups with differential chemotherapeutic responses and outcomes(Konecny et al., 2014; Tan et al., 2009; Tan et al., 2013a; Winterhoff,). Among them, the C5/Stem-A cell lines were found to be more sensitive to inhibitors of microtubule polymerizing agents like vinorelbine and vincristine compared to non-Stem-A/C5 cell lines (Tan, Miow et al., 2013). Strikingly, when cells were treated with vincristine, apoptotic activity was detected only in Stem-A cells with no apoptotic activity detected in non-Stem-A cells.

Microtubules play essential roles in cell growth and division, motility,

intracellular trafficking and bestowing cells the ability to interact with the microenvironment by conforming and adapting to a variety of shapes (Mukhtar et al., 2014). Biological functions of microtubules are regulated predominantly by their polymerization dynamics (figure 5.1) (Mukhtar et al., 2014). Microtubule targeting agents (MTA) can be classified into two groups, inhibitors of microtubule polymerization, which includes several compounds notably the vinca alkaloids, cholchicine and estramustine, while the other group is known as microtubule stabilizing agents, of which drugs such as paclitaxel, docetaxel and epothilones are part of (Mukhtar et al., 2014). At high doses, MTA affects microtubule polymer mass. However, at 10 – 100 fold lower concentrations, most of these compounds act as anti-mitotic agents inhibiting cancer cell proliferation by disrupting the spindle-microtubule dynamics, leading to the slowing or blocking of mitosis at metaphase-anaphase transition, cell cycle arrest and induction of apoptotic cell death (figure 5.2) (Mukhtar et al., 2014).

Vinca alkaloids were originally isolated from periwinkle leaves, *Catharanthus roseus* (Mukhtar et al., 2014). They were first discovered in the 1950's by Canadian scientists, Robert Noble and Charles Beer, for their anti-mitotic and hence, cancer therapeutic potential (Mukhtar et al., 2014). They were initially used in the treatment of childhood leukemia with great success followed by adult haematological malignancies and solid tumour malignancies (Mukhtar et al., 2014). Today, with the increased understanding of their mechanisms of action, vinca alkaloids are used as single agent therapy in breast cancer (Weber et al., 1995) and in combination treatment settings in lung cancer (Winton et al., 2005), bladder malignancies (Maase et al., 2005), urothelial carcinoma (Bellmunt et al., 2013) and adult leukemia (Kantarjian et al., 2000; Thomas et al., 2010). Hitherto, vinca alkaloids are not routinely used as standard of care for the treatment of ovarian cancer.

In the past, the use of vinorelbine has been evaluated in ovarian cancer with several single agent phase I/II trials in recurrent ovarian cancer demonstrating variable response rates from 3 – 30% (Burger et al., 1999; M. J. George et al., 1989; Gershenson et al., 1998; Rothenberg et al., 2004; Sørensen et al., 2001). George *et al* were the first to report the results of a Phase II trial with vinorelbine in recurrent ovarian cancer. An objective response rate (ORR) of 13.2% (5 /37 patients) was observed(M. J. George et al., 1989). Burger *et al* subsequently evaluated vinorelbine in 38 patients with recurrent ovarian cancer; 24 with platinum-sensitive disease, 12 with platinum-resistant disease, and 2 who could not be characterised. ORR of 28.9% was observed with median survival of 13.8 months (Burger et al., 1999). Vinorelbine was administered at a dose of 30 mg/m2 /week in both studies. Bajetta *et al* evaluated 33 patients with recurrent ovarian cancer and observed ORR of 15.2% (5/33) with median PFS and OS of 4 and 10 months, respectively (Bajetta et al., 1996). Interestingly, all five responses observed occurred in patients with platinum-resistant disease (Bajetta et al., 1996). Gershenson *et al*. also performed a phase II trial of vinorelbine which was administered daily for 3 days, once every 3 weeks in women with platinum- and taxane-resistant ovarian cancer and observed ORR of 30% including two patients with complete remissions (Gershenson et al., 1998). Median survival was 11.2 months. Notably, all patients in this study underwent prior treatment with a taxane. In contrast, Rothenberg *et al* observed ORR to vinorelbine monotherapy of only 3% (2/71) in patients previously treated with platinum and taxane (Rothenberg et al., 2004). Nonetheless, despite the diversity in patient selection, differences in dose intensity and prior sensitivity to platinum or taxane treatment, vinorelbine had modest activity comparable with other second line treatment options and was well tolerated (Bajetta et al., 1996; Burger et al., 1999; M. J. George et al., 1989; Gershenson et al., 1998; Sørensen et al., 2001)

Tan *et al,* through an shRNA-based negative genome wide selection screen designed to search for genes necessary for survival/ proliferation of ovarian cancer cells demonstrated that C5/Stem-A cells were dependent on *TUBGCP4, NAT10, GTF3C1, BLOC1S1* and *LRRC59* for cell growth (figure 5.3). However only si*TUBGCP4* and si*NAT10* appeared to suppress cell growth/suvival of C5/Stem-A cell lines compared to non-C5/Stem-A cell lines (figure 5.3) (Tan et al., 2013). *NAT10,* human N-acetyltransferase-like protein 10, is located in the nucleoli and is thought to be involved in cell division and nucleolar assembly (Shen et al., 2009). *NAT10* is also thought to regulate the microtubule by acetylation of alpha tubulin (Shen et al., 2009). This modification enhances microtubule stability and raises resistance to drug-induced disassembly as well as modulates cytokinesis. The molecular mechanisms linking *NAT10* with the C5/Stem-A subtype are still unclear.

Nonetheless, the susceptibility of C5/Stem-A subtype to vinca alkaloids *in vitro* is intriguing and underscores the importance of the role of tubulin polymerization in this subtype. To validate the *in vitro* results of Tan *et al,* we utilized several C5/Stem-A HGSOC PDX from the cohort and assessed their responses to vinorelbine in light of their respective platinum sensitivities. We considered that pre-clinical *in vivo* validation of this hypothesis in our C5/Stem-A HGSOC PDX would allow us to better understand the potential of this approach for the clinic. We subsequently evaluated the influence of *NAT10* in this subtype and its contributory role, if any, to vinorelbine response.

5.2 Results

In vivo activity of vinorelbine, inhibitor of microtubule polymerization, in C5/Stem-A PDX

Currently, vinca alkaloids do not feature as standard of care in the treatment paradigm of HGSOC. Nonetheless, in light of recent findings by Tan *et al*, *in vivo* sensitivity to vinorelbine was examined using six molecularly annotated C5/Stem-A PDX (#PH038, #PH039, #PH077, #PH034, #PH041 and #PH048). A dose of 15mg/kg of vinorelbine administered weekly via the tail vein for three weeks showed initial tumour regression in five out of six C5/Stem-A PDX independent of MYCN expression and platinum response (figure 5.4(A-F). Three platinum sensitive PDX (#PH038, #PH039, #PH077) treated with vinorelbine showed anti-tumour activity with tumour regression (figure 5.4(A-C). Median time to progression of disease (PD) for PDX #PH038, #PH039 and #PH077 treated with IV vinorelbine was 78d, 78d and 15d respectively while the median time to tumour harvest (TTH) was 132d, 96d and 74d respectively for PDX treated with vinorelbine versus 12d, 11d and 33d for vehicle treated PDX (Hazard ratio(HR): 0.17, p value: <0.01; HR: 0.28, p value: <0.01 and HR 0.28, p value: <0.05; respectively) (table 5.1). One platinum resistant PDX (PH#034)(figure 3.5)(Table 3.4) had initial anti-tumour activity evidenced by tumour regression lasting 29 days on vinorelbine (figure 5.3(D) (median TTH: 74.5d vs 38d vehicle; HR 0.26; p value: <0.01) (Table 5.1) while two platinum refractory PDX (#PH041, #PH048) (figure 3.5)(Table 3.4) were subsequently treated with vinorelbine, with #PH041 known to overexpress *CCNE1* mRNA and protein (Table 3.5) while #PH048 shown to overexpress BCL2 protein (Table 3.5), with differing outcomes. PDX #PH041 had significant sustained anti-tumour response with time to PD >100days (figure 5.4(E) (median TTH: 116d vs 42d vehicle; HR 0.21, p value: <0.05) while PDX #PH048 had minimal appreciable anti-tumour activity with a time to PD of 8d (Figure 5.4(F) (median TTH:

46d; HR 0.4; p value: 0.1086) (Table 5.1) implying that the C5/Stem-A subtype are still heterogeneous despite their molecular similarities and perhaps conventional single-subtype assignments adopted to classify tumors based on patterns of gene expression may need to be refined to sufficiently reflect the heterogeneity that exist within each subtype.

The *in vitro* findings published by Tan *et al* which showed increased sensitivity demonstrated by C5/Stem-A cell lines to vinca alkaloids, compared to tubulin stabilizing agents like paclitaxel (Tan, Miow et al., 2013) were indeed intriguing. To gain further insights into this, we evaluated the activity of paclitaxel in the *in vivo* setting. Firstly, non-tumour bearing mice were treated with escalating doses of paclitaxel, in order to establish the maximum tolerated dose (MTD) which was established at 30 mg/kg twice a week. We subsequently applied this dose in tumour-bearing mice but unfortunately had to de-escalate the dose to 25mg/kg due to toxicity. At this dose, one C5/Stem-A HGSOC PDX which we had shown to be sensitive to vinorelbine (PH#039) was treated with 25mg/kg of paclitaxel intra-peritoneally twice a week for 3 weeks. Initial tumour regression was observed (figure 5.5). However, this was not sustained. Despite the observed anti-tumour effects of paclitaxel in PDX PH#039 compared to vehicle (median TTH: 25d vs 9d respectively; p value < 0.0025) (figure 5.5), the anti-tumour activity of PDX PH#039 to paclitaxel was significantly less than that demonstrated with treatment using vinorelbine (median TTH: 25d vs 96d respectively; p value: <0.01). It was not our intention to carry out extensive comparative studies between paclitaxel and vinorelbine in our PDX models. This is because we cannot be certain that the MTD of drugs used in mice is reflective of head to head drug comparisons performed in women in the clinic. Notwithstanding, we do note that in our PDX models, vinorelbine shows impressive efficacy.

Heterogeneous NAT10 protein expression observed in C5/Stem-A and non-C5/Stem-A ovarian cancer cell lines

To further understand the role of *NAT10*, we examined the endogenous protein expression of NAT10 in an array of C5/Stem-A and non-C5/Stem-A cell lines. Variable NAT10 protein expression was observed in both the C5/Stem-A and non-C5/Stem-A cell lines (figure 5.6(A). Most C5/Stem-A cell lines appeared to have appreciable endogenous NAT10 protein expression. However, there appeared to be some C5/Stem-A cell lines that had low endogenous NAT10 expression (OV17R, OAW42) while one C5/Stem-A cell line examined had no appreciable endogenous expression of NAT10 (COV318) (figure 5.6(A). A similar pattern of protein expression was also observed in the non-Stem-A cell lines (figure 5.6(A). The NAT10 protein expression was subsequently quantified (normalised against b-actin controls) and the average NAT10 protein expression appeared to be higher, although not significantly, in non-Stem-A compared to Stem-A cells (figure 5.5(B). Contrary to Tan *et al*, this data suggests that not all C5/Stem-A cells require NAT10 for proliferation/survival, however, we reasoned that perhaps only Stem-A cell lines with appreciable expression of NAT10 are dependent for cell proliferation/survival and perhaps an alternative pathway was responsible for cellular proliferation in cells without appreciable NAT10 expression.

Reduced cellular proliferation with depletion of *NAT10* only observed in C5/Stem-A cells with appreciable endogenous NAT10 protein expression

Next, using siRNA to target the *NAT10* gene, three Stem-A cell lines (PA1, CH1 and COV318) and two non-Stem-A cell lines (SKOV3 and HEY) were used to further evaluate the role of *NAT10*. The short interfering RNA used for the control (sicontrol) targets non-human genomic regions. To eliminate any potential biases derived from the use of the PA-1 cell line (C5/Stem-A non-HGSOC cell line), two other bona fide C5/Stem-A HGSOC cell lines (CH1 and COV318) (Beaufort et al., 2014; Domcke et al.,

2013; Helland et al., 2011; Tan et al., 2013a) were included in subsequent experiments, albeit with opposite NAT10 expression (figure 5.6(A). C5/Stem-A cell lines with high endogenous NAT10 expression showed significant decrease in cell viability 72 hours after targeting by siRNA (figure 5.7(A). For C5/Stem-A cell lines with no appreciable endogenous NAT10 protein expression, COV318, there was no obvious reduction in cell viability 72 hours after *NAT10* depletion (figure 5.7(A). In contrast, there was no significant decrease in cell viability for non-C5/Stem-A cell lines with depletion of *NAT10* despite harboring appreciable levels of endogenous NAT10 protein (figure 5.7(B). Therefore, this suggests that *NAT10* influences cellular proliferation/ survival specifically in C5/Stem-A cell lines with appreciable endogenous expression of NAT10 protein.

C5/Stem-A cells with depleted *NAT10* undergoes anoikis in suspension culture but does not induce apoptosis

Subsequently, we determined if C5/Stem-A cells depleted of *NAT10* would undergo anoikis and apoptosis in suspension culture. *NAT10* depleted C5/Stem-A CH1 and PA-1 cells along with non-C5/Stem-A SKOV3 cells and their corresponding *NAT10* replete controls were seeded in a 10cm ultra-low attachment dish. Cells were incubated for 72 hours and subsequently stained with PI and Annexin V for FACS analysis. *NAT10* depleted PA-1 and CH1 cells were more prone to anoikis as evidenced by the significant increase of Annexin V-positive early apoptotic cells from 9%±1.6% and 12.2%±0.9% in control PA-1 and CH1 cells respectively, compared to 33.2%±1.6% and 25.3%±1.3% respectively in *NAT10* depleted cells (Figure 5.8 (A, B). In contrast, non-C5/Stem-A SKOV3 cells did not undergo anoikis with depletion of *NAT10* as there was no change in Annexin V-positive early apoptotic cell populations compared to controls (Figure 5.8 (C). Notably, *NAT10* depletion did not appear to induce apoptosis in both C5/ Stem-A

and non- C5/ Stem-A cells. This was subsequently confirmed by the lack of cleaved caspase 3 protein expression observed on immunoblotting of *NAT10* depleted PA-1 and CH1cells (figure 5.8(D, E).

Depletion of *NAT10* did not affect acetylation of alpha tubulin in C5/Stem-A cell lines

Recently, it has been suggested that *NAT10* may play a role in maintaining or enhancing the stability of alpha – tubulin and that depletion of *NAT10* lead to G2/M cell cycle arrest or delay in mitotic activity (Shen et al., 2009). Shen *et al* also raised the possibility that *NAT10,* as an acetyltransferase, may play a role in acetylation of alpha tubulin and hence enhance microtubule stability (Shen et al., 2009). To determine *NAT10* modulates acetylation of alpha tubulin, levels of acetylated alpha-tubulin were assessed in *NAT10* depleted and replete CH1 and PA-1 cell lines 72 hours after *NAT10* knockdown. Using western blot to assess protein levels of acetylated alpha tubulin relative to the alpha tubulin expression, we observed no significant reduction in acetylated alpha-tubulin protein levels observed in both the C5/Stem-A as well as non-C5/Stem-A cell lines compared to controls (figure 5.9(A,B).

Depletion of *NAT10* does not enhance sensitivity of C5/Stem-A cells to microtubule targeting agents

Next, to determine whether *NAT10* played a role in modulating the preferential sensitivity of C5/Stem-A ovarian cancer to vinorelbine compared to paclitaxel observed in Tan *et al* (Tan et al., 2013a), dose-response curves were performed using siRNA targeting *NAT10* in CH1, PA-1 and COV318 C5/Stem-A cells as well as SKOV3 and HEY non-C5/Stem-A cell lines. *NAT10* depletion did not significantly enhance sensitivity to vinorelbine or paclitaxel relative to the negative control in both the

C5/Stem-A and non-C5/Stem-A cell lines. Nonetheless, it is worth noting that depletion of *NAT10* resulted in modest reduction of GI50 values, albeit not significantly, in Stem-A cell lines which overexpress NAT10 protein endogenously (CH1 and PA1) (figure 5.10(A,B) compared to C5/Stem-A cell lines that did not endogenously overexpress NAT10 protein (COV318) (figure 5.10(C) or to non- C5/Stem-A cell lines (HEY and SKOV3) (figure 5.10(D,E). Using a larger number of C5/Stem-A and non- C5/Stem-A cell lines, NAT10 protein expression for each cell line was quantified by normalizing to b-actin and subsequently correlated to their respective GI50 values for vinorelbine and paclitaxel (figure 5.10(F,G). Five C5/Stem-A cell lines (CH1, A2780, PA1, OVCAR3 and COV318) and six non- C5/Stem-A cell lines (OVCA433, HEY, A1847, OVCA432, PEO1 and SKOV3) were used for this correlation and not surprisingly, there did not appear to be a correlation between NAT10 protein levels and sensitivity to either one of the microtubule targeting agents (figure 5.10 (F,G).

To determine whether *NAT10* was the target gene in C5/Stem-A PDX treated with microtubule targeting agents, baseline expression of NAT10 protein in the six PDX treated with vinorelbine were initially evaluated. Consistent with reports observed in soft tissue sarcoma where NAT10 protein expression was associated with aggressiveness and poor prognostic malignant lesions(Shen et al., 2009), NAT10 protein expression was found to be ubiquitously overexpressed in the poor prognostic C5/Stem-A HGSOC PDX cohort (figure 5.11(A). Intriguingly, when NAT10 expression levels were further interrogated in one PDX (#PH039) pre vinorelbine/ paclitaxel treatment and 12 hours after second dose of vinorelbine or paclitaxel, no appreciable change in the NAT10 protein expression pre and post vinorelbine or paclitaxel treatment was observed (figure 5.11(B) indicating that the mechanism of action for microtubule targeting agents in this subtype may not be solely related to the expression of a single gene like *NAT10*.

Collectively, these results would suggest that although antitumour activity was observed in C5/Stem-A HGSOC PDX treated with vinorelbine, the underlying mechanisms of action in this subtype is not completely clear. It is apparent that the C5/Stem-A subtype appears to be heterogeneous despite their molecular similarities and understanding the interplay between the underlying oncogenic drivers relevant for each individual tumour as well as modifying the classification to enable a more comprehensive reporting of transcriptomic subtype heterogeneity within the tumour may be the key to better select patients for specific therapeutic strategies.

C5/Stem-A-ness correlates with vinorelbine response in PDX

It has been reported that 95% of ovarian cancer consist of at least four sub-clones within a tumour (Lohr et al., 2014), while 82% of the TCGA cohort (Verhaak et al., 2012) and 42% of the Mayo ovarian cancer cohorts(Konecny et al., 2014) demonstrated co-existence of at least two subtypes. Using a scheme termed molecular assessment of subtype heterogeneity (MASH) to represent the composition of transcriptomic subtypes within a tumour, the heterogeneity of transcriptomic subtypes that co-exist within a tumour was explored (Tan, Heong et al, in press).

To determine whether inherent transcriptomic heterogeneity within each vinorelbine treated C5/Stem-A HGSOC PDX influenced response to vinorelbine treatment, MASH was used to analyse array comparative genomic hybridization (aCGH) data from six C5/Stem-A HGSOC PDX(Weroha et al., 2014) treated with vinorelbine. Of the six C5/Stem-A PDX analysed, tumour from PDX PH#048 demonstrated significant heterogeneity with a large presence of Mes subclone (50%) co-existing with C5/Stem-A (50%) subclone within the tumour (figure 5.12(A) which could explain the relative resistance to vinorelbine treatment. Due to the significant portion of co-existing Mes subclone in this PDX, PH#048 was excluded from the

subsequent analysis as it would confound the findings. The remaning five vinorelbine treated PDX (PH#038, PH#041, PH#039, PH#034 and PH#077) with predominantly C5/Stem-A consisting subclones (>50%) in the tumour were graded using the MASH scheme to produce a C5/Stem-A score based on their gene expression profiles. C5/Stem-A scores of PDX treated with vinorelbine were found to correlate with overall survival as evidenced by a longer TTH, (Rho – 0.74; p value = 0.15) (figure 5.11(B), although this was not significant, likely due to the small numbers analysed.

Collectively, this data demonstrates significant heterogeneity exist within the C5/Stem-A subtype and through MASH, the transcriptomic heterogeneity within this subtype can be quantitatively analysed to better select patients that may respond to subtype specific therapeutic strategies.

5.3 Discussion:

Here we demonstrated that vinorelbine, an inhibitor of microtubule polymerization, had impressive *in vivo* anti-tumour activity in five out of six C5/Stem-A HGSOC PDX tested. While the other PDX (PH#048) did not experience tumour regression, anti-tumour activity from vinorelbine was observed with prolonged stabilization of disease compared to vehicle treated PDX hence validating the *in vitro* data previously published by Tan *et al* (Tan et al., 2013). In addition, data from one PDX, PH#039, suggests that this particular PDX had increased sensitivity to vinorelbine while the antitumour activity of paclitaxel was observed to be significantly less in the same PDX. It is tempting to speculate that this may also be the case in patients with C5/Stem-A HGSOC but the differences in established MTD and drug metabolism differs greatly between mice and humans. Hence, a head to head comparison of these two drugs in the PDX, while tempting, will likely not be reflective of outcomes in women seen in clinical practice. Nonetheless, this is of particular importance, as vinorelbine chemotherapy is not currently used as standard of care to treat ovarian cancer. Furthermore, the response of the C5/Stem-A HGSOC PDX to vinorelbine appears to be irrespective of their platinum response as evident by PDX PH#041, platinum refractory PDX, with prolonged anti-tumour response to vinorelbine. This is of particular interest as patients will eventually become platinum resistant where limited treatment strategies exist with low efficacy rates (Gordon et al., 2004; Mutch et al., 2007; Sehouli et al., 2011). However, it is worth noting that the significant anti-tumour effects shown with vinorelbine treatment in the C5/Stem-A PDX were demonstrated in taxol naïve PDX. It remains unclear if similar responses to vinorelbine will still be observed in previously taxol treated PDX. Nonetheless, these findings suggest that vinorelbine may potentially be efficacious in the platinum-refractory setting for patients where treatment options are currently limited.

Despite recent published reports of the potential relevance of *NAT10* in the C5/Stem-A subtype (Tan et al., 2013a), we found that depletion of *NAT10* resulted in decreased cell viability only in C5/Stem-A cell lines that had high endogenous NAT10 protein levels. For C5/Stem-A cell line COV318, with no appreciable endogenous NAT10 protein expression, and non-C5/Stem-A cell lines (SKOV3 and HEY) no reduction in cell viability was observed. Upon further interrogation, depletion of *NAT10* resulted in an increase in anoikis only in C5/Stem-A cells but did not affect apoptosis or acetylation of alpha- tubulin. These experiments were performed at 72 hours and 96 hours post depletion of *NAT10.* It may be possible that the timepoints chosen contributed to the lack of apoptotic and acetylation activity seen. However, when we attempted to generate stable clones of *NAT10* depleted cells using targeted *NAT10* shRNA, we observed that this resulted in cell death specifically in the C5/Stem-A cell lines, 4-5 days after infection of cells (data not shown). Future works could focus on improving methods to generate stable clones of depleted *NAT10* using newer genome editing techniques to allow a more comprehensive evaluation of the role of this gene in C5/Stem-A HGSOC.

Although *NAT10* is known to influence cytokinesis and modulate the microtubules (Shen et al., 2009), we observed that it did not influence sensitivity to microtubule targeting agents, vinorelbine nor paclitaxel. Nonetheless, as *NAT10* is known to regulate nucleolar assembly and has been shown to increase transcriptional activity of its promoter in response to DNA damage (Shen et al., 2009), further research focusing on the role of *NAT10* in the maintenance of the cell cycle as well as its role in DNA repair may shed some light on potential combinatorial strategies for the C5/Stem-A subtype.

Based on the significant heterogeneity observed within the C5/Stem-A subtype thus far, it is not surprising that attempts at biomarker selection using single genes have

not been successful. Therefore, a more robust biomarker selection, one that takes into account tumoural heterogeneity, may be more reliable. Conventionally, single-subtype assignments are generally utilized to molecularly classify HGSOC (Tan et al., 2013a; TCGA., 2011; Tothill et al., 2008). However, single-subtype assignments may not be adequate to reflect the heterogeneity that exist within the tumour. Based on the MASH analysis performed on the *in vivo* PDX C5/Stem-A data, we demonstrated that for tumours consisting of predominantly C5/Stem-A subtype (> 50% C5/Stem-A) which are not confounded by significant co-existence of other poor prognostic subtype like the Mes/C1 subtype, those with a higher C5/Stem-A score correlated with increased sensitivity to vinorelbine suggesting that analysing tumours based on their intra-tumoural transcriptomic heterogeneity using this scheme could potentially be used for patient selection.

A caveat of our study is the treatment of only PDX from the C5/Stem-A subtype with vinorelbine. HGSOC from other subtypes may also respond favourably to vinorelbine however, that is beyond the scope of this project as we focus on therapies for this poor prognostic subtype where several other apparently promising treatment strategies have failed. Furthermore, the molecular and functional correlation between C5/Stem-A-ness and sensitivity to vinorelbine response using the MASH analysis reinforces the *in vitro* data of increased sensitivity of the C5/Stem-A subtype to vinorelbine.

Despite variable response rates of 3-29% observed in single agent phase II trials of vinorelbine in recurrent OC (Burger et al., 1999; Rothenberg et al., 2004; Sørensen et al., 2001) the compelling *in vivo* and *in vitro* efficacy data in C5/Stem-A HGSOC cannot be ignored. Furthermore, the early clinical trials performed were based on an unselected patient cohort of ovarian cancer patients with confounding differences in dose intensity and regimen of administration as well as prior platinum sensitivity, with

none incorporating patient selection based on pure HGSOC histiotype or a molecular biomarker of response.

In summary, the C5/Stem-A subtype of HGSOC PDX showed significant anti-tumour activity when treated with vinorelbine irrespective of their response to platinum therapy. Despite reports suggesting that C5/Stem-A cells were dependent on NAT10 for cell survival, this dependency was only observed in C5/Stem-A cell lines with high endogenous NAT10 protein expression and depletion of *NAT10* did not affect apoptotic activity or sensitize cells to microtubule targeting agents. Taking into account the heterogeneity within this molecular subtype, MASH analysis correlated the C5/Stem-A-ness of the PDX with its response to vinorelbine treatment. Future works could focus on using the compelling *in vitro* and *in vivo* data of vinca alkaloids in C5/Stem-A HGSOC to inform a clinical trial.

Table 5.1. Relative growth rates of independent HGSOC PDX and median survival following vinorelbine therapy

HGSOC PDX	Time to PD (d) vinorelbine	Median TTH (d) vehicle	Median TTH (d) vinorelbine	n (recipient mice)	Hazard ratio (95% CI)
Responder					
#PH034	29	36	74.5	8, 4	0.26** (0.079 – 0.86)
#PH038	78	12.0	>100	6, 4	0.17** (0.03 – 0.86)
#PH039	78	11	96	7, 3	0.28** (0.08 – 0.99)
#PH041	>100	42	116	5, 5	0.21** (0.05 – 0.89)
#PH077	15	33	74	8, 8	0.28* (0.08 – 0.99)
#PH048	8	19	46	5, 5	0.4^{ns} (0.12-1.3)

Table 5.1. Relative growth rates of independent PDX and median survival following vinorelbine therapy. Recipient mice PDX were randomized to treatment with vehicle or vinorelbine monotherapy 15mg/kg, D1, 8, 18 when tumour volume reached 0.18-0.3 cm^3. Time to Progressive disease (PD) was defined as the time (in days) from beginning of vinorelbine treatment to an increase in average tumor volume (for that treatment group) of >20% from the nadir. Time to Harvest (TTH) was defined as the time (in days) from the beginning of treatment to day of harvest at 0.7 cm^3 and the median TTH was calculated and plotted using Kaplan-Meier curves (Prism version 7). Control growth rates (treatment with vehicle) for independent PDX reveal that the slowest growth rates were observed in PDX, PH#038, PH#039 and PH#041. As seen with the relatively early measure of time to PD, response to vinorelbine was most durable for cisplatin-sensitive PDX, PH#038 and PH#039; cisplatin-resistant PDX PH#034 and cisplatin-refractory PDX PH#041 (TTH 74.5d – 132d; p value for difference between vinorelbine and vehicle significant for all) and minimal response for PH#077 and PH#048 (median TTH of only 46 - 74d; p value for difference between vinorelbine and vehicle not significant for all). Significance determined by Mantel-Cox test. ^{ns} p value not significant; *p value <0.05; **p value <0.01; *** p value <0.005. Hazard Ratio and 95% CI determined by Log Rank analysis

Table 5.2. Relative growth rates of HGSOC PDX #PH039 and median survival following paclitaxel therapy

HGSOC PDX	Time to PD (d) paclitaxel	Median TTH (d) vehicle	Median TTH (d) paclitaxel	n (recipient mice)	Hazard ratio (95% CI)
#PH039	5	9	26	6, 6	0.28** (0.07 – 1.0)

Table 5.2. Relative growth rates of HGSOC PDX #PH039 and median survival following paclitaxel therapy. Recipient mice PDX were randomized to treatment with vehicle or paclitaxel monotherapy 25mg/kg twice a week for three weeks (D1, 4, 8, 11, 15, 18) when tumour volume reached 0.18-0.3 cm^3. Time to Progressive disease (PD) was defined as the time (in days) from beginning of paclitaxel treatment to an increase in average tumor volume (for that treatment group) of >20% from the nadir. Time to Harvest (TTH) was defined as the time (in days) from the beginning of treatment to day of harvest at 0.7 cm^3 and the median TTH was calculated and plotted using Kaplan-Meier curves (Prism version 7). Control growth rates (treatment with vehicle) revealed aggressive tumour biology in PDX #PH039 with median TTH for vehicle treated PDX at D9. Delayed progression was observed in the paclitaxel treatment group (median TTH of 26 days; p value <0.0005 for difference between paclitaxel and vehicle). Significance determined by Mantel-Cox test. ^{ns} p value not significant; *p value <0.05; **p value <0.01. Hazard Ratio and 95% CI determined by Log Rank analysis

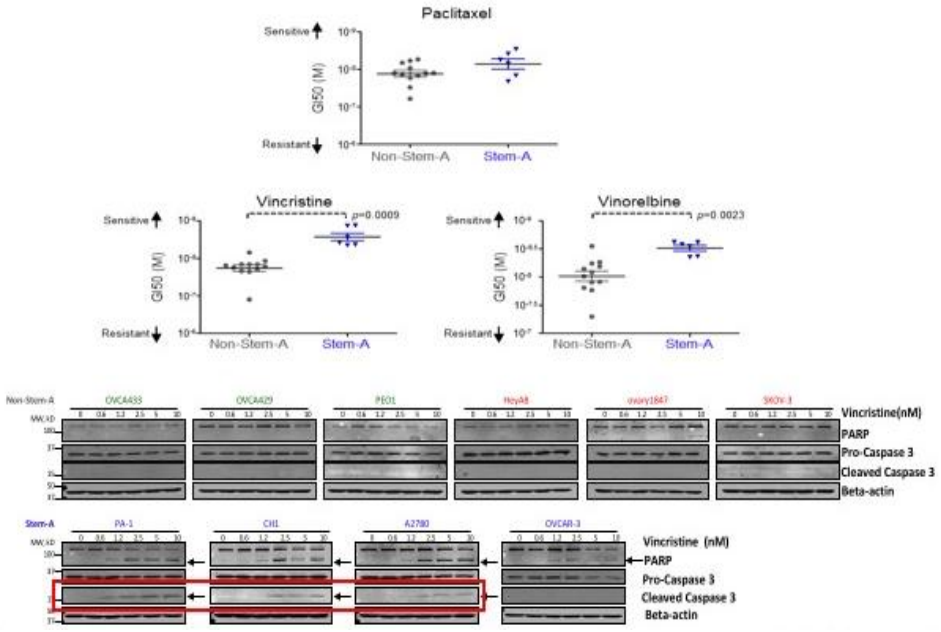

Figure 5.1: Increased sensitivity of C5/Stem-A cell lines to inhibitors of microtubule polymerization. 18 non-Stem A (OVCA433, OVCA429, OVCAR-8, PEO1, OVCA432, OVCA420, HeyA8, HEY, HeyC2, SKOV-3, ovary1847 and DOV 13) and Stem-A (PA-1, CH1, A2780, OVCAR-3, SKOV-4 and SKOV-6) cell lines were analysed for their sensitivity to paclitaxel (Top panel), vincristine (Left bottom panel) and vinorelbine (Right bottom panel). Increased cleaved caspase 3 in Stem-A cell lines (red box) compared to non-Stem-A cell lines after treatment with vinca alkaloid, vincristine. GI50 = 50% growth inhibition. Image adapted from Tan et al EMBO Mol Med 2013

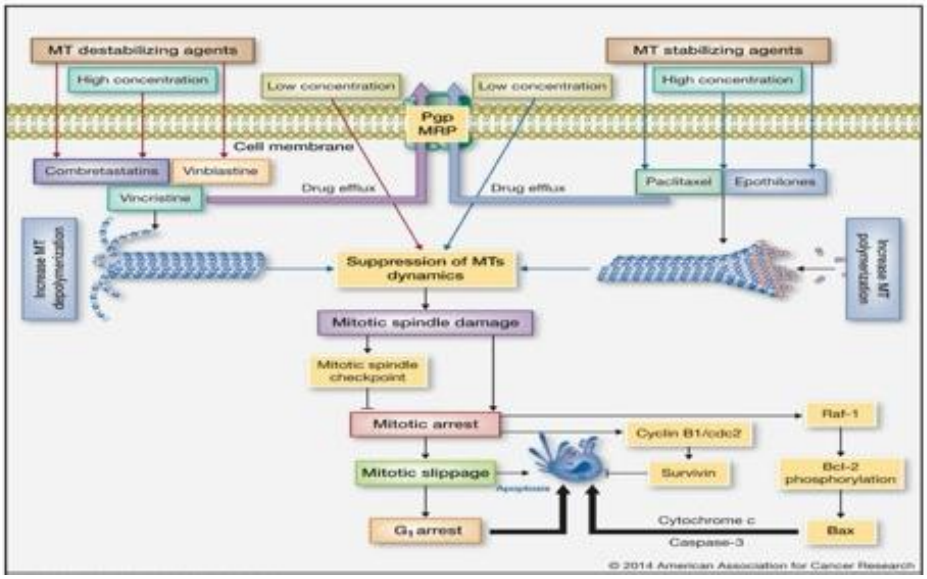

Figure 5.2: Mechanism of action of microtubule targeting agents. Image adapted from Mukhtar et al Mol Cancer Ther 2014

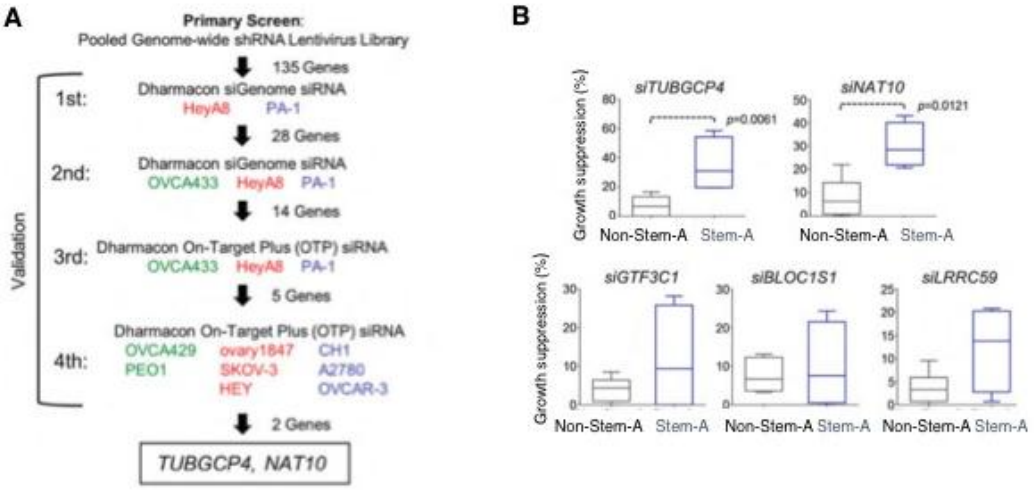

Figure 5.3: *NAT10* gene relevant and specific for C5/Stem-A cell lines (A) Schematic siRNA experiments validating the identified Stem-A- specific growth-promoting genes: TUBGCP4 and NAT10 (B) Inhibition with siTUBGCP4 or siNAT10 significantly suppressed cell growth of Stem-A cell lines as compared to non-Stem-A cell lines. Grey = non-Stem-A cell lines; blue = Stem-A cell lines. Image adapted from Tan et al EMBO Mol Med 2013

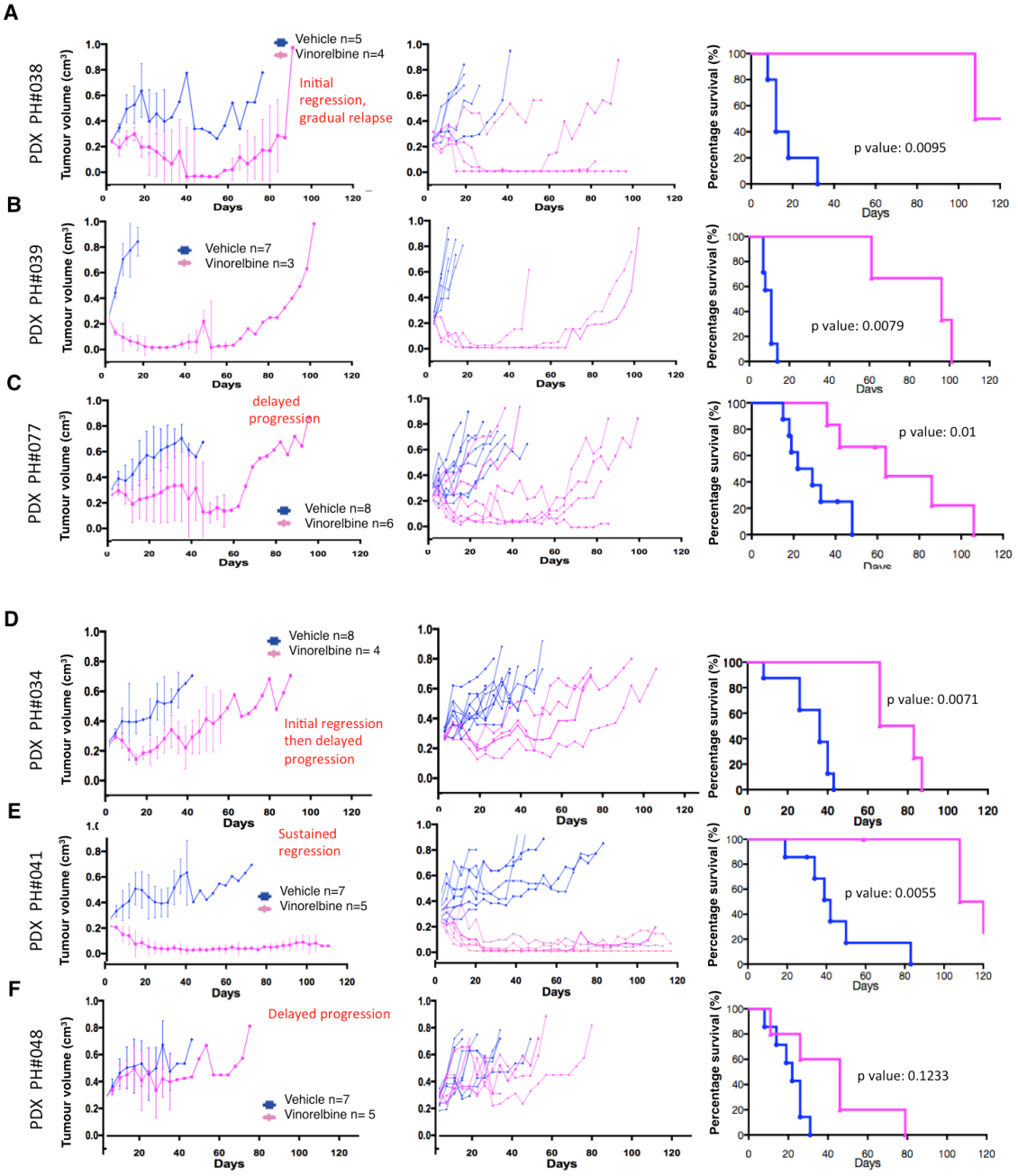
A
PDX PH#038
Tumour volume (cm³)
Vehicle n=5
Vinorelbine n=4
Initial regression, gradual relapse
Days
Percentage survival (%)
p value: 0.0095
B
PDX PH#039
Vehicle n=7
Vinorelbine n=3
p value: 0.0079
C
PDX PH#077
delayed progression
Vehicle n=8
Vinorelbine n=6
p value: 0.01
D
PDX PH#034
Vehicle n=8
Vinorelbine n= 4
Initial regression then delayed progression
p value: 0.0071
E
PDX PH#041
Sustained regression
Vehicle n=7
Vinorelbine n=5
p value: 0.0055
F
PDX PH#048
Delayed progression
Vehicle n=7
Vinorelbine n= 5
p value: 0.1233

Figure 5.4: Vinorelbine shows impressive anti-tumour response irrespective of platinum sensitivity in C5/Stem-A PDX. (A-F) PDX arranged according to platinum sensitivity from most platinum sensitive to least platinum sensitive. Left panel: average tumour volumes of vinorelbine response in each C5/Stem-A cell PDX; Middle panel: Spaghetti plots of each individual mice treated with vehicle or vinorelbine; Right panel: KM graphs depicting overall survival (OS) of each individual mice (OS – time from treatment with vehicle of vinorelbine to time to tumour harvest). 15mg/kg vinorelbine was administered IV on D1, D8 and D18 via tail vein. Where reported, error bars represent SEM. Significance determined by Mantel-Cox test. ^{ns} p value not significant; *p value <0.05; **p value <0.01; *** p value <0.005. Hazard Ratio and 95% CI determined by Log Rank analysis

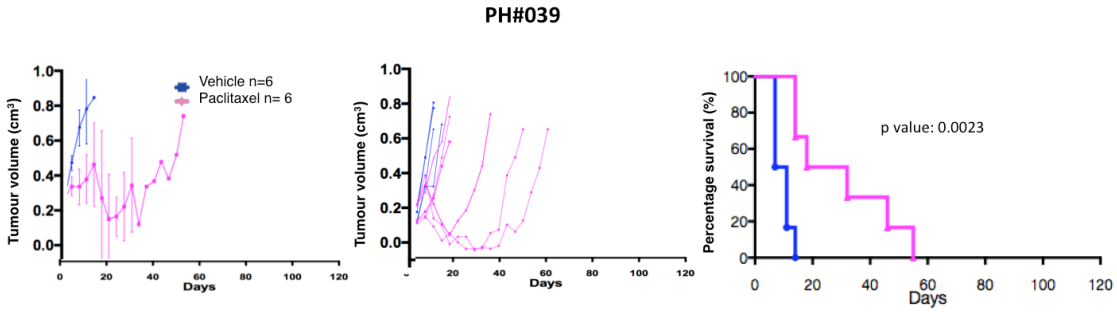

Figure 5.5: Paclitaxel response in PDX PH#039. Anti-tumour activity observed with paclitaxel in PDX PH#039. Left panel: average tumour volumes of vinorelbine response in each C5/Stem-A cell PDX; Middle panel: Spaghetti plots of each individual mice treated with vehicle or vinorelbine; Right panel: KM graphs depicting overall survival (OS) of each individual mice (OS – time from treatment with vehicle of vinorelbine to time to tumour harvest). 25mg/kg paclitaxel was administered intra-peritoneally twice a week for 3 weeks. Where reported, error bars represent SEM. Significance determined by Mantel-Cox test. ^{ns} p value not significant; *p value <0.05; **p value <0.01; *** p value <0.005. Hazard Ratio and 95% CI determined by Log Rank analysis

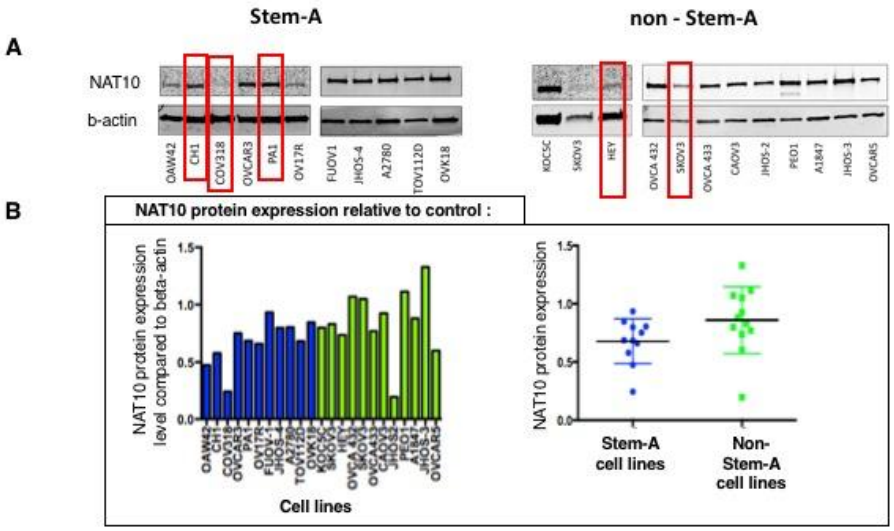

Figure 5.6: Variable NAT10 protein expression in C5/Stem-A and non-C5/Stem-A cell lines. (A) Western blot analysis depicting NAT10 protein expression in an array of C5/Stem-A and non-C5/Stem-A cell lines. Red boxes indicate cell lines used in subsequent experiments. (B) Left panel: Normalized fold changes in band intensities normalized to b-actin controls for NAT10 protein expression of C5/Stem-A and non-C5/Stem-A cell lines used. Right panel: Average (black line) NAT10 protein expression for an array of 11 C5/Stem-A cell lines and 12 non-C5/Stem-A cell lines.

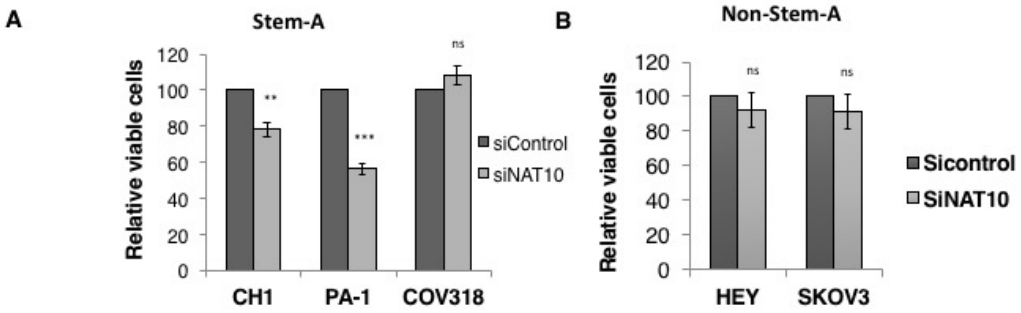

Figure 5.7: Depletion of *NAT10* decreases cell proliferation only in C5/Stem-A cell lines with appreciable endogenous NAT10 protein expression. (A) Reduced cell viability in *NAT10* depleted CH1 and PA-1 C5/Stem-A cell lines. No significant reduction in cell viability in *NAT10* depleted C5/Stem-A cell line, COV318. (B) No reduction in cell viability in non-C5/Stem-A cell lines HEY and SKOV3. Cell viability was measured by the MTS assay, and each value was reported as a percentage of the effect obtained with sicontrol. Where reported, error bars represent SEM. Statistical significance was determined by student's t test **p value <0.01; *** p value <0.005

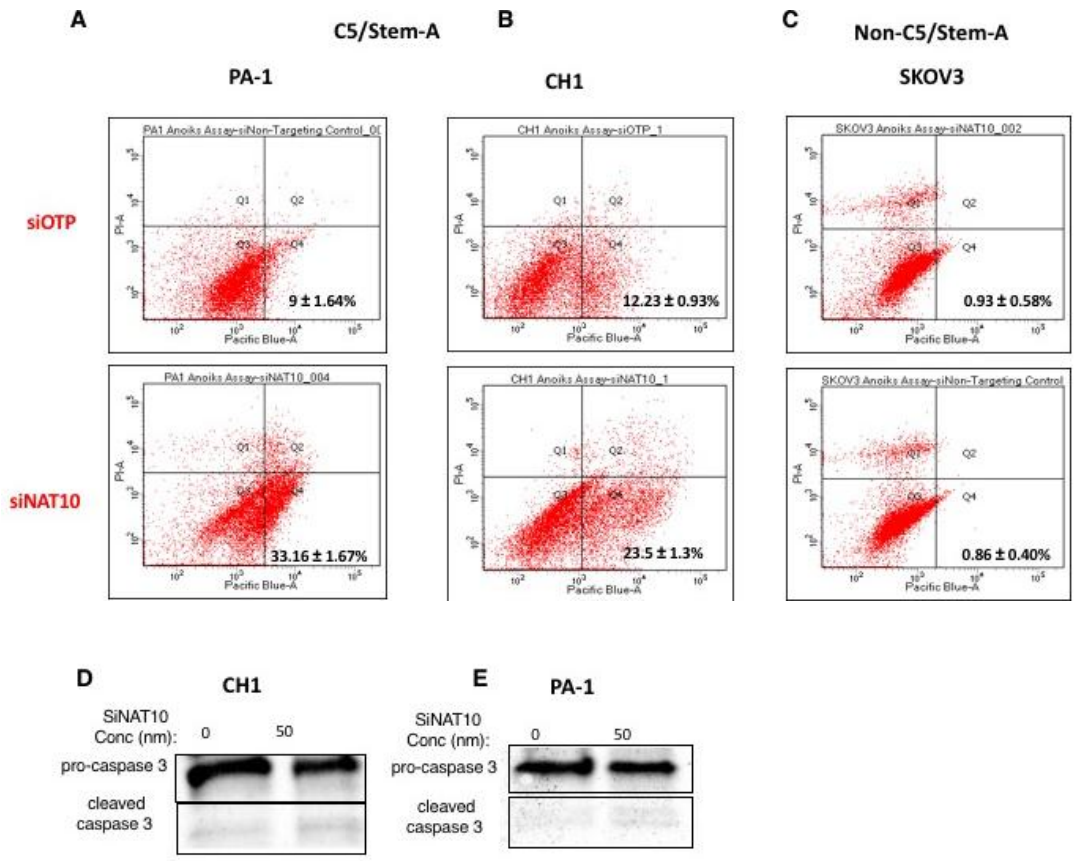

Figure 5.8: *NAT10* knockdown results in anoikis in C5/Stem-A cell lines CH1 and PA-1 but not in non-C5/Stem-A cell lines SKOV3 and does not induce apoptosis. FACS plots of *NAT10* depleted C5/Stem-A cell lines (A,B) shows increase in anoikis with no induction of apoptosis. (C) Anoikis resistance observed with knockdown of *NAT10* in non-C5/Stem-A cell lines SKOV3. Cells were kept in suspension for 72 hours prior to being analysed by FACS analysis. The percentage of Annexin V^+/ PI^- were considered apoptotic. Values recoded in red (Mean ± S.D) denote the percentage of cells undergoing anoikis from at least 3 independent experiments. X axis shows the level of Annexin V tagged with pacific blue and the y- axis shows the level of Propidium Iodide (PI). (D, E) Western blot analysis in two selected C5/Stem-A cell lines with known appreciable NAT10 protein expression, confirms no apoptotic activity 72 hours post *depletion* of NAT10 as evidenced by no appreciable caspase 3 protein expression after 72 hours of siRNA targeting of *NAT10* with 50nm siNAT10 and sicontrol in (D) CH1 and (E) PA-1 cell lines. siRNA targeting non-human genomic regions were used as control.

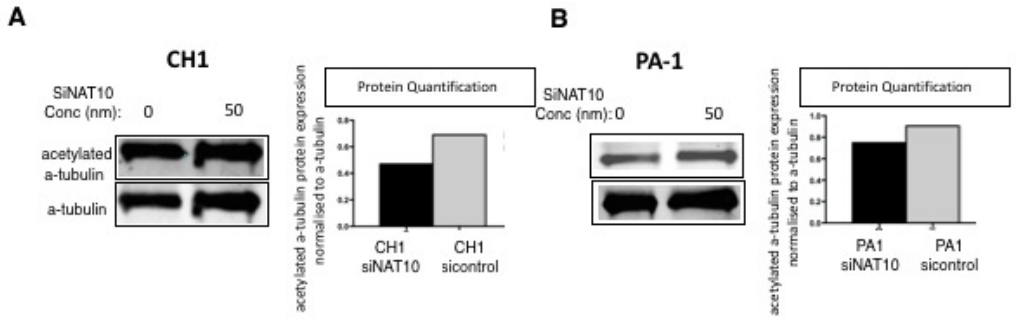

Figure 5.9: No modulation of alpha tubulin with depletion of *NAT10*. Western blot analysis in two selected C5/Stem-A cell lines with known appreciable NAT10 protein expression shows no significant change in protein expression of acetylated alpha tubulin levels after 72 hours of siRNA targeting of *NAT10* with 50nm siNAT10 and control for (A) CH1 cell lines and (B) PA-1 cell line. Protein quantification: Normalized fold changes in band intensities normalized to b-actin controls for acetylated alpha-tubulin protein expression of CH1 and PA-1.

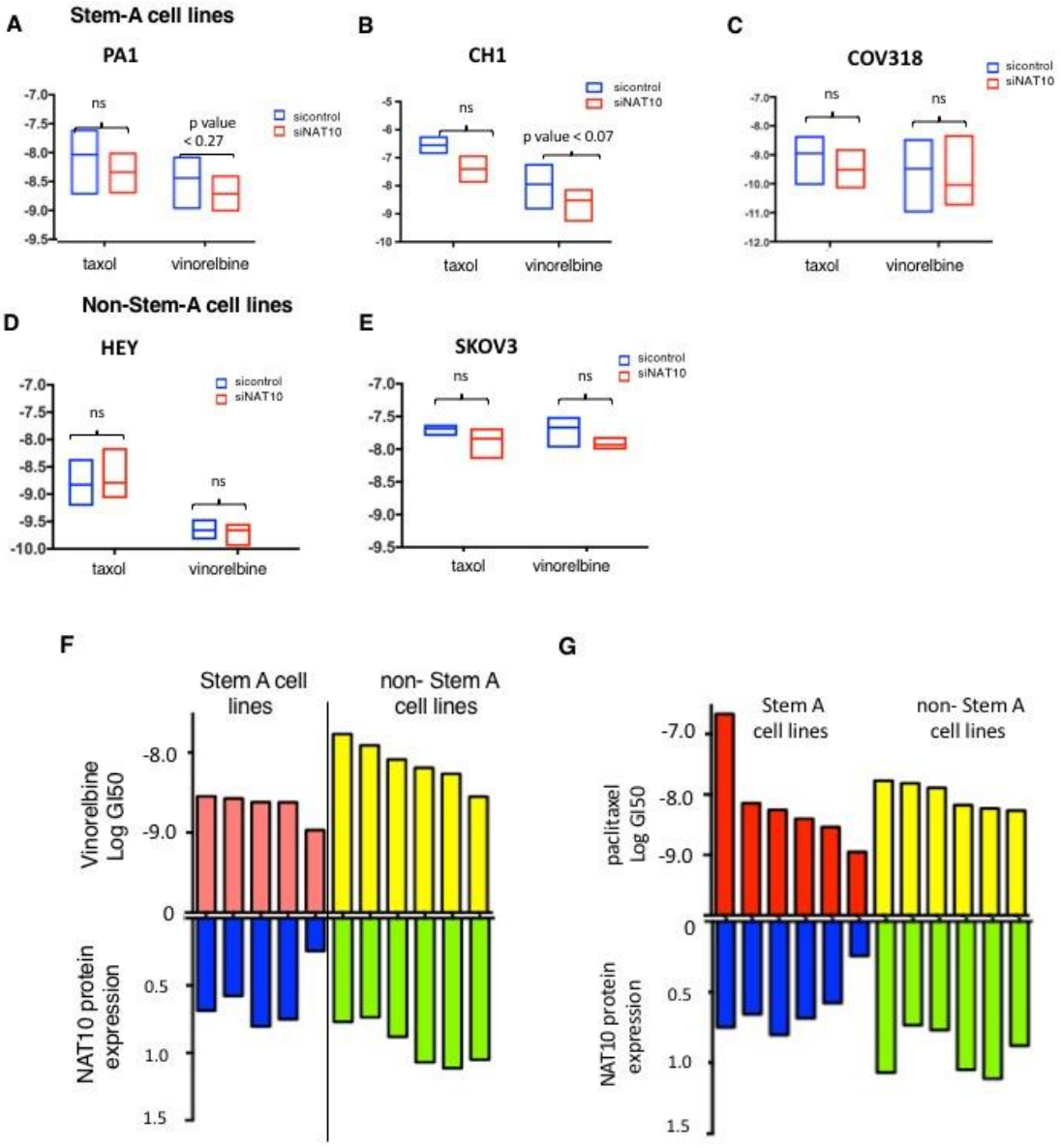
A
Stem-A cell lines
PA1
ns
p value
< 0.27
sicontrol
siNAT10
taxol
vinorelbine
B
CH1
ns
p value < 0.07
C
COV318
ns
ns
D
Non-Stem-A cell lines
HEY
ns
ns
E
SKOV3
ns
ns
F
Stem A cell lines
non- Stem A cell lines
Vinorelbine Log GI50
NAT10 protein expression
G
Stem A cell lines
non- Stem A cell lines
paclitaxel Log GI50
NAT10 protein expression

Figure 5.10: Depletion of NAT10 does not sensitize cells to microtubule targeting agents. Comparison of the Log GI50 values in *NAT10* depleted cells (siNAT10) and control cells (sicontrol) obtained from vinorelbine and paclixel response curves performed under different conditions for C5/Stem-A cell lines (A) PA-1; (B) CH1; (C) COV318 and non-C5/Stem-A cell lines (D) HEY and (E) SKOV3. Log GI50 for (F) vinorelbine and (G) paclitaxel for C5/Stem-A and non-C5/Stem-A cells were compared with their respective NAT10 protein expression. No trend was observed between NAT10 protein expression and sensitivity to microtubule targeting agents. Cell viability was measured using MTS assay and for each value was reported as a percentage of the effect obtained by employing the vehicle (DMSO) alone. Cells were treated for 2 days at varying concentrations of vinorelbine and paclitaxel. Data represent mean of at least 3 technical replicates per cell line. Where reported, error bars represent SEM. Non-significance was determined by paired t test. Protein quantification: Normalized fold changes in band intensities normalized to b-actin controls for NAT10 protein expression of individual cells.

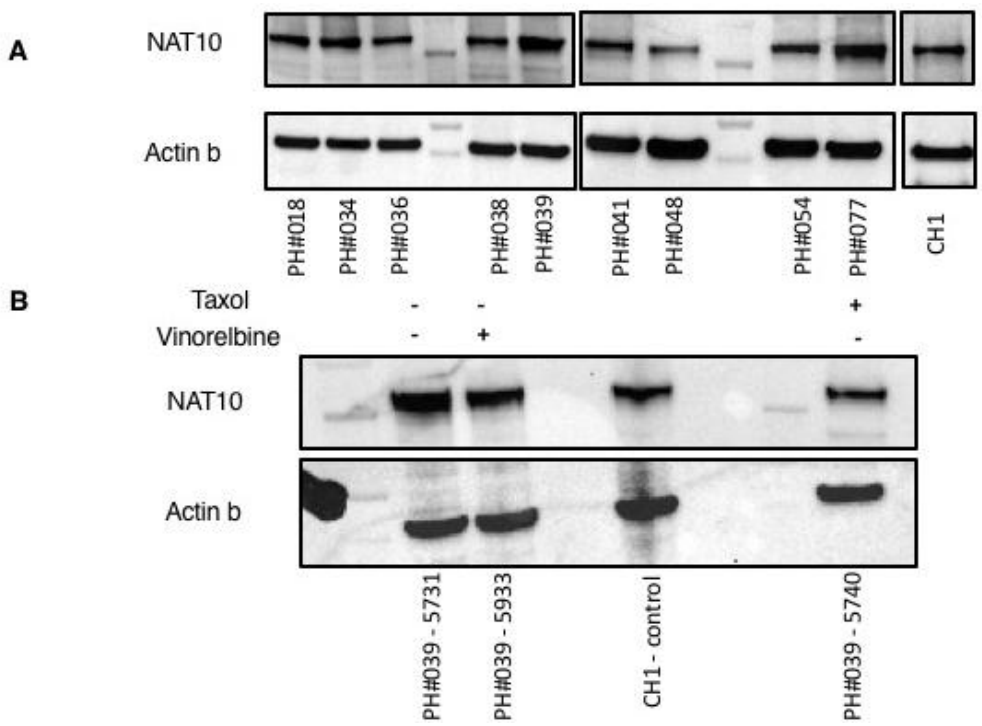

Figure 5.11: Ubiquitous NAT10 protein expression in C5/Stem-A PDX. (A) Western blot shows appreciable baseline NAT10 protein expression in all nine of the C5/Stem-A PDX. (B) No significant reduction in NAT10 expression in PDX PH#039 24 hours after two doses of microtubule targeting agents, vinorelbine or paclitaxel. CH1 C5/Stem-A cell line, known to over-express NAT10 protein was used as positive control (Tan et al., 2013).

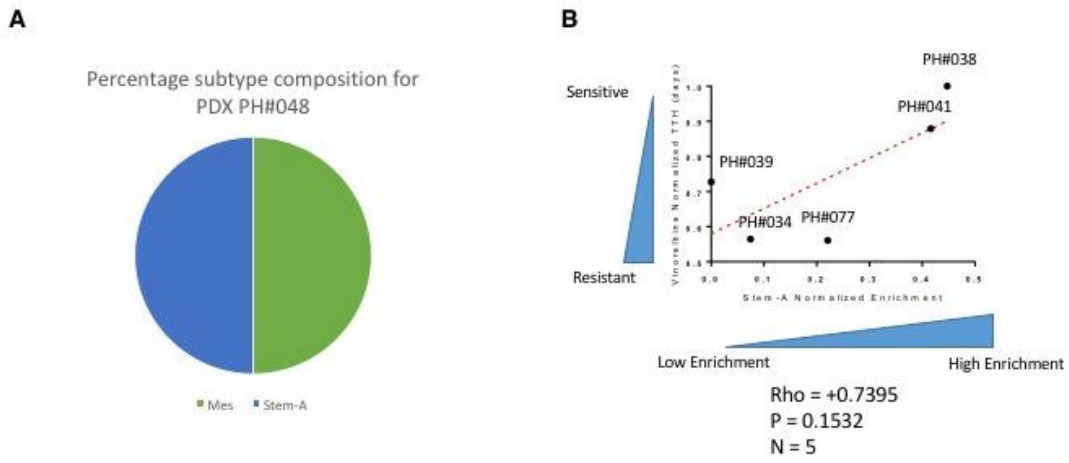

Figure 5.12: Intra-tumour transcriptomic heterogeneity in PDX shows increase in C5/Stem-A-ness correlates with increase vinorelbine response. Utility of MASH to decipher intra-tumoural heterogeneity shows multiple transcriptomic subtypes exist within the tumour as evidenced by (A) PDX PH#048. (B) PDX with higher C5/Stem-A signatures within the tumour showed improved response to vinorelbine. Y-axis: TTH for PDX treated with vinorelbine; x-axis: C5/Stem-A enrichment scores analysed using the MASH scheme.

Rho – 7.4, p value: 0.15. TTH = Time to Tumour Harvest. Shorter = more resistant. Normalized by max TTH, = 132 days

Chapter VI:
Discussion

6.1 Discussion:

EOC is the fifth leading cause of cancer mortality in western women (Ferlay et al., 2014; Vaughan et al., 2011). In Australia there are an estimated 1500 new cases annually and almost 1000 deaths from OC reported in 2010 (AIHW., 2012) while in Singapore, from 2009 – 2013, 1646 new cases of ovarian cancer were diagnosed over five years and 583 deaths were attributed to ovarian cancer (Singapore Cancer Registry, 2015). In 80% of patients with advanced epithelial ovarian cancer (EOC), the disease recurs despite optimal surgical cytoreduction and adjuvant systemic platinum-based chemotherapy. Recurrent EOC is incurable and it remains unclear why patients develop recurrent disease despite the high response rates (~70%) observed during 1st line chemotherapy. At disease recurrence, tumours may be platinum sensitive or resistant, and the spectrum of chemosensitivity may be partially explained by the existence of at least four different histological subtypes of EOC, namely: high grade serous (HGSOC), endometrioid, clear cell, and mucinous ovarian cancer. The clear cell and mucinous carcinomas are particularly chemoresistant tumours. Histological differences alone, however, cannot fully account for the heterogeneity in clinical outcomes because differences in patient outcome and responses to chemotherapy also exist between patients with seemingly identical histological EOC subtypes. Hitherto, the underlying mechanisms that underpin drug resistance in EOC have remained largely elusive. Plausible mechanisms include tumour heterogeneity driven by different molecular aberrations (Alsop et al., 2012; Bowtell et al., 2015; Etemadmoghadam et al., 2010; Tan et al., 2008) or molecular signatures (Tan et al., 2013a; Tothill et al., 2008), clonal evolution and/or chemoresistant stem cell-like populations in the primary tumour (Burrell et al., 2013; Patch et al., 2015)

To date, the one-size fits all approach of chemotherapy agents used in the recurrent disease setting, especially in platinum resistant disease, such as pegylated

liposomal doxorubicin (Gordon et al., 2004), topotecan (Sehouli et al., 2011) and gemcitabine (Mutch et al., 2007), have demonstrated minimal benefits in outcomes (Gordon et al., 2004; Mutch et al., 2007; Sehouli et al., 2011). Alternatively, when therapeutic approaches were targeted to a subgroup of patients either based on molecular biomarkers or underlying mechanisms of action, such as the anti-vascular endothelial growth factor (VEGF) antibody, bevacizumab in high risk patients (Perren et al., 2011) or platinum-resistant disease (Pujade-Lauraine et al., 2014) and olaparib, an inhibitor of the enzyme poly-(ADP ribose) polymerase inhibitor (PARPi) (Ledermann et al., 2012) in patients who harbor a *BRCA1/2* mutation, significant improvement in outcomes were observed. Furthermore, molecular subtypes in HGSOC have been used as biomarkers to predict for response to the angiogenesis inhibitor, bevacizumab in the ICON7 trial (Gourley et al., 2014; Kommoss et al., 2017).

However, opponents of molecular subtyping using gene expression data have argued about the lack of robustness of the subtypes and the relative ambiguity of this classification (Chen et al., 2017.). Indeed, when Chen et al attempted to re-implement three major previously validated subtyping methods (Helland et al., 2011; Tothill et al., 2008; Verhaak et al., 2012), they observed only a minority of HGSOC fell into the four predefined subtypes while a majority of samples (~75%) were not consistently labelled into the pre-specified subtypes (Chen et al., 2017.). This observation may arise in part due to the underlying biology of the disease. As highlighted in previous chapters of this thesis, HGSOC is heterogeneous. Using the MASH scheme, we showed that tumours often consist of several transcriptomic subtypes. Furthermore, the drivers of the subtypes, such as stromal or immune infiltration are continuous variables reflecting the assay used to classify them (ie. gene expression) compared to nominal classifications, ie: point mutations. We suspect that samples with low prediction scores are highly mixed with tumour consisting of several transcriptomic subtypes.

Notably, Chen et al argued that retaining the ambiguous/marginal cases impacts on the overall survival profiles of the subtypes (Chen et al., 2017.). Using the MASH scheme, we found that intra-tumour heterogeneity (ITH), determined using an ITH score to estimate ITH based on the transcriptomic subtype constituents within a tumor, did not correlate with clinical outcomes of overall survival or disease free survival from a database of 3,431 ovarian cancer transcriptomes— CSIOVDB (Tan et al., 2015) (Figure 6.1) (Tan & Heong et al, manuscript submitted). However, regardless of the ITH score, the existence of either one of the two poor prognostic subtypes, C1/Mes or C5/Stem-A, led to poorer outcomes (Figure 6.2). Tumors with Epi-A/Mes or Epi-A/Stem-A subtype had poorer OS and DFS compared to pure Epi-A tumors (HR = 0.619, $p = 0.0752$, and HR = 0.5424, $p = 0.0211$, respectively; Figure 6.2(B). A similar trend was observed with Epi-B/Mes and Epi-B/Stem-A tumors, although the difference was not significant for both OS and DFS when compared to pure Epi-B tumors. The co-existence of Mes/Stem-A subtypes within a tumor was observed to have the poorest OS and DFS, when compared to tumors consisting of pure Mes or Stem-A subtypes (HR = 1.583, $p = 0.0306$ and HR=1.91, $p = 0.0044$, respectively) (Figure 6.2(B).

Collectively, these data suggest that a tumour containing any degree of the poor prognostic Mes and/or Stem-A subtype/s conferred a poorer survival outcome compared to those containing neither of these two subtypes. In addition, the percentage of Mes or Stem-A subtype co-existing within a tumor also appeared to impact on clinical outcomes. Therefore, in future, it may be important to assess proportional scores along with the prediction scores for molecular subtype classification. Moreover, to further address the complexities of intra-tumoural heterogeneity in the C5/Stem-A HGSOC, single-cell RNA sequencing could be employed to enhance our understanding and improve precision molecular subtyping of HGSOC.

In this thesis, clinically relevant models of C5/Stem-A HGSOC were established to evaluate novel therapies. Mechanisms underlying response and resistance to putative C5/Stem-A candidate inhibitors were explored and pre - clinical data from the most promising inhibitor tested in this subtype was used to inform a clinical trial.

6.2 Aim One: To determine the complexity of C5/Stem-A HGSOC biology through characterization of a clinically relevant cohort of C5/ Stem-A PDX.

Little is known about the biology and underlying drivers of the C5/Stem-A HGSOC. PDX models have been used not only for drug discovery and identification of potential targetable pathways but also to recapitulate the diversity of the C5/Stem-A HGSOC molecular subtype and reflect tumour biology and metastatic properties of the original tumour (Whittle et al., 2015). Previously, the only available models for preclinical testing were cell lines and GEMM models, which are now considered to have a number of limitations in their modeling of HGSOC (Domcke et al., 2013). Indeed, our group along with others have successfully set up similar HGSOC PDX cohorts that reflected the primary tumour at both the histological and molecular level (Topp et al., 2014; Weroha et al., 2014). However, none have been selected based on the molecular subtypes of HGSOC. In this thesis, we developed a cohort of C5/Stem-A PDXs that recapitulated the primary tumour at the histological level and subsequently characterized each PDX both molecularly and functionally. This not only enhanced our understanding of the biology of the molecular subtype, but allowed the recapitulation of the diversity of molecular aberrations present in the primary tumour. Through the generation of this clinically relevant cohort, we demonstrated that despite the similarities inherent in their molecular classification, the C5/Stem-A HGSOC are indeed heterogenous, with no single,

unifying underlying oncogenic driver. The establishment of this cohort of C5/Stem-A PDX generated in this project will continue to be a valuable laboratory resource for further *in vivo* testing of novel compounds in a biologically relevant model. More importantly, it will enable further interrogation of resistance mechanisms in light of their individual platinum response and molecular aberrations. Furthermore, the C5/Stem-A PDXs are amenable to expansion, freeze/thaw cycles and can be considered as a renewable source of material for future expreiments.

6.3 Aim Two: To test efficacy of novel candidate inhibitors of C5/Stem-A HGSOC in the established PDX

Using our C5/Stem-A PDX cohort, we were able to validate the efficacy of the vinca alkaloid, vinorelbine in C5/Stem-A HGSOC previously reported in cell lines by Tan et al (Tan et al., 2013a). This clinically relevant model also allowed us to in part, dissect the mechanism of action hypothesized by Tan et al using HGSOC cell lines (Tan et al., 2013a). More importantly, using a biologically relevant model, we were able to demonstrate the lack of efficacy of a novel MYCN inhibitor shown to be efficacious when tested in MYCN-amplified neuroblastoma cell lines (Cheung, 2012). This highlights one of the major issues in drug development, which is the lack of adequate preclinical models that recapitulate the diversity and intra-tumoural heterogeneity often seen in patients (Whittle et al., 2015) and evaluating these new targets using established cell lines is limited by the poor correlation between responsiveness observed in cell lines versus that elicited in the patient (Scott et al., 2013; Johnson et al., 2001) leading to failure of multiple phase III therapeutic studies (Ellis and Fidler, 2010; Gillet et al., 2011).

In addition, using a larger cohort of five clinically relevant C5/Stem-A PDX, we demonstrated that MYCN is not a faithful predictor of response to BET bromodomain inhibitors as was previously shown (Baratta et al., 2015). Only one out of five PDX demonstrated anti-tumour activity to I-BET-762, when tested *in vivo.* This further highlights the need for not only clinically relevant pre clinical models for drug discovery, but also the importance of using more than one PDX for *in vivo* targeted therapeutic testing and biomarker validation.

6.4 Aim Three: To understand biology relevant for response or resistance of C5/Stem-A HGSOC to specific therapy.

We subsequently evaluated underlying mechanism of resistance to the BET bromodomain inhibitor, I-BET-762, and identified the Wnt pathway via the *FZD7-TWIST1* axis as a potential pathway of importance for modulation of BET bromodomain inhibitor response. Furthermore, we demonstrated that inhibition of the *FZD7-TWIST1* axis via sh*FZD7* resulted in C5/Stem-A cells being more vulnerable to I-BET-762 mediated growth suppression and cell death. In addition, inhibition of the *FZD7-TWIST1* axis via the small molecule porcupine inhibitor, C59, mimicked the functional outcomes of the sh*FZD7* model, leading to increased sensitivity to BET bromodomain inhibitor, I-BET-762. Future work from the laboratory will focus on combining the porcupine inhibitor with BET bromodomain inhibitors in the C5/Stem-A PDX and further understanding the mechanism underlying the synergy.

We also evaluated the hypothesis from Tan et al that *NAT10* was responsible for the underlying response of vinorelbine in C5/Stem-A HGSOC (Tan et al., 2013a) and found that *NAT10* was responsible for cellular proliferation in this molecular subtype but the gene did not affect sensitivity to

vinorelbine in the C5/Stem-A HGSOC cells. Several reports have alluded to the preferential sensitivity of individual molecular subtypes to certain compounds (Gourley et al., 2014; Kommoss et al., 2017; Tan et al., 2013a). Using the MASH scheme to interrogate the transcriptomic landscape of individual tumours, we demonstrated that PDX with higher percentage of C5/Stem-A composition were more sensitive to vinorelbine compared to cells with a lower C5/Stem-A composition. Hence, the C5-ness of the tumour impacted on response to targeted therapy. This is particularly relevant for stratification of patients into upcoming molecular subtype trials in HGSOC and highlights the importance of the heterogeneity within the C5/Stem-A HGSOC cohort.

6.5 Aim Four: To identify the most promising compound for C5/Stem-A HGSOC to inform a clinical trial.

Based on the compelling pre-clinical data of vinorelbine in C5/Stem-A HGSOC in both, platinum sensitive as well as platinum resistant PDX, a phase II signal-seeking trial was designed for C5/Stem-A HGSOC patients resistant or refractory to platinum based treatment. This is an international collaboration between Australia (led by investigators: Mileshkin, Bowtell and Scott) and Singapore (led by investigators: Tan, Huang and Heong) and will be the first trial to prospectively stratify patients based on their molecular subtype for therapeutic targeting. The trial was approved and will commence recruitment shortly at both sites, based on the strength of the preclinical data, known clinical parameters for vinorelbine, and the limited options for patients with recurrent platinum resistant/refractory disease.

Patients with platinum resistant recurrent HGSOC will be consented to the study and their surgical archival formalin-fixed paraffin-embedded (FFPE) primary ovarian or fallopian tube or primary peritoneal tumor blocks will be recalled and shipped to

Singapore. Principal investigator Huang and the Cancer Science Institute at National University Singapore (NUS) will perform Nanostring subtyping analysis on RNA generated from the diagnostic block. In a pilot analysis, using one block of archival FFPE tumor sample per patient (>70% tumour within the block), the assay was able to accurately stratify patients for subtype-specific therapeutic approaches. When analyzing metastatic or peritoneal deposits, the C5 subtype required a more thorough analysis with additional tumour blocks to yield similar results(Leong et al., 2015). As there is no clear evidence of whether the C5/Stem-A status changes from initial diagnosis compared to relapse disease, the patients' primary tumour blocks will be screened prospectively as to avoid treatment delays at time of relapse. Once C5/Stem-A subtype confirmation is established on the baseline diagnostic FFPE block (likely to be ~20% of platinum-resistant cases, ie 36 of 160 patients screened), patients who have relapsed disease and deemed platinum resistant or refractory will then be offered participation in this study.

A standard regimen of vinorelbine will be prescribed (30 mg/m^2, maximum 50 mg, Day 1 and 8 of a 21 day cycle, 6-8 cycles). Patients will be monitored with clinical assessments and serum Ca125 levels each cycle (21 days) and imaging (CT scan Chest, Abdomen and Pelvis) every 9 weeks as per standard of care. Toxicity will be assessed as per the CTCAE Version 4.03. Patients will be evaluated following a single arm open label Simon's Optimal two-stage design, with a null hypothesis of response rate of 10%, based on historical response data for platinum resistant recurrent OC with the alternative hypothesis of response rate of 30% or more in patients with C5/Stem-A HGSOC, following treatment with vinorelbine. Ten patients will be enrolled in the first stage between Singapore and Melbourne, for expansion to the second stage, which will involve an additional 19 patients. At a 5% level of significance, 29 patients are required for 80% power of rejecting the null hypothesis

and continuing to stage II if two or more out of ten patients have a response as per RECIST v1.1 to vinorelbine. Key eligibility criteria includes histologically confirmed HGSOC with platinum resistant or refractory disease; defined as progressive disease by imaging ≤ 6 months from last date of most recent platinum-based therapy or rising CA-125 based on GCIG criteria, C5/Stem-A molecular subtype based on nanostring technology; measurable disease as per RECIST v1.1; no prior exposure to vinorelbine; adequate organ function and good performance status (ECOG PS 0-1). Tumour samples via core biopsy and whole blood will also be collected at several timepoints throughout the study for the purpose of translational research (complete trial protocol in Appendix 4)

With this trial, patients with C5/Stem-A HGSOC will know that their cancer belongs to a molecularly-defined subgroup of HGSOC, for which therapies are currently being developed. The drivers and susceptibilities of C5/Stem-A HGSOC will be better understood, with a number of therapies proven to have efficacy in relevant pre-clinical human C5/Stem-A HGSOC models. The clinical trial of vinorelbine will constitute the proof-of-principle that prospective identification of HGSOC molecular subtypes could potentially be used as a biomarker for patient selection for specific therapeutic agents. It is likely that this will spawn a series of "bench to the bedside" clinical trials and a pipeline of C5/Stem-A-directed therapies, based on continuing research. Furthermore, this trial will afford patients with C5/Stem-A relapsed platinum resistant or refractory HGSOC additional treatment options that may potentially have greater benefit than standard chemotherapy.

Leveraging on translational samples from the clinical trial, future work could focus on understanding the molecular drivers and vulnerabilities of this subtype as well as the evolution under therapeutic pressure. The MASH scheme will also be employed to samples in the trial to enhance our understanding of intra-tumour

heterogeneity and its impact on subtype-specific therapy. The ability to dissect molecular events behind drug sensitivity and resistance in patient samples highlights the importance of bench-to-bedside clinical trials with robust translational components that can be exploited to benefit women with this devastating diagnosis

6.6 Concluding remarks

This thesis interrogated a molecular subtype of HGSOC, C5/Stem-A, by establishing a cohort of clinically relevant C5/Stem-A PDX and subsequently characterized the PDX both molecularly and functionally using standard platinum treatment. We also assessed the treatment responses to putative C5/Stem-A inhibitors shown to effective in the literature. We demonstrated that for pre-clinical therapeutic studies to be informative, they should be performed on a number of independent clinically relevant models of the disease before translation into clinical practice. The results from this thesis has informed a clinical trial that is currently recruiting in Singapore (clincaltrials.gov identifier: NCT03188159) and has led to two manuscripts currently under review. Further publications arising from this thesis will contribute to a growing body of work concerning biomarker evaluation and targeted treatment strategies in molecular subtypes of HGSOC. In addition, this PhD also facilitated and strengthened the strong collaboration between Cancer Science Institute, Singapore and the Walter and Eliza Hall Institute of Medical Research, Australia. By working together and building strong collaborations across the globe, we aim to ultimately improve outcomes for patients with ovarian cancer.

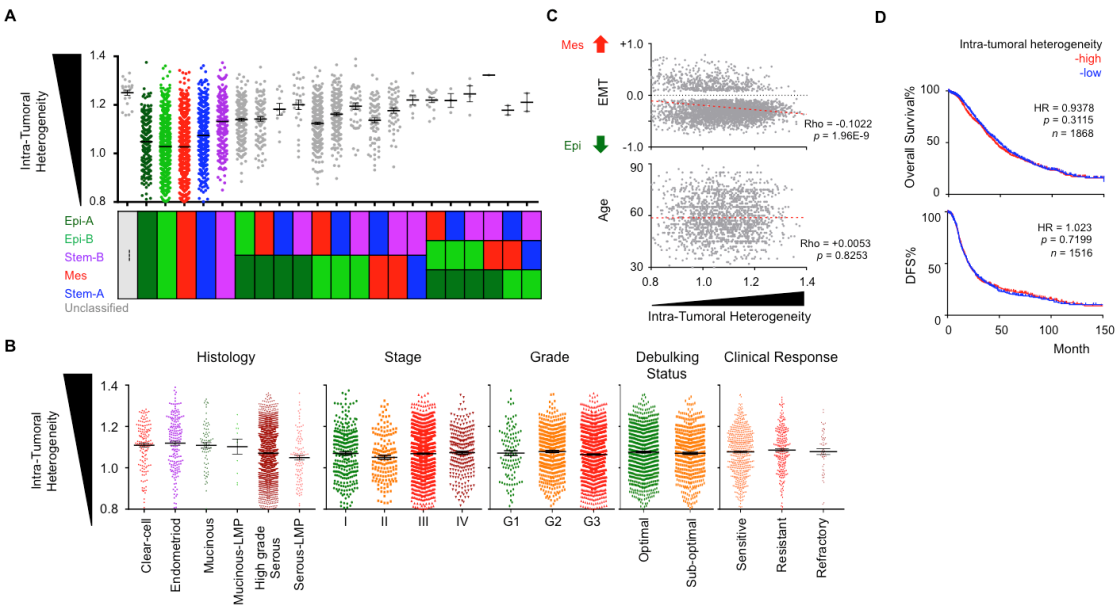

Figure 6.1: Correlation of intra-tumoral heterogeneity score and survival.

Kaplan-Meier analysis of overall- (A) and disease-free (B) survival in all samples with one subtype annotation (left panel), and stratified by ovarian cancer molecular subtypes (right panels). (C) Correlation plots of intra-tumor heterogeneity (*x*-axis) and EMT (*y*-axis; upper panel), and age (*y*-axis; lower panel). Rho and *p*-value is computed by Spearman correlation coefficient test. (D) Kaplan-Meier analysis of intra-tumor heterogeneity in overall (upper panel) and disease-free survival (lower panel). The *p*-value is computed by log-rank test. Median is used to stratify the patients into intra-tumor heterogeneity high (red) or low (blue). Significance is evaluated using log-rank test. Median of intra-tumoral heterogeneity score is used to separate the samples into high (red) and low groups (blue). Percentage bar chart shows the composition of good prognosis subtypes (non-Mes/Stem-A%; light blue) and poor prognosis subtypes (Mes/Stem-A; pink) in the intra-tumoral heterogeneity score-high and low groups. Significance is evaluated using Fisher Exact test. (Tan & Heong et al; manuscript submitted)

Abbrev: HR, hazard ratio.

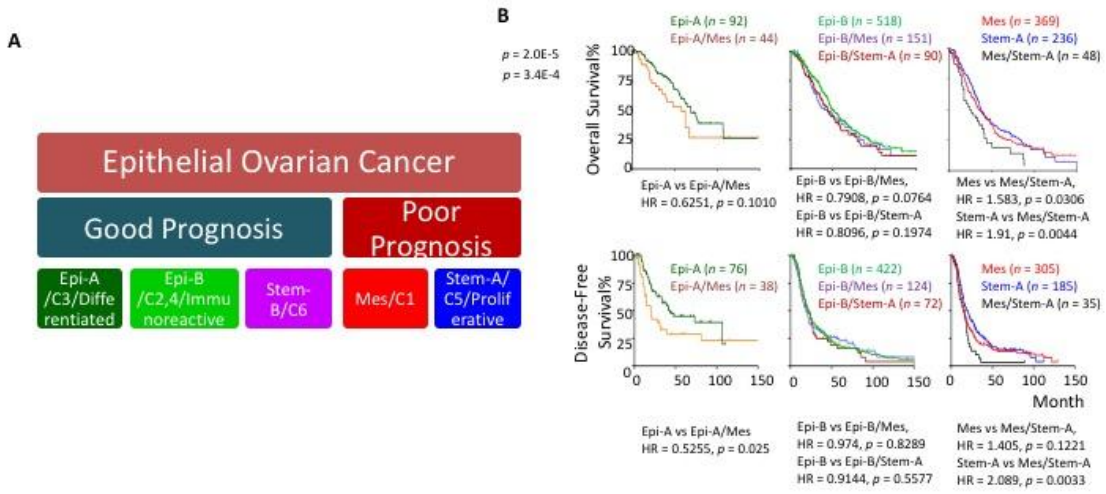

Figure 6.2: Molecular subtype composition is linked to clinical outcome in ovarian cancer.

(A) Epithelial ovarian cancer can be classified into five molecular subtypes: good prognosis (Epi)thelial-A/C3/Differentiated, (Epi)thelial-B/C4/Immunoreactive, (Stem)-like-B/C6; and poor prognosis (Mes)enchymal/C1, (Stem)-like-A/C5/Proliferative. Labels are given in order of Tan et al (Tan et al., 2013a)/ Tothill et al. (Tothill et al., 2008)/ TCGA (TCGA., 2011). (B) Kaplan-Meier analysis of overall- (upper panel) and disease-free (lower panel) survival stratified by molecular subtype compositions: Epi-A vs Epi-A/Mes (left); Epi-B vs Epi-B/Mes and Epi-B/Stem-A (middle); and Mes, Stem-A vs Mes/Stem-A (right). Significance is evaluated using log-rank test. (Tan & Heong et al; manuscript submitted)

Abbrev: HR, hazard ratio; OS, overall survival; DFS, disease-free survival

Subtype color code: Epi-A, dark green; Epi-B, light green; Mes, red; Stem-A, blue; Stem-B, purple.

Bibliography

Ahmed, A.A., Etemadmoghadam, D., Temple, J., Lynch, A.G., Riad, M., 2010. Driver mutations in TP53 are ubiquitous in high grade serous carcinoma of the ovary. J. Pathol. 221, 49–56.

AIHW, 2012. an overview 2012 1–215.

Alsop, K., Fereday, S., Meldrum, C., deFazio, A., Emmanuel, C., George, J., 2012. BRCA Mutation Frequency and Patterns of Treatment Response in BRCA Mutation-Positive Women With Ovarian Cancer: A Report From the Australian Ovarian Cancer Study Group. Journal of Clinical Oncology 30, 2654–2663.

Ansieau, S., Bastid, J., Doreau, A., Morel, A.-P., Bouchet, B.P., Thomas, C., 2008. Induction of EMT by twist proteins as a collateral effect of tumor-promoting inactivation of premature senescence. Cancer Cell 14, 79–89.

Asad, M., Wong, M.K., Tan, T.Z., Choolani, M., Low, J., Mori, S., 2014. FZD7 drives in vitro aggressiveness in Stem-A subtype of ovarian cancer via regulation of non-canonical Wnt/PCP pathway. Cell death and Disease 5, e1346–12.

Bajetta, E., Di Leo, A., Biganzoli, L., Mariani, L., Cappuzzo, F., Di Bartolomeo, 1996. Phase II study of vinorelbine in patients with pretreated advanced ovarian cancer: activity in platinum-resistant disease. J. Clin. Oncol. 14, 2546–2551.

Baratta, M.G., Schinzel, A.C., Zwang, Y., Bandopadhayay, P., Bowman-Colin, C., Kutt, J., 2015. An in-tumor genetic screen reveals that the BET bromodomain protein, BRD4, is a potential therapeutic target in ovarian carcinoma. Proc. Natl. Acad. Sci. U.S.A. 112, 232–237.

Baust, C.S., Kuhn, E., Valle, B.L., 2014. A genetically engineered ovarian cancer mouse model based on fallopian tube transformation mimics human high- grade serous carcinoma development. The Journal of Pathology 233(3), 228 -237.

Beaufort, C.M., Helmijr, J.C.A., Piskorz, A.M., Hoogstraat, M., Ruigrok-Ritstier, K., Besselink, N., 2014. Ovarian Cancer Cell Line Panel (OCCP): Clinical Importance of In Vitro Morphological Subtypes. PLoS ONE 9(9), e103988.

Bellmunt, J., Fougeray, R., Rosenberg, J.E., Maase, von der, H., Schutz, F.A., Salhi, Y., 2013. Long-term survival results of a randomized phase III trial of vinflunine plus best supportive care versus best supportive care alone in advanced urothelial carcinoma patients after failure of platinum-based chemotherapy. Ann. Oncol. 24, 1466 - 1472.

Benito, A., Lerga, A., Silva, M., Leon, J., 1997. Apoptosis of human myeloid leukemia cells induced by an inhibitor of protein phosphatases (okadaic acid) is prevented by Bcl-2 and Bcl-XL. Leukemia 11(7), 940 - 944.

Bois du, A., 2003. A Randomized Clinical Trial of Cisplatin/Paclitaxel Versus Carboplatin/Paclitaxel as First-Line Treatment of Ovarian Cancer. CancerSpectrum Knowledge Environment 95, 1320–1329.

Bois du, A., Reuss, A., Lauraine, E.P., Harter, P., 2009. Role of surgical outcome as prognostic factor in advanced epithelial ovarian cancer: a combined exploratory analysis of 3 prospectively randomized phase 3 multicenter trials. Cancer 115(6), 1234 - 1244.

Boj, S.F., Hwang, C.-I., Baker, L.A., Chio, I.I.C., Engle, D.D., Corbo, V., 2015. Organoid models of human and mouse ductal pancreatic cancer. Cell 160, 324–338.

Bolton, K.L., Chenevix-Trench, G., Goh, C., Sadetzki, S., Ramus, S.J., Karlan, B.Y., Lambrechts, D., EMBRACE, kConFab Investigators, Cancer Genome Atlas Research Network, 2012. Association between BRCA1 and BRCA2 mutations and survival in women with invasive epithelial ovarian cancer. JAMA 307, 382–390.

Bowtell, D.D., Böhm, S., Ahmed, A.A., Aspuria, P.-J., Bast, R.C., Beral, V., Berek, J.S., 2015. Rethinking ovarian cancer II: reducing mortality from high-grade serous ovarian cancer. Nat. Rev. Cancer 15, 668–679.

Brodeur, G.M., 2003. Neuroblastoma: biological insights into a clinical enigma. Nat. Rev. Cancer 3, 203–216.

Brodeur, G.M., Seeger, R.C., Schwab, M., Varmus, H.E., Bishop, J.M., 1984. Amplification of N-myc in untreated human neuroblastomas correlates with advanced disease stage. Science 224, 1121–1124.

Burger, R.A., DiSaia, P.J., Roberts, J.A., O'rourke, M., Gershenson, D.M., Homesley, H.D., Lichtman, S.M., 1999. Phase II trial of vinorelbine in recurrent and progressive epithelial ovarian cancer. Gynecologic Oncology 72, 148–153.

Burrell, R.A., McGranahan, N., Bartek, J., Swanton, C., 2013. The causes and consequences of genetic heterogeneity in cancer evolution. Nature 501, 338–345.

Buys, S.S., Partridge, E., Black, A., Johnson, C.C., 2011. Effect of screening on ovarian cancer mortality: the Prostate, Lung, Colorectal and Ovarian (PLCO) cancer screening randomized controlled trial. JAMA 305, 2295 - 2303.

Cadron, I., Leunen, K., Amant, F., Van Gorp, T., Neven, P., Vergote, I., 2007. The “Leuven” dose-dense paclitaxel/carboplatin regimen in patients with recurrent ovarian cancer. Gynecologic Oncology 106, 354–361.

Collaborative Group on Epidemiological Studies of Ovarian Cancer., 2012. Ovarian Cancer and Body Size: Individual Participant Meta-Analysis Including 25,157 Women with Ovarian Cancer from 47 Epidemiological Studies. PLoS Med. 9, e1001200.

Collaborative Group on Epidemiological Studies of Ovarian Cancer., 2015. Menopausal hormone use and ovarian cancer risk: individual participant meta-analysis of 52 epidemiological studies. The Lancet 385, 1835 - 1842.

Cantilena, S., Pastorino, F., Pezzolo, A., Chayka, O., 2011. Frizzled receptor 6 marks rare, highly tumourigenic stem-like cells in mouse and human neuroblastomas.

Oncotarget 2, 976 - 983.

Chaidos, A., Caputo, V., Gouvedenou, K., Liu, B., Marigo, I., Chaudhry, M.S., Rotolo, A., 2014. Potent antimyeloma activity of the novel bromodomain inhibitors I-BET151 and I-BET762. Blood 123, 697–705.

Chen, G.M., Kannan, L., Geistlinger, L., Kofia, V., Safikhani, Z., Gendoo, D.M.A., Parmigiani, 2017. Consensus on Molecular Subtypes of Ovarian Cancer. bioRxiv 162685; doi:10.1101/162685

Chen, V.W., Ruiz, B., Killeen, J.L., Coté, T.R., Wu, X.C., 2003. Pathology and classification of ovarian tumors. Cancer 97, 2631 - 2642.

Cheng, G.Z., Chan, J., Wang, Q., Zhang, W., Sun, C.D., 2007. Twist transcriptionally up-regulates AKT2 in breast cancer cells leading to increased migration, invasion, and resistance to paclitaxel. Cancer Research 67, 1979 - 1987.

Cheung, L., 2012. The Isolation and Characterisation of Novel Small Molecule Inhibitors of the MYCN Transcriptional Pathway for the Potential Treatment of Childhood Neuroblastoma 1–239.

Chuaqui, R.F., Cole, K.A., Emmert-Buck, M.R., Merino, M.J., 1998. Histopathology and molecular biology of ovarian epithelial tumors. Ann Diagn Pathol 2, 195–207.

Ciriello, G., Miller, M.L., Aksoy, B.A., Senbabaoglu, Y., Schultz, N., Sander, C., 2013. Emerging landscape of oncogenic signatures across human cancers. Nat Genet 45, 1127–1133. doi:10.1038/ng.2762

Cragg, M.S., Harris, C., Strasser, A., Scott, C.L., 2009. Unleashing the power of inhibitors of oncogenic kinases through BH3 mimetics. Nat. Rev. Cancer 9, 321–326. doi:10.1038/nrc2615

Dawson, M.A., Prinjha, R.K., Dittmann, A., Giotopoulos, G., Bantscheff, M., Chan, W.-I., et al 2011. Inhibition of BET recruitment to chromatin as an effective treatment for MLL-fusion leukaemia. Nature 478, 529–533. doi:10.1038/nature10509

Dekkers, J.F., Wiegerinck, C.L., de Jonge, H.R., Bronsveld, I., Janssens, H.M., de Winter-de Groot, K.M., Brandsma, A.M., 2013. A functional CFTR assay using primary cystic fibrosis intestinal organoids. Nat. Med. 19, 939–945. doi:10.1038/nm.3201

Delbridge, A.R.D., Grabow, S., Strasser, A., Vaux, D.L., 2016. Thirty years of BCL-2: translating cell death discoveries into novel cancer therapies. Nat. Rev. Cancer 16, 99–109. doi:10.1038/nrc.2015.17

Delmore, J.E., Issa, G.C., Lemieux, M.E., Rahl, P.B., Shi, J., Jacobs, H.M., Kastritis, E., Gilpatrick, T., et al 2011. BET Bromodomain Inhibition as a Therapeutic Strategy to Target c-Myc. Cell 146, 904–917. doi:10.1016/j.cell.2011.08.017

Deng, J., Shimamura, T., Perera, S., Carlson, N.E., Cai, D., Shapiro, G.I., Wong, K.-K., Letai, A., 2007. Proapoptotic BH3-only BCL-2 family protein BIM connects death

signaling from epidermal growth factor receptor inhibition to the mitochondrion. Cancer Research 67, 11867–11875. doi:10.1158/0008-5472.CAN-07-1961

DeRose, Y.S., Gligorich, K.M., Wang, G., 2013. Patient- Derived Models of Human Breast Cancer: Protocols for In Vitro and In Vivo Applications in Tumor Biology and Translational Medicine. Curr Protoc Pharmacol, Chapter 14 Unit 14.23:1 -52.

Dey, A., Nishiyama, A., Karpova, T., McNally, J., Ozato, K., 2009. Brd4 marks select genes on mitotic chromatin and directs postmitotic transcription. Mol. Biol. Cell 20, 4899–4909. doi:10.1091/mbc.E09-05-0380

Domcke, S., Sinha, R., Levine, D.A., Sander, C., Schultz, N., 2013. Evaluating cell lines as tumour models by comparison of genomic profiles. Nature Communications 4, 1–10. doi:10.1038/ncomms3126

Ellis, L.M., Fidler, I.J., 2010. Finding the tumor copycat: therapy fails, patients don't. Nat. Med. 16, 974 - 975.

Etemadmoghadam, D., George, J., Cowin, P.A., Cullinane, C., Kansara, M., Australian Ovarian Cancer Study Group, Gorringe, K.L., Smyth, G.K., Bowtell, D.D.L., 2010. Amplicon-Dependent CCNE1 Expression Is Critical for Clonogenic Survival after Cisplatin Treatment and Is Correlated with 20q11 Gain in Ovarian Cancer. PLoS ONE 5, e15498. doi:10.1371/journal.pone.0015498.s009

Etemadmoghadam, D., Weir, B.A., 2013. Synthetic lethality between CCNE1 amplification and loss of BRCA1. PNAS 110, 19489 - 19494.

Feng, M., Wang, K., Song, H., Yu, H., Qin, Y., Shi, Q., 2009. Metastasis-induction and apoptosis-protection by TWIST in gastric cancer cells. Clinical & experimental Metastasis 26, 1013 - 1021

Ferlay J, Soerjomataram I, Ervik M, Dikshit R, Eser S, Mathers C, Rebelo M, Parkin DM, Forman D, Bray, F. GLOBOCAN 2012 v1.0, Cancer Incidence and Mortality Worldwide: IARC CancerBase No. 11. Lyon, France: International Agency for Research on Cancer; 2013. Available from: http://globocan.iarc.fr, accessed on day/month/year.

Filippakopoulos, P., Qi, J., Picaud, S., Shen, Y., Smith, W.B., Fedorov, O., Morse, E.M., Keates, T., Hickman, T.T., Felletar, I., Philpott, M., Munro, S., McKeown, M.R., Wang, Y., Christie, A.L., West, N., Cameron, M.J., Schwartz, B., Heightman, T.D., La Thangue, N., French, C.A., Wiest, O., Kung, A.L., Knapp, S., Bradner, J.E., 2010. Selective inhibition of BET bromodomains. Nature 468, 1067–1073. doi:10.1038/nature09504

Fleming, J.M., Miller, T.C., Meyer, M.J., 2010. Local regulation of human breast xenograft models. Journal of cellular Physiology 224, 795 - 806.

Fong, C.Y., Gilan, O., Lam, E.Y.N., Rubin, A.F., Ftouni, S., Tyler, D., Stanley, K., Sinha, D., Yeh, P., Morison, J., Giotopoulos, G., Lugo, D., Jeffrey, P., Lee, S.C.-W., Carpenter, C., Gregory, R., Ramsay, R.G., Lane, S.W., Abdel-Wahab, O., Kouzarides, T., Johnstone, R.W., Dawson, S.-J., Huntly, B.J.P., Prinjha, R.K., Papenfuss, A.T., Dawson, M.A., 2015. BET inhibitor resistance emerges from

leukaemia stem cells. Nature 525, 538–542. doi:10.1038/nature14888

Fong, P.C., Boss, D.S., Yap, T.A., Tutt, A., Wu, P., Mergui-Roelvink, M., Mortimer, P., Swaisland, H., Lau, A., O'Connor, M.J., Ashworth, A., Carmichael, J., Kaye, S.B., Schellens, J.H.M., de Bono, J.S., 2009. Inhibition of poly(ADP-ribose) polymerase in tumors from BRCA mutation carriers. N Engl J Med 361, 123–134. doi:10.1056/NEJMoa0900212

Forshew, T., Murtaza, M., Parkinson, C., Gale, D., Tsui, D.W.Y., Kaper, F., Dawson, S.-J., Piskorz, A.M., Jimenez-Linan, M., Bentley, D., Hadfield, J., May, A.P., Caldas, C., Brenton, J.D., Rosenfeld, N., 2012. Noninvasive identification and monitoring of cancer mutations by targeted deep sequencing of plasma DNA. Science Translational Medicine 4, 136ra68. doi:10.1126/scitranslmed.3003726

Fotopoulou, C., Zang, R., Gultekin, M., Cibula, D., 2013. Value of tertiary cytoreductive surgery in epithelial ovarian cancer: an international multicenter evaluation. Annals of surgical Oncology 20, 1348 - 1354.

Fujii, N., You, L., Xu, Z., Uematsu, K., Shan, J., He, B., Mikami, I., 2007. An Antagonist of Dishevelled Protein-Protein Interaction Suppresses β-Catenin–Dependent Tumor Cell Growth. Cancer Research. 67, 573 - 579.

Garcia, S., Freitas, A.A., 2012. Humanized mice: current states and perspectives. Immunology letters. 146, pp 1-7

George, J., Alsop, K., Etemadmoghadam, D., Hondow, H., Mikeska, T., Dobrovic, A., deFazio, A., for the Australian Ovarian Cancer Study Group, Smyth, G.K., Levine, D.A., Mitchell, G., Bowtell, D.D., 2013. Nonequivalent Gene Expression and Copy Number Alterations in High-Grade Serous Ovarian Cancers with BRCA1 and BRCA2 Mutations. Clinical Cancer Research 19, 3474–3484. doi:10.1158/1078-0432.CCR-13-0066

George, M.J., Heron, J.F., Kerbrat, P., Chauvergne, J., Goupil, A., Lebrun, D., Guastalla, J.P., Namer, M., Bugat, R., Ayme, Y., 1989. Navelbine in advanced ovarian epithelial cancer: a study of the French oncology centers. Semin. Oncol. 16, 30–32.

Gershenson, D.M., Burke, T.W., Morris, M., Bast, R.C., Guaspari, A., Hohneker, J., Wharton, J.T., 1998. A phase I study of a daily x3 schedule of intravenous vinorelbine for refractory epithelial ovarian cancer. Gynecologic Oncology 70, 404–409. doi:10.1006/gyno.1998.5130

Gillet, J.-P., Calcagno, A.M., Varma, S., Marino, M., Green, L.J., Vora, M.I., Patel, C., Orina, J.N., Eliseeva, T.A., Singal, V., Padmanabhan, R., Davidson, B., Ganapathi, R., Sood, A.K., Rueda, B.R., Ambudkar, S.V., Gottesman, M.M., 2011. Redefining the relevance of established cancer cell lines to the study of mechanisms of clinical anti-cancer drug resistance. Proc. Natl. Acad. Sci. U.S.A. 108, 18708–18713. doi:10.1073/pnas.1111840108

Goodnough, L.H., Dinuoscio, G.J., Atit, R.P., 2016. Twist1 contributes to cranial bone initiation and dermal condensation by maintaining Wnt signaling responsiveness. Dev. Dyn. 245, 144–156. doi:10.1002/dvdy.24367

Gordon, A.N., Granai, C.O., Rose, P.G., Hainsworth, J., Lopez, A., Weissman, C., Rosales, R., Sharpington, T., 2000. Phase II study of liposomal doxorubicin in platinum- and paclitaxel-refractory epithelial ovarian cancer. J. Clin. Oncol. 18, 3093–3100.

Gordon, A.N., Tonda, M., Sun, S., Rackoff, W., 2004. Long-term survival advantage for women treated with pegylated liposomal doxorubicin compared with topotecan in a phase 3 randomized study of recurrent and refractory epithelial ovarian cancer. Gynecologic Oncology 95, 1–8. doi:10.1016/j.ygyno.2004.07.011

Gourley C, McCavigan A, Perren T, Paul J, Michie CO, Churchman M, Williams A, McCluggage WG, Parmar M, Kaplan RS et al. 2014. Molecular subgroup of high-grade serous ovarian cancer (HGSOC) as a predictor of outcome following bevacizumab. Journal of Clinical Oncology 32**:** suppl. 5502

Gurney, A., Axelrod, F., Bond, C.J., Cain, J., Chartier, C., Donigan, L., Fischer, M., Chaudhari, A., Ji, M., Kapoun, A.M., Lam, A., Lazetic, S., Ma, S., Mitra, S., Park, I.-K., Pickell, K., Sato, A., Satyal, S., Stroud, M., Tran, H., Yen, W.-C., Lewicki, J., Hoey, T., 2012. Wnt pathway inhibition via the targeting of Frizzled receptors results in decreased growth and tumorigenicity of human tumors. Proc. Natl. Acad. Sci. U.S.A. 109, 11717–11722. doi:10.1073/pnas.1120068109

Harter, P., Bois, du, A., Hahmann, M., Hasenburg, A., 2006. Surgery in recurrent ovarian cancer: the Arbeitsgemeinschaft Gynaekologische Onkologie (AGO) DESKTOP OVAR trial. Annals of surgical Oncology 13, 1702 -1710.

Helland, Å., Anglesio, M.S., George, J., Cowin, P.A., Johnstone, C.N., House, C.M., Sheppard, K.E., Etemadmoghadam, D., Melnyk, N., Rustgi, A.K., Phillips, W.A., Johnsen, H., Holm, R., Kristensen, G.B., Birrer, M.J., Australian Ovarian Cancer Study Group, Pearson, R.B., Børresen-Dale, A.-L., Huntsman, D.G., deFazio, A., Creighton, C.J., Smyth, G.K., Bowtell, D.D.L., 2011. Deregulation of MYCN, LIN28B and LET7 in a Molecular Subtype of Aggressive High-Grade Serous Ovarian Cancers. PLoS ONE 6, e18064. doi:10.1371/journal.pone.0018064.s016

Henssen, A., Althoff, K., Odersky, A., Beckers, A., Koche, R., Speleman, F., Scha fers, S., Bell, E., Nortmeyer, M., Westermann, F., De Preter, K., Florin, A., Heukamp, L., Spruessel, A., Astrahanseff, K., Lindner, S., Sadowski, N., Schramm, A., Astorgues-Xerri, L., Riveiro, M.E., Eggert, A., Cvitkovic, E., Schulte, J.H., 2016. Targeting MYCN-Driven Transcription By BET-Bromodomain Inhibition. Clinical Cancer Research 22, 2470–2481. doi:10.1158/1078-0432.CCR-15-1449

Horowitz, N.S., Miller, A., Rungruang, B., 2015. Does aggressive surgery improve outcomes? Interaction between preoperative disease burden and complex surgery in patients with advanced-stage ovarian cancer: An Analysis of GOG182. Journal of Clinical Oncology 8, 937- 943.

Hosono, S., Kajiyama, H., Terauchi, M., 2007. Expression of Twist increases the risk for recurrence and for poor survival in epithelial ovarian carcinoma patients. British journal of Cancer 96, 314 - 320.

Howe, L.R., Watanabe, O., Leonard, J., Brown, A., 2003. Twist is up-regulated in

response to Wnt1 and inhibits mouse mammary cell differentiation. Cancer Research. 63, 1906 - 1913.

Huang, R.Y.-J., Wong, M.K., Tan, T.Z., Kuay, K.T., Ng, A.H.C., Chung, V.Y., Chu, Y.-S., Matsumura, N., Lai, H.-C., Lee, Y.F., Sim, W.-J., Chai, C., Pietschmann, E., Mori, S., Low, J.J.H., Choolani, M., Thiery, J.-P., 2013. An EMT spectrum defines an anoikis-resistant and spheroidogenic intermediate mesenchymal state that is sensitive to e-cadherin restoration by a src-kinase inhibitor, saracatinib (AZD0530) 4, e915–13. doi:10.1038/cddis.2013.442

Ince, T.A., Sousa, A.D., Jones, M.A., Harrell, J.C., 2015. Characterization of twenty-five ovarian tumour cell lines that phenocopy primary tumours. Nature Communications 6, 7419

Johnson, J.I., Decker, S., Zaharevitz, D., 2001. Relationships between drug activity in NCI preclinical in vitro and in vivo models and early clinical trials. British journal of Cancer 84, 1424 - 1431.

Jones, S., Wang, T.L., Shih, I.M., Mao, T.L., 2010. Frequent mutations of chromatin remodeling gene ARID1A in ovarian clear cell carcinoma. Science 330, 228 - 231.

Kang, J.-H., Rychahou, P.G., Ishola, T.A., Qiao, J., Evers, B.M., Chung, D.H., 2006. MYCN silencing induces differentiation and apoptosis in human neuroblastoma cells. Biochemical and Biophysical Research Communications 351, 192–197.

Kantarjian, H.M., O'Brien, S., Smith, T.L., Cortes, J., Giles, F.J., Beran, M., Pierce, S., Huh, Y., Andreeff, M., Koller, C., Ha, C.S., Keating, M.J., Murphy, S., Freireich, E.J., 2000. Results of treatment with hyper-CVAD, a dose-intensive regimen, in adult acute lymphocytic leukemia. J. Clin. Oncol. 18, 547–561.

Karst, A.M., Levanon, K., Drapkin, R., 2011. Modeling high-grade serous ovarian carcinogenesis from the fallopian tube. Proc. Natl. Acad. Sci. U.S.A. 108, 7547–7552.

Kelemen, L.E., Köbel, M., 2011. Mucinous carcinomas of the ovary and colorectum: different organ, same dilemma. Lancet Oncol. 12, 1071 - 1080.

Kenny, H.A., Chiang, C.Y., White, E.A., 2014. Mesothelial cells promote early ovarian cancer metastasis through fibronectin secretion. The Journal of clinical Investigtion 124, 4614 - 4628.

Kenny, H.A., Lal-Nag, M., White, E.A., Shen, M., Chiang, C.-Y., Mitra, A.K., Zhang, Y., Curtis, M., Schryver, E.M., Bettis, S., Jadhav, A., Boxer, M.B., Li, Z., Ferrer, M., Lengyel, E., 2015. Quantitative high throughput screening using a primary human three-dimensional organotypic culture predicts in vivo efficacy. Nature Communications 6, 6220.

Kim, J., Coffey, D.M., Ma, L., Matzuk, M.M., 2015. The ovary is an alternative site of origin for high-grade serous ovarian cancer in mice. Endocrinology.156, 1975 - 1981.

Kinde, I., Bettegowda, C., Wang, Y., Wu, J., 2013. Evaluation of DNA from the

Papanicolaou test to detect ovarian and endometrial cancers. Science translational Medicine 5, 167ra4

Kindelberger, D.W., Lee, Y., Miron, A., 2007. Intraepithelial carcinoma of the fimbria and pelvic serous carcinoma: evidence for a causal relationship. The American journal of Surgical Pathology 31, 161-169.

Kolfschoten, G.M., Pinedo, H.M., Scheffer, P.G., 2000. Development of a panel of 15 human ovarian cancer xenografts for drug screening and determination of the role of the glutathione detoxification system. Gynecologic Oncology 76, 362 - 368.

Kommoss, S., Winterhoff, B., Oberg, A., Konecny, G.E., 2017. Bevacizumab may differentially improve ovarian cancer outcome in patients with proliferative and mesenchymal molecular subtypes. Clinical Cancer Research 23, 3794 - 3801.

Konecny, G.E., Wang, C., Hamidi, H., Winterhoff, B., Kalli, K.R., Dering, J., Ginther, C., Chen, H.-W., Dowdy, S., Cliby, W., Gostout, B., Podratz, K.C., Keeney, G., Wang, H.-J., Hartmann, L.C., Slamon, D.J., Goode, E.L., 2014. Prognostic and therapeutic relevance of molecular subtypes in high-grade serous ovarian cancer. CancerSpectrum Knowledge Environment 106.

Kortmann, U., McAlpine, J.N., Xue, H., Guan, J., Ha, G., Tully, S., Shafait, S., Lau, A., Cranston, A.N., O'Connor, M.J., Huntsman, D.G., Wang, Y., Gilks, C.B., 2011. Tumor Growth Inhibition by Olaparib in BRCA2 Germline-Mutated Patient-Derived Ovarian Cancer Tissue Xenografts. Clinical Cancer Research 17, 783–791.

Kotsopoulos, J., Lubinski, J., Gronwald, J., 2015. Factors influencing ovulation and the risk of ovarian cancer in BRCA1 and BRCA2 mutation carriers. International journal of cancer. 137, pp1136 - 1146.

Köbel, M., Kalloger, S.E., Carrick, J., 2009. A limited panel of immunomarkers can reliably distinguish between clear cell and high-grade serous carcinoma of the ovary. The American journal of Surgical Pathology 33, 14 - 21.

Kuhn, E., Kurman, R.J., Vang, R., Sehdev, A.S., 2012. TP53 mutations in serous tubal intraepithelial carcinoma and concurrent pelvic high- grade serous carcinoma—evidence supporting the clonal relationship of the two lesions. The Journal of Pathology 226, 421 - 426.

Kuo, K.T., Mao, T.L., Jones, S., Veras, E., Ayhan, A., 2009. Frequent activating mutations of PIK3CA in ovarian clear cell carcinoma. The American journal of Pathology 174, 1597.

Kurimchak, A.M., Shelton, C., Duncan, K.E., Johnson, K.J., Brown, J., O'Brien, S., Gabbasov, R., Fink, L.S., Li, Y., Lounsbury, N., Abou-Gharbia, M., Childers, W.E., Connolly, D.C., Chernoff, J., Peterson, J.R., Duncan, J.S., 2016. Resistance to BET Bromodomain Inhibitors Is Mediated by Kinome Reprogramming in Ovarian Cancer. Cell Rep 16, 1273–1286.

Kurman, R.J., Shih, I.-M., 2010. The origin and pathogenesis of epithelial ovarian cancer: a proposed unifying theory. Am. J. Surg. Pathol. 34, 433–443.

Kuroda, J., Puthalakath, H., Cragg, M.S., Kelly, P.N., Bouillet, P., Huang, D.C.S., Kimura, S., Ottmann, O.G., Druker, B.J., Villunger, A., Roberts, A.W., Strasser, A., 2006. Bim and Bad mediate imatinib-induced killing of Bcr/Abl+ leukemic cells, and resistance due to their loss is overcome by a BH3 mimetic. Proc. Natl. Acad. Sci. U.S.A. 103, 14907–14912.

Kwong, J., Chan, F.L., Wong, K.-K., Birrer, M.J., Archibald, K.M., Balkwill, F.R., 2009. Inflammatory cytokine tumor necrosis factor alpha confers precancerous phenotype in an organoid model of normal human ovarian surface epithelial cells. Neoplasia 11, 529–541.

Le, D.T., Uram, J.N., Wang, H., Bartlett, B.R., Kemberling, H., Eyring, A.D., 2015. PD-1 Blockade in Tumors with Mismatch-Repair Deficiency. N Engl J Med 372, 2509–2520. doi:10.1056/NEJMoa1500596

Ledermann, J., Harter, P., Gourley, C., Friedlander, M., Vergote, I., Rustin, G., 2012. Olaparib maintenance therapy in platinum-sensitive relapsed ovarian cancer. N Engl J Med 366, 1382–1392. doi:10.1056/NEJMoa1105535

Lee, Y., Miron, A., Drapkin, R., Nucci, M.R., Medeiros, F., Saleemuddin, A., 2007. A candidate precursor to serous carcinoma that originates in the distal fallopian tube. J. Pathol. 211, 26–35. doi:10.1002/path.2091

Leong, H.S., Galletta, L., Etemadmoghadam, D., George, J., The Australian Ovarian Cancer Study, Köbel, M., Ramus, S.J., Bowtell, D., 2015. Efficient molecular subtype classification of high-grade serous ovarian cancer. J. Pathol. n/a–n/a. doi:10.1002/path.4536

Levanon, K., Ng, V., Piao, H.Y., Zhang, Y., Chang, M.C., Roh, M.H., Kindelberger, D.W., Hirsch, M.S., Crum, C.P., Marto, J.A., Drapkin, R., 2010. Primary ex vivo cultures of human fallopian tube epithelium as a model for serous ovarian carcinogenesis. Oncogene 29, 1103–1113. doi:10.1038/onc.2009.402

Li, Q.Q., Xu, J.D., Wang, W.J., Cao, X.X., Chen, Q., Tang, F., 2009. Twist1-mediated adriamycin-induced epithelial-mesenchymal transition relates to multidrug resistance and invasive potential in breast cancer cells. Clinical Cancer Research

Liu, H., Patel, M.R., Prescher, J.A., Patsialou, A., Qian, D., Lin, J., Wen, S., Chang, Y.-F., Bachmann, M.H., Shimono, Y., Dalerba, P., Adorno, M., Lobo, N., Bueno, J., Dirbas, F.M., Goswami, S., Somlo, G., Condeelis, J., Contag, C.H., Gambhir, S.S., Clarke, M.F., 2010. Cancer stem cells from human breast tumors are involved in spontaneous metastases in orthotopic mouse models. Proc. Natl. Acad. Sci. U.S.A. 107, 18115–18120. doi:10.1073/pnas.1006732107

Liu, Y., Beyer, A., Aebersold, R., 2016. On the dependency of cellular protein levels on mRNA abundance. Cell.165, 535 - 550.

Lockwood, W.W., Zejnullahu, K., Bradner, J.E., Varmus, H., 2012. Sensitivity of human lung adenocarcinoma cell lines to targeted inhibition of BET epigenetic signaling proteins. Proc. Natl. Acad. Sci. U.S.A. 109, 19408–19413. doi:10.1073/pnas.1216363109

Lohr, J.G., Stojanov, P., Carter, S.L., Cruz-Gordillo, P., 2014. Widespread genetic heterogeneity in multiple myeloma: implications for targeted therapy. Cancer Cell.

Luo, G.Q., Li, J.H., Wen, J.F., Zhou, Y.H., Hu, Y.B., 2008. Effect and mechanism of the Twist gene on invasion and metastasis of gastric carcinoma cells. World journal of Gastroenterology. 14, 2487 -2493.

Maase, von der, H., Sengelov, L., Roberts, J.T., Ricci, S., Dogliotti, L., Oliver, T., Moore, M.J., Zimmermann, A., Arning, M., 2005. Long-term survival results of a randomized trial comparing gemcitabine plus cisplatin, with methotrexate, vinblastine, doxorubicin, plus cisplatin in patients with bladder cancer. J. Clin. Oncol. 23, 4602–4608. doi:10.1200/JCO.2005.07.757

Madan, B., Virshup, D.M., 2015. Targeting Wnts at the source--new mechanisms, new biomarkers, new drugs. Molecular Cancer Therapeutics 14, 1087–1094.

Maestro, R., Tos, A.D., Hamamori, Y., 1999. Twist is a potential oncogene that inhibits apoptosis. Genes Dev. 13, 2207 -17.

Mani, S.A., Guo, W., Liao, M.-J., Eaton, E.N., Ayyanan, A., Zhou, A.Y., Brooks, M., Reinhard, F., Zhang, C.C., Shipitsin, M., Campbell, L.L., Polyak, K., Brisken, C., Yang, J., Weinberg, R.A., 2008. The epithelial-mesenchymal transition generates cells with properties of stem cells. Cell 133, 704–715.

Marcotte, R., Sayad, A., Brown, K.R., Sanchez-Garcia, F., Reimand, J., Haider, M., Virtanen, C., Bradner, J.E., Bader, G.D., Mills, G.B., Pe'er, D., Moffat, J., Neel, B.G., 2016. Functional Genomic Landscape of Human Breast Cancer Drivers, Vulnerabilities, and Resistance. Cell 164, 293–309. doi:10.1016/j.cell.2015.11.062

Maris, J.M., Matthay, K.K., 1999. Molecular biology of neuroblastoma. J. Clin. Oncol. 17, 2264–2279. doi:10.1200/JCO.1999.17.7.2264

McGuire, W.P., Hoskins, W.J., Brady, M.F., Kucera, P.R., Partridge, E.E., Look, K.Y., Clarke-Pearson, D.L., Davidson, M., 1996. Cyclophosphamide and cisplatin compared with paclitaxel and cisplatin in patients with stage III and stage IV ovarian cancer. N Engl J Med 334, 1–6. doi:10.1056/NEJM199601043340101

Ledermann, J., Harter, P., Gourley, C., Friedlander M., Vergote, I., Rustin, G., et al 2014. Olaparib maintenance therapy in patients with platinum- sensitive relapsed serous ovarian cancer: a preplanned retrospective analysis of outcomes by. Lancet Oncology 15, 852–861. doi:10.1016/S1470-2045(14)70228-1

Mei, H., Nakatsu, M.N., Baclagon, E.R., Deng, S.X., 2014. Frizzled 7 maintains the undifferentiated state of human limbal stem/progenitor cells. Stem cells. 32, 938 - 945.

Menon, U., Ryan, A., Kalsi, J., Gentry-Maharaj, A., 2015. Risk algorithm using serial biomarker measurements doubles the number of screen-detected cancers compared with a single-threshold rule in the United Kingdom Collaborative Trial of Ovarian Cancer Screening. Journal of Clinical Oncology. 33, 2062 - 2071

Mertz, J.A., Conery, A.R., Bryant, B.M., Sandy, P., Balasubramanian, S., Mele, D.A.,

Bergeron, L., Sims, R.J., 2011. Targeting MYC dependence in cancer by inhibiting BET bromodomains. Proc. Natl. Acad. Sci. U.S.A. 108, 16669–16674. doi:10.1073/pnas.1108190108

Miow, Q.H., Tan, T.Z., Ye, J., Lau, J.A., Yokomizo, T., Thiery, J.-P., Mori, S., 2014. mesenchymal status renders differentialresponses to cisplatin in ovarian cancer 34, 1899–1907. doi:10.1038/onc.2014.136

Mukhtar, E., Adhami, V.M., Mukhtar, H., 2014. Targeting Microtubules by Natural Agents for Cancer Therapy. Molecular Cancer Therapeutics 13, 275–284. doi:10.1158/1535-7163.MCT-13-0791

Mutch, D.G., Orlando, M., Goss, T., Teneriello, M.G., Gordon, A.N., McMeekin, S.D., Wang, Y., Scribner, D.R., Marciniack, M., Naumann, R.W., Secord, A.A., 2007. Randomized Phase III Trial of Gemcitabine Compared With Pegylated Liposomal Doxorubicin in Patients With Platinum-Resistant Ovarian Cancer. J. Clin. Oncol. 25, 2811–2818. doi:10.1200/JCO.2006.09.6735

Nara, K., Kusafuka, T., Yoneda, A., Oue, T., Sangkhathat, S., Fukuzawa, M., 2007. Silencing of MYCN by RNA interference induces growth inhibition, apoptotic activity and cell differentiation in a neuroblastoma cell line with MYCN amplification. Int. J. Oncol. 30, 1189–1196.

Nicodeme, E., Jeffrey, K.L., Schaefer, U., Beinke, S., Dewell, S., Chung, C.-W., Chandwani, R., Marazzi, I., Wilson, P., Coste, H., White, J., Kirilovsky, J., Rice, C.M., Lora, J.M., Prinjha, R.K., Lee, K., Tarakhovsky, A., 2011. Suppression of inflammation by a synthetic histone mimic. Nature 468, 1119–1123. doi:10.1038/nature09589

O Donnell, R.L., McCormick, A., Mukhopadhyay, A., Woodhouse, L.C., Moat, M., Grundy, A., Dixon, M., Kaufman, A., Soohoo, S., Elattar, A., Curtin, N.J., Edmondson, R.J., 2014. The use of ovarian cancer cells from patients undergoing surgery to generate primary cultures capable of undergoing functional analysis. PLoS ONE 9, e90604. doi:10.1371/journal.pone.0090604

Ohkawara, B., Glinka, A., Niehrs, C., 2011. Rspo3 binds syndecan 4 and induces Wnt/PCP signaling via clathrin-mediated endocytosis to promote morphogenesis. Dev. Cell 20, 303–314. doi:10.1016/j.devcel.2011.01.006

Ozols, R.F., 2003. Phase III Trial of Carboplatin and Paclitaxel Compared With Cisplatin and Paclitaxel in Patients With Optimally Resected Stage III Ovarian Cancer: A Gynecologic Oncology Group Study. Journal of Clinical Oncology 21, 3194–3200. doi:10.1200/JCO.2003.02.153

Patch, A.-M., Christie, E.L., Etemadmoghadam, D., Garsed, D.W., George, J., Fereday, S., Nones, K., Cowin, P., Alsop, K., Bailey, P.J., Kassahn, K.S., Newell, F., Quinn, M.C.J., Kazakoff, S., Quek, K., Wilhelm-Benartzi, C., Curry, E., Leong, H.S., Hamilton, A., Mileshkin, L., Au-Yeung, G., Kennedy, C., Hung, J., Chiew, Y.-E., Harnett, P., Friedlander, M., Quinn, M., Pyman, J., Cordner, S., O'Brien, P., Leditschke, J., Young, G., Strachan, K., Waring, P., Azar, W., Mitchell, C., Traficante, N., Hendley, J., Thorne, H., Shackleton, M., Miller, D.K., Arnau, G.M.,

Tothill, R.W., Holloway, T.P., Semple, T., Harliwong, I., Nourse, C., Nourbakhsh, E., Manning, S., Idrisoglu, S., Bruxner, T.J.C., Christ, A.N., Poudel, B., Holmes, O., Anderson, M., Leonard, C., Lonie, A., Hall, N., Wood, S., Taylor, D.F., Xu, Q., Fink, J.L., Waddell, N., Drapkin, R., Stronach, E., Gabra, H., Brown, R., Jewell, A., Nagaraj, S.H., Markham, E., Wilson, P.J., Ellul, J., McNally, O., Doyle, M.A., Vedururu, R., Stewart, C., Lengyel, E., Pearson, J.V., Waddell, N., deFazio, A., Grimmond, S.M., Bowtell, D.D.L., 2015. Whole–genome characterization of chemoresistant ovarian cancer. Nature 521, 489–494. doi:10.1038/nature14410

Patel, A.G., Sarkaria, J.N., Kaufmann, S.H., 2011. Nonhomologous end joining drives poly(ADP-ribose) polymerase (PARP) inhibitor lethality in homologous recombination-deficient cells. Proc. Natl. Acad. Sci. U.S.A. 108, 3406–3411. doi:10.1073/pnas.1013715108

Pennington, K.P., Walsh, T., Harrell, M.I., Lee, M.K., Pennil, C.C., Rendi, M.H., Thornton, A., Norquist, B.M., Casadei, S., Nord, A.S., Agnew, K.J., Pritchard, C.C., Scroggins, S., Garcia, R.L., King, M.-C., Swisher, E.M., 2014. Germline and somatic mutations in homologous recombination genes predict platinum response and survival in ovarian, fallopian tube, and peritoneal carcinomas. Clin. Cancer Res. 20, 764–775. doi:10.1158/1078-0432.CCR-13-2287

Perets, R., Wyant, G.A., Muto, K.W., Bijron, J.G., Poole, B.B., Chin, K.T., Chen, J.Y.H., Ohman, A.W., Stepule, C.D., Kwak, S., Karst, A.M., Hirsch, M.S., Setlur, S.R., Crum, C.P., Dinulescu, D.M., Drapkin, R., 2013. Transformation of the fallopian tube secretory epithelium leads to high-grade serous ovarian cancer in Brca;Tp53;Pten models. Cancer Cell 24, 751–765. doi:10.1016/j.ccr.2013.10.013

Perren, T.J., Swart, A.M., Pfisterer, J., Ledermann, J.A., Pujade-Lauraine, E., Kristensen, G., Carey, M.S., Beale, P., Cervantes, A., Kurzeder, C., Bois, A.D., Sehouli, J., Kimmig, R., Stähle, A., Collinson, F., Essapen, S., Gourley, C., Lortholary, A., Selle, F., Mirza, M.R., Leminen, A., Plante, M., Stark, D., Qian, W., Parmar, M.K.B., Oza, A.M., 2011. A Phase 3 Trial of Bevacizumab in Ovarian Cancer. N Engl J Med 365, 2484–2496. doi:10.1056/NEJMoa1103799

Peterson, J.K., Houghton, P.J., 2004. Integrating pharmacology and in vivo cancer models in preclinical and clinical drug development. EUROPEAN JOURNAL OF CANCER. 40, 837 - 844.

Phesse, T., Flanagan, D., Vincan, E., 2016. Frizzled7: A Promising Achilles' Heel for Targeting the Wnt Receptor Complex to Treat Cancer. Cancers 8, 50. doi:10.3390/cancers8050050

Piek, J.M., van Diest, P.J., Zweemer, R.P., Jansen, J.W., Poort-Keesom, R.J., Menko, F.H., Gille, J.J., Jongsma, A.P., Pals, G., Kenemans, P., Verheijen, R.H., 2001. Dysplastic changes in prophylactically removed Fallopian tubes of women predisposed to developing ovarian cancer. J. Pathol. 195, 451–456. doi:10.1002/path.1000

Platt, R.J., Chen, S., Zhou, Y., Yim, M.J., Swiech, L., 2014. CRISPR-Cas9 knockin mice for genome editing and cancer modeling. Cell.159, p440 - 455.

Press, J.Z., Kenyon, J.A., Xue, H., Miller, M.A., De Luca, A., Miller, D.M., Huntsman,

D.G., Gilks, C.B., McAlpine, J.N., Wang, Y.Z., 2008. Xenografts of primary human gynecological tumors grown under the renal capsule of NOD/SCID mice show genetic stability during serial transplantation and respond to cytotoxic chemotherapy. Gynecologic Oncology 110, 256–264. doi:10.1016/j.ygyno.2008.03.011

Puissant, A., Frumm, S.M., Alexe, G., Bassil, C.F., Qi, J., Chanthery, Y.H., Nekritz, E.A., Zeid, R., Gustafson, W.C., Greninger, P., Garnett, M.J., McDermott, U., Benes, C.H., Kung, A.L., Weiss, W.A., Bradner, J.E., Stegmaier, K., 2013. Targeting MYCN in Neuroblastoma by BET Bromodomain Inhibition. Cancer Discovery 3, 308–323. doi:10.1158/2159-8290.CD-12-0418

Pujade-Lauraine, E., Hilpert, F., Weber, B., Reuss, A., Poveda, A., Kristensen, G., Sorio, R., Vergote, I., Witteveen, P., Bamias, A., Pereira, D., Wimberger, P., Oaknin, A., Mirza, M.R., Follana, P., Bollag, D., Ray-Coquard, I., 2014. Bevacizumab Combined With Chemotherapy for Platinum-Resistant Recurrent Ovarian Cancer: The AURELIA Open-Label Randomized Phase III Trial. Journal of Clinical Oncology 32, 1302–1308. doi:10.1200/JCO.2013.51.4489

Qin, L., Liu, Z., Chen, H., Xu, J., 2009. The steroid receptor coactivator-1 regulates twist expression and promotes breast cancer metastasis. Cancer Research 69, 3819–3827. doi:10.1158/0008-5472.CAN-08-4389

Qin, Q., Xu, Y., He, T., Qin, C., Xu, J., 2011. Normal and disease-related biological functions of Twist1 and underlying molecular mechanisms. Nature Publishing Group 22, 90–106. doi:10.1038/cr.2011.144

Quintana, E., Shackleton, M., Sabel, M.S., Fullen, D.R., Johnson, T.M., Morrison, S.J., 2008. Efficient tumour formation by single human melanoma cells. Nature 456, 593–598. doi:10.1038/nature07567

Rathert, P., Roth, M., Neumann, T., Muerdter, F., Roe, J.-S., Muhar, M., Deswal, S., Cerny-Reiterer, S., Peter, B., Jude, J., Hoffmann, T., Boryń, Ł.M., Axelsson, E., Schweifer, N., Tontsch-Grunt, U., Dow, L.E., Gianni, D., Pearson, M., Valent, P., Stark, A., Kraut, N., Vakoc, C.R., Zuber, J., 2015. Transcriptional plasticity promotes primary and acquired resistance to BET inhibition. Nature 525, 543–547. doi:10.1038/nature14898

Reinhold, M.I., Kapadia, R.M., Liao, Z., Naski, M.C., 2006. The Wnt-inducible transcription factor Twist1 inhibits chondrogenesis. Journal of Biological Chemistry 281, 1381 - 1388.

Roberts, A.W., Davids, M.S., Pagel, J.M., Kahl, B.S., Puvvada, S.D., Gerecitano, J.F., Kipps, T.J., Anderson, M.A., Brown, J.R., Gressick, L., Wong, S., Dunbar, M., Zhu, M., Desai, M.B., Cerri, E., Heitner Enschede, S., Humerickhouse, R.A., Wierda, W.G., Seymour, J.F., 2016. Targeting BCL2 with Venetoclax in Relapsed Chronic Lymphocytic Leukemia. N Engl J Med 374, 311–322. doi:10.1056/NEJMoa1513257

Rothenberg, M.L., Liu, P.Y., Wilczynski, S., Nahhas, W.A., Winakur, G.L., Jiang, C.S., Moinpour, C.M., Lyons, B., Weiss, G.R., Essell, J.H., Smith, H.O., Markman, M., Alberts, D.S., 2004. Phase II trial of vinorelbine for relapsed ovarian cancer: a

Southwest Oncology Group study. Gynecologic Oncology 95, 506–512. doi:10.1016/j.ygyno.2004.09.004

Sachs, N., Clevers, H., 2014. ScienceDirectOrganoid cultures for the analysis of cancer phenotypes. Current Opinion in Genetics & Development 24, 68–73. doi:10.1016/j.gde.2013.11.012

Sato, T., Stange, D.E., Ferrante, M., Vries, R., Van Es, J.H., 2011. Long-term expansion of epithelial organoids from human colon, adenoma, adenocarcinoma, and Barrett's epithelium. Gastroenterology. 141, 1762 - 1772.

Sausville, E.A., Burger, A.M., 2006. Contributions of human tumor xenografts to anticancer drug development. Cancer Research. 66 (7), 3351- 3354.

Schwarz, R.F., Ng, C.K.Y., Cooke, S.L., Newman, S., Temple, J., Piskorz, A.M., Gale, D., Sayal, K., Murtaza, M., Baldwin, P.J., Rosenfeld, N., Earl, H.M., Sala, E., Jimenez-Linan, M., Parkinson, C.A., Markowetz, F., Brenton, J.D., 2015. Spatial and Temporal Heterogeneity in High-Grade Serous Ovarian Cancer: A Phylogenetic Analysis. PLoS Med. 12, e1001789. doi:10.1371/journal.pmed.1001789.s025

Scott, C.L., Becker, M.A., Haluska, P., Samimi, G., 2013. Patient-derived xenograft models to improve targeted therapy in epithelial ovarian cancer treatment. Front Oncol 3, 295. doi:10.3389/fonc.2013.00295

Scott, C.L., Mackay, H.J., Haluska, P., Jr, 2014. Patient-derived xenograft models in gynecological malignancies. Am Soc Clin Oncol Educ Book. e258 - e266.

Scott, C.L., Swisher, E.M., Kaufmann, S.H., 2015. Poly (ADP-Ribose) Polymerase Inhibitors: Recent Advances and Future Development. J. Clin. Oncol. 33, 1397–1406. doi:10.1200/JCO.2014.58.8848

Scully, R.E., 1987. Classification of human ovarian tumors. Environ. Health Perspect. 73, 15–25.

Seeger, R.C., Brodeur, G.M., Sather, H., 1985. Association of multiple copies of the N-myc oncogene with rapid progression of neuroblastomas. The New England Journal of Medicine. 313, 1111 - 1116.

Sehouli, J., Stengel, D., Harter, P., Kurzeder, C., Belau, A., Bogenrieder, T., Markmann, S., Mahner, S., Mueller, L., Lorenz, R., Nugent, A., Wilke, J., Kuznik, A., Doering, G., Wischnik, A., Sommer, H., Meerpohl, H.G., Schroeder, W., Lichtenegger, W., Oskay-Oezcelik, G., 2011. Topotecan Weekly Versus Conventional 5-Day Schedule in Patients With Platinum-Resistant Ovarian Cancer: A Randomized Multicenter Phase II Trial of the North-Eastern German Society of Gynecological Oncology Ovarian Cancer Study Group. J. Clin. Oncol. 29, 242–248. doi:10.1200/JCO.2009.27.8911

Shen, Q., Zheng, X., McNutt, M.A., Guang, L., Sun, Y., Wang, J., Gong, Y., Hou, L., Zhang, B., 2009. NAT10, a nucleolar protein, localizes to the midbody and regulates cytokinesis and acetylation of microtubules. Experimental Cell Research 315, 1653–1667. doi:10.1016/j.yexcr.2009.03.007

Shi, J., Wang, Y., Zeng, L., Wu, Y., Deng, J., Zhang, Q., Lin, Y., Li, J., Kang, T., Tao, M., Rusinova, E., Zhang, G., Wang, C., Zhu, H., Yao, J., Zeng, Y.-X., Evers, B.M., Zhou, M.-M., Zhou, B.P., 2014. Disrupting the Interaction of BRD4with Diacetylated Twist Suppresses Tumorigenesis in Basal-like Breast Cancer. Cancer Cell 25, 210–225. doi:10.1016/j.ccr.2014.01.028

Shih, I.-M., Kurman, R.J., 2004. Ovarian tumorigenesis: a proposed model based on morphological and molecular genetic analysis. The American Journal of Pathology 164, 1511–1518.

Shu, S., Polyak, K., 2017. BET Bromodomain Proteins as Cancer Therapeutic Targets. Cold Spring Harb Symp Quant Biol 030908.

Song, L., Webb, N.E., Song, Y., Tuan, R.S., 2006. Identification and functional analysis of candidate genes regulating mesenchymal stem cell self- renewal and multipotency. Stem cells. 24, 1707 - 1718.

Swisher, E.M., Lin, K.K., Oza, A.M., Scott, C.L., Giordano, H., Sun, J., 2017. Rucaparib in relapsed, platinum-sensitive high-grade ovarian carcinoma (ARIEL2 Part 1): an international, multicentre, open-label, phase 2 trial. Lancet Oncol. 18, 75–87. doi:10.1016/S1470-2045(16)30559-9

Sørensen, P., Høyer, M., Jakobsen, A., Malmström, H., Havsteen, H., Bertelsen, K., 2001. Phase II Study of Vinorelbine in the Treatment of Platinum-Resistant Ovarian Carcinoma. Gynecologic Oncology 81, 58–62.

Tan, D.S.P., Rothermundt, C., Thomas, K., Bancroft, E., Eeles, R., Shanley, S., Ardern-Jones, A., Norman, A., Kaye, S.B., Gore, M.E., 2008. “BRCAness” Syndrome in Ovarian Cancer: A Case-Control Study Describing the Clinical Features and Outcome of Patients With Epithelial Ovarian Cancer Associated With BRCA1 and BRCA2 Mutations. J. Clin. Oncol. 26, 5530–5536.

Tan, D.S.P., Lambros, M.B.K., Rayter, S., Natrajan, R., Vatcheva, R., Gao, Q., Marchio, C., Geyer, F.C., Savage, K., Parry, S., Fenwick, K., Tamber, N., Mackay, A., Dexter, T., Jameson, C., McCluggage, W.G., Williams, A., Graham, A., Faratian, D., El-Bahrawy, M., Paige, A.J., Gabra, H., Gore, M.E., Zvelebil, M., Lord, C.J., Kaye, S.B., Ashworth, A., Reis-Filho, J.S., 2009. PPM1D Is a Potential Therapeutic Target in Ovarian Clear Cell Carcinomas. Clinical Cancer Research 15, 2269–2280.

Tan, D.S.P., Yap, T.A., Hutka, M., Roxburgh, P., Ang, J., Banerjee, S., Grzybowska, E., Gourley, C., Gore, M.E., Kaye, S.B., 2013. Implications of BRCA1 and BRCA2 mutations for the efficacy of paclitaxel monotherapy in advanced ovarian cancer. Eur. J. Cancer 49, 1246–1253.

Tan, S., Wang, R.-H., Niu, H.-X., Shi, C.-H., Mao, C.-Y., Zhang, R., Song, B., Sun, S.-L., Liu, X.-J., Hou, H.-M., Liu, Y.-T., Gao, Y., Fang, H., Kong, X.-D., Xu, Y.-M., 2015. Functional genomics identifies five distinct molecular subtypes with clinical relevance and pathways for growth control in epithelial ovarian cancer supplementary data. Chin. Med. J. 128, 291–294. doi:10.4103/0366-6999.150087

Tan, T.Z., Miow, Q.H., Huang, R.Y.-J., Wong, M.K., Ye, J., Lau, J.A., Wu, M.C., Bin Abdul Hadi, L.H., Soong, R., Choolani, M., Davidson, B., Nesland, J.M., Wang, L.-Z., Matsumura, N., Mandai, M., Konishi, I., Goh, B.-C., Chang, J.T., Thiery, J.P., Mori, S., 2013. Functional genomics identifies five distinct molecular subtypes with clinical relevance and pathways for growth control in epithelial ovarian cancer. EMBO Mol Med 5, 1051–1066.

Tan, T.Z., Yang, H., Ye, J., Low, J., Choolani, M., Tan, D., 2015. CSIOVDB: a microarray gene expression database of epithelial ovarian cancer subtype. Oncotarget. 6, 43843 - 43852.

The Cancer Genome Atlas Research Network. 2011. Integrated genomic analyses of ovarian carcinoma. Nature 474, 609–615.

Thisse, B., Stoetzel, C., Gorostiza-Thisse, C., 1988. Sequence of the twist gene and nuclear localization of its protein in endomesodermal cells of early Drosophila embryos. EMBO J. 7, 2175 - 83.

Thomas, D.A., O'Brien, S., Faderl, S., Garcia-Manero, G., Ferrajoli, A., Wierda, W., Ravandi, F., Verstovsek, S., Jorgensen, J.L., Bueso-Ramos, C., Andreeff, M., Pierce, S., Garris, R., Keating, M.J., Cortes, J., Kantarjian, H.M., 2010. Chemoimmunotherapy with a modified hyper-CVAD and rituximab regimen improves outcome in de novo Philadelphia chromosome-negative precursor B-lineage acute lymphoblastic leukemia. Journal of Clinical Oncology 28, 3880–3889. doi:10.1200/JCO.2009.26.9456

Topp, M.D., Hartley, L., Cook, M., Heong, V., Boehm, E., McShane, L., Pyman, J., McNally, O., Ananda, S., Harrell, M., Etemadmoghadam, D., Galletta, L., Alsop, K., Mitchell, G., Fox, S.B., Kerr, J.B., Hutt, K.J., Kaufmann, S.H., Study, A.O.C., Swisher, E.M., Bowtell, D.D., Wakefield, M.J., Scott, C.L., 2014. ScienceDirect. Mol Oncol 8, 656–668. doi:10.1016/j.molonc.2014.01.008

Tothill, R.W., Tinker, A.V., George, J., Brown, R., Fox, S.B., Lade, S., Johnson, D.S., Trivett, M.K., Etemadmoghadam, D., Locandro, B., Traficante, N., Fereday, S., Hung, J.A., Chiew, Y.E., Haviv, I., Australian Ovarian Cancer Study Group, Gertig, D., deFazio, A., Bowtell, D.D.L., 2008. Novel Molecular Subtypes of Serous and Endometrioid Ovarian Cancer Linked to Clinical Outcome. Clinical Cancer Research 14, 5198–5208. doi:10.1158/1078-0432.CCR-08-0196

Trabert, B., Ness, R.B., Lo-Ciganic, W.H., 2014. Asprin, Nonasprin Anti-inflammatory drug, and acetaminophen use and risk of invasive epithelial ovarian cancer: a pooled analysis in the Ovarian Cancer Association Consortium. Journal of the National Cancer Institute 106, djt431

Vaillant, F., Merino, D., Lee, L., Breslin, K., Pal, B., Ritchie, M.E., Smyth, G.K., Christie, M., Phillipson, L.J., Burns, C.J., Mann, G.B., Visvader, J.E., Lindeman, G.J., 2013. Targeting BCL-2 with the BH3 Mimetic ABT-199 in Estrogen Receptor-Positive Breast Cancer. Cancer Cell 24, 120–129. doi:10.1016/j.ccr.2013.06.002

Valsesia-Wittmann, S., Magdeleine, M., Dupasquier, S., Garin, E., Jallas, A.-C., Combaret, V., Krause, A., Leissner, P., Puisieux, A., 2004. Oncogenic cooperation

between H-Twist and N-Myc overrides failsafe programs in cancer cells. Cancer Cell 6, 625–630. doi:10.1016/j.ccr.2004.09.033

van de Wetering, M., Francies, H.E., Francis, J.M., 2015. Prospective derivation of a living organoid biobank of colorectal cancer patients. Cell. 161, 933- 945.

van Meurs, H.S., Tajik, P., Hof, M., Vergote, I., 2013. Which patients benefit most from primary surgery or neoadjuvant chemotherapy in stage IIIC or IV ovarian cancer? An exploratory analysis of the European Organisation for Research and Treatment of Cancer 55971 randomised trial. European Journal of Cancer 49, 3191 - 3201.

Vaughan, S., Coward, J.I., Bast, R.C., Berchuck, A., Berek, J.S., Brenton, J.D., Coukos, G., Crum, C.C., Drapkin, R., Etemadmoghadam, D., Friedlander, M., Gabra, H., Kaye, S.B., Lord, C.J., Lengyel, E., Levine, D.A., McNeish, I.A., Menon, U., Mills, G.B., Nephew, K.P., Oza, A.M., Sood, A.K., Stronach, E.A., Walczak, H., Bowtell, D.D., Balkwill, F.R., 2011. Rethinking ovarian cancer: recommendations for improving outcomes. Nature Rev. Cancer, pp. 719–725. doi:10.1038/nrc3144

Vergote, I., Tropé, C.G., Amant, F., 2010. Neoadjuvant chemotherapy or primary surgery in stage IIIC or IV ovarian cancer. The New England Journal of Medicine 363, 943 - 953.

Verhaak, R.G.W., Tamayo, P., Yang, J.-Y., Hubbard, D., Zhang, H., Creighton, C.J., Fereday, S., Lawrence, M., Carter, S.L., Mermel, C.H., Kostic, A.D., Etemadmoghadam, D., Saksena, G., Cibulskis, K., Duraisamy, S., Levanon, K., Sougnez, C., Tsherniak, A., Gomez, S., Onofrio, R., Gabriel, S., Chin, L., Zhang, N., Spellman, P.T., Zhang, Y., Akbani, R., Hoadley, K.A., Kahn, A., Köbel, M., Huntsman, D., Soslow, R.A., deFazio, A., Birrer, M.J., Gray, J.W., Weinstein, J.N., Bowtell, D.D., Drapkin, R., Mesirov, J.P., Getz, G., Levine, D.A., Meyerson, M., The Cancer Genome Atlas Research Network, 2013. Prognostically relevant gene signatures of high-grade serous ovarian carcinoma. J. Clin. Invest. 123, 5167 - 525. doi:10.1172/JCI65833DS1

Vesuna, F., Lisok, A., Kimble, B., Raman, V., 2009. Twist modulates breast cancer stem cells by transcriptional regulation of CD24 expression. Neoplasia. 11, 1318 - 28.

Vidal, A., Munoz, C., Guillen, M.J., Moretó, J., Sara, P., 2012. Lurbinectedin (PM01183), a new DNA minor groove binder, inhibits growth of orthotopic primary graft of cisplatin-resistant epithelial ovarian cancer. Clinical Cancer Research 18, 5399 - 5411.

Walsh, T., Casadei, S., Lee, M.K., Pennil, C.C., Nord, A.S., Thornton, A.M., Roeb, W., Agnew, K.J., Stray, S.M., Wickramanayake, A., Norquist, B., Pennington, K.P., Garcia, R.L., King, M.-C., Swisher, E.M., 2011. Mutations in 12 genes for inherited ovarian, fallopian tube, and peritoneal carcinoma identified by massively parallel sequencing. Proc. Natl. Acad. Sci. U.S.A. 108, 18032–18037. doi:10.1073/pnas.1115052108

Weber, B.L., Vogel, C., Jones, S., Harvey, H., Hutchins, L., Bigley, J., Hohneker, J., 1995. Intravenous vinorelbine as first-line and second-line therapy in advanced

breast cancer. J. Clin. Oncol. 13, 2722–2730.

Weroha, S.J., Becker, M.A., Enderica-Gonzalez, S., Harrington, S.C., Oberg, A.L., Maurer, M.J., Perkins, S.E., AlHilli, M., Butler, K.A., McKinstry, S., Fink, S., Jenkins, R.B., Hou, X., Kalli, K.R., Goodman, K.M., Sarkaria, J.N., Karlan, B.Y., Kumar, A., Kaufmann, S.H., Hartmann, L.C., Haluska, P., 2014. Tumorgrafts as In Vivo Surrogates for Women with Ovarian Cancer. Clinical Cancer Research 20, 1288–1297. doi:10.1158/1078-0432.CCR-13-2611

Whittle, J.R., Lewis, M.T., Lindeman, G.J., Visvader, J.E., 2015. Patient-derived xenograft models of breast cancer and their predictive power. Breast Cancer Res. 17, 17. doi:10.1186/s13058-015-0523-1

Winterhoff, B., Kommos, S., Oberg, A., Wang, C., Riska, S., Konecny, G., Fan, J.B., et al. 2014. Bevacizumab and improvement of progression-free survival (PFS) for patients with the mesenchymal molecular subtype of ovarian cancer. Journal of Clinical Oncology 32**:** suppl. 5509

Winton, T., Livingston, R., Johnson, D., Rigas, J., Johnston, M., Butts, C., Cormier, Y., Goss, G., Inculet, R., Vallieres, E., Fry, W., Bethune, D., Ayoub, J., Ding, K., Seymour, L., Graham, B., Tsao, M.-S., Gandara, D., Kesler, K., Demmy, T., Shepherd, F., National Cancer Institute of Canada Clinical Trials Group, National Cancer Institute of the United States Intergroup JBR.10 Trial Investigators, 2005. Vinorelbine plus cisplatin vs. observation in resected non-small-cell lung cancer. N Engl J Med 352, 2589–2597. doi:10.1056/NEJMoa043623

Wyce, A., Ganji, G., Smitheman, K.N., Chung, C.-W., Korenchuk, S., Bai, Y., Barbash, O., Le, B., Craggs, P.D., McCabe, M.T., Kennedy-Wilson, K.M., Sanchez, L.V., Gosmini, R.L., Parr, N., McHugh, C.F., Dhanak, D., Prinjha, R.K., Auger, K.R., Tummino, P.J., 2013. BET Inhibition Silences Expression of MYCN and BCL2 and Induces Cytotoxicity in Neuroblastoma Tumor Models. PLoS ONE 8, e72967. doi:10.1371/journal.pone.0072967.s007

Yang, J., Mani, S.A., Donaher, J.L., Ramaswamy, S., 2004. Twist, a master regulator of morphogenesis, plays an essential role in tumor metastasis. Cell.117, 927 - 939.

Yang, Z., Yik, J.H.N., Chen, R., He, N., Jang, M.K., Ozato, K., Zhou, Q., 2005. Recruitment of P-TEFb for stimulation of transcriptional elongation by the bromodomain protein Brd4. Mol. Cell 19, 535–545.

Yuen, H.-F., Chua, C.-W., Chan, Y.-P., Wong, Y.-C., Wang, X., Chan, K.-W., 2007. Significance of TWIST and E-cadherin expression in the metastatic progression of prostatic cancer. Histopathology 50, 648–658. doi:10.1111/j.1365-2559.2007.02665.x

Zaino, R.J., Brady, M.F., Lele, S.M., Michael, H., Greer, B., 2011. Advanced stage mucinous adenocarcinoma of the ovary is both rare and highly lethal. Cancer.117, 554 - 562.

Zhang, Z., Rankin, S.A., Zorn, A.M., 2013. Different thresholds of Wnt-Frizzled 7 signaling coordinate proliferation, morphogenesis and fate of endoderm progenitor cells. Developmental biology. 378, pp 1-12.

Zorn, K.K., Bonome, T., Gangi, L., Chandramouli, G., 2005. Gene expression profiles of serous, endometrioid, and clear cell subtypes of ovarian and endometrial cancer. Clinical Cancer Research 11, 6422 - 6430.

Zuber, M.T., 2011. Planetary science: Making mountains out of a moon. Nature 476, 36–37. doi:10.1038/476036a

Appendix 1:

***TWIST1 – FZD7* signature:**

Index	Gene	Index	Gene
6795	FZD7	384	MLLT11
10705	TWIST1	5499	RAB31
4370	MMP2	3490	DACT1
8942	EDNRA	963	COL11A1
8608	FSTL1	669	MXRA8
7964	MN1	7209	FN1
5171	PMP22	3924	ISLR
10506	FZD1	12187	SRPX
11707	ROR2	3098	DCN
10541	PCOLCE	3828	THBS1
1661	ZCCHC24	6581	ANTXR1
4662	CDH11	8572	PDZRN3
4050	FBN1	5190	MFAP4
9707	SPARC	3922	LOXL1
46	PDPN	4179	CHSY1
11432	RECK	3669	SEC23A
3122	NUAK1	7577	PTGIS
7174	COL5A2	8864	
334	OLFML3	96	CLIC4
1355	LOC100996668 ///ZEB1	9244	FBXL7
11242	SNAI2	2033	SERPINH1
3632	EFS	5915	AXL
7832	TIMP3	9221	PDLIM3
10444	AEBP1	10980	PDGFRL
5636	TCF4	1534	HTRA1
733	MFAP2	1592	KIAA1462
3119	GLT8D2	8886	PKD2
806	COL16A1	1607	CXCL12
8968	PALLD	12153	KAL1
6773	COL3A1	9687	DPYSL3
8248	TMEM45A	2929	KCNJ8
3097	LUM	9985	DSE
4352	TGFB1I1	3654	PRKD1
5584	COLEC12	1686	SORBS1
10266	BACH2	3735	LTBP2
823	COL8A2	6894	PXDN
10391	FSCN1	261	DNAJB4
10616	CALD1	8618	HEG1
11700	GAS1	2214	DKK3
		1834	PARVA

Appendix 2:

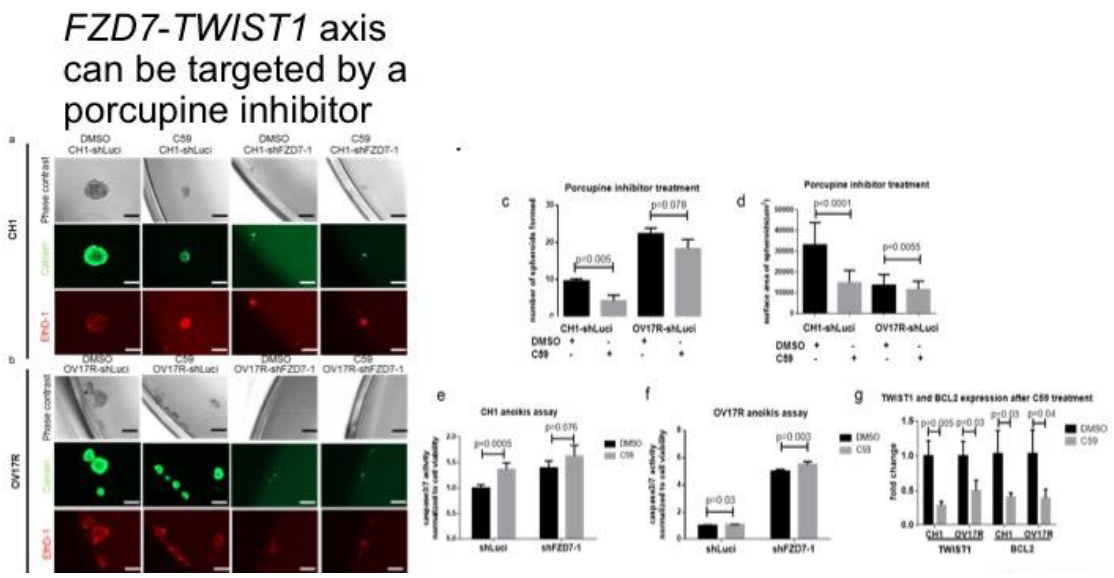

Figure 8. PORCN inhibitor C59 treatment in CH1 and OV17R clones

(a) CH1-shLuci, CH1-sh*FZD7*-1 cells were seeded at a density of 200 cells per well and (b) OV17R-shLuci, OV17R-sh*FZD7*-1 cells were seeded at a density of 500 cells per well in flat bottom ULA 96-well plates for 10 wells per clone. After 10 days in culture with DMSO or C59 treatment, phase contrast images, Calcein-AM staining for viable cells and ethidium homodimer-1 (EthD-1) staining for dead cells were analyzed. Scale bars represented 200 µm. Bar charts showing (c) the numbers and (d) the surface areas of spheroids formed by CH1-shLuci and OV17R-shLuci with DMSO or C59 treatment for 10 days in suspension. Only spheroids with a diameter greater than 50µm were counted. Bar charts showing caspase3/7 activities (y-axis) of DMSO (black bars) or C59 (grey bars) treated (e) CH1-Luci, CH1-sh*FZD7*-1 and (f) OV17R-Luci, OV17R-sh*FZD7*-1 clones. Cells were seeded at a density of 10,000 cells per well in flat bottom ULA 96-well plates for 3 wells per clone. After 72h, cell viability for live cells was measured by Luminescent Cell Viability Assay and cell death was measured by the caspase3/7 activity. (g) Bar charts showing the fold change of *TWIST1* (left) and *BCL2* (right) mRNA expression (2-ΔCt) (y-axis) in CH1-shLuci and OV17R-shLuci with DMSO or C59

treatment for 3 days. mRNA expression levels were measured by qPCR normalized with a panel of housekeeping genes, *ACTB*, *B2M*, *GAPDH*, *RPL13A*, and *HPRT1*.

C59 was used to treat cells at a final concentration of 10 nM. Unpaired T-tests were performed for statistical significance. (Tan, Asad & Heong; manuscript submitted)

Appendix 3:

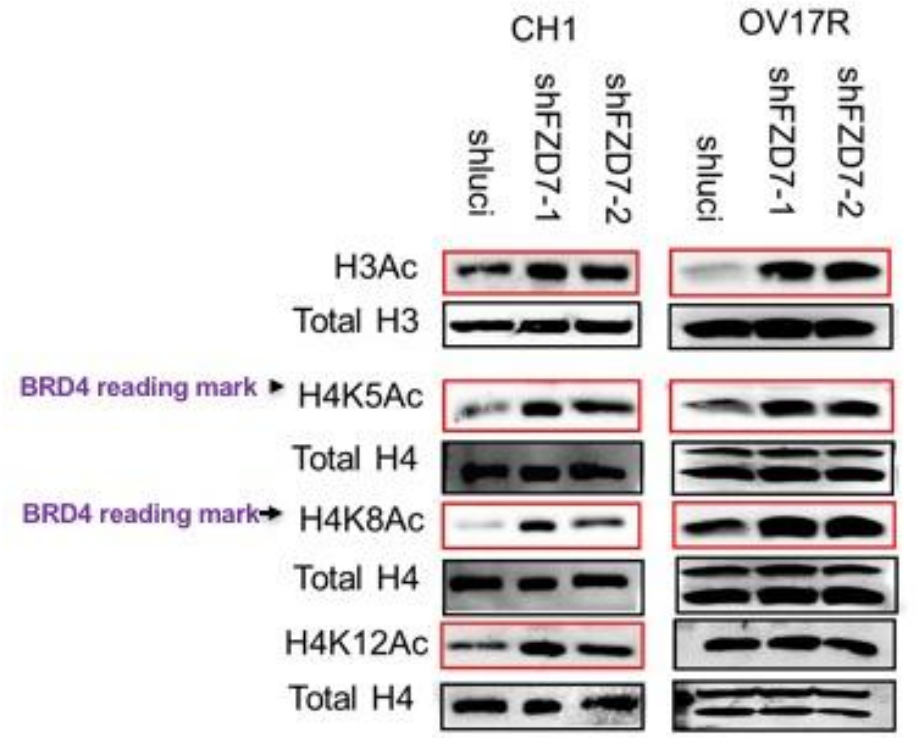

Inhibition of *FZD7* – *TWIST1* axis by depletion of *FZD7* increases histone acetylation. Depletion of *FZD7* **(**shFZD7.1 and shFZD7.2) show increase in acetylation of histone H4K8Ac and H4K5Ac (histones known to bind BRD4).

Appendix 4: VIP clinical trial protocol

Protocol Title:
Phase II study of Intravenous Vinorelbine in Patients with Relapsed Platinum Resistant or Refractory C5 High Grade Serous, Endometrioid, or Undifferentiated Primary Peritoneum, Fallopian Tube or Ovarian Cancer (VIP)

1. Synopsis

Title	Phase II study of Intravenous Vinorelbine in Patients with Relapsed Platinum Resistant or Refractory C5 High Grade Serous, Endometrioid, or Undifferentiated Primary Peritoneum, Fallopian Tube or Ovarian Cancer (VIP)
Short Title	VIP
Protocol Number	GY01/05/16
Protocol Version	Version 4 dated 28 July 2017
Phase	Phase 2
Methodology	Single arm trial
Study Duration	5 years
Study Center(s)	National University Hospital, Singapore National Cancer Centre Singapore KK Women's & Children's Hospital, Singapore
Primary Objective	To determine the activity of IV vinorelbine as defined by response rates
Number of subjects	36 patients
Diagnosis and Main inclusion criteria	Recurrent platinum resistant high-grade serous or endometrioid, undifferentiated ovarian, primary peritoneal or fallopian tube cancer. • Patients must have at least three cores of archival formalin fixed paraffin embedded (FFPE) tumor sample available from the primary tumor or three to five cores from metastatic deposit for central molecular profiling. Molecular subtyping by nanostring technology must confirm C5 subtype
Study product, dose, route, regimen	IV Vinorelbine 25mg/m^2 administered on D1 and D8 of a 3 weekly cycle until the appearance of significant treatment-related toxicity or disease progression
Duration of administration	Continue until the appearance of significant treatment-related toxicity or disease progression
Reference therapy	None
Statistical analysis	Single arm open label Simon's Optimal two-stage design, with a null hypothesis of response rate of 10% with the alternative hypothesis of a response rate of 30% or more

Table of Content

2. STUDY PERSONNEL AND ROLES

Principal Investigator:
Dr David SP Tan (National University Hospital, Singapore)

Site Principal Investigators:
Dr Chay Wen Yee (National Cancer Centre Singapore)
Dr Lim Sheow Lei (KK Women's & Children's Hospital, Singapore)

Study Sites
National University Hospital, Singapore
National Cancer Centre Singapore
KK Women's & Children's Hospital, Singapore

Study Statistician

A/Prof Tai Bee Choo

Study Sponsor
National University Hospital, Singapore

3. Background and introduction

3.1 Background Disease Information

Ovarian Cancer (OC) is the fifth most common cause of cancer death in western women(1). In Australia there are an estimated 1500 new cases annually and almost 1000 deaths from OC reported in 2010 (2). The incidence of ovarian cancer increases with age. More than 70% of patients with OC are diagnosed with advanced disease. Survival rates have hardly changed in the last two decades, with median overall survival rates remaining around 40% (1).

The standard therapy for advanced ovarian cancer consist of radical debulking surgery followed by post-operative platinum-based chemotherapy (3-5). Since 1996, platinum and paclitaxel combination therapy has become the standard-of-care first line chemotherapy with response rates of around 80% (3,6-8). However, the success of this approach is limited and approximately 70% of patients fail to achieve complete responses, or experience disease relapse after a varying disease-free interval. For patients who relapse within 6 months of their last platinum dose, i.e. platinum resistant patients, response rates to further 2nd line chemotherapy significantly reduces to about 20% (9,10) and the 6 months progression free survival rates decline to 15-20% (11-13).

Despite the involvement of over 12,000 women in phase III clinical trials of OC, it has been difficult to progress beyond platinum-based therapy for the treatment of OC (14). This is mainly because OC is still largely treated as a single entity. A number of sub-classifications of the most common OC histiotype, high-grade serous ovarian cancer (HGSOC), suggests that more specific therapeutic approaches may be useful (15-17). Tothill and colleagues identified four molecular subtypes of HGSOC – C1, C2, C4 and C5 (15) which have been validated by The Cancer Genome Atlas (16), and the same pattern of association of subtype with clinical outcome observed in independent studies (18). The C5 subtype which comprises about 20% of HGSOC, is of special interest as it is associated with a poor outcome (Figure 1) (15), stem cell like behaviours (18) and potential oncogenic drivers have been identified, including members of the MYCN pathway (18,19). Tan and colleagues identified a subtype of HGSOC that they named Stem A (17), which corresponds closely to C5.

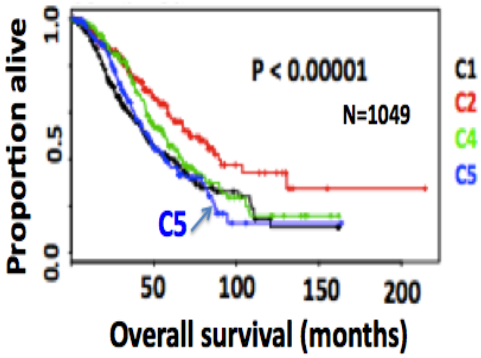

Figure 1

Tothill et al Clinc Canc Res 2008

3.2 Background Therapeutic Information

In ovarian cancer, several single agent phase II trials of vinorelbine in recurrent OC have shown variable response rates of 3 – 30%. However, previous studies have involved "all-comers" and no reported trials have selected patients based on confirmed pure HGSOC or a biomarker of relevance (12,13,20,21).

3.3 Preclinical Data

Drs Huang, Jean Paul Thiery, and colleagues at the Cancer Science Institute, Singapore, performed an shRNA screen of Stem A/C5-like cell lines, revealing a specific dependency on genes involved in microtubule dynamics (17), which is significantly over-expressed in C5 tumours in the AOCS dataset (p=1.1e-09). Importantly, sensitivity was demonstrated of C5-like cell lines to tubulin depolymerising agents vincristine and vinorelbine, but not to the tubulin stabilizing agent paclitaxel.
This hypothesis was tested using patient derived xenograft (PDX) models of C5 HGSOC. These C5-like PDX were obtained from consecutive cohorts of HGSOC PDX shown to represent the clinical spectrum (22,23). Each individual PDX was identified as "C5-like" using *MYCN* pathway (*MYCN, HMGA2, LIN28B)* expression analysis by qRT-PCR (22) or by Affymetrix gene expression analysis (23). *In vivo* response to vinorelbine (delivered I.V on D1, D8 and D18) was evaluated in light of the individual molecular phenotype and platinum response of each PDX. Preliminary analyses of vinorelbine response (figure 2) revealed two PDX of four tested to date (PH038 and PH041) responded for more than 50 days when treated with vinorelbine, one of which (PH041) was refractory to cisplatin; with another (PH038) being sensitive to cisplatin. A third PDX (PH048), also refractory to cisplatin, had disease stabilization with vinorelbine. A fourth PDX (PH077) displayed a mixed response. These preclinical proof of principle experiments demonstrated that vinorelbine could be an effective therapeutic option in targeting the C5 subclass of HGSOC, including in platinum resistant or refractory disease.

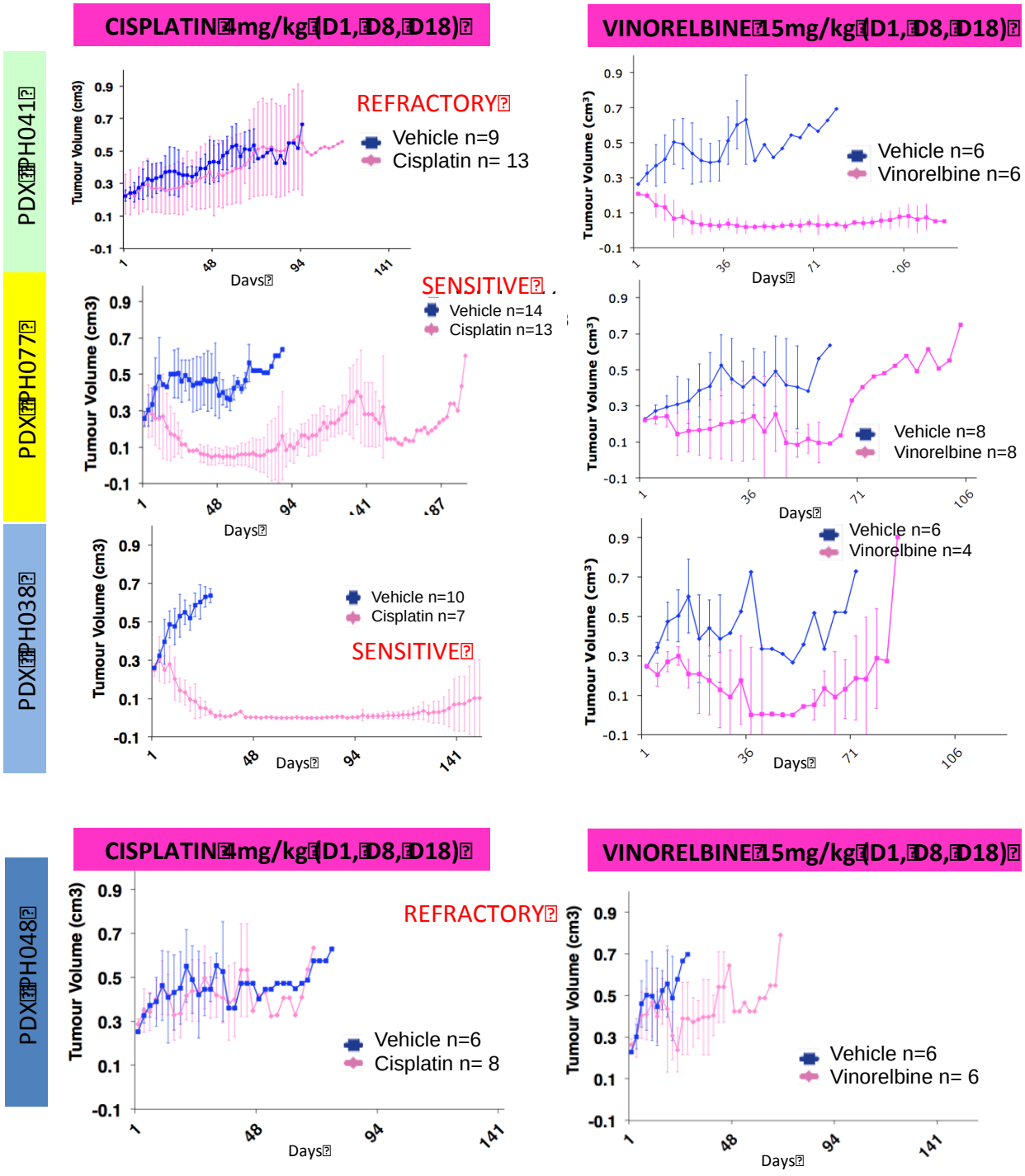

3.4 Risk/ Benefit of Intervention

Vinorelbine is a hemisynthetic vinca alkaloid that is traditionally administered intravenously via an infusion. The mechanism of action is disruption of microtubules by their reversible binding to tubulin resulting in mitotic spindle dissolution and metaphase arrest in dividing cells. The current *in vitro* preclinical data has provided significant information for this trial as 1) there is precedent for use of vinorelbine in platinum resistant HGSOC, 2) the toxicity of vinorelbine is well-understood, 3) there are no other indicators of a better treatment approach for platinum resistant disease in C5 HGSOC

patients. In summary, the strength of the preclinical data, known clinical parameters for vinorelbine, and the limited options for patients with recurrent platinum resistant/refractory disease provide a strong justification for a small signal seeking trial of C5 subtype patient. .

With this trial, patients with C5 HGSOC will know that their cancer belongs to a molecularly-defined subgroup of HGSOC, for which therapies are being developed. The drivers and susceptibilities of C5 HGSOC will be better understood, with a number of therapies proven to have efficacy in relevant pre-clinical human C5 HGSOC models. The clinical trial of vinorelbine will constitute the proof of principle of identification of this patient subset. It is likely that this will spawn a series of "bench to the bedside" clinical trials and a pipeline of C5-directed therapies, based on continuing research (Huang/Bowtell/Scott laboratories). This trial will afford patients with C5 relapsed platinum resistant or refractory HGSOC additional treatment options that may potentially have greater benefit than standard chemotherapy.

3.5 Tolerability

The main dose limiting toxicity associated with IV vinorelbine in lung cancer is myelosuppression with Grade 3-4 neutropenia seen in up to 46% of patients(12,13,25,26,29). However, the febrile neutropenia rate was low at <5%. (25,29). Mild to moderate gastrointestinal toxicity was observed with nausea and vomiting being the most common adverse effect. Grade 3/4 nausea or vomiting occurred in 7% - 17% of patients and primary prophylaxis is recommended. Neurotoxicity was also reported with the use of vinorelbine. Peripheral neuropathy was observed in up to 11% of patients, (25,31)and neuroconstipation was documented to affect up to 24% of patients, however most of these cases were mild, grade 1-2. A similar toxicity profile was observed in patients with platinum resistant ovarian cancer treated with vinorelbine. Leukopenia was the most common dose limiting toxicity followed by anemia, fatigue and nausea (12,13).

4. Aim and Objectives of the trial

The purpose of this trial is to determine if targeting platinum resistant or refractory C5 high-grade serous, high grade endometrioid or undifferentiated ovarian, primary peritoneal and fallopian tube with vinorelbine can improve patient outcomes. The objectives of this study are:

Primary Objective:

- To determine the activity of vinorelbine as defined by response rates when patients with recurrent platinum resistant or refractory C5 high-grade serous, endometrioid or undifferentiated ovarian, primary peritoneal or fallopian tube cancer are treated with IV vinorelbine based on RECISTv1.1

Secondary Objectives:

- To assess progression free survival when patients with recurrent platinum resistant C5 high-grade serous, endometrioid or undifferentiated ovarian, primary peritoneal and fallopian tube cancer are treated with IV vinorelbine
- To evaluate the clinical efficacy (as measured by CA 125 GCIG responses) when patients with recurrent platinum resistant C5 high-grade serous, endometrioid or

undifferentiated ovarian, primary peritoneal and fallopian tube cancer are treated with IV vinorelbine
- To assess the adverse event profile of IV vinorelbine in this patient population

Exploratory Objectives:
- To identify predictive novel markers of response and resistance to IV vinorelbine in C5 high-grade serous and endometrioid ovarian, primary peritoneal and fallopian tube cancer.
- To validate use of a Nanostring classifier in recurrent disease by comparing archival HGSOC with pre treatment biopsy samples and relating these findings to treatment response to IV vinorelbine
- To determine the prevalence of MDR1 fusion/ upregulation in the recurrent disease setting and it's association with vinorelbine resistance
- To determine C5 status using a Nanostring classifier on pre-treatment biopsies of HGSOC to determine consistency of the C5 status between metastatic deposits and primary ovarian tumour and to identify whether treatment post platinum changes subtype status.

5. Trial Design

This is a phase II study in patients with recurrent platinum resistant or refractory C5 high-grade serous, endometrioid or undifferentiated ovarian, primary peritoneal or fallopian tube cancer. All patients with high-grade serous, endometrioid or undifferentiated primary peritoneum, fallopian tube or ovarian cancer will be eligible to be screened for this trial and will be required to sign a pre-screening consent form.

As genomic testing is being increasingly utilized in routine clinical practice, institutions have developed the ability to routinely analyze archival blocks to determine suitability of patients for inclusion into various available clinical trials at the respective institutions (ie: *BRCA1/2*, nanostring). As such, a prescreening consent form will be used to prospectively screen patients at time of initial diagnosis or during the course of their initial treatment.

The molecular analysis will be conducted using the molecular classifier (nanostring platform) in NCCS ICP Lab (National Cancer Centre of Singapore Integrated Genomic Platform). Data will be analysed by Cancer Science Institute (CSI) and Transcend. This molecular classifier will be used to screen RNA from archival formalin fixed paraffin embedded (FFPE) primary ovarian or fallopian tube tumor blocks to molecularly define them into 4 subclasses (C1, C2, C4 or C5). This platform uses a 48-gene nanostring-based assay to classify FFPE HGSOC samples into 4 subtypes with 80% accuracy when compared to gene expression microarray analysis{Leong:2015ho}. The platform had a high level of specificity when primary ovarian or fallopian tumor blocks were available for analysis. By using one block of archival FFPE tumor sample per patient, the assay was able to accurately stratify patients for subtype-specific therapeutic approaches. When analyzing metastatic or peritoneal deposits, the C5 subtype required a more thorough analysis with additional tumor blocks to yield similar results{Leong:2015ho}. As there is no clear evidence of whether the C5 status changes from initial diagnosis compared to relapse disease, the patients primary tumor blocks will be screened prospectively as to avoid treatment delays at time of relapse.

Once C5 confirmation is established on archival primary ovarian tumor blocks via the nanostring platform, patients who have relapsed disease and deemed platinum resistant

or refractory will then be offered participation in this study. Single agent intravenous vinorelbine at a dose of 25mg/m^2 weekly will be administered to all patients, with allowances for dose reductions due to treatment related toxicities.

CA-125 assessment will occur prior to every cycle but will not be utilized to determine disease progression. Tumor measurements will be assessed by radiological assessment with CT Chest/Abdomen/Pelvis at baseline and every 9 weeks (every three cycles) until disease progression.

For the exploratory endpoints of this study, prior to starting treatment, patients may consent to the following:

1. Mandatory pre-treatment biopsy of accessible lesions (radiological-guided). Tissue samples will then be used to determine:
    a. Consistency of the C5 status using the nanostring platform between metastatic deposits and primary ovarian tumor post-platinum treatment.
    b. Association of somatic mutations in *BRCA1/2* and other genes assessed in archival samples and tumor biopsies with tumor response and patient outcome following treatment with IV vinorelbine
    c. Mechanisms of drug resistance by assessing gene expression profiles in pre-treatment tumor biopsies of both responders and non-responders

Patients will be treated until disease progression or unacceptable toxicity. Treatment with vinorelbine may be delayed to allow recovery from treatment-related toxicities and to consider if dose reductions are appropriate for continued therapy with IV vinorelbine.

Objective tumor response using RECIST v1.1 will be evaluated after 3 cycles and after every nine weeks (ie: after every third cycle) thereafter for the duration of study participation.

6. Patient Selection Criteria

Study eligibility will be based on the inclusion and exclusion criteria listed below.

6.1 Patient Inclusion Criteria

Patients will be eligible for inclusion in this study if all of the following criteria apply:

1. Provided written informed consent
2. Patients must have platinum resistant or refractory HGSOC; defined as progressive disease by imaging ≤ 6 months from last date of most recent platinum-based therapy or rising CA-125 based on GCIG criteria
3. Have histological confirmation of high-grade serous or high-grade endometrioid or undifferentiated tumour of the primary peritoneum, fallopian tube cancer or ovary
4. Molecular subtyping by Nanostring technology must confirm C5 subtype on primary ovarian surgical sample or on appropriate cores for recurrent disease
5. Patients must not have received more than 3 prior chemotherapy regimens, which may include chemotherapy, biologics or other targeted therapies (this does not include maintenance treatment or hormonal therapy) for platinum resistant disease
6. Measurable disease by RECIST criteria (version 1.1).
7. At time of registration, if the patient has had previous treatment it must have been at least 28 days since major surgery or radiation therapy; 28 days from any other

previous anti-cancer therapy including biologics; 14 days since hormone therapy. Patients must have recovered to ≤ grade 1 from their treatment-related events with the exception of alopecia.

8. Age ≥ 18 years of age (Age ≥ 21 years of age for Singapore sites)
9. Have clinically acceptable laboratory screening results within certain limits specified below:
    - AST and ALT ≤ 2.5 times upper limit of normal (ULN)
    - Total bilirubin ≤ ULN
    - Creatinine ≤ 1.5 x UL
    - Absolute neutrophil count ≥ 1500 cells/mm
    - Platelets ≥ 100,000/mm3
    - Hemoglobin ≥ 9.0 g/dl
10. Have an ECOG performance status of ≤ 2.
11. Women of child-producing potential must agree to use effective contraceptive methods prior to study entry, during study participation, and for at least 30 days after the last administration of study medication.
12. Have the ability to understand the requirements of the study, provide written informed consent, abide by the study restrictions, and agree to return for the required assessments.
13. Able to tolerate IV medication.
14. Life expectancy greater than 6 months

6.2 Patient Exclusion Criteria

Patients will not be eligible for inclusion in this study if any of the following criteria apply:

1. Women who are pregnant or nursing
2. Previous exposure to vinorelbine
3. Patients known to be hypersensitive to vinorelbine or any vinca alkaloids previously
4. Persistent toxicities (≥ Common Terminology Criteria for Adverse Event (CTCAE) v4.03 grade 1) caused by previous cancer therapy, excluding alopecia
5. Have active, acute, or chronic clinically significant infections or bleeding.
6. Have active angina pectoris, stroke, myocardial infarction, or any other pre-existing uncontrolled cardiovascular condition within the last 6 months.
7. Have additional uncontrolled serious medical or psychiatric illness.
8. Require therapeutic doses of anti-coagulation with warfarin or warfarin derivatives. However, treatment with low molecular weight heparin (LMWH) is allowed.
9. Known symptomatic CNS metastases. Treated brain metastatis that are stable for more than ≥4 weeks are allowed.
10. Psychiatric disorders that would hinder compliance with study protocol
11. History of other malignancies within the past 5 years except for curatively treated skin BCC or SCC or cervical carcinoma in situ. Patients who have had curatively treated breast cancer, with completion of adjuvant chemotherapy more than three years before are allowed.
12. Require treatment with drugs known to be potent inducers or inhibitors of CYP3A4 at the time of registration
13. Subjects known to be HIV positive or with active and untreated Hepatitis B or Hepatitis C infection. Patients with controlled Hepatitis B or Hepatitis C infection on treatment with antiviral medication are allowed.

6.3 Patient Discontinuation

Individual patients may be discontinued from the study by the investigator at any time if it is felt to be in the patient's best interest. Patients will be encouraged to complete the study; however they may voluntarily withdraw at any time. The Investigator or designee will document the reason for discontinuation.

A patient may be discontinued from the study for the following medical or administrative reasons:

- **Significant adverse event:** If a patient suffers an AE that, in the judgment of a Co-Investigator or the Principal Investigator presents an unacceptable consequence or risk to the patient, whether or not the AE is considered related to study medication, the patient may be discontinued from study treatment. Patients will be followed until the AE resolves (return to normal or baseline values), becomes stabilized, is no longer related, or the patient is lost to follow-up or deceased (see section 8.1.4).
- **Pregnancy:** If a female patient becomes pregnant at any time during the study, she will be discontinued from further participation and treatment.
- **Administrative Discontinuation:** A patient may be discontinued from the study for the following reasons related to noncompliance:
    1. Failure to receive or refusal of study medication.
    2. Failure to comply with protocol requirements. The patient has a serious deviation from the protocol that would compromise the integrity of the study data. All occurrences of noncompliance must be documented on the appropriate CRF pages.
    3. Discontinued at the discretion of the Investigator for any reason.
- **Disease progression:** Patients who have documented disease progression based on RECIST v1.1 will be discontinued from the study.
- **Consent withdrawn:** The patient chooses to terminate participation in the study.
- **Study completion**: Patients will be discontinued after a maximum of 12 months on treatment with vinorelbine**:** The patient chooses to terminate participation

7 Study Treatment

Treatment is with 25mg/m^2 intravenous vinorelbine on day1 and day8 every 3 weeks. Individual patient therapy will continue until the appearance of significant treatment-related toxicity or disease progression.

7.1 Dose Rationale

The rationale for the starting dose of intravenous 25mg/m^2 for this planned clinical study is derived from several studies in advanced breast cancer{Weber:1995wq} and non small cell lung cancer {Gridelli:1999wy}. This regimen was well tolerated with granulocytopenia the predominant dose limiting toxicity and asthenia, nausea and constipation being the most common non-hematologic toxicity{Weber:1995wq}. All grade peripheral neuropathy was recorded as 10% - 13%{Weber:1995wq, Gridelli:1999wy} when used as 1st line treatment in patients with NSCLC and breast cancer. However, the rate increased to 23% (all grade) when vinorelbine was used in subsequent lines{Weber:1995wq}. An Italian study in patients over the age of 70 demonstrated that vinorelbine provided improved survival and quality of life over best supportive care. It was well tolerated in this patient group{Gridelli:2003ur}

7.2 Dosages and Doses

The planned dose for this study is 25 mg/m^2 intravenously on day-1 and day-8 of a 3 week cycle to commence following confirmation of eligibility into the study for a maximum of 12 months, until disease progression, intolerable toxicity or withdrawal of patient consent (whichever event occurs first).

Anti emetics will be used concomitantly with IV vinorelbine. Dexamethasone 4mg and granisetron 2mg (or an equivalent 5HT3 antagonist) orally are recommended on day 1 prior to the vinorelbine. Patients are also recommended to have metoclopramide (10mg-20mg) or prochlorperazine (5-10mg) orally every 6 hours when necessary.

Prophylactic laxatives should be prescribed to prevent constipation related to the use of vinca alkaloids

7.3 Dose Delays and Modification for Toxicity

Treatment with IV vinorelbine may be delayed in order to allow recovery from treatment-related toxicities or intercurrent illness, and to consider if dose reductions are appropriate for continued therapy with vinorelbine. Local institution or local practice guidelines applies for dose modifications while on chemotherapy. If treatment cannot be delivered on day 8 then that treatment should be omitted rather than delayed. Treatment for the next cycle should proceed on the date originally scheduled and should incorporate dose modifications as appropriate Below are suggested dose modification guidelines that could be used if required.

Dose Adjustment Guideline for physician's choice chemotherapy	Recommended Action
Hematological toxicity ANC X 10^9 0.5 - <1.5 <0.5 Febrile neutropenia Platlets X10^9 50 - <100 <50	 Delay treatment until recovery Delay treatment until recovery and consider reducing chemotherapy **to dose level -1** Delay treatment until recovery and consider reducing chemotherapy **to dose level -1** Delay treatment until recovery Delay treatment until recovery and consider reducing chemotherapy **to dose level -1** **All hematological toxicity:** **1st occurrence: No dose reduction** **2nd occurrence: Reduce chemotherapy to dose level -1** **3rd occurrence: Reduce chemotherapy to dose level -2** **4th occurrence: Omit chemotherapy**
Mucositis Grade 2: Grade 3 or Grade 4:	Delay treatment until toxicity has resolved to Grade 1 or less and reduce the dose for subsequent cycles as follow: **1st occurrence: No dose reduction** **2nd occurrence: Reduce chemotherapy to dose level -1** **3rd occurrence: Reduce chemotherapy to dose level -2** **4th occurrence: Omit chemotherapy** Delay treatment until toxicity has resolved to Grade 1 or less and reduce the dose for subsequent cycles as follow: 1st occurrence: Reduce chemotherapy **to dose level -1** 2nd occurrence: Omit chemotherapy
Peripheral neuropathy CTC Grade 2 CTC Grade 3 or 4	 Reduce vinorelbine to dose level -1 if persists, reduce vinorelbine to dose level -2 Omit vinorelbine
Renal dysfunction	No dose modifications necessary
Hepatic dysfunction ALT or AST >2.5 – 3.0 X ULN ALT or AST >3.0 – 5.0 X ULN : ALT or AST > 5.0 – 20.0 X ULN :	 Reduce vinorelbine to dose level -1 Reduce vinorelbine to dose level -2 Omit vinorelbine

Dose adjustment guideline for vinorelbine -related toxicity*	Recommended action
Clinically significant Grade 2 toxicity that is deemed intolerable OR Clinically significant Grade ≥3 toxicity	• Hold dose until toxicity resolves to ≤ Grade 1 or baseline (maximum 21 days). • If the patient is benefiting from treatment but toxicity does not resolve to ≤ Grade 1 or baseline within 21 days of discontinuation of study drug, then study drug will be discontinued permanently. • If the toxicity resolves to ≤ Grade 1 or baseline within 14-21 days, restart drug administration at dose level -1 shown below.
First Occurrence	• Allow toxicity to resolve to Grade ≤1 or baseline, then restart dosing at dose level -1
Second Occurrence	• Hold dose until toxicity resolves to ≤ Grade 1 or baseline (maximum 21 days). • If the patient is benefiting from treatment but toxicity does not resolve to ≤ Grade 1 or baseline within 21 days of discontinuation of study drug, then study drug will be discontinued permanently. • If the toxicity resolves to ≤ Grade 1 or baseline within 14-21 days then restart dosing at a dose level -2
Third Occurrence	• Discontinue study medication. • If patient is benefiting from therapy, discuss with PI.

* excluding alopecia

Dose de-escalation schedule	
Dose Level	**Dose (D1 and D8 every 3 weeks):**
Level 1	25 mg/m^2
Level -1	20 mg/m^2
Level -2	16 mg/m^2

In general, any persistent (i.e. lasting more than 3 weeks despite optimal medical intervention, e.g. intolerable Grade 2 nausea and vomiting for 2 weeks despite appropriate anti-emetic treatment) Grade 2 toxicity that is deemed intolerable or Grade 3 toxicity considered to be study drug related should warrant study drug interruption or reduction according to the Table shown above. Grade 2-3 toxicity which is not considered clinically significant such as alopecia or isolated asymptomatic laboratory results eg. lymphopenia does not require a dose delay or reduction

Two dose reductions will be allowed, Dose -1 will be 20mg/m^2 and Dose -2 will be 16 mg/m^2.

Dosing interruptions/delays of up to three weeks will be allowed for recovery from toxicities or inter-current illness (equivalent of 2 missed doses in every cycle). Longer interruptions or lower doses may be considered if the patient is benefiting from therapy

with vinorelbine as described in table above. These cases have to be discussed with the Principal Investigator.

7.4 Concomitant Medication(s)/Treatment(s) Permitted

All prescription and non-prescription concomitant medications should be recorded on the appropriate page of the case report form (CRF).

The *in vitro* studies implicate the involvement of cytochrome P450 enzymes CYP3A4 in the pathways involved in the metabolism of IV vinorelbine. Hence, IV vinorelbine metabolism is expected to be modulated by the drugs that are able to potently inhibit or induce CYP3A activity. Patients who require such agents on the list in Appendix 1 will be excluded from enrolling in the study. Patients who require such an agent as a result of being on trial, may be allowed to continue treatment if the following apply: they have stable or responding disease; no alternative treatment is available; they are closely clinically monitored while they are enrolled in the clinical trial; the individual case has been discussed and agreed with the PI.

Grapefruit juice is also a well-known inhibitor of CYP3A4 and should not be consumed during participation in the trial.

Any other medication which is considered necessary for the patient's welfare, and which is not expected to interfere with the evaluation of the study drug, may be given at the discretion of the Investigator. No other investigational agents are permitted during the entire duration of treatment with study drug.

7.5 Patient Compliance / Dose Administration

Authorized site personnel will administer the Day 1 dose of IV vinorelbine.. Routine blood test will be carried out prior to day 8 of vinorelbine treatment. If treatment cannot be delivered on day 8 then that treatment should be omitted rather than delayed. Treatment for the next cycle should proceed on the date originally scheduled and should incorporate dose modifications as appropriate..

Information regarding study medication administration and compliance will be recorded in the CRF.

7.6 Packaging and Labeling

- Vinorelbine is available in a minibag

7.7 Ordering and Shipping

- As per institutional guidelines

7.8 Handling and Storage

- As per institutional guidelines

7.9 Preparation of vinorelbine for administration

- Vinorelbine is available in a minibag and should be administered intravenously via intravenous cannula, PORT or central venous cannula over 5 – 10minutes
- Care should be taken when administering vinorelbine as it is vesicant. ensure vein is patent and monitor for signs of extravasation throughout administration
- Flush with flush with ~250 mL of sodium chloride 0.9%

8 Study Procedures

Information provided during the Study Initiation Visit and the appendices of this clinical study protocol will be used as further information regarding this investigational product. Details of the procedures to be followed during the course of this study are as follows

8.1 Time and Events Schedule

8.1.1 Pre- Screening Period:

Using a prescreening consent form unique to each site, patients will be prospectively consented for analysis of primary surgical ovarian, fallopian tube or metastatic tumour blocks at time of initial diagnosis or during first line chemotherapy. Six consecutive sections (5 X 5 microns unstained sections and 1 H & E stained section) from three primary surgical blocks will be centrally analyzed using the nanostring platform in the clinical pathological laboratory at Cancer Science Institute or Transcend, Singapore as previously outlined. If one block is found to be positive for C5, a repeat analysis will be performed on the positive block and an additional two primary blocks will also be evaluated to confirm the diagnosis. If primary tumor is unavailable, six consecutive sections (5 X 5 microns unstained sections and 1 H & E stained section) from three to five metastatic blocks (ie: omentum) will be used to confirm C5 status with at least one from primary site.

For non-Singapore sites, tumour samples should be batched for shipping (4 patients at a time – 3 samples per patient) to the lab in Singapore. Turn-around time for results is expected to be between 2 – 4 weeks with the report being disseminated via email to the site PI or study co-ordinator. Sites should notify Ms Ye Jieru via email jieruye@nus.edu.sg a week prior to shipping of samples. However, for urgent sample processing, please also contact Ms Ye Jieru via email jieruye@nus.edu.sg and alternate arrangements may be made for urgent samples.

Positive C5 results from the nanostring classifier will be returned to the kept confidential until the patient develops platinum resistant or refractory disease. Once a patient with confirmed C5 status using the molecular classifier develops platinum resistant or refractory ovarian, fallopian tube or primary peritoneal carcinoma, she will be invited to participate in this study.

8.1.2 Screening Period (D-28 – D-1):

Prior to performing any study procedures, the Investigator, or designee, will obtain written informed consent from the patient. Baseline evaluations are to be conducted within 28 days prior to day 1, unless otherwise indicated (table 3). The Physical Examination, Height, Weight, ECOG, Vital Signs, Hematology, Chemistry, Urinalysis, liver function test and CA-125 are to be assessed within 7 days prior to day 1. In the event that the patient's condition is deteriorating, laboratory evaluations should be repeated within 48 hours prior to initiation of the next cycle of therapy. Following procedures will be performed during the Screening Visit (Table 2):

- Informed Consent
- Review of eligibility criteria
- Medical history and demographics
- Complete physical exam
- Performance Status
- Vitals signs, weight and height
- Tumor biopsy
- Review of prior/concomitant medications
- Imaging by CT/MRI
- Clinical laboratory tests for:
    - Hematology (see Table 2)
    - Clinical chemistry (see Table 2)
    - Coagulation (PT, PTT, INR)
    - Creatinine Clearance
    - Serum pregnancy test (for women of childbearing potential only)
    - Hepatitis B and C serology
    - HIV testing

8.1.3 Treatment Period:

A cycle is 21 days. Assessments at each clinic visit for the first 3 weeks (cycle 1) must be completed within 3 days of the indicated visit day and thereafter, each three weekly visit must be completed within 7 days of the indicated visit day. Single agent IV vinorelbine at a dose of 25 mg/m^2 will be administered on day 1 and day 8 of a 3 weekly cycle to all patients, with allowances for dose reductions due to treatment related toxicities. Patients will be evaluated for treatment-emergent adverse events (AEs) during study participation, and toxicity will be assessed according to the National Cancer Institute (NCI) Common Terminology Criteria for Adverse Events, Version 4.0. Treatment with vinorelbine may be delayed to allow recovery from treatment-related toxicities and to consider if dose reductions are appropriate as per section 4.3. Dosing interruptions/delays of up to three weeks will be allowed for recovery from toxicities or inter-current illness. Longer interruptions may be considered following discussion with the principal investigator if the patient is benefiting from therapy with vinorelbine.

CA-125 assessment will occur prior to every cycle but will not be utilized to determine disease progression. Tumor measurements will be assessed by radiological assessment with CT Chest/Abdomen/Pelvis at baseline and every 9 weeks (every three cycles) until disease progression. Response will be determined based on Response Evaluation Criteria

in Solid Tumors (RECIST) criteria 1.1 and CA-125 assessment based on GCIG criteria for response. Progression free survival (PFS) is defined as the time from the first day of treatment to the first observation of disease progression or death due to any cause or last follow-up. Duration of overall response is measured from the time measurement criteria are first met for CR/PR (whichever is first recorded) until the first date that recurrent or progressive disease is objectively documented (taking as reference for progressive disease the smallest measurements recorded on study).

8.1.4 Duration of Follow Up

The End of Study Drug Administration visit should take place at the time the patient is removed from the treatment period of the study. Patients who discontinue vinorelbine without documented progressive disease will continue to be followed every 9 weeks for documented radiological progression.
All patients will be followed for ongoing adverse events until 30 days from the end of study drug administration. Patients who specifically discontinue vinorelbine for unacceptable adverse events will be followed until the AE resolves (return to normal or baseline values), becomes stabilized, is no longer related, or the patient is lost to follow-up or deceased.

		Follow-Up Period	
		30 days from the End of Study Drug Administration	Monthly until resolution of adverse event(s)**
Reason Patients Removed study	Objective Disease Progression	X	
	Clinical Progression/ Symptomatic Deterioration	X	
	Unacceptable Adverse Events	X	X
	All other patients	X	

Table 1
** Until the AE resolves (return to normal or baseline values), becomes stabilized or is no longer related

8.1.5 Clinical Laboratory Assessments, including Pregnancy Tests

Non-fasting blood specimens for the measurement and evaluation of clinical chemistry, hematology/coagulation and pregnancy hormones (female patients with childbearing potential) will be collected as described in Table 2. Approximately 20 mL of blood will be collected for the clinical laboratory assessments at the specified times. A positive pregnancy test prior to dosing will exclude the patient from enrollment in the study.

Values for the following parameters will be obtained:

HEMATOLOGY	**CLINICAL**	**OTHER**

Hemoglobin Hematocrit Platelet Count White Blood Cell Count Differential, including: Neutrophils, Lymphocytes, Basophils, Monocytes, Eosinophils	Total protein Albumin Creatinine Uric acid Bilirubin (total) Alkaline phosphatase AST(SGOT) ALT (SGPT) Glucose Calcium	Serum Pregnancy Test (according to study schedule) HIV Test Hepatitis B and C Serology Test
COAGULATION TESTS	Phosphorus	
Prothrombin time (PT) or International Normalized Ratio (INR), Partial thromboplastin time (PTT)	Bicarbonate Chloride Sodium Potassium Magnesium Creatinine clearance	

Table 2

Table 3	Screening	Cycle 1[a]			Cycle 2+ [a]		End of Study Drug Administration [h i]
Measurement/Treatment		**D1**	**D8**	**D15**	**D1**	**D8**	
Inclusion/Exclusion	X						
Informed Consent	X						
Medical/Cancer History including status, tumor grade, cell type, stage, primary site, and prior therapy/dates/response	X						
Physical Examination	X	X[b]			X		X
Height, Weight	X[k]						
Vital Signs (HR, temp, RR, BP)	X	X[b]	X	X	X		X
ECOG Performance Status	X	X[b]			X		X
Hematology [c]	X	X[b]	X	X	X		X
Clinical Chemistry [c]	X	X[b]	X	X	X		X
Coagulation Tests [c]	X	X[b]					
Serum Pregnancy Test [d]	X						
HIV Test, Hepatitis B and C Serology Test	X						
IV Vinorelbine		X	X		X	X	
Tumor Marker CA-125 [e]	X	X[b]			X		X
Radiographic Tumor Evaluation [f]	X				X (every 9 weeks)		X
Biopsy and blood for translational research	X[j]						X (optional)
AE Monitoring	X	---------- X[g] ----------					

Concomitant Medications [g]	X	---------- X ----------	X
Follow up			X[l]

AE = adverse event; BP = blood pressure; HR = heart rate; RR = respiratory rate

a. Each visit following Day 1 must be completed within 3 days of the indicated visit day and each monthly visit must be completed within 7 days of the indicated visit day.
b. Repeat only if more than 7 days between baseline screening assessment and the first dose. Assessments must continue to be acceptable if repeated at baseline.
c. Specific tests are listed in the protocol in table 2
d. Women of childbearing potential only; to be completed within 72hrs prior to initiation of therapy.
e. Tumor markers shall be assessed at the beginning of each cycle and at end of study drug administration. Tumor markers alone will not be used to determine progressive disease. The same laboratory must be used to follow CA-125 levels.
f. Scans must be done within 28 days prior to entering study. Objective tumor response will be evaluated every 9 weeks until disease progression. CT of abdomen and pelvis must be performed in all patients; additional scans should be obtained depending on where baseline disease was known. Information on prior radiotherapy must be provided to the central radiologist for determination of which lesions cannot be selected as target lesions for response assessments.
g. AEs and concomitant medications are monitored continually while on study and until resolution of AE to < CTCAE v4.03 Gd 1. (Patients can call with AE symptoms between scheduled visits)
h. End of study drug administration visit shall occur at the time the patient discontinues treatment with study drug.
i. Ongoing adverse events must be followed until 30 days from the end of study drug administration.
j. Fresh tumor tissue biopsies will be taken from subjects who have accessible tumor tissues based on the Investigator's judgment. Fresh tumor tissue collections are to be obtained 2 weeks prior to starting study drug but not less than 3 days prior to starting treatment. Optional fresh tumor tissue biopsies will be taken from subjects who have accessible tumor tissues based on the Investigator's judgment at the time of disease progression.
k. Baseline height and weight to be assessed 3 days prior to registration to determine starting dose.

l. Follow up every month until resolution of AE to < CTCAE v4.03 Gd 1 and thereafter every 6 months telephone conversation for OS follow up

9 Efficacy Assessments

9.1 Objective Tumor Responses/Benefit Assessments

Tumor responses in patients will be determined by the RECIST guidelines (version 1.1). In the absence of significant treatment-related toxicity or clinical evidence of progressive disease, patients will be allowed to continue on 3-week cycles of IV vinorelbine. The frequency and timing of the assessment of tumor burden/clinical benefit are described in Table 3. Unscheduled assessments may be conducted when clinically indicated during the study.

Cytology:

- The cytological confirmation of the neoplastic origin or any effusion that appears or worsens during treatment when the measurable tumor has met criteria for response or stable disease is encouraged if safe to do so, in order to differentiate between response or stable disease (an effusion may be a side effect of the treatment) and progressive disease.

Note:

- Patients with a global deterioration of health status requiring discontinuation of treatment without objective evidence of disease progression at that time should be reported as "symptomatic deterioration." Every effort should be made to document the objective progression even after discontinuation of treatment.
- In some circumstances, it may be difficult to distinguish residual disease from normal tissue. When the evaluation of complete response depends upon this determination, it is recommended that the residual lesion be investigated if safe to do so (fine needle aspirate/biopsy) before confirming the complete response status.

9.2 Guidelines for Evaluation of Measurable Disease and Response

The same method of assessment and the same technique is to be used to characterize each identified and reported lesion at baseline and during follow-up. Imaging-based evaluation should always be done rather than clinical examination.

10Endpoints

Primary Endpoints:
Response rates following treatment with IV vinorelbine. Objective Response Rate defined as the percentage of subjects with a confirmed CR or PR as per RECIST v1.1 criteria (see Appendix 2) will be used to evaluate response. Response will be evaluated every three cycles (every 9 weeks) of treatment

Secondary Endpoints:

- Progression free survival: Progression free survival (PFS) is defined as the time from the first day of treatment to the first observation of disease progression or death due to any cause or last follow-up. PFS will be censored for patients who are alive and free of progression at the time of last follow-up.
- Clinical efficacy: defined as the percentage of subjects with a confirmed response as per a CA-125 response by GCIG criteria (see Appendix 3). CA-125 assessment will

be performed prior to each cycle and response will be evaluated based on GCIG criteria for response.
- Adverse event profile of IV vinorelbine in this patient population as measured by CTCAE v4.03

Exploratory endpoints:
- To validate use of a nanostring classifier on archival HGSOC to enrich for responders to vinorelbine
- To determine C5 status using a nanostring classifier on pre-treatment biopsies of HGSOC to determine whether treatment post platinum changes C5 status
- Association of somatic mutations in *BRCA1/2* and other genes assessed in archival samples and tumor biopsies with tumor response and patient outcome following treatment with vinorelbine.
- To understand mechanisms of drug resistance by assessing gene expression profiles in pre-treatment tumor biopsies of both responders and non-responders

10.1 Patient Discontinuation

Individual patients may be discontinued from the study by the Investigator or PI at any time if it is felt to be in the patient's best interest. Patients will be encouraged to complete the study; however they may voluntarily withdraw at any time. The Investigator or designee will document the reason for discontinuation.

A patient may be discontinued from the study for the following medical or administrative reasons:
- **Significant adverse event:** If a patient suffers an AE that, in the judgment of a Co-Investigator or the Principal Investigator presents an unacceptable consequence or risk to the patient, whether or not the AE is considered related to study medication, the patient may be discontinued from study treatment. Patients will be followed until the AE resolves (return to normal or baseline values), becomes stabilized, is no longer related, or the patient is lost to follow-up or deceased
- **Pregnancy:** If a female patient becomes pregnant at any time during the study, she will be discontinued from further participation and treatment.
- **Administrative Discontinuation:** A patient may be discontinued from the study for the following reasons related to noncompliance:
  - Failure to receive or refusal of study medication.
  - Failure to comply with protocol requirements. The patient has a serious deviation from the protocol that would compromise the integrity of the study data. All occurrences of noncompliance must be documented on the appropriate CRF pages.
  - Discontinued at the discretion of the Investigator for any reason.
- **Disease progression:** Based on RECIST v1.1 criteria radiologically and clinical deterioration as deemed by the investigator. Progression will not be determined by CA-125 levels alone.
- **Consent withdrawn:** The patient chooses to terminate participation in the study

11Adverse Events/ Intercurrent Illnesses

The Investigator and clinical staff will note all AEs offered by the patient prior to and during administration of study drug. All AEs will be recorded in the source documents. All AEs, including clinically significant abnormal laboratory AEs, will be entered in the electronic CRFs from the time of the first dose of study medication until up to 30 days after the end of study drug administration or until alternate therapy is initiated, whichever occurs first. The Investigator must record whether or not the AE meets the definition of serious.

11.1 Definition of an Adverse Event

- Any untoward medical occurrence (including an abnormal laboratory finding), symptom, or disease temporally associated with the use of a medicinal (investigational) product in a patient administered a pharmaceutical product and which does not necessarily have to have a causal relationship with treatment
- **CTCAE term (AE description) and grade:** The descriptions and grading scales found in the revised NCI Common Terminology Criteria for Adverse Events (CTCAE) version 4.0 will be utilized for AE reporting. All appropriate treatment areas should have access to a copy of the CTCAE version 4.0. A copy of the CTCAE version 4.0 can be downloaded from the CTEP web site http://ctep.cancer.gov/protocolDevelopment/electronic_applications/ctc.htm.
- The Investigator must assess the **attribution** of the AE to the study medication as:

- Definite – The AE *is clearly related* to the study treatment.
- Probable – The AE *is likely related* to the study treatment.
- Possible – The AE *may be related* to the study treatment.
- Unlikely – The AE *is doubtfully related* to the study treatment.
- Unrelated – The AE *is clearly NOT related* to the study treatment.

11.2 Clinical Laboratory Abnormalities

All abnormal laboratory values should be captured on source documentation and assessed for clinical significance by the Investigator at the site. Only abnormal laboratory values deemed clinically significant should be listed as AEs in the CRFs. All clinically significant abnormal laboratory results will be followed up to 30 days after the end of study drug administration or until an alternate therapy is initiated, whichever occurs first.

11.3 Definition of a Serious Adverse Event (SAE)

As provided in Title 21 Code of Federal Regulations (CFR) Part 312, a serious adverse event is an AE occurring at any dose that results in any of the following outcomes:

- Death
- A life-threatening AE
  (The patient was, in the view of the Investigator, at immediate risk of death from the event as it occurred. It does not mean that the event, had it occurred in a more severe form, might have caused death).
- Hospitalization or prolongation of existing hospitalization
  (Complications that occur during hospitalization are AEs. If a complication prolongs hospitalization or fulfills any other serious criteria, the event is serious. Hospitalization for elective treatment of a pre-existing condition that did not worsen from baseline is not considered to be an AE).
- A persistent or significant disability/incapacity

(A substantial disruption of a person's ability to conduct normal life functions. This definition is not intended to include experiences of relatively minor medical significance such as uncomplicated headache, nausea, vomiting, diarrhea, influenza, accidental trauma (i.e., sprained ankle) that may interfere or prevent everyday life functions but do not constitute a substantial disruption).

- A congenital anomaly/birth defect
- Important medical events that may not result in death, be life-threatening, or require hospitalization may be considered serious when, based upon appropriate medical judgment, they may jeopardize the patient and may require medical or surgical intervention to prevent one of the outcomes listed in this definition (Examples include allergic bronchospasm requiring intensive treatment in an emergency room or at home, blood dyscrasias or convulsions that do not result in hospitalization or the development of drug dependency or drug abuse).

11.4 Expedited Adverse Event and Serious Adverse Event Reporting

- AE reporting must be done through the CRFs.
- Any SAE that occurs after starting study drug administration must be reported to the central office within 2 business days of the Investigator at the site learning of the event. All SAEs must be reported via a written report (Serious Adverse Event Reporting Form), signed by the Investigator and faxed to SCRI.
- All SAEs must be followed until they are resolved (return to normal or baseline values), stabilized, or the patient is lost to follow-up or deceased. Supplemental measurements and/or evaluations may be necessary to fully investigate the nature and/or causality of an AE or SAE. This may include additional laboratory tests, diagnostic procedures, or consultation with other healthcare professionals.
- Any malignancy possibly related to cancer treatment (including AML/MDS) should also be reported. A second malignancy is one unrelated to the treatment of a prior malignancy (and is NOT a metastasis from the initial malignancy).
- A death on study requires reporting regardless of causality and attribution to treatment or other cause must be provided. Death due to progressive disease should be reported as grade 5 "Neoplasms benign, malignant and unspecified (including cysts and polyps) - Other (Progressive Disease)" under the system organ class (SOC) of the same name. Evidence that the death was a manifestation of underlying disease (*e.g.*, radiological changes suggesting tumor growth or progression: clinical deterioration associated with a disease process) should be submitted. Deaths that occur beyond 30 days after the end of study drug administration/initiation of an alternate therapy, do not qualify as SAEs.

11.5 Pregnancy Information

The effects of vinorelbine on the developing human fetus are unknown. Due to potential teratogenic effects, women of child-bearing potential must agree to use effective contraceptive methods prior to study entry, during study participation, and for at least 30 days after the last administration of study medication. Should a woman suspect she is pregnant while she is participating in this study, she should inform her treating physician immediately. If any female patient becomes pregnant while enrolled in the clinical trial, she will be withdrawn immediately. Any dispensed study medication must be returned to the clinical site. The Investigator must notify within **24 hours** of learning about the pregnancy.

Any unintended pregnancy, pregnancy complication or elective termination of a pregnancy for medical reasons will be recorded as an AE or SAE and will be followed as such. A spontaneous abortion is always considered to be an SAE.

12Translational Research/Pharmacodynamics Studies

Within 2 weeks (up to 3 days) prior to starting treatment with IV vinorelbine and at time of disease progression (for all Singapore and Australian sites), fresh tumor tissue biopsies will be taken from subjects who have accessible tumor tissue and safe to biopsy based on the Investigator's judgment, and up to 20ml blood at each time point, for the purpose of translational research. Time points for collection of tumour biopsy and blood for purpose of translational research are as below:

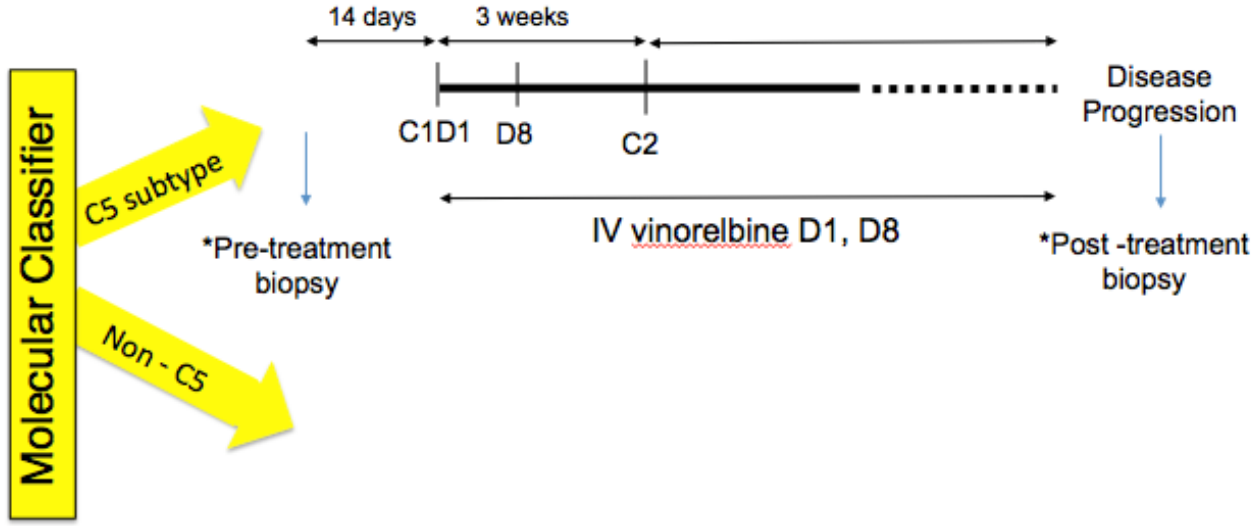

12.1 List of the material to be obtained for each patient for translational research:

- 20ml of whole blood will be obtained each during pre-treatment and post-treatment.
- One archival tumor block or 5 unstained slides if blocks cannot be released, will be obtained.
- Fresh tumor tissue biopsies will be taken from subjects who have safe and accessible tumor tissue based on the Investigator's judgment

12.2 Translational Studies

- Patients' tumors and whole blood samples may be subject to additional molecular analysis to identify additional pharmacodynamic markers of IV vinorelbine and/or predictive biomarkers of response to IV vinorelbine.
- Molecular analysis including but not restricted to gene mutation profiling, gene expression profiling, protein expression profiling will be performed.

- Patient samples collected could be stored in a biobank for further research at Cancer Science Institute and NUHS Transcend for five years after publication (roughly for 10 years).

13Statistical Considerations

13.1 Sample Size

Sample size for primary endpoint of Response Rates
Patients will be evaluated following a single arm open label Simon's Optimal two-stage design, with a null hypothesis of response rate of 10%, based on historical response data for platinum resistant recurrent OC with the alternative hypothesis of response rate of 30% or more in patients with C5 HGSOC, following treatment with vinorelbine. Ten patients will be enrolled in the first stage between Singapore and Australia, for expansion to the second stage, which will involve an additional 19 patients. At a 5% level of significance, 29 patients are required for 80% power of rejecting the null hypothesis and continuing to stage II if two or more out of 10 patients have a response as per RECIST1.1 to vinorelbine. However, a total of 36 patients will be recruited to the trial to account for drop outs of 20% (29 patients + 20% drop out = 35 patients)

13.2 Analysis Populations

All enrolled patients who receive at least one dose of study medication will constitute the safety population. The safety population will be used for all demographic and baseline characteristic analyses and for all safety analyses. All patients who complete one cycle of therapy will be considered evaluable. Patients who discontinue treatment before completing one cycle for reasons other than progression will be replaced.

13.3 Significance Level

For the study population, analysis of response rates will be completed using one-sided tests at the 5% level of significance

13.4 Study Termination

This study is an open-label trial; patients will be allowed to continue study drug treatment until disease progression or toxicity occurs. No interim analysis or data safety monitoring beyond that described in this protocol will be conducted for this study.

13.5 Statistical Methodology

The data collected in this study will be summarized in tables listing the mean, standard deviation, median, minimum, maximum, and number of patients for continuous data, or in tables listing count and percentage for categorical data, where appropriate.
Demographics and baseline characteristics for each dose group will be summarized and compared descriptively. Patient accountability will be summarized for the safety population. The following patient accountability information will be presented:
- Number of patients enrolled, completed, and discontinuing prematurely
- Number of patients by reason for discontinuation

In addition, a listing of the patients who discontinued prematurely will be presented.

13.5.1 Efficacy

Patients will be evaluated for clinical benefit as determined by tumor response and progression free survival using RECIST. The endpoint of objective response rate will be based on RECIST criteria (version 1.1). The best overall response will be summarized by using the number and percent of patients in each tumor response category along with the two-sided exact binomial 95% confidence intervals. The overall response rate (CR + PR) and clinical efficacy rate (RECIST and/or CA125 responses) will also be summarized.

13.5.2 Safety and Tolerability

AE data as per CTCAE v4.03 will be listed individually and summarized by body system and preferred terms within a body system for each treatment group. Each AE (based on preferred terminology) will be counted only once for a given patient. If the same AE occurs on multiple occasions, the highest severity and most conservative estimate of relationship to study drug will be assumed. If two or more AEs are reported as a unit, the individual terms will be reported as separate experiences. The number of patients reporting AEs within body systems will be analyzed descriptively.

Treatment-emergent AEs will be defined as those AEs that begin on or after the date/time of study medication administration or are present at the start of screening and worsen following initiation of treatment with the study medication. Drug-related AEs will include those AEs that are reported by the Investigator as possible, probable, or definite relationship to the study medication. With the exception of the treatment-emergent AEs by severity summary, all summaries will present the number and percent of patients having an AE by system organ class and by specific AE preferred term. If there are any deaths in the study, a similar listing of all treatment-emergent AEs for patients who died will be provided.

14Direct Access to Source Data Documents

This study will be performed in accordance with current NHMRC and World Medical Assembly Statements. All trial-related records will be made available upon request of the sponsor or clinical monitor, auditor or FDA.

14.1 Study Monitoring

This is an investigator initiated study and study monitoring will be performed by Singapore Clinical Research Institute (SCRI) for Singapore sites or other selected CRO/s for overseas sites. Data will be reviewed on a regular basis and quality assurance measures will be performed. Electronic data queries as well as paper query letters may be issued to the site.

15Study and Site Closure

Upon completion of the study, the following activities, when applicable, must be conducted in conjunction with the Investigator, as appropriate:

- Collection of study materials (i.e., specimen collection kits, drug shippers, etc.)
- Data clarifications and/or resolutions

- Accounting, reconciliation, and final disposition of used and unused study medication
- Review of site study records for completeness

If the Sponsor, Investigator, designate monitor(s), or appropriate regulatory officials discover conditions arising during the study that indicate that the study should be halted or that the study center should be terminated, this action may be taken after appropriate consultation among the Sponsor, Investigator, and designate monitor(s). Conditions that may warrant termination of the study include, but are not limited to, the following:

- The discovery of an unexpected, serious, or unacceptable risk to the patients enrolled in the study
- A decision on the part of the Sponsor to suspend or discontinue testing, evaluation, or development of the product
- Failure of the Investigator to comply with pertinent regulations of appropriate regulatory authorities
- Submission of knowingly false information from the research facility to the Sponsor, Study Monitor, or appropriate regulatory authority
- Refusal of the Investigator to supply source documentation of work performed in this clinical trial

Study termination and follow-up will be performed in compliance with the conditions set forth in the International Conference on Harmonisation (ICH) sixth efficacy publication (E6) on Good Clinical Practice.

16Quality Control and Quality Assurance

The Principal Investigator is responsible for ensuring that the trial is conducted and data are generated, documented, and reported in compliance with the protocol, GCP guidelines, and applicable regulatory requirements.

16.1 Regulatory Requirements

- All investigators must have an up-to-date CV (signed within 2 years) on file
- Laboratory certification/accreditation and normal ranges are required
- Investigators and site staff are required to complete ICH GCP training modules depending on delegated tasks
- Consent forms must be reviewed by the Central Office before submission to the local ethics regulatory board and must include a statement that 1) information will be sent to and 2) medical records will be reviewed
- A Membership list of the local ethics board is required.
- A copy of the initial approval letter from the ethics board must be submitted
- A completed Site Participant List/Training Log is required and must be submitted to the Central Office

References

1. Vaughan S, Coward JI, Bast RC, Berchuck A, Berek JS, Brenton JD, et al. Rethinking ovarian cancer: recommendations for improving outcomes. 2011. pp. 719–25.

2. AIHW. an overview 2012. 2012 Nov 13;:1–215.

3. McGuire WP, Hoskins WJ, Brady MF, Kucera PR, Partridge EE, Look KY, et al. Cyclophosphamide and cisplatin compared with paclitaxel and cisplatin in patients with stage III and stage IV ovarian cancer. N Engl J Med. 1996 Jan 4;334(1):1–6.

4. ICON2: randomised trial of single-agent carboplatin against three-drug combination of CAP (cyclophosphamide, doxorubicin, and cisplatin) in women with ovarian cancer. ICON Collaborators. International Collaborative Ovarian Neoplasm Study. Lancet. 1998 Nov 14;352(9140):1571–6.

5. Omura G, Blessing JA, Ehrlich CE, Miller A, Yordan E, Creasman WT, et al. A randomized trial of cyclophosphamide and doxorubicin with or without cisplatin in advanced ovarian carcinoma. A Gynecologic Oncology Group Study. Cancer. 1986 May 1;57(9):1725–30.

6. Cadron I, Leunen K, Amant F, Van Gorp T, Neven P, Vergote I. The “Leuven” dose-dense paclitaxel/carboplatin regimen in patients with recurrent ovarian cancer. Gynecologic Oncology. 2007 Aug;106(2):354–61.

7. Ozols RF. Phase III Trial of Carboplatin and Paclitaxel Compared With Cisplatin and Paclitaxel in Patients With Optimally Resected Stage III Ovarian Cancer: A Gynecologic Oncology Group Study. Journal of Clinical Oncology. 2003 Sep 1;21(17):3194–200.

8. Bois du A. A Randomized Clinical Trial of Cisplatin/Paclitaxel Versus Carboplatin/Paclitaxel as First-Line Treatment of Ovarian Cancer. CancerSpectrum Knowledge Environment. 2003 Sep 3;95(17):1320–9.

9. Alsop K, Fereday S, Meldrum C, deFazio A, Emmanuel C, George J, et al. BRCA Mutation Frequency and Patterns of Treatment Response in BRCA Mutation-Positive Women With Ovarian Cancer: A Report From the Australian Ovarian Cancer Study Group. Journal of Clinical Oncology. 2012 Jul 18;30(21):2654–63.

10. Gordon AN, Granai CO, Rose PG, Hainsworth J, Lopez A, Weissman C, et al. Phase II study of liposomal doxorubicin in platinum- and paclitaxel-refractory epithelial ovarian cancer. J Clin Oncol. 2000 Sep;18(17):3093–100.

11. Pujade-Lauraine E, Hilpert F, Weber B, Reuss A, Poveda A, Kristensen G, et al. Bevacizumab Combined With Chemotherapy for Platinum-Resistant Recurrent Ovarian Cancer: The AURELIA Open-Label Randomized Phase III Trial. Journal of Clinical Oncology. 2014 Apr 25;32(13):1302–8.

12. Sørensen P, Høyer M, Jakobsen A, Malmström H, Havsteen H, Bertelsen K. Phase II Study of Vinorelbine in the Treatment of Platinum-Resistant Ovarian Carcinoma. Gynecologic Oncology. 2001 Apr;81(1):58–62.

13. Rothenberg ML, Liu PY, Wilczynski S, Nahhas WA, Winakur GL, Jiang CS, et al. Phase II trial of vinorelbine for relapsed ovarian cancer: a Southwest Oncology Group study. Gynecologic Oncology. 2004 Dec;95(3):506–12.

14. Bookman MA. First-line chemotherapy in epithelial ovarian cancer. Clin Obstet Gynecol. 2012 Mar;55(1):96–113.

15. Tothill RW, Tinker AV, George J, Brown R, Fox SB, Lade S, et al. Novel Molecular Subtypes of Serous and Endometrioid Ovarian Cancer Linked to Clinical Outcome. Clinical Cancer Research. 2008 Aug 15;14(16):5198–208.

16. Network TCGAR, Network TCGAR, sites DWGATS, Medicine GSCBCO, Broad Institute, Washington University in St Louis, et al. Integrated genomic analyses of ovarian carcinoma. Nature. Nature Publishing Group; 2012 Apr 12;474(7353):609–15.

17. Tan TZ, Miow QH, Huang RY-J, Wong MK, Ye J, Lau JA, et al. Functional genomics identifies five distinct molecular subtypes with clinical relevance and pathways for growth control in epithelial ovarian cancer. EMBO Mol Med. 2013 May 13;5(7):1051–66.

18. Helland Å, Anglesio MS, George J, Cowin PA, Johnstone CN, House CM, et al. Deregulation of MYCN, LIN28B and LET7 in a Molecular Subtype of Aggressive High-Grade Serous Ovarian Cancers. Tan P, editor. PLoS ONE. 2011 Apr 13;6(4):e18064.

19. Molenaar JJ, Domingo-Fernández R, Ebus ME, Lindner S, Koster J, Drabek K, et al. LIN28B induces neuroblastoma and enhances MYCN levels via let-7 suppression. Nat Genet. 2012 Oct 7;44(11):1199–206.

20. Burger RA, DiSaia PJ, Roberts JA, O'rourke M, Gershenson DM, Homesley HD, et al. Phase II trial of vinorelbine in recurrent and progressive epithelial ovarian cancer. Gynecologic Oncology. 1999 Feb;72(2):148–53.

21. Gershenson DM, Burke TW, Morris M, Bast RC, Guaspari A, Hohneker J, et al. A phase I study of a daily x3 schedule of intravenous vinorelbine for refractory epithelial ovarian cancer. Gynecologic Oncology. 1998 Sep;70(3):404–9.

22. Topp MD, Hartley L, Cook M, Heong V, Boehm E, McShane L, et al. Molecular correlates of platinum response in human high-grade serous ovarian cancer patient-derived xenografts. Mol Oncol. 2014 Jan 24.

23. Weroha SJ, Becker MA, Enderica-Gonzalez S, Harrington SC, Oberg AL, Maurer MJ, et al. Tumorgrafts as In Vivo Surrogates for Women with Ovarian Cancer. Clinical Cancer Research. 2014 Mar 2;20(5):1288–97.

24. Liu G, Franssen E, Fitch MI, Warner E. Patient preferences for oral versus intravenous palliative chemotherapy. J Clin Oncol. 1997 Jan;15(1):110–5.

25. Jassem J, Ramlau R, Karnicka-Młodkowska H, Krawczyk K, Krzakowski M, Zatloukal P, et al. A multicenter randomized phase II study of oral vs. intravenous vinorelbine in advanced non-small-cell lung cancer patients. Ann Oncol. 2001 Oct;12(10):1375–81.

26. Depierre A, Freyer G, Jassem J, Orfeuvre H, Ramlau R, Lemarie E, et al. Oral vinorelbine: feasibility and safety profile. Ann Oncol. 2001 Dec;12(12):1677–81.

27. Marty M, Fumoleau P, Adenis A, Rousseau Y, Merrouche Y, Robinet G, et al. Oral vinorelbine pharmacokinetics and absolute bioavailability study in patients with solid tumors. Ann Oncol. 2001 Nov;12(11):1643–9.

28. Vokes EE, Rosenberg RK, Jahanzeb M, Craig JB, Gralla RJ, Belani CP, et al. Multicenter phase II study of weekly oral vinorelbine for stage IV non-small-cell lung cancer. J Clin Oncol. 1995 Mar;13(3):637–44.

29. Freyer G, Delozier T, Lichinister M, Gedouin D, Bougnoux P, His P, et al. Phase II study of oral vinorelbine in first-line advanced breast cancer chemotherapy. J Clin Oncol. 2003 Jan 1;21(1):35–40.

30. Bartsch R, Wenzel C, Altorjai G, Pluschnig U, Bachleitner-Hoffmann T, Locker GJ, et al. Results from an observational trial with oral vinorelbine and trastuzumab in advanced breast cancer. Breast Cancer Res Treat. 2007 May;102(3):375–81.

31. Gridelli C, Manegold C, Mali P, Reck M, Portalone L, Castelnau O, et al. Oral vinorelbine given as monotherapy to advanced, elderly NSCLC patients: a multicentre phase II trial. EUROPEAN JOURNAL OF CANCER. 2004 Nov;40(16):2424–31.

32. Bonneterre J, Chevalier B, Focan C, Mauriac L, Piccart M. Phase I and pharmacokinetic study of weekly oral therapy with vinorelbine in patients with advanced breast cancer (ABC). Ann Oncol. 2001 Dec;12(12):1683–91.

33. Mansour M, Mourad C. Phase II study of single agent oral vinorelbine as first-line treatment in patients with HER-2 negative metastatic breast cancer. Cancer Chemother Pharmacol. 2013 Jun 26;72(2):429–35.

Appendix 1: List of prohibited inducers and inhibitors of CYP3A4

Inhibitors	Inducers
protease inhibitors: ritonavir indinavir nelfinavir saquinavir	anticonvulsants, mood stabilizers: phenytoin (anticonvulsant) carbamazepine oxcarbazepine
macrolide antibiotics: erythromycin telithromycin clarithromycin	Barbiturates: Phenobarbital
azole antifungals: fluconazole ketoconazole itraconazole	non-nucleoside reverse transcriptase inhibitors: efavirenz nevirapine etravirine
nefazodone (psychoactive and antidepressant)	rifampicin & rifabutin (bactericidal)
bergamottin (constituent of grapefruit juice)	modafinil (stimulant)
quercetin (nutritional supplement)	hyperforin (constituent of St Johns Wort)
aprepitant (antiemetic)	cyproterone (antiandrogen, progestin)
verapamil & diltiazem (calcium channel blocker)	pioglitazone & troglitazone (antidiabetics)
chloramphenicol (antibiotic)	

Appendix 2: Guidelines for Evaluation of Disease

- *Measurable and Non-measurable Definitions*

Measurable lesion:

A non nodal lesion that can be accurately measured in at least one dimension (longest dimension) of

≥10 mm with MRI or CT when the scan slice thickness is no greater than 5mm. If the slice thickness is greater than 5mm, the minimum size of a measurable lesion must be at least double the slice thickness (e.g., if the slice thickness is 10 mm, a measurable lesion must be ≥20 mm).
≥10 mm calliper/ruler measurement by clinical exam or medical photography.
≥20 mm by chest x-ray.
Additionally lymph nodes can be considered pathologically enlarged and measurable if

≥15mm in the short axis when assessed by CT or MRI (slice thickness recommended to be no more than 5mm). At baseline and follow-up, only the short axis will be measured [**Error! Reference source not found.**].

Non-measurable lesion:

All other lesions including lesions too small to be considered measurable (longest diameter <10 mm or pathological lymph nodes with ≥ 10 mm and <15 mm short axis) as well as truly non-measurable lesions, which include: leptomeningeal disease, ascites, pleural or pericardial effusions, inflammatory breast disease, lymphangitic involvement of the skin or lung, abdominal masses/abdominal organomegaly identified by physical exam that is not measurable by reproducible imaging techniques [**Error! Reference source not found.**, 2009].

Measurable disease: The presence of at least one measurable lesion. Palpable lesions that are not measurable by radiologic or photographic evaluations may not be utilized as the only measurable lesion.

Non-Measurable only disease: The presence of only non-measurable lesions. Note: non-measurable only disease is not allowed in Phase II per protocol.

- **Response Criteria**

- ***Evaluation of target lesions***

Definitions for assessment of response for target lesion(s) are as follows:

Complete Response (CR): Disappearance of all target lesions. Any pathological lymph nodes must be <10mm in the short axis.
Partial Response (PR): At least a 30% decrease in the sum of the diameters of target lesions, taking as a reference, the baseline sum of the diameters (e.g. percent change from baseline).
Stable Disease (SD): Neither sufficient shrinkage to qualify for PR nor sufficient increase to qualify for progressive disease.
Progressive Disease (PD): At least a 20% increase in the sum of the diameters of target lesions, taking as a reference, the smallest sum of diameters recorded since the treatment started (e.g. percent change from nadir, where nadir is defined as the smallest sum of diameters recorded since treatment start). In addition, the sum must have an absolute increase from nadir of 5mm.

Not Applicable (NA): No target lesions at baseline.
Not Evaluable (NE): Cannot be classified by one of the five preceding definitions.
Note:

If lymph nodes are documented as target lesions the short axis is added into the sum of the diameters (e.g. sum of diameters is the sum of the longest diameters for non-nodal lesions and the short axis for nodal lesions). When lymph nodes decrease to non-pathological size (short axis <10mm) they should still have a measurement reported in order not to overstate progression.

If at a given assessment time point all target lesions identified at baseline are not assessed, sum of the diameters cannot be calculated for purposes of assessing CR, PR, or SD, or for use as the nadir for future assessments. However, the sum of the diameters of the assessed lesions and the percent change from nadir should be calculated to ensure that progression has not been documented. If an assessment of PD cannot be made, the response assessment should be NE.

All lesions (nodal and non-nodal) should have their measurements recorded even when very small (e.g 2 mm). If lesions are present but too small to measure, 5 mm should be recorded and should contribute to the sum of the diameters, unless it is likely that the lesion has disappeared in which case 0 mm should be reported.

If a lesion disappears and reappears at a subsequent time point it should continue to be measured. The response at the time when the lesion reappears will depend upon the status of the other lesions. For example, if the disease had reached a CR status then PD would be documented at the time of reappearance. However, if the response status was PR or SD, the diameter of the reappearing lesion should be added to the remaining diameters and response determined based on percent change from baseline and percent change from nadir.

- ***Evaluation of non-target lesions***

Definitions for assessment of response for non-target lesions are as follows:

Complete Response (CR): The disappearance of all non-target lesions. All lymph nodes identified as a site of disease at baseline must be non-pathological (e.g. <10 mm short axis).

Non-CR/Non-PD: The persistence of 1 or more non-target lesion(s) or lymph nodes identified as a site of disease at baseline ≥ 10 mm short axis.

Progressive Disease (PD): Unequivocal progression of existing non-target lesions.

Not Applicable (NA): No non-target lesions at baseline.

Not Evaluable (NE): Cannot be classified by one of the four preceding definitions.

Note:

In the presence of measurable disease, progression on the basis of solely non-target disease requires substantial worsening such that even in the presence of SD or PR in target disease, the overall tumour burden has increased sufficiently to merit discontinuation of therapy.

Sites of non-target lesions, which are not assessed at a particular timepoint based on the assessment schedule, should be excluded from the response determination (e.g. non-target response does not have to be "Not Evaluable").

- ***New lesions***

New malignancies denoting disease progression must be unequivocal. Lesions identified in follow-up in an anatomical location not scanned at baseline are considered new lesions.

Any equivocal new lesions should continue to be followed. Treatment can continue at the discretion of the investigator until the next scheduled assessment. If at the next assessment the new lesion is considered to be unequivocal, progression should be documented.

- ***Evaluation of overall response***

Table presents the overall response at an individual time point for all possible combinations of tumor responses in target and non-target lesions with or without the appearance of new lesions for subjects with measurable disease at baseline.

Table 1 Evaluation of Overall Response for Subjects with Measurable Disease at Baseline

Target Lesions	Non-Target Lesions	New Lesions	Overall Response
CR	CR or NA	No	CR
CR	Non-CR/Non-PD or NE	No	PR
PR	Non-PD or NA or NE	No	PR
SD	Non-PD or NA or NE	No	SD
NE	Non-PD or NA or NE	No	NE
PD	Any	Yes or No	PD
Any	PD	Yes or No	PD
Any	Any	Yes	PD
CR=complete response, PR = partial response, SD=stable disease, PD=progressive disease, NA= Not applicable, and NE=Not Evaluable			

- ***Evaluation of best overall response***

The best overall response is the best response recorded from the start of the treatment until disease progression/recurrence and will be determined programmatically by GSK (or designee) based on the investigators assessment of response at each time point.

To be assigned a status of SD, follow-up disease assessment must have met the SD criteria at least once after first dose at a minimum interval of 63 days.

If the minimum time for SD is not met, best response will depend on the subsequent assessments. For example if an assessment of PD follows the assessment of SD and SD does not meet the minimum time requirement the best response will be PD. Alternative subjects lost to follow-up after an SD assessment not meeting the minimum time criteria will be considered not evaluable.

Appendix 3

- **Efficacy Assessment by GCIG CA 125 Criteria**

Disease progression and response evaluations determined according to the definitions established by GCIG [**Error! Reference source not found.**.

To calculate CA 125 responses accurately the following rules apply:

5 Intervening CA 125 values and the 28-day confirmatory value must be less than or equal to (within an assay variability of 10%) the previous values

6 Variations within the reference range of CA 125 levels will not interfere with the response definition.

7 For each subject, the same assay method must be used, and the assay must be tested in a quality control scheme.

8 Subjects are not evaluable by CA 125 if they have received mouse antibodies, medical or surgical manipulation of the peritoneum or pleura during the previous 28 days.

- **Assessment of Subject Completion**

If the last CA 125 assessment was more than 3 weeks prior to withdrawal from study and progressive disease has not been documented, an assessment should be obtained at the time of withdrawal from study.

- **Response Criteria**

A subject is categorized as a CA 125 **partial responder** if the CA 125 level has decreased by a minimum of 50%. The date when the CA 125 level is first reduced by 50% is the date of the CA 125 response.

A subject is categorized as a **complete CA 125 responder** if the CA 125 level has decreased by a minimum of 50% AND normalized, i.e. is within the reference range.

Subjects who have a decrease in CA 125 to within the reference range but whose initial CA 125 was less than twice the upper limit of the reference range have not had a CA 125 response and cannot therefore be classified as a CA 125 complete responder. All CA 125 responses require confirmation with a repeat evaluation within 28 days.

Progression is defined as below:

9 Subjects with elevated CA 125 pretreatment and normalization of CA 125 must show evidence of CA 125 ≥ the upper limit of the reference range on 2 occasions at least 1 week apart **OR**

10 Subjects with elevated CA 125 pretreatment which never normalizes, must show evidence of Ca 125 ≥ 2 x nadir value on 2 occasions at least 1 week apart **OR**

11 Subjects with CA 125 in the reference range pretreatment must show evidence of CA 125 ≥ 2 x upper limit of the reference range at least 1 week apart

Subject who progress solely based on CA -125 values should continue to receive study treatment per protocol.

- **Efficacy Assessment Incorporating RECIST 1.1 and GCIG CA 125 Criteria**

Disease progression and response evaluations determined according to the definitions established by GCIG [**Error! Reference source not found.**].

See Section **Error! Reference source not found.** and for guidelines of how to assess subjects using RECIST 1.1 and GCIG CA 125 criteria.

- **Assessment of Subject Completion**

If the last radiographic and/or CA 125 assessment was more than 3 weeks prior to withdrawal from study and progressive disease has not been documented, an assessment should be obtained at the time of withdrawal from study.

- **Response Criteria**

The date of response will be date of the earlier of the two events.

Table 2 Best overall response in subjects with measurable disease and who are also evaluable by CA 125

Target Lesion[a]	Nontarget[b]	New Lesion	CA 125	Overall Best Response
CR	CR	No	Normal	CR
CR	Non-CR/Non-PD	N o	Not PD	PR
CR	CR	No	PR but not normal	PR
CR	NE[e]	No	PR	PR
PR	Non-PD or NAE[e]	No	Not PD	PR
NAE[e]	Non-PD	No	PR	PR
PD or New > 28 days from CA 125 PR[c]	Any	Yes or No	PR	PR
SD[d]	Non-PD	No	PR	PR
SD[d]	Non-PD or NAE[e]	No	Not PR and not PD	SD
PD or New ≤28 days from CA 125 PR	Any		PR	PD
PD	Any	Yes or No	Any	PD
Any	PD	Yes or No	Any	PD
Any	Any	Yes	Any	PD
Any	Any	Yes or No	PD	PD

a. Target lesions include up to 5 measurable lesions (2 per organ) as defined by RECIST 1.1
b. Nontarget lesions include ascites and peritoneal thickening which are not measurable according to RECIST 1.1
c. Subjects who have a CA 125 response that occurs more than 28 days from PD according to RECIST 1.1 are considered a PR, according to best response but PD if the RECIST 1.1 PD is within 28 days of CA 125 response
d. Disease must be stable for 24 weeks to be considered SD
e. NE = Not evaluated; NAE = not all evaluated

- **Criteria for progression**

In assigning date of progression, PD by RECIST 1.1 should always take precedence over CA 125 should it occur first.

Table 3 Definition of Progression per GCIG Criteria (RECIST 1.1 and CA 125)

RECIST Measurable/Nonmeasurable Disease		CA 125
Compared to baseline (or lowest sum while on study if less than baseline), a 20% increase in sum or diameters **OR** any new lesions **OR** unequivocal increase in nontarget disease	AND	CA 125 $\geq$ 2 x ULRR[a] documented on 2 occasions at least 1 week apart
Same as above	OR	CA 125 $\geq$ 2 x nadir value on 2 occasions at least 1 week apart
Same as above	OR	CA 125 $\geq$ 2 x ULRR[a] documented on 2 occasions at least 1 week apart

a. ULRR = upper limit of reference range

Appendix 5:

Deciphering intra-tumoral heterogeneity using Molecular Assessment of Subtype Heterogeneity to guide personalized medicine in ovarian cancer.

Tuan Zea Tan[1*], Valerie Heong[1,2,3*], Jieru Ye[1], Diana Lim[4,5], Jeffrey Low[6], Mahesh Choolani[6], Clare Scott[3], David Shao Peng Tan[1,2,7] and Ruby Yun-Ju Huang[1,6,8]

[1]Cancer Science Institute of Singapore, National University of Singapore, Center for Translational Medicine, 14 Medical Drive,MD6 #12-01, Singapore 117599

[2]Department of Haematology-Oncology, National University Cancer Institute Singapore, Level 8 NUH Medical Center, 5 Lower Kent Ridge Road, Singapore 119074

[3]Walter and Eliza Hall Institute of Medical Research, Parkville, Victoria 3052, Australia

[4]Department of Pathology, National University Health System, 1E KentRidge Road Singapore 119228

[5]Department of Pathology, Yong Loo Lin School of Medicine, National University of Singapore, 4 Medical Drive, MD4 #04-01, Singapore 117597

[6]Department of Obstetrics and Gynecology, National University Health System, 1E Kent Ridge Road Singapore 119228

[7]Department of Medicine, Yong Loo Lin School of Medicine, National University of Singapore. 1E Kent Ridge Road, NUHS Tower Block, Level 10, Singapore 119228.

[8]Department of Anatomy, Yong Loo Lin School of Medicine, National University of Singapore, 4 Medical Drive, MD4 #04-01, Singapore 117597

*Equally contributing authors

Corresponding author: RYH

Address: Cancer Science Institute of Singapore, National University of Singapore, Center for Translational Medicine, 14 Medical Drive, #11-01, Singapore 117599

Phones: +65 6516 1148

Email: csihyjr@nus.edu.sg

Abstract

The evaluation of intra-tumoral heterogeneity (ITH) from a transcriptomic point of view is limited. Single-cell cancer studies reveal significant genomic and transcriptomic ITH within a tumor and it is no longer adequate to employ single-subtype assignment as this does not reflect the ITH that exist. Molecular assessment of subtype heterogeneity (MASH) was developed to comprehensively report on the composition of all transcriptomic subtypes within a tumor lesion. We demonstrate that by employing MASH on clinical ovarian samples, (i) a poor clinical outcome is determined by the presence or absence of poor prognosis subtypes within the tumor make-up, and (ii) when ovarian tumors recur, they unanimously express poor prognosis subtypes within their tumor composition. We utilized MASH on cell lines and observed that the intended preferential therapeutic responses of certain drugs, as previously reported, significantly correlated with the enrichment levels of the corresponding subtype. Hence, in-depth identification of transcriptomic subtypes within a tumor using MASH could potentially be useful in informing personalized therapeutic strategies and may warrant the translation of the MASH into a clinical assay.

Keyword: Intra-tumor heterogeneity/Microarray Gene Expression/Molecular Subtype/Ovarian Cancer

Introduction

The existence of inter-tumoral and intra-tumoral heterogeneity (ITH) have posed great challenges to the practice of precision medicine in oncology. Inter-tumoral heterogeneity has been extensively documented by The Cancer Genome Atlas (TCGA) projects identifying various distinct molecular subtypes within a tumor type. These molecular subtypes have distinct clinicopathologic outcomes and hence are relevant for therapeutic intervention (1-3). For example, the PAM50 subtyping identifies HER2-positive breast cancer patients who would derive greater benefit from trastuzumab treatment with longer disease-free survival and higher pathological complete response rates (4). Therefore, it would be reasonable to stratify patients based on markers derived from analysis of inter-tumoral heterogeneity. However, the existence of ITH complicates this approach. Several studies exploring ITH have addressed the clonal evolution of genomic (refers to both genomic and genetic) alterations such as the spatial and temporal mutation patterns (5-8), and concluded that spatially separated subclones are genomically diverse and would acquire distinct mutations in the same gene, protein complex or signal transduction pathway. Therefore, this diversity strongly argues against the clinical exploitation of genomic alteration profiles as biomarkers. ITH has been documented using single-cell analysis across multiple tumor types including carcinoma of the breast (9), renal (6), lung (10), prostate (11), ovarian (12), glioblastoma (13), melanoma (14), lymphoblastic leukemia (15) and multiple myeloma (16). These studies suggest that the existence of heterogeneity lies not only at the genomic level, but also at the epigenomic and transcriptomic levels. While the genomic composition of ITH has been well-documented, our understanding of the other constituents that influence heterogeneity within a tumor lesion, like transcriptomic subtype, is lacking.

Conventionally, the molecular subtype analysis deploys single-subtype assignment to each tumor biopsy sample. Given the existence of ITH, a single-subtype annotation is largely inadequate for classifying tumors as it ignores the co-existence of other subtype clones within that particular tumor. Many subclones co-exist within a tumor and display significant genomic, epigenomic, and transcriptomic diversity (6, 11). Therefore, alternative annotation methods that comprehensively report the co-existence and the relative frequency of good and poor prognosis signatures (6), drug-resistant and drug-sensitive populations (10) would better reflect the diversity that exist within a tumor lesion. This would provide a more comprehensive landscape of the tumor composition to allow for relevant identification of clinical biomarkers and realistic stratification of patients.

In this study, a new scheme termed molecular assessment of subtype heterogeneity (MASH) was used to represent the composition of transcriptomic subtypes within a tumor. As a proof-of-concept study, the proposed MASH scheme was applied to five cohorts of ovarian cancer to illustrate its utility and strength. Ovarian cancer, the most lethal of gynecological malignancies can be molecularly divided into 4-6 subtypes with the use of the single transcriptomic subtype annotation scheme(17-19). Despite being heterogeneous, ovarian cancer has been treated as a single entity with platinum/taxane-based chemotherapy over the past 20 years (20). Although there is limited clinical evidence currently to suggest these transcriptomic subtypes can robustly predict therapeutic outcomes in patients with ovarian cancer, recent retrospective analysis revealed that bevacizumab was reported to show benefit in the poor prognosis molecular subtypes, but not the others (21-23). There have also been reports to suggest these poor prognosis subtypes exhibit preferential response to platinum, paclitaxel,

vincristine and vinorelbine (17, 21, 23-25). With novel therapeutic options for ovarian cancer in the horizon, the need to explore the clinical relevance of these transcriptomic subtypes and how it may inform personalized therapeutic strategies is imminent. When validated, the MASH scheme may also be applicable to other tumour types particularly for the cancer agnostic clinical trials such as National Cancer Institute Molecular Analysis Therapy Choice (NCI-MATCH; NCT02465060).

Results

Ovarian cancer displays diverse inter- and intra-tumoral heterogeneity

Molecularly, ovarian cancer can be classified into five gene expression subtypes (17) based on transcriptomic profiling (Fig. 1A): Epithelial-A (Epi-A), Epithelial-B (Epi-B), Stem-like B (Stem-B), Mesenchymal (Mes) and Stem-like A (Stem-A). These subtypes were found to be highly concordant with other subtype annotations reported by several other groups (18, 19, 26) (Fig. 1A) confirming the robust representation of inter-tumoral heterogeneity. It has been reported that 95% of ovarian cancer consist of at least four subclones in a tumor (16), and 82% of TCGA (27) and 42% of the Mayo (28) ovarian cancer cohorts displayed properties of at least two subtypes. To understand the extent of ITH that exist within each transcriptomic subtype, we explored the prevalence of multiple co-existent transcriptomic subtypes within a tumor from a database of 3,431 ovarian cancer transcriptomes— CSIOVDB (26). We developed predictors for each transcriptomic subtype using Lasso regression (Fig. S1; Materials and Methods; Supplementary Info). Using the Lasso regression predictive models, we derived subtype scores and subsequently mapped out all co-existent subsets from each clinical sample from CSIOVDB. The threshold was selected based on the margin of each subtype versus non-subtype scores (Fig. S1A). The predictive models had an overall accuracy of 92.06% in subtype prediction (Fig. S1B). Not surprisingly, ovarian cancer exhibited extreme ITH where majority of the sample showed moderate to high scores for multiple subtypes (Fig. 1B). Approximately 30% of tumors showed gene expression signatures of more than one subtype under a stringent threshold (Fig. 1C; Materials and Methods). When stratified by histology, ovarian endometrioid carcinomas were found to most commonly display more than one subtype annotation followed by serous carcinoma (Fig. S2A).

We next evaluated whether there were any specific patterns of co-occurrence amongst the transcriptomic subtypes. There was no mutual exclusiveness between which two molecular subtypes could co-exist (Fig. 1D). Epi-B, being the most prevalent transcriptomic subtype in ovarian cancer, commonly co-existed with other subtypes (22.4%) (Fig. 1D). Stem-B, on the other hand, was observed to rarely co-exist with other subtypes (4.2%) (Fig. 1D) likely because Stem-B is a transcriptomic subtype that mainly consist of low grade non-serous carcinoma. We further explored whether there would be any preferential coupling of subtypes among histotypes. The most frequent transcriptomic subtype mixture for clear cell, endometrioid, and mucinous carcinoma were Epi-B/Stem-B (48.8%), Epi-A/Stem-B (20.3%), and Mes/Stem-B (59.1%), respectively (Fig. S2B). However, for serous carcinoma, the mixtures of any other subtype with Stem-B accounted for a mere 4.4% among all the mixtures that occurred within serous carcinoma (0.6% in Epi-A/Stem-B + 1.4% in Epi-B/Stem-B + 2% in Mes/Stem-B + 0.4% in Stem-A/Stem-B; Fig. S2B), confirming that the Stem-B signature was a useful predictor for non-serous histotypes. Interestingly, the rate of co-occurrence of a good prognosis subtype (Epi-A, Stem-B, Epi-B) with a bad prognosis subtype within the same tumor lesion was approximately 19.8% (3.3% + 9% + 1.5% in Mes, 0.4% + 5.3% + 0.3% in Stem-A; Fig. 1D). This intriguing finding posed further questions of the impact on survival outcomes.

Ovarian cancer clinical outcome is linked to the presence of poor prognostic transcriptomic subtypes.

We subsequently evaluated whether a higher degree of transcriptomic ITH would correlate with poorer clinical outcomes. We developed an ITH score to estimate ITH

based on the transcriptomic subtype constituents within a tumor (Materials and Methods). We observed tumors classified as single-subtype (‘pure’) exhibited a wide range of heterogeneity scores (Fig. S3A). This was due to multiple underlying subclones of transcriptomic signatures within the tumor that lead to significant heterogeneity but were insufficient to reach the subtype calling threshold set by Lasso regression. In general, there was no significant association between ITH score with clinicopathological parameters (Fig. S3B, C, D): histology, stage, grade, surgical debulking status, age, clinical response, EMT, overall survival (OS) and disease-free survival (DFS; inclusive of progression-, recurrence-, and metastasis-free survival). However, when we focused only on the good prognostic subtypes, surprisingly, we observed a correlation between ITH score and outcomes (Hazard Ratio = 0.7963; *p*-value = 0.0028) (Fig. 2). This impact on OS was particularly evident within tumors annotated as Epi-A (HR = 0.227; $p < 0.0001$) or Epi-B (HR = 0.748; $p = 0.0174$). In addition, multivariate Cox regression analyses with age, stage, grade, histology and debulking status further supported the role of the heterogeneity score as an independent prognostic factor in Epi-A ($p = 0.0191$), with a trend to significance in Epi-B tumors ($p = 0.0792$; Table S1) for OS but not DFS. To understand why the ITH score correlated with OS only in the good prognostic subtypes, Epi-A and Epi-B, but not the other subtypes, we evaluated the composition of good (Epi-A, Epi-B, Stem-B) and poor prognostic subtypes (Mes, Stem-A) in each tumor. We observed that in Epi-A and Epi-B, the difference in survival outcomes between ITH low and high groups were attributed to the degree of poor prognostic subtype/s within the tumor composition (Fig. 2). However, when we interrogated tumors from the poor prognostic subtypes, Mes and Stem-A, we observed that the level of ITH did not lead to differences in clinical outcomes. This is likely due to the overwhelming influence of the poor prognostic subtype, which constitutes the majority of the tumor make up, negating any potential

influence exerted by the good prognosis subtype/s that may co-exist. We note that in Stem-B tumors, the presence of poor prognostic subtype/s did not change the survival outcome. We believe the results may be confounded by the presence of low-grade tumors and diversity of multiple histotypes, leading to significant heterogeneity and non-uniformity of clinical outcomes. Collectively, the data lead us to hypothesize that the degree of poor prognosis subtype/s within a tumor composition is the predominant factor affecting clinical outcomes.

Intriguingly, regardless of the ITH score, the existence of either one of the two poor prognostic subtypes, Mes or Stem-A, led to a more aggressive phenotype linked to EMT (29) (Fig. 3). The co-existence of Mes or Stem-A increased EMT-ness of the tumor (Fig. 3A). Tumors with Epi-A/Mes or Epi-A/Stem-A subtype had poorer OS and DFS compared to pure Epi-A tumors (HR = 0.619, p = 0.0752, and HR = 0.5424, p = 0.0211, respectively; Fig. 3B). Epi-A/Mes and Epi-A/Stem-A tumors were combined due to low number of samples with available clinical information in Epi-A/Stem-A (n = 6). Comparing Epi-B/Mes and Epi-B/Stem-A tumors to pure Epi-B tumors, there was no significant difference for both OS and DFS, even though hazard ratio indicates that pure Epi-B has relatively better OS and DFS. The co-existence of Mes/Stem-A subtypes within a tumor was observed to have the poorest OS, when compared to tumors consisting of pure Mes or Stem-A subtypes (HR = 1.583, p = 0.0306 and HR=1.91, p = 0.0044, respectively). Similarly, Mes/Stem-A tumors have significantly poorer DFS than Stem-A tumors (HR = 2.089, p = 0.0033), and Mes tumors (HR = 1.405, p = 0.1221), albeit the difference is not significant in the later. The only exception observed was the Mes/Stem-B subtype, which had exceptionally longer median survival compared to Mes/non-Stem-B subtypes (undefined vs 57.8 months in Mes/Epi-A, 44.1 months in Mes/Epi-B, 24.5 months in Mes/Stem-A). Upon further scrutiny, these

Mes/Stem-B tumors were found to be mostly early stage or non-high grade serous tumors (Table S2), which may be a confounding factor for the exceptionally good outcome observed. We subsequently validated the analysis using an independent cohort of 409 primary ovarian cancer tumors (Materials and Methods; Supplementary Info) and observed the same trend with survival outcomes (Fig. S4A). Because of small sample size and limited number of events, the difference in outcome between the Mes/Stem-A and pure Mes or Stem-A tumors was not significant ($p = 0.476$, and $p = 0.172$). Yet, the combination of Mes/Stem-A trended a worse outcome than Mes or Stem-A alone, as indicated by the hazard ratio (HR = 0.6382, and HR = 0.3695). There were insufficient samples for comparisons between Epi-A with Epi-A mixtures ($n = 4$; Fig. S4A), and hence a survival analysis was not performed. In Epi-B and Epi-B/Mes or Epi-B/Stem-A tumors of the validation cohort, the trend is concordant with the previously described CSIOVDB cohort where significant differences in OS was observed but not in DFS (HR = 0.1506, $p < 0.0001$; and HR = 0.8515, $p = 0.4964$, respectively; Fig. S4A). It is worth noting that the Epi-B/Mes and Epi-B/Stem-A tumors were combined due to low number of samples with Epi-B mixture.

Armed with the knowledge that the co-existence of Mes and Stem-A conferred the worst outcome, we explored whether the degree of Mes/Stem-A mixture would also impact patient outcomes. We analysed the percentages of Mes/Stem-A mixture within a tumor, using the MASH scheme, and correlated them with clinical outcomes (Fig. 3E). We grouped the tumors into three nominal categories (no, partial, or full Mes/Stem-A) according to the degree of Mes/Stem-A mixture. As expected, the degree of Mes/Stem-A mixture within a tumor significantly correlated with OS and DFS in the CSIOVDB cohort (Fig. 3E; $p < 0.0001$). Ovarian cancer patients without the Mes/Stem-A trait showed longer median survival than those with full Mes/Stem-A trait in the CSIOVDB

cohort (55 vs 36 months in OS, and 24 vs 16 months in DFS, respectively). In the validation cohort, the OS and DFS outcomes for the three categories of no, partial, or full Mes/Stem-A displayed highly similar trends (Fig. S4B; $p = 0.0212$ and $p = 0.0048$, respectively). In the International Cancer Genome Consortium-Australian Ovarian Cancer Study (ICGC-AOCS) chemoresistant ovarian cancer cohort (release 19) (30), the degree of Mes/Stem-A mixture within a tumor significantly correlated with OS ($p = 0.0473$) but not with DFS ($p = 0.4371$). Patients with low Mes/Stem-A trait were observed to have a longer median survival than those with high Mes/Stem-A trait (44 vs 21 months in OS, and 7 vs 4 months in DFS, respectively). It should be noted that different stratification methods were used in the CSIOVDB and ICGC-AOCS cohorts because limited number of tumors were annotated with no Mes/Stem-A traits ($n = 9$) and full Mes/Stem-A traits ($n = 0$) in the ICGC-AOCS cohort. The decreased significance in the ICGC-AOCS cohort could be due to the fact that it was a smaller cohort with 24.4% genes in the microarray-derived subtype predictors not available by RNA-seq (Supplementary Info). When stratifying patients by the percentage of Mes or Stem-A subtype using the MASH scheme, there was a significant correlation between increasing Mes/Stem-A percentage and poorer OS and DFS outcomes (Fig. S5A).

Collectively, these data suggests that transcriptomic ITH using the MASH scheme was predictive of clinical outcomes in ovarian cancer. Importantly, a tumour composition containing Mes and/or Stem-A subtype/s conferred a poorer survival outcome compared to those containing neither of these two subtypes. In addition, the percentage of Mes or Stem-A subtype co-existing within a tumor also appeared to play a significant role.

Ovarian cancer metastasis and recurrence is enriched with Mes and Stem-A subtypes

To further evaluate the evolution of the subtypes during disease progression, we explored transcriptomic ITH using the MASH scheme by analyzing paired samples or ascitic fluid from the same patient. Intriguingly, regardless of the initial MASH annotation of the primary tumor, the omentum metastasis GSE30587 (31), peritoneum metastasis FRTLO (32), and ascitic fluid of patients (GSE94598), showed an increase in the percentage of Mes or Stem-A subtype (Fig. 4A). The same trend of Mes or Stem-A enrichment was also seen in platinum-resistant relapsed disease compared to the primary tumors in two independent cohorts E-MTAB-611 (33), ICGC-AOCS (30) (Supplementary Info). When paired primary -metastatic tumors were analyzed, there was significant enrichment of Mes/Stem-A in the metastatic deposits when compared to primary tumors (p = 0.0063; Fig. 4B). Enrichment of the Mes subtype in metastatic lesions was most common (p = 0.0006; Fig. S5B) followed by Stem-A (p = 0.149; Fig. S5B). We subsequently explored whether the poor prognostic subtypes influenced response to chemotherapy, we observed no significant enrichment of Mes/Stem-A in tumors that did not respond to chemotherapy (p = 0.9468; Fig. S5C).

To assess the relationship of molecular subtype composition in paired primary-metastasis/chemoresistant relapse, we estimated the conditional probability of subtype switching during primary to metastasis or chemoresistant relapse (Fig. 4C), based on the assumption that the subtypes of metastatic/relapsed tumors are dependent on the subtypes of primary tumors (Materials and Methods). The results suggest that all subtypes had a higher tendency to be annotated to Mes after metastasis or acquiring chemoresistance. In addition, good prognosis subtype Epi-A had relatively higher

tendency to maintain the original subtype or to switch to Mes. In contrast, Stem-A showed preferred subtype switching only to Mes (Fig. 4C). The Mes subtype was very stable maintaining as Mes without subtype switch (Fig. 4C). The Mes molecular subtype has previously been shown to be linked to a higher incidence of metastasis (17, 26). The Mes subtype was enriched in the relapsed setting and in metastasis to the omentum as well as peritoneum but was relatively scarce in ascites (Fig. 4A). We also asked whether the subtype switch observed from primary lesion to metastatic deposit was due to either one of three scenarios (i) clonal conversion - the disappearance of a subtype clone initially observed in primary tumor from the metastatic lesion, (ii) clonal expansion - expansion of a subtype clone in the metastatic deposit that was pre-existing in the primary tumor, or (iii) *de novo* – the appearance of a subtype in the metastatic deposit which was not originally seen in the primary tumor (Fig. 4C). By looking at the subtype annotation of paired primary tumors and metastatic deposits, the Mes subtype had the highest probability to undergo clonal expansion, and appear in metastasis or chemoresistant relapse. In contrast, the Stem-A and Epi-B subtypes were more likely to undergo clonal conversion to other subtypes. Interestingly, looking at the probability of clonal conversion and *de novo* clone formation in the Stem-A subtype, it was very unlikely to acquire this subtype during disease progression unless there was a pre-existing Stem-A clone in the primary tumor (Fig. 4C). This likely reflects the stem cell-like nature of the Stem-A subtype. However, these observations on clonal conversion and *de novo* clone formation should be taken with caution. The probability of clonal expansion may be underestimated in our analysis due to the lack of multiple biopsies taken from the primary and metastatic tumor samples to confirm the presence of spatially separated existing subclones. Another preliminary finding worth noting was that almost all subtypes (except Stem-A) showed medium probability to be annotated as Epi-B in the metastatic lesion. In accordance, Epi-B also had the second highest

probability to form *de novo* clones in metastatic lesions. Since Epi-B is correlated with the immune reactive subtype from TCGA, this finding is intriguing and raises the question regarding the impact of local microenvironmental cues in ITH and disease progression. It also sheds light on the relationship between the microenvironment and the immune signature in its effect on biological function and even therapeutic responses. Collectively, these results indicate that during ovarian cancer progression, transcriptomic subtype clones undergo clonal evolution according to several distinct patterns as a result of either clonal expansion, clonal conversion, or *de novo* clone formation leading to significant intra-tumoral and inter-tumoral heterogeneity observed between paired samples of primary tumor and metastatic/ relapsed lesions.

Using the MASH scheme to inform therapeutic strategies

Several reports have alluded to the preferential sensitivity of individual molecular subtypes to certain compounds (17, 23, 24). To evaluate the effect of ITH has on therapeutic response, we employed the MASH scheme to molecularly dissect individual tumors derived from the CSIOVDB cohort and interrogated the relationship between underlying functional pathways and the co-existing molecular subtypes. Based on previous work from our lab, the Stem-A and Mes tumors demonstrated preferential sensitivity to vinca alkaloids (17) and R428 (AXL inhibitor) (34) respectively. Hence we performed analysis of AXL and microtubule-related signaling pathways on these tumors and found that ovarian tumors either partially or completely consisting of the Stem-A subtype had significant enrichment of microtubule pathway genes compared with tumors without the Stem-A molecular subtype (p = 9.42E-154; Fig. 5A). Similarly, ovarian tumors consisting predominantly of Mes or a mixture of Mes subtype demonstrated significant higher enrichment of AXL signaling genes (p ~= 0; Fig. 5A)

with the higher percentage of Mes subtype within the tumor correlating with increased AXL pathway enrichment (p = 4.5E-31).

To determine whether employing MASH to delineate co-existing transcriptomic subtypes is able to predict functional outcomes, we applied MASH to ovarian cancer cell lines where the 50% growth inhibitory concentration (IC50) for vinca alkaloid, vincristine, and AXL inhibitor, R428, were previously established (Fig. 5B). By correlating the subtype composition with the IC50 values, we demonstrated that cells with higher percentage of Stem-A composition were more sensitive to vincristine compared to cells with a lower Stem-A composition. This could be due to inhibition of microtubule pathways highly enriched in the Stem-A subtype, as previously shown, by vincristine. We also found that Stem-B was the most resistant subtype to vincristine, followed by Mes and Epi-A. Likewise for AXL inhibitor R428, we found that Mes is the only subtype that was sensitive, whereas Epi-B was the most resistant to R428, followed by Epi-A, and Stem-A (Fig. 5B; Table S3A). We subsequently extended the analysis to CCLE (version 2015.02.24) (35) and SANGER COSMIC (release v79 version 17) (36) cohort where drug sensitivity data were available for 231 compounds (Fig. 5C; Table S3B). We focused mainly on identifying agents that could target both the poor prognostic subtypes effectively. Only PPM1D phosphatase inhibitor, CCT007093, showed moderate activity (*Rho* ~= -0.3) in both Mes and Stem-A subtypes (Fig. 5C). Of note, the Mes or Stem-A subtype were not particularly sensitive or resistant to cisplatin or paclitaxel. Intriguingly, most compounds were found to be efficacious in either one of the subtypes but not to both. Moreover, we noticed that the ERK, MAPK pathway inhibitors demonstrated increased activity in the Mes subtype, consistent with previous reports that the Mes subtype has sustained ERK activation (34). To a lesser extent, the Stem-A subtype was more sensitive to PI3K pathway

inhibitors (Fig. 5C). Collectively, these observations imply that the utility of MASH in enhancing our understanding of the molecular constituents within a tumor was useful in informing therapeutic strategies and warrants further investigation.

Ovarian cancer MASH assay development

As our data demonstrated a potential for clinical utility of MASH, we have outlined a possible strategy to implement the scheme as a clinical assay for ovarian tumors. The scheme is depicted in Fig. 6A. For this experiment, we used NanoString gene expression profiling for each ovarian cancer sample. The gene expression profile is subsequently fed into the classifier that computes the enrichment scores for each of the 5 molecular subtypes. Altogether FFPE samples collected from 80 patients from 2006 – 2014 were used as a training set. Sixteen regression models were trained using the Nanostring dataset with the best one used for analysis (Fig. 6B; Material and Methods). Receiver-operating characteristic (ROC) curves for each subtype show significant accuracy of the classifier based on the training cohort (Fig. 6C; Material and Methods). Of interest, the age of FFPE tumor samples did not affect accuracy of the classifier, with some samples analysed noted to be >10 years old. Encouragingly, concordance of the MASH analysis on the Nanostring training dataset was 93.75% for exact match of MASH profile while the propensity to accurately detect the poor prognostic subtypes, Mes or Stem-A, was 98.75% (Fig. 6D). Collectively, these results demonstrate the feasibility of accurately implementing the MASH scheme as a clinical assay using FFPE samples.

Discussion

As we enter the era of precision medicine, managing the underlying heterogeneity within tumors continues to be one of the most challenging tasks. Many studies have looked at the mutational landscape using next-generation sequencing (NGS) which have helped shed some light in this field. With sequencing tools at the single-cell level becoming more widely available, the appreciation of the dynamic intricacies of inter- and intra-tumoral heterogeneity (ITH) has been greatly highlighted. Yet, there are still limitations before these technologies can be readily translated into the clinical setting and offered as robust diagnostic tests. In this study, we reassessed the classic transcriptomic profiling analysis and asked the question: can gene expression signatures derived from the whole tumor bulk reflect the clonal heterogeneity within? We utilized ovarian cancer as the proof-of-concept disease model in part because of our prior experience (17), but also because of recent findings from the translational subgroup analysis of the ICON7 trial which suggested certain transcriptomic subtypes may derive preferential benefit when treated with bevacizumab in addition to standard chemotherapy (21, 23). Furthermore, we felt the conventional single-subtype assignment was inadequate to encompass the heterogeneous nature of ovarian cancer (12, 27, 28). Hence, we proposed a scheme termed— molecular assessment of subtype heterogeneity (MASH) — to describe a tumor by its molecular subtype composition.

The MASH scheme proposed is based on the assumption that any ovarian tumor will fit into the classification characterized by the five transcriptomic subtypes: good prognosis Epi-A, Epi-B, Stem-B; and poor prognosis Mes, and Stem-A. However, in this study, there were 17 (0.5%) ovarian cancer samples that did not express any of the transcriptomic subtype signatures under the stringent threshold set by Lasso regression. This may be the result of poor sample quality, problematic microarray hybridization, or

simply a matter of threshold choices. From our data, we showed that even dissecting the percentage of enrichment of certain subtype signatures within a tumor can be prognostic, and may have therapeutic implications. Furthermore, monitoring the evolution of these subtype signatures over space and time would also be informative as demonstrated by the paired sample analysis.

The MASH scheme provided a means to measure ITH without the use of single-cell/nucleus technologies. Single-cell/nucleus technologies, while an extremely useful tool to quantify and study ITH, may not be cost-effective for use in clinical practice. We demonstrated that the MASH scheme with appropriate optimization, can feasibly be applied to existing clinically validated technologies such as microarrays, Fluidigm® and NanoString®, to facilitate translation into clinical practice. In addition, the MASH annotation using the bulk tumor transcriptome could circumvent a crucial technical issue encountered in single-cell/nucleus analysis: how many single cells are required to accurately represent the lesion in question? Nonetheless, this study is still limited by the fact that the archival samples were all derived from a single random biopsy. The extensive diversity in tumors poses significant challenges in resolving the full spectrum of cancer pathway aberrations through a single biopsy sampling bias and may not be representative of the entire tumor (6). Consequently, this raises concerns whether the subtype annotation derived from a single biopsy would adequately depict the genetically distinct subclonal populations of cells driving phenotypic variation of the actual tumor. However, the fact that the presence of clonal heterogeneity itself was prognostic within the single subtype annotated group was rather intriguing. This indicated that an alternative surrogate could be used to score heterogeneity particularly within the seemingly good prognostic group. Furthermore, the above concerns could be somewhat reassured by the temporal evolution of the poor prognostic signatures demonstrated in

this study where the presence of poor prognostic subtypes—Mes and/or Stem-A within a tumor determined the clinical outcome. In addition, we showed that these traits were significantly enriched in recurrent and metastatic tumors implying that the Mes and/or Stem-A traits are likely to be the "default" state during disease progression to evade the effects of chemotherapy. As the Mes signature is enriched in processes related to extracellular matrix modeling, stroma and fibroblast[11], it is plausible that ovarian cancer preferentially elicits stromal reactions similar to fibrosis in response to platinum-taxane chemotherapy.

The multiple molecular subtypes in the tumor make-up has relevant implications to the management of ovarian cancer and further supports the notion that we should move away from the conventional "one-size-fit-all" therapeutic approach. The co-existence of multiple molecular subtypes or subclones within a tumor implies that more sophisticated therapeutic strategies are required in order to successfully target all the specific subtypes (4, 7). Treatment regimens targeting only one subtype might inevitably spare the other co-existing subtypes resulting in the expansion or conversion to more resistant clones (7, 14, 15). This is of particular importance for tumors that contain both the Mes and Stem-A subtypes. Not only does this portend the worst prognosis, but no one drug from our limited screen appeared to effectively target both the subtypes with drugs sensitive in Mes appearing to be resistant in Stem-A, and vice versa. Hence, a combination approach that targets the different clones within a tumor is likely required (37). Furthermore, we showed that targeting of unique aberrant pathways responsible for driving the individual poor prognostic subtypes, Mes and Stem-A, resulted in preferential sensitivity to the relevant therapeutic targets. Moreover, the inverse correlation between the composition of Mes or Stem-A and the dose of relevant

targeted therapeutic strategy further highlights the utility of the MASH analysis in the application of personalized medicine.

An ambiguous point of contention is the extent of subclone presents that would be considered relevant for therapeutic targeting. This is an important consideration highlighted in the KEYNOTE-010 study where consistent benefit of PD-L1 inhibition by pembrolizumab was only demonstrated in non-small cell lung cancer patients with ≥ 50% of PD-L1 expression in tumor, but ambiguous for patients with PD-L1 expression < 50% (38). Another important aspect not covered in this study was the inter-subclone cooperation (39). Co-existing molecular subtypes within a tumor might interact and cooperate or compete in response to microenvironment cues and cytotoxic stress. While it may be plausible to use the MASH scheme to analyze such interaction, the results will at best be correlative and therefore, limited in value. In this aspect, single-cell transcriptome analysis is still the preferred method when evaluating inter-subclone competition and cooperation functionally. Nonetheless, this study has shown that the application of the MASH scheme in deciphering intra-tumoral heterogeneity warrants further validation as a clinical tool. Thus, the proposed MASH scheme may provide a promising strategy in informing personalized management of a patient.

Materials and Methods

National University Hospital cohort

From 2006 to 2014, frozen archival epithelial ovarian cancer tumors from the Department of Obstetrics & Gynecology, National University of Singapore were collected according to protocols approved by the Institution Review Board. Frozen tumor samples were kept frozen at all times prior to disruption. Each set of mortar and pestle was chilled in liquid nitrogen. Each frozen tumor sample was placed directly into the chilled mortar filled with liquid nitrogen. The frozen samples were crushed with pestle to fine powder, and collected into a pre-chilled microfuge tube, followed by homogenization in Trizol (Life Technologies, Carlsbad, CA) using sterile 1ml syringe and 21G Hypodermic needle (BD Precision, Oxford, AL). After the samples were homogenized, RNA was purified using miRNeasy kit as per manufacturer's protocol (Qiagen, Hilden, Germany). The quality of purified RNA obtained was determined using Eukaryote Total RNA Nano Series II, 2100 Bioanalyzer (Agilent Technologies, Santa Clara, CA) prior to microarray profiling.

Cells from patients' ascites fluid were harvested by filtering the ascites fluid through 100µm, 70µm, and 40µm cell strainers in descending order. Cells collected on 70µm and 40µm cell strainers were retained. Harvested cells were then split to two parts, a part for *in-vitro* culture, while the other portion was lysed and homogenized in RLT buffer (Qiagen, Hilden, Germany) to obtain RNA. Homogenized samples were purified using RNeasy kit as per manufacturer's protocol. The quality of RNA samples were determined by Eukaryote Total RNA Nano Series II, 2100 Bioanalyzer (Agilent Technologies, Santa Clara, CA) prior to microarray profiling.

Affymetrix GeneChip® Human Gene 1.0 ST Array

RNA samples with RIN value above 6.5 were subjected to Affymetrix GeneChip® Human Gene 1.0 ST Array (Affymetrix, Inc., Santa Clara, CA) analysis. The microarray data was deposited in Gene Expression Omnibus (GEO; http://www.ncbi.nlm.nih.gov/sites/entrez?db=gds) with the accession id GSE94598. The data was first RMA-normalized and standardized with GSE69207 (26) using Affymetrix Power Tool version 1.15.0 and ComBat (40), respectively (Supplementary Info). Subsequently, paired primary tumor-ascites data were extracted from the combined data.

Ovarian cancer database and subtype predictive model

Ovarian cancer molecular subtype information was extracted from CSIOVDB (26) curated from 48 cohorts of 3,431 clinical samples. Binary predictive models were developed to classify each subtype from the rest using Lasso regression and 10-fold cross-validation. The predicted subtype scores were scale-normalized across the samples to [0.0, 1.0], and a threshold of 0.4 was selected to call the presence of a subtype (Fig. S1A). The procedure is repeated to derive subtype predictive model for ovarian cancer cell lines.

Several datasets were downloaded from GEO and ArrayExpress (http://www.ebi.ac.uk/microarray-as/ae/) for validation. Preprocessed data of E-MTAB-611 (33) were downloaded from ArrayExpress. Processed data from Australian Ovarian Cancer Study (AOCS) recurrent ovarian cancer and ascites were downloaded from International Cancer Genome Consortium (ICGC; http://icgc.org/). Validation dataset GSE17260 (41), GSE32062 (42), and GSE32063 (42) hybridized on Agilent platform,

were downloaded from GEO, normalized using R version 3.3.1, limma version 3.28.21 and combined using ComBat (40) (EV Info). The MASH analysis of these samples were estimated using the predictive model developed from CSIOVDB.

Subtype heterogeneity score

To estimate intra-tumoral heterogeneity, a quantitative measurement scheme was derived based on the scores computed by the five subtype predictors. This score is based on the assumption that a tumor must show at least one primary molecular subtype, and that the secondary subtypes constitute the intra-tumor molecular subtype heterogeneity. Given the molecular subtype scores, $Score_s$, where $s \in \mathbf{SUBTYPE}$, and $\mathbf{SUBTYPE} = \{\text{Epi-A, Epi-B, Mes, Stem-A, Stem-B}\}$, the intra-tumoral heterogeneity, denoted as $Tumor_{Heterogeneity}$, is estimated as

$$Tumor_{Heterogeneity} = \sum_{s \in \text{SUBTYPE}}^{5} Score_s - \max_{s \in \text{SUBTYPE}} (Score_s),$$

$$Tumor_{Heterogeneity} \in [-1.0, 4.0]$$

The intra-tumoral heterogeneity score was applied to the clinical samples. Tumors with more than one subtype annotation expectantly showed a higher heterogeneity score, indicating the validity of the scoring system (Fig. S3A).

MASH assay

As the subtype signatures available on NanoString platform were derived previously from a cohort of 1,538 samples (17), new classifiers were developed for each subtype. For each subtype classifier, five-fold cross-validation was performed on the 80 FFPE samples of NUH cohort, using regressionLearner function from Matlab 2017b pre-release, and MASH profile deducted from this study. In total, 16 regression models

were tested as subtype classifier and the best were selected based on least root mean square error.

nanoString Codeset and processing

The 187 signature genes from previous subtype analysis (17) were sent to NanoString for designing and customizing the nCounter CodeSets. FFPE samples from NUH cohort (n = 80) that have corresponding fresh frozen samples included in CSIOVDB were chosen and analyzed via NanoString nCounter gene expression profiling. The normalization of nanoString data was performed using nSolver analysis software version 3.0 (NanoString Technologies Inc; Seattle, WA). The raw count from nanoString was subjected to background subtraction, positive control normalization and housekeeping genes (*ACTB*, *B2M*, *GAPDH*, *HPRT1*, *HSP90*, *RPL90)* normalization. The normalized counts were then log2-transformed prior to down-stream analysis.

Statistical Analysis

Statistical analyses were conducted using Matlab® R2012a version 7.14.0.739, and statistics toolbox version 8.0 (MathWorks; Natick, MA). Statistical significance of differential expression was evaluated using either Kruskal-Wallis (for paired comparison) or Mann-Whitney *U*-test. A Spearman correlation coefficient test was applied to assess significance of correlation. Kaplan-Meier analyses were conducted using GraphPad Prism® version 5.04 (GraphPad Software; La Jolla, CA). Statistical significance of the Kaplan-Meier analysis was calculated by log-rank test. Pathway enrichment scoring is based on Kolmogorov-Smirnov method described previously (24). Microtubule-related pathway geneset was taken from (17), and AXL signaling signature from (34).

Conditional probability of subtype is estimated by counting the number of samples having subtype score > 0.4. Prior of each subtype is estimated by $P(subtype) = \frac{count_{subtype}}{N}$, where *N* is the total number of sample. The co-occurrence probability is computed by

$$P(subtype_{primary} AND\ subtype_{metastatsis}) = \frac{Count\ of\ Co-occurrence}{N}.$$

Conditional probability is subsequently computed by

$$P(subtype_{metastasis} | subtype_{primary}) = P(subtype_{primary} AND\ subtype_{metastasis}) \Big/ P(subtype_{primary})$$

For *de novo* clone formation, the conditional probability is computed by

$$P(subtype_{de\ novo\ metastasis} | subtype_{non-existence\ in\ primary}) = P(subtype_{de\ novo\ metastasis} AND\ subtype_{non-existense\ in\ primary}) \Big/ [1 - P(subtype_{primary})]$$

Acknowledgements

This work is supported by National Research Foundation (NRF) Singapore and the Singapore Ministry of Education under its Research Centres of Excellence initiative to R.Y.H.; National Medical Research Council (NMRC) under its Centre Grant scheme to National University Cancer Institute (NCIS) to R.Y.H.

Authors Contribution

R.Y.H, T.Z.T, D.S.P.T., J.L, and M.C designed and conceptualized the study. J.Y performed sample collection and experiments. T.Z.T. performed bioinformatics analysis. R.Y.H, T.Z.T, V.H., D.S.P.T., J.L, and M.C analysed the data, interpret the results, and wrote the manuscript.

Conflicts of interest

The authors declare that they have no competing interests.

References

1. Cancer Genome Atlas N. Genomic Classification of Cutaneous Melanoma. Cell. 2015;161:1681-96.

2. Cancer Genome Atlas Research N, Kandoth C, Schultz N, Cherniack AD, Akbani R, Liu Y, et al. Integrated genomic characterization of endometrial carcinoma. Nature. 2013;497:67-73.

3. Cancer Genome Atlas Research N, Linehan WM, Spellman PT, Ricketts CJ, Creighton CJ, Fei SS, et al. Comprehensive Molecular Characterization of Papillary Renal-Cell Carcinoma. The New England journal of medicine. 2016;374:135-45.

4. Prat A, Bianchini G, Thomas M, Belousov A, Cheang MC, Koehler A, et al. Research-based PAM50 subtype predictor identifies higher responses and improved survival outcomes in HER2-positive breast cancer in the NOAH study. Clin Cancer Res. 2014;20:511-21.

5. de Bruin EC, McGranahan N, Swanton C. Analysis of intratumor heterogeneity unravels lung cancer evolution. Mol Cell Oncol. 2015;2:e985549.

6. Gerlinger M, Rowan AJ, Horswell S, Larkin J, Endesfelder D, Gronroos E, et al. Intratumor heterogeneity and branched evolution revealed by multiregion sequencing. N Engl J Med. 2012;366:883-92.

7. McGranahan N, Swanton C. Biological and therapeutic impact of intratumor heterogeneity in cancer evolution. Cancer Cell. 2015;27:15-26.

8. Venkatesan S, Swanton C. Tumor Evolutionary Principles: How Intratumor Heterogeneity Influences Cancer Treatment and Outcome. American Society of Clinical Oncology educational book / ASCO American Society of Clinical Oncology Meeting. 2016;35:e141-9.

9. Zardavas D, Irrthum A, Swanton C, Piccart M. Clinical management of breast cancer heterogeneity. Nat Rev Clin Oncol. 2015;12:381-94.

10. Kim KT, Lee HW, Lee HO, Kim SC, Seo YJ, Chung W, et al. Single-cell mRNA sequencing identifies subclonal heterogeneity in anti-cancer drug responses of lung adenocarcinoma cells. Genome Biol. 2015;16:127.

11. Brocks D, Assenov Y, Minner S, Bogatyrova O, Simon R, Koop C, et al. Intratumor DNA methylation heterogeneity reflects clonal evolution in aggressive prostate cancer. Cell Rep. 2014;8:798-806.

12. McPherson A, Roth A, Laks E, Masud T, Bashashati A, Zhang AW, et al. Divergent modes of clonal spread and intraperitoneal mixing in high-grade serous ovarian cancer. Nat Genet. 2016.

13. Reardon DA, Wen PY. Glioma in 2014: unravelling tumour heterogeneity-implications for therapy. Nat Rev Clin Oncol. 2015;12:69-70.

14. Kemper K, Krijgsman O, Cornelissen-Steijger P, Shahrabi A, Weeber F, Song JY, et al. Intra- and inter-tumor heterogeneity in a vemurafenib-resistant melanoma patient and derived xenografts. EMBO Mol Med. 2015;7:1104-18.

15. Landau DA, Carter SL, Stojanov P, McKenna A, Stevenson K, Lawrence MS, et al. Evolution and impact of subclonal mutations in chronic lymphocytic leukemia. Cell. 2013;152:714-26.

16. Lohr JG, Stojanov P, Carter SL, Cruz-Gordillo P, Lawrence MS, Auclair D, et al. Widespread genetic heterogeneity in multiple myeloma: implications for targeted therapy. Cancer Cell. 2014;25:91-101.

17. Tan TZ, Miow QH, Huang RY, Wong MK, Ye J, Lau JA, et al. Functional genomics identifies five distinct molecular subtypes with clinical relevance and pathways for growth control in epithelial ovarian cancer. EMBO Mol Med. 2013;5:983-98.

18. Tothill RW, Tinker AV, George J, Brown R, Fox SB, Lade S, et al. Novel molecular subtypes of serous and endometrioid ovarian cancer linked to clinical outcome. Clin Cancer Res. 2008;14:5198-208.

19. Cancer Genome Atlas Research N. Integrated genomic analyses of ovarian carcinoma. Nature. 2011;474:609-15.

20. Narod S. Can advanced-stage ovarian cancer be cured? Nat Rev Clin Oncol. 2016;13:255-61.

21. Gourley C, McCavigan A, Perren T, Paul J, Michie CO, Churchman M, et al. Molecular subgroup of high-grade serous ovarian cancer (HGSOC) as a predictor of outcome following bevacizumab. Journal of Clinical Oncology. 2014;32:suppl. 5502.

22. Winterhoff BJN, Kommoss S, Oberg AL, Wang C, Riska SM, Konecny GE, et al. Bevacizumab and improvement of progression-free survival (PFS) for patients with the mesenchymal molecular subtype of ovarian cancer. Journal of Clinical Oncology,. 2014;32:5509.

23. Kommoss S, Winterhoff B, Oberg A, Konecny GE, Wang C, Riska SM, et al. Bevacizumab may differentially improve ovarian cancer outcome in patients with proliferative and mesenchymal molecular subtypes. Clin Cancer Res. 2017.

24. Tan TZ, Miow QH, Miki Y, Noda T, Mori S, Huang RY, et al. Epithelial-mesenchymal transition spectrum quantification and its efficacy in deciphering survival and drug responses of cancer patients. EMBO Mol Med. 2014;6:1279-93.

25. Miow QH, Tan TZ, Ye J, Lau JA, Yokomizo T, Thiery JP, et al. Epithelial-mesenchymal status renders differential responses to cisplatin in ovarian cancer. Oncogene. 2015;34:1899-907.

26. Tan TZ, Yang H, Ye J, Low J, Choolani M, Tan DS, et al. CSIOVDB: a microarray gene expression database of epithelial ovarian cancer subtype. Oncotarget. 2015;6:43843-52.

27. Verhaak RG, Tamayo P, Yang JY, Hubbard D, Zhang H, Creighton CJ, et al. Prognostically relevant gene signatures of high-grade serous ovarian carcinoma. J Clin Invest. 2013;123:517-25.

28. Konecny GE, Wang C, Hamidi H, Winterhoff B, Kalli KR, Dering J, et al. Prognostic and therapeutic relevance of molecular subtypes in high-grade serous ovarian cancer. J Natl Cancer Inst. 2014;106.

29. Nieto MA, Huang RY, Jackson RA, Thiery JP. Emt: 2016. Cell. 2016;166:21-45.

30. Patch AM, Christie EL, Etemadmoghadam D, Garsed DW, George J, Fereday S, et al. Whole-genome characterization of chemoresistant ovarian cancer. Nature. 2015;521:489-94.

31. Brodsky AS, Fischer A, Miller DH, Vang S, MacLaughlan S, Wu HT, et al. Expression profiling of primary and metastatic ovarian tumors reveals differences indicative of aggressive disease. PLoS One. 2014;9:e94476.

32. Malek JA, Martinez A, Mery E, Ferron G, Huang R, Raynaud C, et al. Gene expression analysis of matched ovarian primary tumors and peritoneal metastasis. J Transl Med. 2012;10:121.

33. Marchini S, Fruscio R, Clivio L, Beltrame L, Porcu L, Fuso Nerini I, et al. Resistance to platinum-based chemotherapy is associated with epithelial to mesenchymal transition in epithelial ovarian cancer. Eur J Cancer. 2013;49:520-30.

34. Antony J, Tan TZ, Kelly Z, Low J, Choolani M, Recchi C, et al. The GAS6-AXL signaling network is a mesenchymal (Mes) molecular subtype-specific therapeutic target for ovarian cancer. Sci Signal. 2016;9:ra97.

35. Barretina J, Caponigro G, Stransky N, Venkatesan K, Margolin AA, Kim S, et al. The Cancer Cell Line Encyclopedia enables predictive modelling of anticancer drug sensitivity. Nature. 2012;483:603-7.

36. Iorio F, Knijnenburg TA, Vis DJ, Bignell GR, Menden MP, Schubert M, et al. A Landscape of Pharmacogenomic Interactions in Cancer. Cell. 2016;166:740-54.

37. Willyard C. Cancer therapy: an evolved approach. Nature. 2016;532:166-8.

38. Herbst RS, Baas P, Kim DW, Felip E, Perez-Gracia JL, Han JY, et al. Pembrolizumab versus docetaxel for previously treated, PD-L1-positive, advanced non-small-cell lung cancer (KEYNOTE-010): a randomised controlled trial. Lancet. 2016;387:1540-50.

39. Cleary AS, Leonard TL, Gestl SA, Gunther EJ. Tumour cell heterogeneity maintained by cooperating subclones in Wnt-driven mammary cancers. Nature. 2014;508:113-7.

40. Johnson WE, Li C, Rabinovic A. Adjusting batch effects in microarray expression data using empirical Bayes methods. Biostatistics. 2007;8:118-27.

41. Yoshihara K, Tajima A, Yahata T, Kodama S, Fujiwara H, Suzuki M, et al. Gene expression profile for predicting survival in advanced-stage serous ovarian cancer across two independent datasets. PloS one. 2010;5:e9615.

42. Yoshihara K, Tsunoda T, Shigemizu D, Fujiwara H, Hatae M, Fujiwara H, et al. High-risk ovarian cancer based on 126-gene expression signature is uniquely characterized by downregulation of antigen presentation pathway. Clinical cancer research : an official journal of the American Association for Cancer Research. 2012;18:1374-85.

Figure Legends

Figure 1: Ovarian cancer is extremely heterogeneous between tumors and within tumors.

A. Epithelial ovarian cancer can be classified into five molecular subtypes: good prognosis (Epi)thelial-A/C3/Differentiated, (Epi)thelial-B/C4/Immunoreactive, (Stem)-like-B/C6; and poor prognosis (Mes)enchymal/C1, (Stem)-like-A/C5/Proliferative. Labels are given in order of Tan et al. (17)/Tothill et al. (18)/TCGA (19).

B. Subtype score heatmap from the five subtype predictor (black = low score, red = high score). The color bar indicates the subtype assigned in CSIOVDB.

C. Pie chart of CSIOVDB samples exhibiting multiple subtypes. The threshold of normalized subtype score 0.4 was deemed if a subtype properties are expressed. Color code: 1 subtype, black; 2 subtype, red; 3 subtype, pink.

D. Table of subtype co-occurrence frequency in CSIOVDB samples. Frequency percentage is given in parentheses. Frequency of single subtype is left empty and colored grey. Diagonal cells (repeat) are also colored grey. Total is the column sum indicating co-occurrence involving that particular subtype.

The frequency percentage in C, D is computed based on CSIOVDB sample size of 3,431. *Subtype color code*: Epi-A, dark green; Epi-B, light green; Mes, red; Stem-A, blue; Stem-B, purple.

Figure 2: Correlation of intra-tumoral heterogeneity score and survival.

Kaplan-Meier analysis of overall- (A) and disease-free (B) survival in all samples with one subtype annotation (left panel), and stratified by ovarian cancer molecular subtypes (right panels). Significance is evaluated using log-rank test. Median of intra-tumoral heterogeneity score is used to separate the samples into high (red) and low groups

(blue). Percentage bar chart shows the composition of good prognosis subtypes (non-Mes/Stem-A%; light blue) and poor prognosis subtypes (Mes/Stem-A; pink) in the intra-tumoral heterogeneity score-high and low groups. Significance is evaluated using Fisher Exact test.

Abbrev: HR, hazard ratio.

Figure 3: Molecular subtype composition is linked to clinical outcome in ovarian cancer.

A. Dot plot of epithelial-mesenchmal transition (EMT) score (*y*-axis; mean±SEM) in various molecular subtype compositions (*x*-axis) found in ovarian cancer from CSIOVDB (*n* = 3,431). Significance is evaluated using Mann-Whitney test. Selected comparisons are shown.

B. Kaplan-Meier analysis of overall- (upper panel) and disease-free (lower panel) survival stratified by molecular subtype compositions: Epi-A vs Epi-A/Mes (left); Epi-B vs Epi-B/Mes and Epi-B/Stem-A (middle); and Mes, Stem-A vs Mes/Stem-A (right). Significance is evaluated using log-rank test.

Bar plot indicating the median overall- (C) and disease-free (D) survival (*y*-axis) in month. Bar color indicates the molecular subtype compositions. Number of sample in each subtype composition is labeled beside the bar. (E) Kaplan-Meier analysis of overall and disease-free survival in CSIOVDB (left panel) and in ICGC-ACOS cohorts, where ovarian cancers are stratified into no (% = 0) or low (lowest 33%) Mes/Stem-A (green), partially (0 < % < 100) or intermediate (medium 33%) Mes/Stem-A (red), and fully (% = 100) or high (highest 34%) Mes/Stem-A (maroon). The shown *p*-value is computed by log-rank test.

Abbrev: HR, hazard ratio; OS, overall survival; DFS, disease-free survival

Subtype color code: Epi-A, dark green; Epi-B, light green; Mes, red; Stem-A, blue; Stem-B, purple.

Figure 4: Ovarian cancer metastasis composed of predominantly Mes or Stem-A subtype.

A. Bar plots showing the MASH percentage of primary ovarian cancer and metastasis (omental, peritoneal, or other distant) or ascites from five dataset. A bar plot showing the poor prognosis Mes and Stem-A subtypes composition percentage is shown each on the right of the MASH bar plots.

B. Frequency plot of Mes and Stem-A percentage (% > 0, red; % = 0, black) within a tumor in primary and metastasis/relapsed ovarian cancer. The shown *p*-value is computed by Fisher exact test.

C. Heatmap showing the conditional probability of metastasis subtype given the primary subtype. Blue = low and red = high probability.

Abbrev: Mets, metastasis; MASH, molecular assessment of subtype heterogeneity.

Subtype color code: Epi-A, dark green; Epi-B, light green; Mes, red; Stem-A, blue; Stem-B, purple.

Figure 5: MASH impact on drug treatment

A. Enrichment score (*y*-axis; mean±SEM) dot plot of microtubule-related pathway (upper panel) and AXL signaling pathway (lower panel) in various molecular subtype compositions (*x*-axis) found in ovarian cancer from CSIOVDB (*n* = 3,431). Significance is evaluated using Mann-Whitney test. Selected comparisons are shown.

B. Bar plot of MASH percentage (left *y*-axis) and growth inhibitory concentration (IC50; right *y*-axis) in ovarian cancer cell lines. The cells were aligned from most

sensitive to most resistant to vincristine (left panel; *n* = 18) and to R428, an AXL inhibitor (right panel; *n* = 10).

C. Scatter plot of Spearman correlation *Rho* comparing IC50 of 231 compounds and MASH compositions of Stem-A (*y*-axis) and Mes (*x*-axis). The purple quadrant (top right) shows compounds sensitive to Mes and Stem-A, while the blue quadrant (top left) shows compounds sensitive to Stem-A but resistant to Mes. Conversely, the pink quadrant (bottom right) shows compounds sensitive to Mes but resistant to Stem-A. Data is from ovarian cancer cell lines in CCLE (*n* = 20-25) and COSMIC (*n* = 17-40). Selected compounds and corresponding putative targets in parentheses are labelled: ERK, MAPK signaling inhibitors (diamond; black); PI3K signaling inhibitors (square; dark grey).

Abbrev: MASH, molecular assessment of subtype heterogeneity.

Subtype color code: Epi-A, dark green; Epi-B, light green; Mes, red; Stem-A, blue; Stem-B, purple.

Figure 6: MASH implementation as clinical assay.

A. Scheme of implementing MASH into a clinical assay.

B. Boxplot of regression models (*n* = 16) accuracy in 1/RMSE (*y*-axis) for each subtype classifier (*x*-axis). Whiskers indicate min and max, whereas the box indicate 1st, 2nd, and 3rd quantiles.

C. Classifier ROC curves of poor prognosis Mes, Stem-A and good prognosis subtypes Epi-A, Epi-B and Stem-B developed using FFPE samples from NUH cohort (*n* = 80) on NanoString.

D. Comparison of MASH predictions from microarray and NanoString. Top heatmap indicates FFPE year (darker color = older FFPE). Second heatmap indicates MASH

from microarray and third heatmap shows MASH prediction from NanoString (black = predicted present). Concordance of MASH profile and Mes/Stem-A detection are indicated using black bars. Concordance percentage is given on the right of the bars. Abbrev: ES, enrichment score; RMSE, root mean square error; ROC, receiver operative characteristic curve; AUC, area under the curve.

Subtype color code: Epi-A, dark green; Epi-B, light green; Mes, red; Stem-A, blue; Stem-B, purple.

Figures 1:

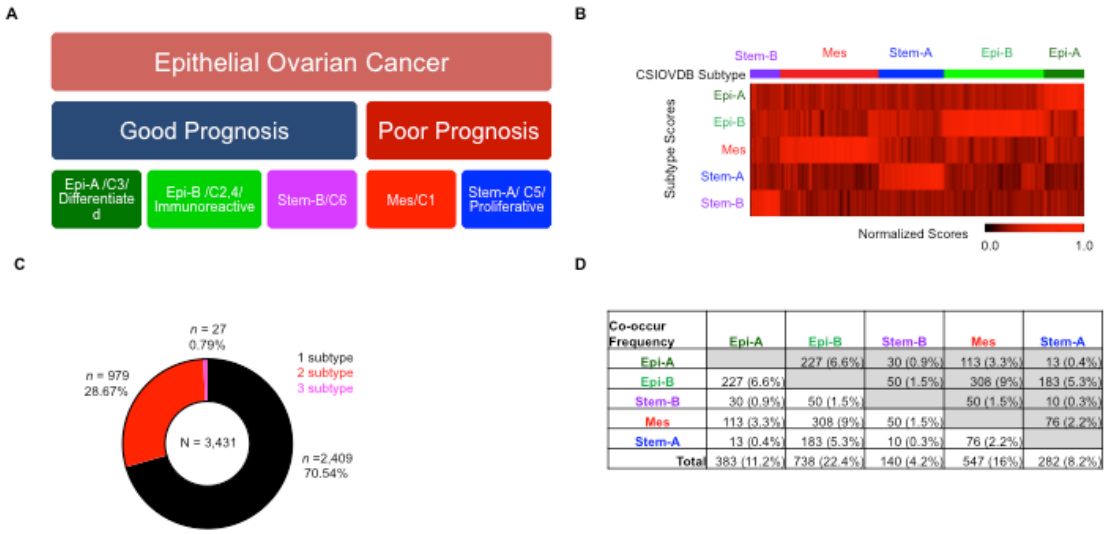

Co-occur Frequency	Epi-A	Epi-B	Stem-B	Mes	Stem-A
Epi-A		227 (6.6%)	30 (0.9%)	113 (3.3%)	13 (0.4%)
Epi-B	227 (6.6%)		50 (1.5%)	308 (9%)	183 (5.3%)
Stem-B	30 (0.9%)	50 (1.5%)		50 (1.5%)	10 (0.3%)
Mes	113 (3.3%)	308 (9%)	50 (1.5%)		76 (2.2%)
Stem-A	13 (0.4%)	183 (5.3%)	10 (0.3%)	76 (2.2%)	
Total	383 (11.2%)	738 (22.4%)	140 (4.2%)	547 (16%)	282 (8.2%)

Figure 2:

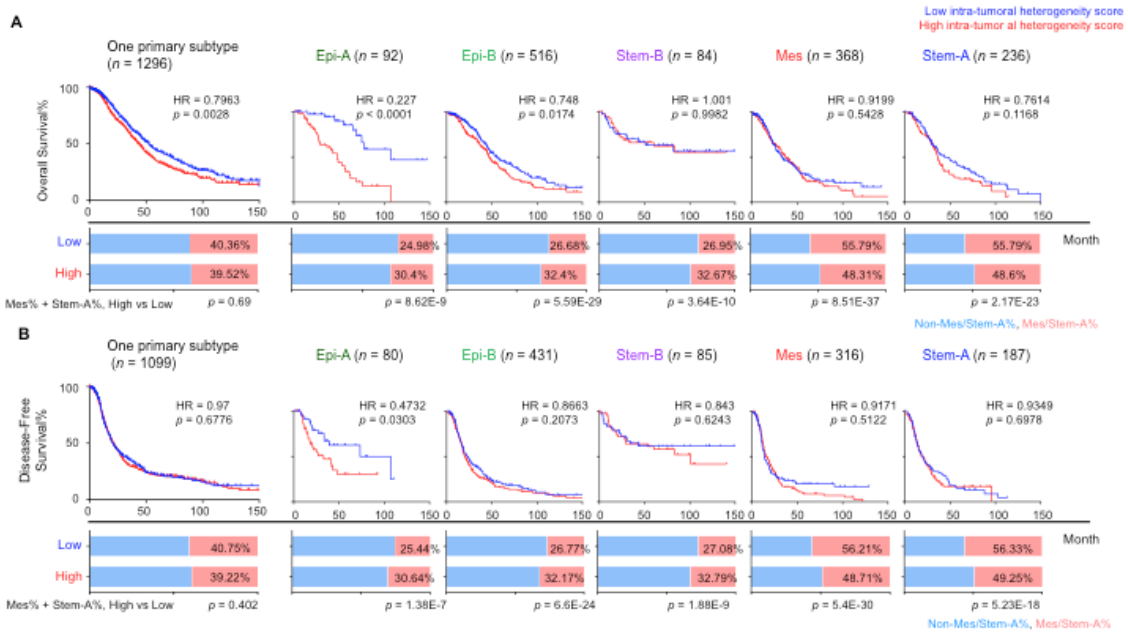

Figure 3:

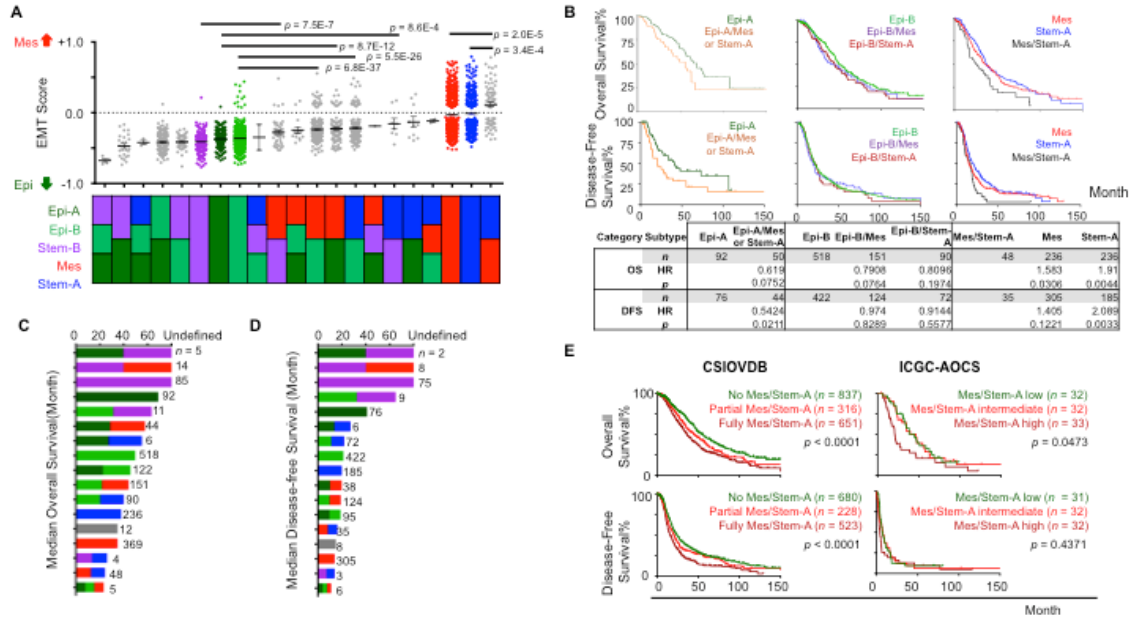

Figure 4:

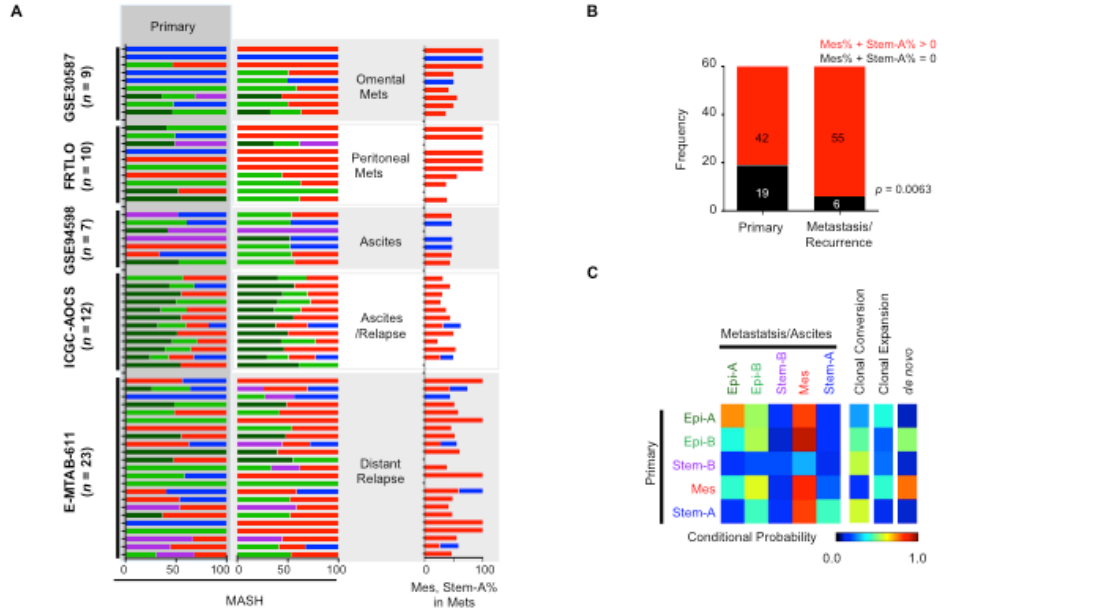

Figure 5:

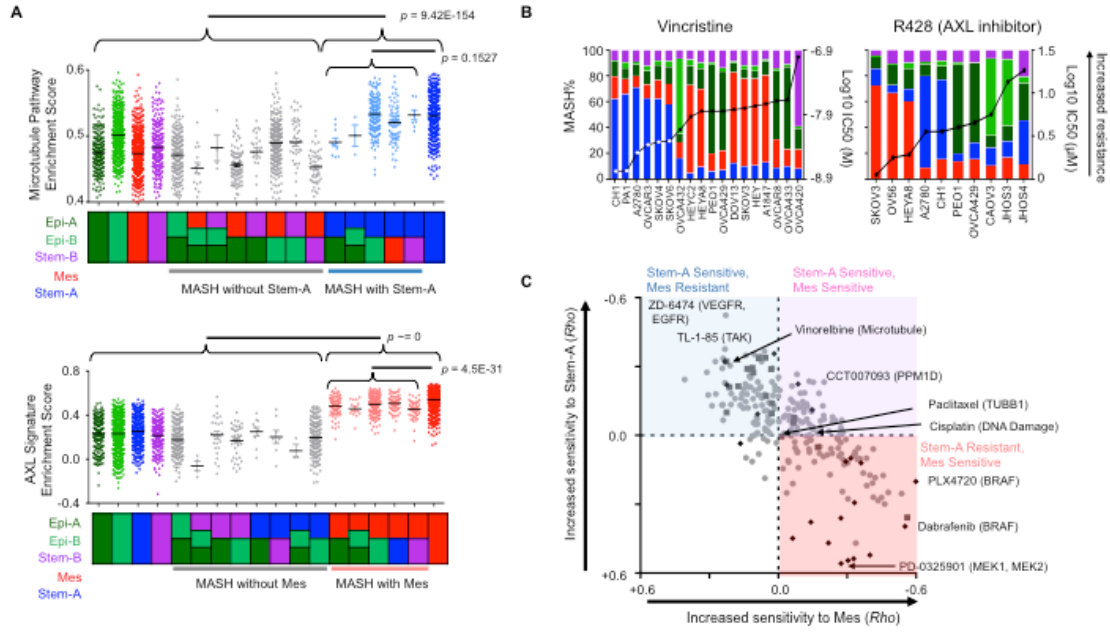

Figure 6:

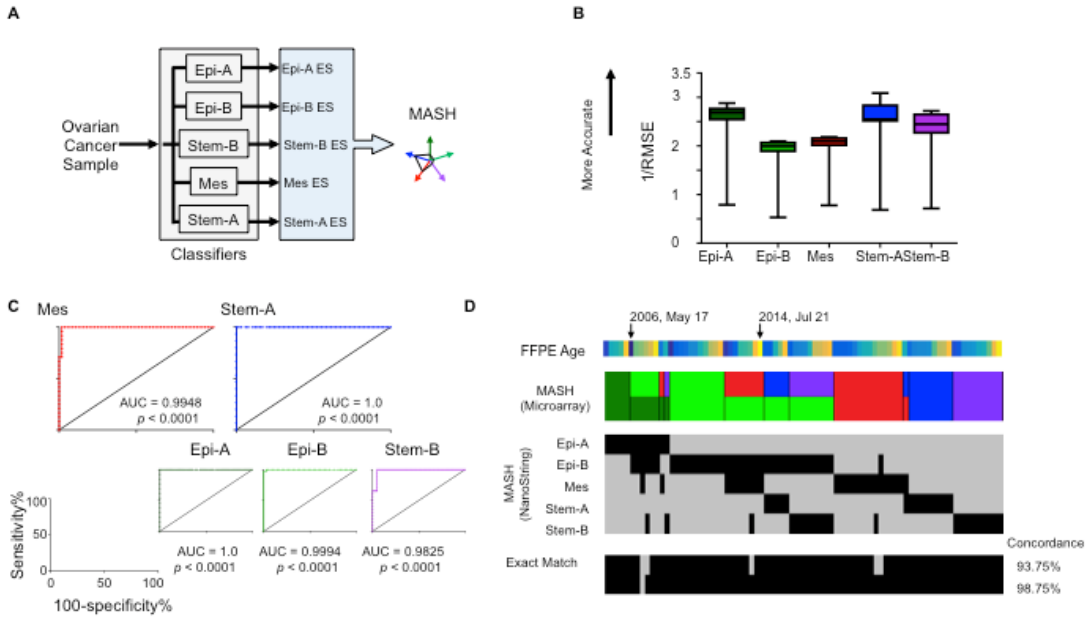
A
Ovarian Cancer Sample
Epi-A
Epi-B
Stem-B
Mes
Stem-A
Epi-A ES
Epi-B ES
Stem-B ES
Mes ES
Stem-A ES
MASH
Classifiers
B
More Accurate
1/RMSE
3.5
3
2
1
0
Epi-A
Epi-B
Mes
Stem-A
Stem-B
C
Mes
Stem-A
AUC = 0.9948
p < 0.0001
AUC = 1.0
p < 0.0001
Epi-A
Epi-B
Stem-B
AUC = 1.0
p < 0.0001
AUC = 0.9994
p < 0.0001
AUC = 0.9825
p < 0.0001
Sensitivity%
100
50
0
0
50
100
100-specificity%
D
2006, May 17
2014, Jul 21
FFPE Age
MASH (Microarray)
MASH (NanoString)
Epi-A
Epi-B
Mes
Stem-A
Stem-B
Concordance
Exact Match
93.75%
98.75%